On the development of a digital elevation model over South Africa using ground and satellite data

By: Mihlali Malindi

MLNMIH002

Department of Architecture, Planning and Geomatics: Division of Geomatics

Faculty of Engineering and the Built Environment

Thesis submitted in fulfilment of the requirements for the Degree of

Master of Science in Engineering (Geomatics) at the

University of Cape Town

Supervisor:

Associate Professor Patroba Achola Odera

September 2022

Copyright Declaration

Authorship Declaration

I know that plagiarism is wrong and that I cannot use another author's work and pretend that it is my own. This thesis is my own work.

Each significant contribution to, and quotation in this thesis from the work(s) of other people has been attributed and has been cited and referenced.

The work in this thesis has not previously been published in whole or in part for the award of any degree.

Signature: Signed by candidate **Date:** 12/09/2022

Research Ethics Declaration

Application for Approval of Ethics in Research (EiR) Projects
Faculty of Engineering and the Built Environment, University of Cape Town

ETHICS APPLICATION FORM

Please Note:
Any person planning to undertake research in the Faculty of Engineering and the Built Environment (EBE) at the University of Cape Town is required to complete this form **before** collecting or analysing data. The objective of submitting this application *prior* to embarking on research is to ensure that the highest ethical standards in research, conducted under the auspices of the EBE Faculty, are met. Please ensure that you have read, and understood the **EBE Ethics in Research Handbook** (available from the UCT EBE, Research Ethics website) prior to completing this application form: http://www.ebe.uct.ac.za/ebe/research/ethics1

APPLICANT'S DETAILS		
Name of principal researcher, student or external applicant		Mihlali Malindi
Department		Architecture, Planning and Geomatics
Preferred email address of applicant:		www.minmih002@myuct.ac.za
If Student	Your Degree: e.g., MSc, PhD, etc.	MSc in Engineering specialising in Geomatics
	Credit Value of Research: e.g., 60/120/180/360 etc.	180
	Name of Supervisor (if supervised):	Dr Patroba Achola Odera
If this is a researchcontract, indicate the source of funding/sponsorship		N/A
Project Title		Towards development of an accurate digital elevation model from ground and satellite data over South Africa

I hereby undertake to carry out my research in such a way that:

- there is no apparent legal objection to the nature or the method of research; and
- the research will not compromise staff or students or the other responsibilities of the University;
- the stated objective will be achieved, and the findings will have a high degree of validity;
- limitations and alternative interpretations will be considered;
- the findings could be subject to peer review and publicly available; and
- I will comply with the conventions of copyright and avoid any practice that would constitute plagiarism.

APPLICATION BY	Full name	Signature	Date
Principal Researcher/ Student/External applicant	Mihlali Malindi		05/05/2020
SUPPORTED BY	**Full name**	**Signature**	**Date**
Supervisor (where applicable)	Dr Patroba Odera		5/5/2020

APPROVED BY	Full name	Signature	Date
HOD (or delegated nominee) Final authority for all applicants who have answered NO to all questions in Section 1; and for all Undergraduate research (including Honours).	Simon Hull		26 May 2020
Chair: Faculty EIR Committee For applicants other than undergraduate students who have answered YES to any of the questions in Section 1.			

Page 1 of 1

Abstract

A digital elevation model (DEM) represents the bare land surface of the Earth. DEMs are used in a wide range of applications, including geological studies, geomorphology, water resources and hydrology, evaluation of natural hazards, and vegetation surveys. In recent years, DEMs have increasingly been used in geographic information systems (GIS), mainly due to the availability of free satellite-based DEMs, some with global coverage.

The satellite-based DEMs over South Africa provide topographic surface representation but are associated with errors, and in recent decades there have been significant efforts to improve accuracy. In South Africa, the ground levelling (trigonometrical beacon) data is more capable of representing the terrain heights accurately. However, the data points are farther apart, which makes it difficult for accurate continuous terrain representation.

In this research, contributions are made towards the development of an accurate digital elevation model from ground and satellite data over South Africa. This is achieved by preparing satellite-based DEMs (AW3D30, SRTM, ASTER, TanDEM-X, and MERIT), assessing the quality of the satellite-based DEMs, selecting candidate DEMs for fusion, modelling candidate DEM errors, and fusing DEMs. The aerial-based DEM from LiDAR is also applied in the assessment of the quality of satellite-based DEMs, although this was only possible in selected areas due to a lack of LiDAR data covering the whole of South Africa.

Following removal of outliers from each DEM, a different number of ground levelling data is used in the assessment of the DEMs (26364, 25728, 23773, 25967 and 24485) ground levelling points for AW3D30, SRTM, ASTER, TanDEM-X and MERIT, respectively. The vertical quality assessment results indicate that the standard deviations of the differences between ground levelling and DEMs heights are ±5.09, ±7.03, ±9.20, ±4.99 and ±8.36 m for AW3D30, SRTM, ASTER, TanDEM-X and MERIT, respectively. In general, the vertical accuracies of the satellite-based DEMs are relatively lower in higher areas than in low areas.

The results of height differences between satellite-based and LiDAR DEMs heights in different geomorphological ranges indicate that the AW3D30 and TanDEM-X are better candidate DEMs for generating a new DEM over South Africa. Applying a combination of linear regression, multiple regression, and adaptive terrain-dependent methods to these DEMs, their vertical accuracies improved. The standard deviations of the differences between ground levelling and the improved DEMs at 8,657 points over South Africa decreased from ±5.745 to ±4.995 m for AW3D30 and ±5.073 to ±4.582 m for TanDEM-X.

A fused DEM was developed from improved AW3D30 and TanDEM-X DEMs using a combination of different fusion methods (linear combination, weighted averaging, and simple averaging) over South Africa. The fused DEM was assessed using 8,657 ground levelling points over South Africa. The standard deviation of the height differences between ground levelling and the fused DEM is ±4.290 m, indicating the superiority of the fused DEM over all the satellite-based DEMs used in this study.

The fused DEM can be applied in areas with a slope less than 20° where an accuracy of less than 4.3 m is achievable. In the steepest areas, it can still achieve better vertical accuracies compared to other satellite-based DEMs tested.

Acknowledgements

I would like to express my sincere gratitude to my supervisor Associate Professor Patroba Odera for his patience, availability, enthusiasm, and immense knowledge. His guidance helped me in all the time of research and writing of this thesis. I could not have imagined having a better supervisor for my thesis. I acknowledge the National Research Foundation, URC Building Research Active Academic Staff Grant, and Vice-Chancellor's Research Grant for providing me with scholarship funding.

I would like to thank the TanDEM-X-Geoservice, United States Geological Survey, Earthdata, Japan Aerospace Exploration Agency, Yamazaki lab, and International Service for the Geoid for providing the data for free. I would also like to thank the Chief Directorate: National Geospatial Information and the City of Cape Town for providing necessary datasets used in this study.

Dedication

First and foremost, I would like to praise and thank God Almighty, my creator, pillar of strength, source of inspiration, wisdom, and knowledge. Throughout this program, I have been strengthened by Him. A special feeling of gratitude goes to my family, with whom I dedicate this work.

Table of Contents

List of Tables

List of Figures

List of Abbreviations

ALOS	Advanced Land Observing Satellite
ASTER	Advanced Space- borne Thermal Emission and Reflection Radiometer
AW3D30	ALOS World 3D – 30 m
CD: NGI	Chief Directorate: National Geospatial Information
CZO	Critical Zone Observation
DTED	Digital Terrain Elevation Data
DEM	Digital Elevation Model
DEMSA	Digital Elevation Model of South Africa
DLR	German Space Agency
DSM	Digital Surface Model
DTM	Digital Terrain Model
EGM	Earth Gravitational Models
EROS	Earth Resources Observation and Science
GDEM	Global Digital Elevation Model
GLAS	Geoscience Laser Altimeter System
GPS	Global Positioning System
GRASS	Geographic Resources Analysis Support System
GRID	Global Resource Information Database
GSI	Geographical Survey Institute
HRS	High-Resolution Stereoscopic
ICESat	Ice, Cloud, and Elevation Satellite
INEG	Instituto Nacional de Estadistica Geografica
InSAR	Interferometric Synthetic Aperture Radar
JPL	Jet Propulsion Laboratory
LAI	Leaf Area Index
LASER	Light Amplification by Stimulated Emission of Radiation
LiDAR	Light Detection and Ranging
MERIT	Multi-Error-Removed Improved-Terrain DEM
MOMS	Modular Optoelectronic Multispectral Stereo Scanner
NASA	National Aeronautics and Space Administration
NASADEM	National Aeronautics and Space Administration Digital Elevation Model
NED	National Elevation Dataset
PALSAR	Phased Array type L-band Synthetic Aperture Radar
RADAR	Radio Detection and Ranging
RMSE	Root Mean Squared Error
RTK	Real-Time Kinematic
SANSA	South African National Space Agency
SAR	Synthetic Aperture Radar
SCAR	Scientific Committee on Antarctic Research
SNAMP	Sierra Nevada Adaptive Management Project
SPOT	Système Pour l'Observation de la Terre
SRTM	Shuttle Radar Topography Mission
SUDEM	Stellenbosch University Digital Elevation Model
TanDEM-X	TerraSAR-X add-on for Digital Elevation Measurement
UNEP	United Nations Environment Programme
USAID	U.S. Agency for International Development

USGS	United States Geological Surveys
WGS84	World Geodetic System of 1984

Chapter One: INTRODUCTION

1.1 Background

A DEM is one of the basic and most frequently used digital representations of bare earth. Earth surfaces are represented by raster or regular grid points with a value representing an elevation. DEMs have many applications, including but not limited to view-shed visibility analysis, landscaping, water modelling, marine observation, and geological land observation (Singh, 2019; ElSayed and Ali, 2016; Tian et al., 2018). In accordance with Yamazaki et al. (2017), DEMs are also important datasets for geodetic survey applications, since precise terrain representation is essential in geodetic survey for applications such as earthquake motion analysis, flooding overflow modelling, soil erosion prediction, and sediment yield prediction.

Different techniques that vary in production cost, time, sampling density, and pre-processing requirements to generate DEMs have been developed. These techniques include ground field surveys such as GPS surveys, conventional contour maps, photogrammetry, Airborne Laser Scanning, and satellite remote sensing (ElSayed and Ali, 2016). The ground field surveying technique generates DEMs with high accuracies, but their applications are restricted to small areas as they are time-consuming and costly, especially in mountainous and rugged terrain (Tian et al., 2018). Photogrammetry has become a frequently used technique to generate DEMs compared to field ground surveying techniques and conventional maps (Gómez et al., 2012). Photogrammetry uses satellite or aerial images to generate DEMs, which makes it cheaper and less time-consuming. High resolution and good light conditions (cloudless view) are required to achieve better accuracies in photogrammetric techniques (ElSayed and Ali, 2016).

Light detection and ranging (LiDAR) technology generates high precision DEMs but, using this technology is also expensive, limiting its application, especially in developing countries (O'Loughlin et al., 2016). In developed nations, the LiDAR DEMs cover a small percentage of the earth's land-surface (O'Loughlin et al., 2016). In the past years, satellite remote sensing techniques have provided a quick and cheap way for DEM generation. Stereo matching of a pair of optical images (optical stereoscopy) and Interferometry Synthetic Aperture Radar (InSAR) images are the most regularly applied satellite techniques (Karkee et al., 2008).

InSAR and optical stereoscopy use different sensing technologies to generate DEM's. The InSAR technique uses two or more SAR images to generate a DEM by taking the phase difference between the waves returning to the satellite or aircraft. The optical stereoscopy technique is based on image parallax in which a difference in coordinates between conjugate points in two partially overlapping images is found, and elevation is extracted based on the image geometry (Karkee et al., 2008). The satellite-based DEMs generated either from InSAR or optical stereoscopy are the most used DEMs, due to their almost global coverage. Until now, the most popular near-global DEMs include the Shuttle Radar Topography Mission (SRTM), TerraSAR-X add-on for Digital Elevation Measurement (TanDEM-X), ALOS World 3D 30 m (AW3D30) and Advanced Space- borne Thermal Emission and Reflection Radiometer (ASTER).

The DEMs have been used by many scientists for different scientific studies (O'Loughlin et al., 2016). Advances in satellite remote sensing techniques over the years have improved the accuracy of terrain elevation representation. For example, the 90 m SRTM DEM was the only SRTM DEM that regions outside the United States could access freely before 2013. However, 30 m SRTM DEM become freely

accessible to everyone thereafter (Jing et al., 2013). Global DEMs, such as ASTER (30 m), TanDEM-X (90 m), and AW3D30 (30 m) are also freely accessible, (i.e., they are public).

As a result of difficulties such as clouds and rain, slanted radar sensing, and shadows when satellites acquire data, the InSAR and optical stereoscopic techniques do not produce accurate results. The InSAR technique sometimes fails to give a good estimate of elevation due to non-linear distortion of the image, temporal decorrelation, layover in images, and atmospheric condition change during the acquisitions (Karkee et al., 2008). In some cases, stereo images contain radiometric variation, cloud cover, and low levels of texture, which may lead to poor image matching in the optical stereoscopic technique. (Weydahl et al., 2005). Due to these challenges, satellite-based DEMs contain many observation errors, which cannot be ignored for some applications.

The satellite-based DEMs are, furthermore, affected by errors such as spatial scale into short-wavelength speckle noise, medium wavelength strip noise, long-wavelength absolute biases and land cover (Yamazaki et al., 2017). According to Rodríguez et al. (2006), the speckle noise is a random error with a very short wavelength of pixels and can be noted in a radar image by the grainy salt and pepper pattern. The strip noise is a constant height undulation with a wavelength of 500 m to 100 km (Tarekegn and Sayama, 2013). According to Yamazaki et al. (2017), the absolute bias is a shift in the average elevation over a large domain.

South Africa has some national DEMs that have been used in scientific research. These include the Chief Directorate: National Geo-Spatial Information (CD: NGI) DEM, Stellenbosch University Digital Elevation Model (SUDEM), and Computamaps^{TM} South African Digital Terrain Model (SADTM). The CD: NGI DEM is available for free, while the SUDEM and SADTM are available at a cost. The SUDEM is part of the efforts being made in South Africa to produce a high-resolution national DEM that reduces anomalies in satellite-based DEMs.

1.2 Statement of the problem

The publicly available free 25 m resolution DEM provided by the CD: NGI produced from hybrid methods has limitations. From a preliminary assessment and analysis conducted by the author, the DEM does not provide the full coverage of the country, some tiles are missing, and some tiles contain pixels with incorrect height information. In addition, the NGI 25 m DEM, when validated using 12,460 ground levelling (trigonometrical beacon) has a standard deviation of approximately ±4.60 m and ±5.88 m when validated using 189 LiDAR data, but it has a lot of inconsistencies in terms of coverage including missing pixels.

The LiDAR data available provides a small percentage coverage of the country as it only covers certain locations such as the City of Cape Town. As part of the efforts being made to address the issue of inconsistencies in terms of coverage and pixels missing, the SUDEM was developed. It has full national coverage and reduces anomalies in satellite-based DEMs. The DEM is, however, expensive, and not available to the public.

The South African ground levelling (trigonometrical beacon) data heights have a precision of about ± 0.1 m and are more capable of representing the terrain height accurately. However, the ground levelling data points are farther apart, making it difficult to accurately represent the topographical surface over South Africa. A surface or contours interpolated from ground levelling data points (trigonometrical beacons) can only represent a topographical surface at an accuracy of ±10 m over South Africa. This is because interpolation cannot estimate above maximum or below minimum

values, and therefore does not replicate the bare continuous earth surface. This means that there is a chance to improve topographic representation in South Africa using satellite- and aerial- based digital elevation models.

The satellite-based DEMs provide an accurate surface replication but are associated with speckle noise, strip noise, voids, and vegetation errors, limiting their applications. The results from different parts of the world indicate an average vertical accuracy range of ±7 to ±16 m. Now the challenge is how to incorporate ground levelling data and satellite-based DEMs to develop a more accurate DEM over South Africa that draws from the strengths of the two and reduces errors to improve its applications. The intended solution to the problem is to use the ground levelling and LiDAR data to model DEM systematic error and use fusion techniques to develop an accurate national DEM for South Africa.

1.3 Research objectives

The main objective of this research is to contribute to the development of a digital elevation model with vertical accuracy better than 5 m from ground and satellite data over South Africa. The following are the specific objectives.

- To empirically select candidate global DEMs for fusion to develop a more accurate DEM over South Africa

- To empirically select the optimal fusion technique(s) and develop a fused DEM for South Africa based on freely available DEMs and ground levelling data

1.4 Study area

The study site is the whole of South Africa, and it is located between latitudes 22^{o} - 35^{o}S and longitudes 17^{o} - 33^{o}E. It has an area of approximately 1.22 million km^{2}. The region consists of high, middle, and low-level terrain with a mountain height range of up to 3,475 m. The physical features range from grasslands, forests, deserts, bushveld, mountain peaks and coastal wetlands. Figure 1 shows the study area.

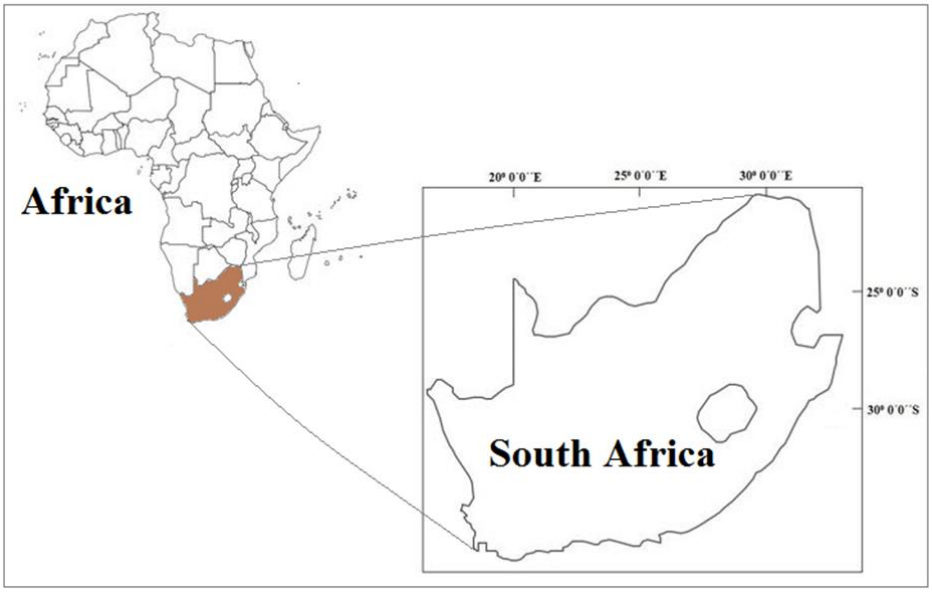

Figure 1: Study area

1.5 Thesis outline

Following this introduction is chapter 2. It starts by discussing the theory of digital elevation models. In theory, the techniques for deriving ground-based, aerial-based, and satellite-based DEMs are presented. The second part of chapter 2 discusses the assessment of the vertical accuracy of DEMs. This includes methods for assessing the vertical accuracy and methods for modeling errors in DEMs. The third part focuses on the fusion of DEMs. Here the discussion is on the different methods used in fusing DEMs. The final part of this chapter discusses the most common DEMs in South Africa. This includes a discussion on ground-based, satellite-based, and fused DEMs in South Africa. Chapter 2 concludes with a presentation of problems with DEMs in South Africa.

In chapter 3, the methodology towards the development of an accurate digital elevation model from ground and satellite data over South Africa is presented. The section shows the dataset acquired and how it is processed to achieve the objectives. There are four processes which include preparing satellite-based DEMs, assessment of the satellite-based DEMs over South Africa using ground levelling and LiDAR, modeling errors on selected candidate DEMs, and finally the fusion of the error modelled DEMs.

In chapter 4, the prospects for the development of an accurate digital elevation model from ground and satellite data over South Africa are presented. This includes the data sources, methods, and techniques to be considered for the development of accurate DEMs over South Africa in the future. In chapter 5, the approach is reviewed by revisiting the stated research objectives, identifying weaknesses, and exploring avenues for future research.

Chapter Two: LITERATURE REVIEW

2.1 Digital elevation models

A digital elevation model (DEM) represents the elevation of the earth's bare surface as digital images where each pixel represents the elevation at the pixel's center point. The Digital Terrain Model (DTM) and Digital Surface Model (DSM) are common terms related to DEMs. DTM is a model that represents the bare Earth's surface, as well as topographic information, such as information about slopes, and aspects of the terrain (Oksanen, 2021). Due to the widespread use of airborne laser scanning and satellite radar, digital surface models (DSM) have become commonplace. These models represent the highest elevation of the terrain, including land cover. DSM only represents the bare earth's surface in open areas, whereas in other regions, the model follows forest canopy and building roofs (Oksanen, 2021).

Before the development of DEMs, country-wide elevation data was stored on contour lines, printing plates, and paper maps (Oksanen, 2021). Even though contours remain a good way of visualising topography, they have two inadequacies in terms of data storage:

- Contours are not continuous representations of surfaces, and the surfaces that form between a contour interval are largely unknown.
- For contours to be generated, visualisation is necessary, which forces the use of generalisation rules in cartography. In this process, some details of the topography are removed, while others are deliberately over-emphasized.

A DEM can be represented as a raster (a grid of squares) or as a vector-based triangular irregular network (TIN). The TIN dataset is also referred to as a primary (measured) DEM, whereas the raster DEM is referred to as a secondary (computed) DEM (Ronald, 1987). The TIN representation has the primary advantage of requiring fewer points to represent the terrain with the same level of accuracy, but its disadvantage is that it is relatively more difficult (than a raster grid) to determine elevation from the model (Mikhail et al., 2001).

Among many other uses and applications, the DEMs are used for climate impact studies, hydrological, and hydraulic analyses and models, cartographic representations, geological applications, visibility analyses, road and dam planning, flood risk analysis, planning of telecommunication networks, agriculture and forestry applications, geophysical modelling, palaeogeographical mapping, cut-and-fill analysis, automatic drainage basin delineation, biogeographical, analysis of landscape dynamics, water management, ortho-rectification of aerial photographs, 3D visualisations, and geomorphological analysis.

2.1.1 Generation of digital elevation models based on ground field surveys

Ground-based DEMs are obtained from interpolation using field measurements. Ground levelling surveying techniques are used to obtain field measurements by determining unknown elevations or heights using known heights or elevations. In land surveying, a ground levelling survey can be described as vertical measurement and is considered important as it generates data for construction, mapping, and engineering design. Different ground levelling survey methods include but are not limited to barometric, GNSS, precise or geometric, and trigonometric levelling.

Barometric levelling determines the relative unknown elevation or height by measuring the air pressure difference using a barometer. The method has disadvantages as air pressure is also affected by other elements such as temperature. The trigonometric levelling method determines the height of an unknown point by taking vertical angular observations and the distance between the points using a theodolite or total station. Geometric or precise levelling involves using a telescope to take observations of staves and using the observations together with a known height to evaluate a height difference to find an unknown height. GNSS levelling involves using satellite-positioning systems and the geoid to determine unknown heights or elevation (normal, orthometric, or non-orthometric heights).

Due to the high accuracy of ground levelling survey data, a DEM produced from them is accurate. However, the costs and time-consuming nature of these techniques limit their use to small areas or means that they are used as references or to complement other types of DEM. A brief description of trigonometric levelling in South Africa is provided here because trigonometrical beacon data has been used in the current study.

The erection and surveying of trigonometrical beacons in South Africa began in 1834. Once a robust country-wide geodetic network had been established by 1936, secondary and tertiary triangulation began and was completed in the early 1980s. South African coordinates were referred to the Cape Datum using the Clarke 1880 modified ellipsoid. The Cape Datum has its origin at trigonometrical beacon Buffelsfontein, No. 130, in degree square 3325. The geodetic latitude of Buffelsfontein was determined from several adjacent astronomical stations. Its geodetic longitude was determined from the Royal Observatory in Cape Town's triangulation chain.

A telegraph time signal from Greenwich was used to determine the Royal Observatory's longitude. The development of computing systems and the introduction of satellite positioning in the 1970s, notably the establishment of the Global Positioning System (GPS) in the 1980s, enabled a recalculation of the South African reference frame. Throughout the country, a GPS baseline survey campaign began in 1990, surveying trigonometrical beacons of zero-order, each approximating 100km in length.

The work ended in the Hartebeesthoek94 Datum, which was officially introduced on the 1st of January 1999. The Hartebeesthoek94 Datum is referred to the World Geodetic System 1984 ellipsoid (WGS84), with the Hartebeesthoek Radio Astronomy telescope as the datum origin. The heights of the trigonometrical beacons were calculated using trigonometrical heightening techniques and are referred to the Land Levelling Datum. South Africa has a network of approximately 28,000 trigonometrical beacons.

There are 9 types of trigonometrical beacon: standard concrete pillars with 1.26 m or 1.89 m signals, standard beacon on platform, standard up-station, pipe beacon, 10-11 m block beacon, metal tripod beacon, 15 m windmill tower beacon, 6.3 m or 8.82 m windmill tower beacon and block beacon higher than 10 - 11m. At each trigonometrical station, a minimum of three witness marks are placed and surveyed. These witness marks are used to confirm the beacon position during subsequent surveys.

2.1.2 Aerial based digital elevation models

Aerial-based DEMs are derived from data collected by high-precision sensors mounted on moving aircraft and collecting information about the bare earth surface over which the aircraft flies. Popular DEMs derived from aerial surveys are photogrammetric and LiDAR DEMs.

Photogrammetric DEMs: Photogrammetry is the science of obtaining reliable information about surface properties and objects without actual physical contact, measuring and interpreting this information. Photogrammetry takes its name from the three Greek words phos or phot, which means light, gramma, which means letter, or something drawn, and metrein, which means measurement (Schenk, 2005). According to Baqersad et al. (2017), photogrammetry is a measurement technique that uses photographs or digital images to calculate the geometry, displacement, and deformation of a structure. The earliest applications of photogrammetry were aerial and terrestrial, motivated mostly by military reconnaissance. As digital cameras and high-resolution cameras became more affordable, the applications expanded into other fields of science such as civil and mechanical engineering.

In aerial photogrammetry, as an aircraft flies over bare earth's surface, high precision metric cameras photograph the terrain. In most instances, the optical axis of the camera is perpendicular to the ground. The most prominent products of photogrammetry are maps. They are produced at a variety of scales and accuracy levels. The photogrammetric DEM generation technique involves extracting 3D data or information from two or more overlapping aerial photographs (also called stereo pairs). In general, extraction techniques assume that all camera parameters (internal and external) are well-known (Mikhail et al., 2001). In built-up areas, it is relatively common for DSMs, which represent heights of the tallest surfaces at that point, to be generated from optical image matching (Ismail and Jaafar, 2013).

Airborne laser scanning (LiDAR) DEMs: In a LiDAR technique, a laser range-measurement beam scans the terrain beneath the aircraft, typically by whiskbroom. In this process, the LiDAR system emits EM pulses to the surface, which reflect off the target surface and are detected by the LiDAR system. Laser scanning using pulsed laser beams is the preferred method for airborne scanning (Vermeer and Ayehu, 2018).

Among other things, this technique can be used to construct geocentric terrain height models of high precision (a few centimetres depending on the terrain type) and resolution (sub-m^2) (Vermeer and Ayehu, 2018). Having a GNSS-equipped scanning aircraft positioned in a geocentric reference frame is essential to the success of airborne laser scanning. The LiDAR process is largely automated, unlike photogrammetry. This explains a portion of its current popularity; however, precisely calibrating the laser scanner and connecting its origin with the electromagnetic center of the GNSS antenna is challenging (Vermeer and Ayehu, 2018).

With modern instruments, it is possible to record and use multiple reflections, such as those from the canopy, mid-level foliage, understorey, and the forest floor. One can then construct either a DSM which represents the heights of the tallest surfaces at that point or a DTM which represents ground elevation from the point cloud generated (Vermeer and Ayehu, 2018). For constructing a DTM in urban areas, buildings must be removed, either manually or automatically.

Comparison of the techniques: In any operative condition, it has become clearer that neither photogrammetric nor airborne laser scanning techniques can guarantee complete and consistent results as both techniques have their advantages and limits (Szabó et al., 2016). The way that LiDAR collects data makes it more reliable than photogrammetry because LiDAR allows the acquisition of full-waveform data by collecting thousands of points per second. According to Csanyi and Toth (2007), because of the footprint, the horizontal accuracy of the LiDAR is worse than vertical accuracy. According to Nex and Rinaudo (2011), it is impossible to directly obtain radiometric and semantic information from LiDAR.

On the other hand, the photogrammetric technique is biased by vegetation as it can only produce surface models. According to Nex and Rinaudo (2011), it is not possible to generate accurate point

clouds without errors under every operational condition (especially on the terrestrial). One of the major obstacles to automation in photogrammetry is the complicated and sometimes unreliable matching procedure, especially when dealing with converged imagery with significant depth differences or with the presence of bad-textured areas (Nex and Rinaudo, 2011).

LiDAR is generally the preferred source for elevation modelling data due to its ability to collect more detailed depth data, but photogrammetry can provide detailed visual information on the environment, which is invaluable to many researchers (Mapware, 2020). LiDAR is, however, extremely expensive, so it is typically flown only over small- high-value areas, like cities, with photogrammetry used for large-scale data collection.

2.1.3 Satellite-based digital elevation models

Satellite-based DEMs are generated by remote sensing techniques, which provide a relatively cheaper and quicker way for DEM generation compared to ground and aerial-based methods. The remote sensing process (deployed in satellite-based data acquisition techniques) involves the process of obtaining information about an object, area, or phenomenon under investigation via the analysis and interpretation of data acquired by a sensor-device on a satellite that is not in contact with the subject. The DEMs generated from data collected by optical and radar remote sensing systems, and those derived from fusing the data from these systems are discussed below. It is important to note that the DEMs described refer to Digital Surface Models (DSMs). This is due to the low penetration of SRTM and TanDEM-X radar signals in dense vegetation and the canopy sensitivity of optical images used to generate ASTER GDEM and AW3D30.

Shuttle Radar Topography Mission (SRTM): SRTM's mission research generated Digital Elevation Models (DEMs) on a near-global scale from 60°N to 56°S. Between the 11th and the 22nd of February 2000, the SRTM mapped the earth's surface to provide a high-resolution digital topographic database consisting of digital elevation data, covering about 80% of the world landmass (Roth et al., 2002). The C-and X-band interferometric radar data were used to generate the SRTM elevation data. During the mission, two antenna pairs working at different frequencies were operated, and the SRTM recorded the earth's topography and processed it at 30 m resolution. The SRTM DEM has a vertical error of no more than 16 m at a 90% confidence level (Tian et al., 2018). The DEM is in the geographic coordinate system and based on the WGS84 ellipsoid horizontal datum with vertical datum as EGM96 (Tran et al., 2014).

Advanced Space- borne Thermal Emission and Reflection Radiometer (ASTER): The U.S. National Aeronautics and Space Administration (NASA), Japan's Industry, Trade, and Ministry of Economy jointly released the first Global Digital Elevation Model (GDEM) version in July 2009 which was formed from 1.7 million stereo images captured by the ASTER and released to the public at no cost covering the earth's surface from 83° North to 83° South (Abrams, 2016).

There was a shortcoming in the first version of ASTER in the sense that there was missing data. Therefore, the second version, which had an additional 260 000 stereo-pairs scenes to cover the short falling by filling in the missing data, eliminating many artefacts, mostly those caused by remains of cloud edges, was released in 2011 (Mohamed and Saleh, 2018). According to Tachikawa et al. (2011), the vertical accuracy for the first version is estimated to be 20 m at 95% confidence level. The second released version also had some uncorrected artefacts. Therefore, the US and Japan jointly released

version 3 of the Global DEM (GDEM) in 2016, which was produced by stereo correlation of 2 million ASTER scenes covering the earth's surface from 82° North to 82° South (Abrams, 2016).

The released ASTER DEM version 3 has a 30 m resolution and has been improved from the previously released versions, as areas with missing data have been filled with more acquired data, and any artifacts which previously occurred are corrected. This version also contains separate data that identified water bodies (Abrams, 2016). According to Gesch et al. (2016), the ASTER Global DEM (GDEM) third version has been reported to have a vertical accuracy of lower than ±16 m at a 95 % confidence level. The DEM is in the geographic coordinate system and based on the WGS84 ellipsoid horizontal datum with vertical datum as EGM96.

Advanced Land Observing Satellite World 3D – 30m (AW3D30): AW3D is the latest generation high resolution global DSM released by Japan Aerospace Exploration Agency (JAXA). AW3D uses 3 million scene records to cover the global land areas. The records were collected from 2006 to 2011 by the PRISM panchromatic stereo mapping sensor on the Advanced Land Observing Satellite "DAICHI" (Japan Aerospace Exploration Agency, 2021). The AW3D30 has a 30 m resolution and was generated from resampling the AW3D, available at a resolution of 5 m, and it is considered the most accurate open-source DEM (Tian et al., 2018). Due to its late release, there are also a few studies testing vertical accuracy. The DEM is in the geographic coordinate system and based on the WGS84 ellipsoid horizontal datum with vertical datum as EGM96.

Multi-Error-Removed Improved Terrain (MERIT): MERIT-DEM is a high accuracy global DEM with a horizontal resolution of approximately 90 m at the equator (3 arc-second). The DEM was produced by removing major error components from space-borne DEMs (SRTM3 v2.1 and AW3D30). Yamazaki (2018) used datasets from multiple satellites and filtering techniques to eliminate speckle noise, tree height bias, absolute bias, and strip noise. After the removal of the biases, land areas mapped with 2m, or better vertical accuracy were increased from 39% to 58%. Remarkable improvements after error removal were in flat areas, and landscapes such as river networks and hill-valley structures became more visible. The DEM is in the geographic coordinate system and based on the WGS84 ellipsoid horizontal datum with vertical datum as EGM96.

TerraSAR-X and TanDEM-X: TerraSAR-X and TanDEM-X are imaging, radar and earth observation, satellite missions for commercial and scientific applications. The satellites are managed by DLR (German Aerospace Center) and supported by BMBF (German Ministry of Education and Science). The satellites are owned and operated by DLR, with the scientific rights also held by the DLR. On the 15th of June 2007, the satellite TerraSAR-X was launched, and since January 2008, it has been operating, then on the 21st of June 2010, the TanDEM-X was launched (Airbus, 2015).

The two satellites (TerraSAR-X and TanDEM-X) operate close to each other, separated by a distance of a few hundred meters and record data synchronously. Both satellites acquire the databases for the Global World DEM, presenting an unrivaled quality, accuracy, and coverage with the worldwide and homogeneous DEM available from 2014 (Airbus, 2015). The TerraSAR-X and TanDEM-X acquire radar images at higher quality for the entire Earth while circulating in a sun-synchronous orbit at an altitude of 514 km on the equator and provide data independent of weather conditions. Both satellites have an operational life of 5 years and are reliable providers of high-resolution radar images. The satellites acquire radar data in three modes, which are the spotlight, strip map, and scanSAR (Airbus, 2015). The application of the high-resolution TanDEM-X and TerraSAR-X imagery includes but is not limited to change detection, land use/cover mapping, environmental applications, defense and security applications, topographic mapping, and surface movement (Airbus, 2015).

The TanDEM-X global digital elevation model is as the result of merging at least two different acquisitions of the same area, which are from the TerraSAR-X and TanDEM-X imaging radar earth observation satellite missions. The DEM is available with a pixel spacing in latitude direction of 0.4 arc-second, 1 arcsecond, and 3 arcseconds, corresponding to approximately 12 m, 30 m, and 90 m, respectively. The DEM has been generated on all overland surfaces with a relative vertical accuracy of 2 m for slopes less than 20° and 6 m for slope greater than 20° (Han et al., 2021). The DEM is in the geographic coordinate system and based on the WGS84 ellipsoid for horizontal and vertical datum.

2.2 Assessment of vertical accuracy of existing public digital elevation models

2.2.1 Considerations when assessing vertical accuracy

Vertical accuracy is one of the most important aspects of a DEM. Vertical accuracy refers to how close a modeled height obtained from a DEM represents/replicates the actual height of the topographical surface. DEMs generated from different techniques such as photogrammetry, radar, LiDAR, and satellite sensors, among others, have different levels of accuracy.

A focus in most DEM evaluations is on absolute vertical accuracy rather than relative vertical accuracy (Luebke, 2019). Absolute vertical accuracy accounts for all effects of systematic and random errors and relates the DEM heights to the true height with respect to an established vertical datum. Relative accuracy is a measure of the point-to-point vertical accuracy of models against another reference model that has higher vertical accuracy. Since in DEMs, elevations are an average over the chosen area, the vertical accuracy is correlated to horizontal resolution. In flat areas, the effect of averaging is minimal, while in hilly terrain, the effect is large, especially for lower resolution DEMs (Luebke, 2019).

2.2.2 Validation of digital elevation models

To judge the validity of an accuracy assessment, the selection of a test site is critical. Assessment should either occur on a very large site or several different sites with different variations of the terrain. Depending on the available data, the point-based, profile-based, and surface-based are different methodological approaches for the assessment of the DEMs (Luebke, 2019).

The point-based approach is used if the reference data is provided as a set of points with accurate height information and scattered over the area of interest. Differences in heights are determined for each point independently, and the vertical accuracy is determined for the entire set of points. The profile-based approach is used to provide more understanding of the quality of the DEM if the reference data is collected along with a linear feature. In addition, relative vertical accuracy can be calculated along with each profile after removing the errors of the starting point. The surface-based approach is used if the reference data is provided as a grid. In this approach, a difference in surface is determined, and a validity mask is used to exclude anomalies in any of the input datasets or any differences due to temporal changes.

Irrespective of any approach used, the DEMs must be referenced to the same vertical datums before being assessed. The transformation must be performed if the vertical datums are different. The validation is essential in deciding on the DEM's suitability for utilization towards the development of an accurate digital elevation model(s).

2.2.3 Selected case studies on vertical accuracy of freely available global digital elevation models

Many authors have conducted DEM validation studies in various parts of the world. Only four case studies (Uuemaa et al., 2020; Santillan et al., 2016; Mahesh et al., 2021; Han et al., 2021) are discussed here.

Uuemaa et al. (2020) evaluated the vertical accuracy of freely available DEMs (AW3D30 version 3.1, 1 arc-second SRTM version 3, 3 arc-second MERIT, 1 arc-second NASADEM, 3 arc-second TanDEM-X version 1, and 1 arc-second ASTER version 2), using locally derived LiDAR-based DEM; and the Pleiades 1A data as reference models. To validate the DEMs, error raster's were generated by subtracting the reference models from corresponding DEMs and descriptive statistics (median, mean, and root mean square error (RMSE)) were calculated for the height differences (Uuemaa et al., 2020). In addition, land cover, slope aspect, and slope angle were taken into consideration when assessing vertical accuracy. The study was conducted by Uuemaa et al. (2020) in four areas in various parts of the world (China, Estonia, New Zealand, and Norway).

The Estonian study area was in southern Estonia and had an area of approximately 225 km^2. The area was characterized by relatively flat topography, with some hilly landscapes in the eastern part with elevations ranging from 40 to 218 m. 28% of the land cover was cultivated/ arable, 17% open forest, and 52% closed forest. In this area, the ASTER, AW3D30, MERIT, TanDEM-X, SRTM, and NASADEM had a RMSE of 10.36, 7.92, 3.01, 7.16, 6.59, and 6.39 m, respectively (Uuemaa et al., 2020). The study area in China was in the Ningxia Hui Autonomous, covering an area of approximately 103 km^2. The area contained mountains and had tectonic faults that resulted in a diverse relief with an elevation ranging from 1063 to 1766 m. 20% of the land cover in this area was grasslands, 24% artificial landscapes, and 52% was sparsely vegetated. In this area, the ASTER, AW3D30, MERIT, TanDEM-X, SRTM, and NASADEM had a RMSE of 13.52, 7.18, 12.43, 11.1, 10, and 8.53 m, respectively (Uuemaa et al., 2020).

The New Zealand study area was in the southern part of the North Island with an area of approximately 111 km^2. The topography of the area is characterised by mountains and gorges, with elevations ranging from 32 to 828 m. In this area, the ASTER, AW3D30, MERIT, TanDEM-X, SRTM, and NASADEM had a RMSE of 11.7, 11.42, 13.58, 15.05, 13.07, and 12.08 m, respectively (Uuemaa et al., 2020). The Norway study area was used only in the assessment of the AW3D30, MERIT, ASTER, and TanDEM-X DEMs. The study area was located between the Jotunheimen and Rondane mountainous areas and had an area of approximately 193 km^2. The area had a relatively flat topography with an elevation ranging from 335 to 1662 m. 12% of the land cover/use in this area was open forest, 37% grassland, and 44% forested. In this area, the ASTER, AW3D30, MERIT, and TanDEM-X had a RMSE of 9.22, 4.98, 10.49, and 6.84 m, respectively (Uuemaa et al., 2020).

Assessment results for all the GDEMs in the study areas indicated that, the AW3D30 was the most robust and stable performing DEM, followed by the NASADEM, and SRTM, respectively. MERIT and TanDEM-X performed better than ASTER, despite their low resolution. The ASTER DEM had the highest ambiguities and least performance when compared against the reference data in all the study areas (Uuemaa et al., 2020). The slope was found to be the most significant factor influencing DEM accuracy. Flat areas (slope less than 5°) had the smallest bias in elevation values, and this bias increased with slope, resulting in higher variations in errors (Uuemaa et al., 2020). There was no systematic effect of aspect on DEM performance. In densely forested areas, all DEMs overestimated height. MERIT, however, was less impacted by the forested areas, primarily due to vegetation removal procedures.

Santillan et al. (2016) conducted the vertical accuracy assessment of the 30 m GDEMs (AW3D, SRTM, and ASTER) in north-eastern Mindanao, Philippines. The DEMs were assessed against 274 ground control points (GCP) scattered over different land cover/use classes. The ground control points were derived using the 3rd order differential levelling using a high precision digital level. The horizontal coordinates for these points were derived using GPS. The area had 5 different land covers/uses (grassland, cultivated areas, brushland, built-up areas, and dense vegetation).

To validate the vertical accuracy of these DEMs, the elevations of the DEM and GCPs were compared. ArcGIS 9.3 software was used to extract DEM elevations at each point. Following that, the differences in elevation were calculated by subtracting the GCP elevation from its corresponding DEM elevation, resulting in the measured DEM errors (Santillan et al., 2016). Based on these measured errors, the mean error and root mean square error (RMSE) for each DEM were calculated, along with their standard deviations. According to Santillan et al. (2016), the results indicated that the AW3D30 performed better than the SRTM and ASTER. The SRTM also showed a greater performance compared to the ASTER DEM. The AW3D30, SRTM, and ASTER had a Root Mean Square Error (RMSE) of 5.68, 8.28, and 11.98 m, respectively.

Mahesh et al. (2021) assessed the vertical accuracy of open source 30 m DEMs (AW3D30, SRTM, Carto, and ASTER) using the Ice, Cloud, and Elevation Satellite/ Geoscience Laser Altimeter System (ICESat/GLAS) and Real-Time Kinematic Global Positioning System (RTK GPS) data for reference. The study was conducted in the Tamil Nadu state, located in the south-eastern part of India. The study region had an area of approximately 130,058 km^2 and was characterized by a greater variation in relief, with the highest elevation as 2,637 m. The study was also conducted over a 10 km long coastline, covering approximately 8,863 km^2.

To validate the vertical accuracy, ArcGIS software was used to extract elevation values from raster DSM/DEMs, using the ICESat/GLAS point shape files. A difference in elevation was calculated between these DSM/DEMs and ICESat/GLAS. A minimum, maximum, mean, and standard deviation were calculated for the elevation points, and any differences exceeding 100 m between the ICESat/GLAS and the DSM/DEMs were excluded (Mahesh et al., 2021). Key statistical parameters such as mean error, standard deviation and root mean square error (RMSE) were computed for the elevation difference.

Mahesh et al. (2021) suggested that AW3D30 represents terrain elevation values the best, followed by SRTM and Carto DEMs. Results from the validation of the DEMs against the ICESat/GLAS indicated that AW3D30 had the least Root Mean Square Error (RMSE) compared to the SRTM, Carto, and ASTER, in the Tamil Nadu region and over the coastline (Mahesh et al., 2021). In the Tamil Nadu study area, the RMSE for the AW3D30, SRTM, Carto, and ASTER were 2.48, 3.02, 3.88, and 8.02 m, respectively, while the RMSE in the Coastline were 2.29, 3.10, 3.93, and 8.98 m, for AW3D30, SRTM, Carto, and ASTER, respectively (Mahesh et al., 2021).

Han et al. (2021) assessed the vertical quality of the 1 arc-second DEMs (TanDEM-X, ASTER, and SRTM). Reference data was taken from ICESat/GLAS points with 14-cm absolute vertical accuracy but 70-m diameter, and 12-m resolution TanDEM-X DEMs with less than 10-m absolute vertical accuracy. The study was conducted in four areas located in China, with the first two areas located in Xinjiang province, then the last two areas each located in Sichuan and Inner Mongolia. All the areas had coverage of $1^\circ \times 1^\circ$ (Han et al., 2021).

The four study areas were chosen based on two main criteria: diversity in land use/cover and topographic environments (flat, hilly, and mountainous areas), and free availability of TanDEM-X data in the area. 91% of Xinjiang (A) land cover was grassland/cropland/bare land, and in Xinjiang (B),

approximately 16% of the land was covered by forest and 74% by cropland/grassland/bare land. Approximately 56% of Sichuan land was covered by forest, and 40% was cropland/bare land/ grassland. In Mongolia, 2% of the land cover was shrubland, 3% was forest, and 86% was cropland/grassland/ bare land (Han et al., 2021).

Han et al. (2021) used two main methods used for evaluating the accuracy of DEMs. One method was the comparison between the DEM and ICESat/GLAS points. The other comparison was made between the DEM and 12-m TanDEM-X. In this study, differences were evaluated in terms of not only geographic features, but also how DEMs were created. The quality assessment results indicated that the TanDEM-X had a better performance compared to the SRTM and ASTER DEM. The ASTER DEM had the worst performance results (Han et al., 2021). As the slope increases, the quality of these DEMs decreases. The slope has the greatest impact on the vertical quality of ASTER GDEM followed by the SRTM. There was no systematic effect of aspect on ASTER GDEM and SRTM. The SRTM and TanDEM-X have lower quality when vegetation covers are denser, since denser vegetation makes it difficult for the InSAR band to penetrate vegetation, which makes it challenging to obtain the true surface elevation land (Han et al., 2021). The TanDEM-X and SRTM have superior accuracy in obtaining elevations in vegetation-covered areas than optical techniques (i.e., ASTER). The land cover has little effect on ASTER GDEM.

A focus of this section was on studies previously conducted on the vertical accuracy of free satellite global digital elevation models. A review of methods for validating DEM vertical accuracy was conducted, along with evaluations of satellite-based DEMs that perform best and worst, as well as evaluations of land cover and topography conditions that affect vertical accuracy. As indicated in the case studies, there are two main methods to evaluate the accuracy of DEMs. A DEM can be compared with more accurate points, such as GPS data and elevation control points, obtained from a large-scale topographic map. One other way to determine the DEM's accuracy is to compare it to higher-accurate DEMs, such as topographic maps, LiDAR DEMs, or other high-accuracy DEMs.

From these case studies it can be drawn that the AW3D30 is the most robust reliable DEM available in comparison to the SRTM (30 m), ASTER (30 m), TanDEM-X (90 m), NASADEM (30 m), and MERIT (90 m). Due to TanDEM-X (30 m) not being accessible to the public for free, no large-scale comparison of its performance with AW3D30 has been conducted yet. In comparison to SRTM (30 m), TanDEM-X (30 m) performs better. The MERIT (90 m) and TanDEM-X (90 m) performs better than the ASTER (30 m), despite their low spatial resolution. The ASTER (30 m) DEM has the highest ambiguities and least performance in comparison to all the implied DEMs. It can also be found that slope is the most significant factor affecting DEM accuracy, while the aspect had no significant effect. Vertical accuracy of DEMs is also affected by changes in land cover. The low penetration capacity of SRTM and TanDEM-X radar signals in dense vegetation and the canopy sensitivity of the optical images used to generate AW3D30 and ASTER GDEM, results in low vertical accuracies in these DEMs.

In these studies, the DEMs were assessed vertically over small areas of not more than 140,000 km^2 with a less spatially distributed ground control network. Therefore, this research will also focus on evaluation of vertical accuracy of the satellite-based DEMs (AW3D30, ASTER (30 m), SRTM (30 m), MERIT (90 m), and TanDEM-X (30 m) on a larger scale (> 500,000 km^2) against a more spatially distributed ground control network. Also, satellite-based DEMs are to be compared with high-accuracy DEM (i.e., LiDAR).

2.2.4 Modelling errors in digital elevation models

Two common techniques for modelling errors in elevation models are discussed in the subsequent sections. They include regression and adaptive terrain dependent methods.

2.2.4.1 Regression

The simplest relationship between the dependent and independent variables is linear. Simple linear regression is used in modelling a relationship between two continuous variables. Usually, the intention is to predict the value of an output variable based on an input variable. The general equation for the simple linear regression model is given as follows,

$$y_i = \beta_0 + \beta_1 \chi_i \tag{2.1}$$

where, y_i is the dependent variable, x_i is the explanatory variable and β_0, β_1 are the unknown regression coefficient parameters. The simple regression coefficients β_0 and β_1 can be determined using the Ordinary Least Squares (OLS), which minimizes the sum of squares of residuals v_i, where v_i = $y_i - \hat{y}_i$, and $\hat{y}_i$ is the true /expected/ estimated value of y_i. The multiple regression model refers to how a particular response variable $\boldsymbol{y}$ changes linearly based on several predictor variables. The multiple regression model is given as,

$$y_i = \beta_0 + \beta_1 \chi_{1i} + \beta_2 \chi_{2i} + \ldots\ldots + \beta_n \chi_{ni} + \varepsilon_i \tag{2.2}$$

where, y_i is the dependent variable and x_s are the independent variables, β_s represent the unknown regression coefficient parameters, and ε_i represent the residuals of the observation i . The multiple regression model coefficients can be determined using several techniques, and the most used technique to solve for the parameters is the OLS method, which minimizes the sum of the squares of the residuals. The robust least square is an alternative method as it reduces the influence of outliers.

Several authors have used regression for modelling errors in DEMs in various parts of the world. We only include a few such studies that have reported improvement of accuracy of DEMs using repression in various parts of the world. They include the United States of America (Shortridge and Messina, 2011; Su and Guo, 2014; Su et al., 2015), Egypt (ElSayed and Ali, 2016; Ali et al., 2018), China (Tian et al., 2018) and Thailand (Gorokhovich and Voustianiouk, 2006).

The methods by Shortridge and Messina (2011), Gorokhovich and Voustianiouk (2006), Tian et al. (2018), Su and Guo (2014), and Su et al. (2015) demonstrated reliable performances with reference to land cover and terrain types. A multiple regression model using the variables (slope, aspect, landcover/use, and ecoregion) proposed by Shortridge and Messina (2011) explained nearly 60% of the total variation in SRTM (90 m) error and it is believed that the model has a potential of improving the worldwide SRTM data using globally available datasets.

Su and Guo (2014) proposed a multilinear regression model based on three variables (slope, vegetation height, and leaf area index (LAI)) that reduced the SRTM (30 m) DEM's mean error by 89% and the standard deviation by 11%. According to (Su et al., 2015), a multiple linear regression (tree height and canopy from a multisource dataset, slope from SRTM DEM) reduced the SRTM (30 m) mean height difference from 12.15 m to 0.82 m, while the standard deviation decreased by 2 m after the correction was applied.

Gorokhovich and Voustianiouk (2006) observed that there was a strong correlation between elevation errors and geomorphological characteristics (slope and aspect). Results showed that the application of the multiple regression model improved the SRTM (90 m), but for slope values less than 10°, the improvement was insignificant. The application of the multiple regression model showed a significant improvement in areas with slope values of more than 10° (Gorokhovich and Voustianiouk, 2006).

Tian et al. (2018), fitted simple curves on the slope and error distribution data and observed that the correlation coefficients were higher than 0.9, and this was an indicator showing that a simple linear regression model could be used to improve the accuracy of the fused DEM (AW3D30–SRTM (30 m)) in the study. From the results, it was observed that the vertical accuracy of the DEM was improved by 13.6% and 16% in low relief and mountainous areas, respectively (Tian et al., 2018). The polynomial regression methods by ElSayed and Ali (2016), and Ali et al. (2018) demonstrated reliable performances. Ali et al. (2018) Improved the vertical accuracy of the SRTM (30 m), and ASTER (30 m) by nearly 80% and 50 %, respectively. ElSayed and Ali (2016) improved the SRTM DEMs of 90 and 30 m resolutions to be closer to the GPS DEM.

The methods in this section demonstrate reliable performance. The research will therefore test all methods (polynomial regression, linear and multiple linear regression based on the variables (geomorphological factors and semantic information)) on candidate DEMs for fusion and choose the method that performs the best.

2.2.4.2 Adaptive terrain dependent method

The adaptive terrain method was proposed by Zhou et al. (2020) for the correction of the SRTM DEM over mountainous areas. The method considers the errors that are dependent on the local terrain and global error trend, to correct the SRTM DEM over mountainous areas based on the Bayesian Information Criterion and uses the robust estimation method (M- estimator) and OLS method to solve for the coefficients of the model. An adaptive terrain dependent method matrix in formation is given as (Zhou et al., 2020):

$$\Delta \mathrm{H} = \mathrm{B} \cdot \mathrm{X} \tag{2.3}$$

where X and B denotes the model parameters, and model factor vectors, respectively, and ΔH is expressed as,

$$\Delta \mathrm{H} = \begin{bmatrix} 1 & \sin E & \cos\left(90^{\circ} - N\right) & H & S & A & S^2 & SA & A^2 & A^3 & SA^2 & S^2A & A^4 & SA^3 & S^2A^2 \end{bmatrix} \begin{bmatrix} a_0 \\ a_1 \\ \vdots \\ \vdots \\ a_{14} \end{bmatrix} \tag{2.4}$$

where, H, S, A are corresponding DEM elevations, slopes, and aspect to the height differences (ΔH). $a_0, a_1 \cdots \cdots a_{14}$ are the unknown model coefficients to be determined. E and N are geographical longitudes and latitudes, respectively.

A study was conducted in China in Hunan Province in an area called Zhangjiajie to test the method by Zhou et al. (2020). The northern part of the area had flat terrain with an elevation ranging from 118 to 630 m and slopes ranging from 0° to 13°. The southern part of the area had mountains with elevations ranging from 130 to 1452 m and slopes ranging from 0° to 72°. The area was dominated by high land cover/ use. The results from the study indicated a 20% improvement in the accuracy of the SRTM DEM (Zhou et al., 2020). The method has been shown to deliver reliable results. As a result, the method will be tested on candidate DEMs for fusion, and if it improves them, it will be adopted.

2.3 Fusion of digital elevation models

In this section, different methods, and summaries of different published literature on the development of accurate digital elevation models using different fusion techniques are presented. Due to a lack of accurate continuous reference DEM and the lack of computing capacity required to implement advanced fusion techniques over large areas, this research adopted the simple fusion techniques (Weighted averaging, Linear combination fusion, and Averaging fusion) after weighing the minimal gains in accuracy between simple and advanced fusion methods. In the first three sections, an overview of these methods used in the analysis to fuse the candidate DEMs is provided.

2.3.1 Weighted averaging fusion

The weighted averaging fusion algorithm is the most frequently used approach and is given as (Tran et al., 2014; Mohamed and Saleh 2018):

$$DEM\ \ fusion = \frac{\sum_{i=1}^{n} \omega_i X_i}{\sum_{i=1}^{n} \omega_i} \tag{2.5}$$

where, n is the number of datasets (DEMs), X_i represents data values to be averaged, and w_i are non-negative weights applied to X_i. Data with high weights always contribute more to the weighted average than to low weights. Weights for weighted averaging DEM fusion are usually derived from the discrepancies between the investigated DEMs and the reference data. A challenge arises when the reference data is not available or only covers a small area. In most cases, the error maps from satellite-based DEMs are unavailable (Papasaika et al., 2011).

Tran et al. (2014) fused free DEMs (3-arc second SRTM and 1-arc second ASTER) using the weighted averaging technique. The study area was in the city of Danang, which is in Middle Central Vietnam. The study area was about 950 km^2 and had a height ranging from 0 to 1664 m. The area has a varying topography that ranged from flat to mountainous. After fusion, the DEM was then filtered to reduce mismatches and noisy data. The final fused DEM accuracy improved from 14.9 m RMSE in ASTER and 14.8 m RMSE in SRTM to 11.6 m RMSE in fused DEM from ASTER and SRTM (Tran et al., 2014).

Bagheri et al. (2018) proposed a weighted averaging technique for DEM fusion. Weights used in the techniques were derived from weight maps which are generated by a specially trained artificial neural network (ANN). The technique was tested between the TanDEM-X and the Cartosat-1 DEM over urban areas. The test sites were in Munich, Bavaria, which is covered by LiDAR data used as a reference to assess the technique.

According to Bagheri et al. (2018), the result from the test indicated that the proposed fusion strategy can significantly improve the DEM quality. Over industrial areas, TanDEM-X, Cartosat-1, and weighted fused DEM had RMSE of 5.11, 3.56, and 3.46 m, respectively, over the inner city, 8.41 m, 8.13 m, and 7.75 m over high buildings, 2.61, 2.45, and 2.33 m in residential areas, 4.82, 4.65, and 4.18 m over forested areas, and 0.84, 0.81, and 0.68 m over agricultural areas.

Mohamed and Saleh (2018) fused (ASTER and SRTM) using weighted averaging. The weights were derived from the DEM height errors. The study was conducted over an area located in Egypt. The area was located along the Nile River as a part of Banisuif, Elfayoum, and Giza governorates and had an area of about 81 x 54 km. The RMSE for SRTM, ASTER, and weighted fused DEM were ±6.94, ±7.97, and ±6.71 m, respectively (Mohamed and Saleh, 2018).

Roth et al. (2002) fused digital elevation models from different sources using the weighted averaging technique with fusion weights derived from height error maps. The technique was applied in a study conducted in the southwest of Germany. The site covered about 110 km x 140 km of the Black Forest and the southern Rhine Valley with, elevation ranging from 140 to 1500 m. The dataset used included the SRTM/X-SAR, MOMS-2P, and the ERS tandem. According to Roth et al. (2002), after mosaicking and applying the fusion technique, the resulting DEM showed a quality improvement.

Reinartz et al. (2005) fused SPOT-5 HRS, and DEM derived from C-band and X-band radar data acquired during the SRTM mission using the weighted averaging technique. A test was conducted in two areas. The first test site was in the south-eastern part of Bavaria and had an area of about 40 x 50 km, with an elevation ranging from 400 to 2000 m. The second site was in Catalonia (Spain) and had an area of about 60 km x 60 km.

According to Reinartz et al. (2005), the fusion technique of the three DEM (C-band=C, X-band=X, SPOT-5=5) leads to fused DEMs (CX, C5, X5, CX5) of higher accuracies. The C-band, X-band, Spot5, CX, C5, X5, CX5, had standard deviations of 9.8, 5.6, 5.1, 6.5, 5.3, 4.8, and 4.9 m, respectively over the fields. In the suburbs of Barcelona, the C-band, X-band, Spot5, CX, C5, X5, CX5, had standard deviations of 2.8, 4.3, 3.3, 3.3, 2.6, 3.2, and 3.0 m, respectively. Over forest areas, the C-band, X-band, Spot5, CX, C5, X5, CX5, had standard deviations of 12.3, 10.5, 8.9, 10.1, 8.4, 8.8, and 8.6 m, respectively.

2.3.2 Linear combination fusion

The linear combination fusion method estimates optimum weights using the variance and correlation of errors for sites that have reference data (Pham et al., 2018). These weights are then regionalized by relating them to the topographic slope. This method has been widely used in other studies to improve the accuracy of climatic and hydrologic forecasts such as sea surface temperature, precipitation, soil moisture, and rainfall-runoff models (Pham et al., 2018). The original DEMs in this method are first normalized before being used in the derivation of fusion weights using the equation (2.6), so that the resulting weight values are between 0 and 1.

$$Z_{normalised} = \left(Z_{original} - \overline{Z_{original}}\right) \times \frac{std\left(Z_{ref}\right)}{std\left(Z_{original}\right)} + \overline{Z_{ref}} \tag{2.6}$$

where, $Z_{normalised}$, $Z_{original}$, $\overline{Z_{original}}$, and $std(Z_{original})$ are the normalised, original, mean, and standard deviation of the DEMs, respectively. $std(Z_{ref})$ and $\overline{Z_{ref}}$ are the standard deviation and mean of the reference data, respectively (Pham et al., 2018). The method for determining weights by

Bates and Granger (1969) is used to derive weights for DEM fusion using the variance and correlation of errors for sites that have reference data. The aim of the method is to produce a combined forecast with low errors.

Bates and Granger (1969) assumed that performance of the individual forecasts would be consistent over time in the sense that the variance of errors could be expressed as follows: by σ_1^2 and σ_2^2 for all values of time, t. Additionally, both forecasts were assumed to be unbiased (either naturally or after correction). The combined forecast would be obtained by a linear combination of the two sets of forecasts, with k being the weight of the first set and $(1-k)$ being the weight of the second, so that the combined forecast would be unbiased (Bates and Granger, 1969). As a result of the combined forecast, σ_c^2, the variance can be expressed as follows:

$$\sigma_c^2 = k^2\sigma_1^2 + (1-k)^2\sigma_2^2 + 2\rho k\sigma_1(1-k)\sigma_2, \tag{2.7}$$

where ρ is the correlation coefficient between the errors in the first set of forecasts and the errors in the second set and k is the proportionate weight given to the first set of forecasts. The choice of k should be made so that the errors of the combined forecast are small; in particular, aiming to minimize the overall variance, σ_c^2. Differentiating with respect to k, and equating to zero, we get the minimum of σ_c^2 occurring when:

$$k = \frac{\sigma_2^2 - \rho\sigma_1\sigma_2}{\sigma_1^2 + \sigma_2^2 - 2\rho\sigma_1\sigma_2} \tag{2.8}$$

The linear combination fusion is expressed as follows,

$$DEM\ \ fusion = kZ_{DEM1} + (1-k)Z_{DEM2} \tag{2.9}$$

where, k is the optimum weight and Z_{DEM} are elevations from the DEMs.

Pham et al. (2018) applied the linear combination technique to fuse SRTM and ASTER DEMs. The research was conducted in two studies and two test sites. The first study site was in Western Washington at Mount Rainier National Park. The area was characterized by a mountainous landscape. The test site was located at the Valles Caldera National Preserve in New Mexico State. The area was also characterized by a mountainous landscape. The second study site was in Benton County in northwest Indiana and contained a flat landscape with major land use/cover being agricultural. The second test site was in Whitley County in northeast Indian and has mostly cropland use. The results indicated that combined DEMs demonstrate a 47% and 20% reduction in mean bias over a mountainous site, and 16% and 58% at a low-relief site when compared to SRTM and ASTER GDEM, respectively (Pham et al., 2018).

2.3.3 Averaging fusion

In this method, equal weights are used in fusing the DEM's. The fusion formula is given as,

$$DEM\ \ fusion = \frac{\sum_{i=1}^{n} X_i}{n} \tag{2.10}$$

where, n, and X_i are the number of items, and data values to be averaged, respectively. Mohamed and Saleh (2018) fused ASTER and SRTM using the averaging technique. The RMSE for SRTM, ASTER, and averaging fused DEM were ±7.04, ±12.65, and ±8.80 m, respectively. These results indicated that the fusion enhanced the ASTER accuracy but not the SRTM.

2.3.4 Sparse representation fusion

According to the physiological characteristics of the human visual system, sparse representation describes the natural sparsity of signals. A sparse representation method is a transformation-based approach that is widely used to classify, super-resolve, identify, extract characteristics, deblur, analyse, and combine multimodal images (Li et al., 2018). This method was first implemented in image fusion by Yang and Li (2010).

The fusion using the sparse representation technique with the support of weight maps was applied by Papasaika et al. (2011) to three DEMs (30 m SPOT1 Reference 3D DEM, 15 m ALOS/PALSAR2 DEM, and 25 m ERS3 DEM) at a test site located at Thun, Switzerland. The area was characterized by different morphology and land cover. The results from an assessment performed against 2 m LiDAR reference DEM to validate the accuracy of the initial and fused DEM showed that the RMSE for ALOS, SPOT, ERS, fused DEM(ALOS-SPOT), fused DEM(ERS-SPOT), and fused DEM(ALOS-ERS), were 19.4, 15.5, 10.7, 11.0, 9.7, and 10.9 m, respectively (Papasaika et al., 2011).

2.3.5 Frequency domain fusion

The frequency domain fusion technique uses the Fast Fourier Transform (FFT) to convert the input DEMs into a spatial frequency domain, as described in Honikel (1998). The low-pass and high-pass filters are then applied to remove the erroneous frequency components, then after the filtering process, the DEM spectra are summed, and the inverse FFT is applied to convert the fused DEM back into a spatial domain. The filtering operation is given as (Karkee et al., 2008):

$$F_{1p}(p,q) = F(p,q)H_{1p}(p,q) \tag{2.11}$$

where p, q are the frequency domain indices, $F_{1P}(p,q)$ is the resulting filtered DEM 2D spectrum, $F(p,q)$ is the original stereo optical DEM 2D spectrum, and $H_{1P}(p,q)$ is a filter (either low or high pass).

Karkee et al. (2008) used the frequency domain fusion technique to improve the quality of ASTER and SRTM. The research was conducted at about 25 km east of Kathmandu in the central region of Nepal,

which has an area of about 60 km^2. The area consisted of plains, valleys, and uneven, rocky hilly regions. A contour map was used to produce a reference DEM and the assessment results showed that the RMSE for SRTM, ASTER, and fused DEM, were 18.3, 28.3, and 16.4 m, respectively (Karkee et al., 2008).

2.3.6 Multi scale fusion

In the Multi scale fusion, a Wavelet Transform (WT), bidimensional empirical mode decomposition (BEMD), and nonlinear adaptive multiscale decomposition (N-AMD) analysis methods are applied to the DEMs to decompose them into n-level frequency domains. A fusion rule is then developed based on the analysis of the decomposition (Tian et al., 2018).

The wavelet transform is a multi-resolution time-frequency analysis method. In the low-frequency section, this method has a high-frequency resolution, and in the high-frequency section, it has a high time resolution. The empirical mode decomposition is a novel time-frequency analysis method that was proposed by Huang et al. (1998). In this technique, there is no Fourier transform involved and it can be used for nonlinear, nonstationary signal linearization and smooth processing. The Nonlinear adaptive multi-scale decomposition is a recent nonlinear adaptive multi-scale decomposition method. The method can determine any trend signal without prior knowledge and can reduce the noise of time series data more effectively than the linear filters, wavelet shrinkage, and chaos-based noise reduction scheme (Tian et al., 2018).

Tian et al. (2018) applied the multi-scale fusion technique to the 1-arc-second SRTM and AW3D30. The research was conducted in two study areas. The first study area was in the City of Chuxiong, Yunnan Province in Southwestern China. The area is mountainous and has complex terrain. The flora in the area is mainly perennial trees. The second study area was in Xilinhot, in the Inner Mongolia Province of Northern China. It has a gently undulating surface with a landscape that is mostly grassland. The resulting fused DEM was compared against the ICESat, used as the reference ground elevation. The RMSE of the newly created DEM from multi-scale fusion improved by 29,6% and 19.3% over the mountainous area, and by 27.4% and 15.5% over a low-relief region compared to the 1-arc-second SRTM and AW3D30, respectively (Tian et al., 2018).

2.3.7 Active surface fusion

Active surface fusion is a generalization of snakes or active contours developed by Kass et al. (1988). In this technique, the less accurate (active surface) is adjusted towards the most accurate (reference surface). As the active surface approaches the reference surface, it is constrained by rigidity terms. The shape of the surface is determined by internal forces that constrain it to be piecewise smooth and external forces that drive it to coincide with geomorphological features throughout the reference surface (Kass et al., 1988).

A 4m grid IKONOS-based DEM and 2 m regular spacing LiDAR-based DEM were fused using the active surface technique in a study conducted in Switzerland around the town of Thun (Papasaika et al., 2009). The area is made up of smooth hilly regions, steep mountains, and flat areas with elevations ranging from 530 to 2190 m. It was observed from the results that the fusion methodology can improve initial input DEM accuracy, especially in cases of building updates, and enhancement of hedges. Papasaika et al. (2009) revealed that the availability of land cover maps on areas that show

inconsistent accuracies can help in understanding the characteristics of the area and derive DEM quality measures.

2.3.8 Ordinary cokriging fusion

The concept of cokriging can be considered as an interpolation of points. A point map is an input into the function, and a raster map is returned, along with estimations and optional error maps (Johnston et al., 2004). The technique is a multivariate variant of the ordinary Kriging operation: It calculates estimates for a poorly sampled variable from a well-sampled variable. According to Johnston et al. (2004), ordinary cokriging can be expressed as,

$$Z_1(s) = \mu_1(s) + \varepsilon_1(s) Z_2(s) = \mu_2(s) + \varepsilon_2(s) \quad (2.12)$$

where $Z_1(s)$ and $Z_2(s)$ are the input variables, decomposed into deterministic trends $\mu_1(s)$ and $\mu_2(s)$ having random autocorrelated errors as $\varepsilon_1(s)$ and $\varepsilon_2(s)$. There would be autocorrelation for each of them and cross-correlation between them.

Setiyoko et al. (2019) applied cokriging fusion technique to height point data extracted from Cartosat-1 stereo imagery and GPS data measurement in a hilly area covered by plantations. It was also applied to height point data extracted from ALOS PRISM stereo imagery and topographic map in a flat area covered by plantations with elevation ranging from 700.26 to 717.86 m. Results from the experiment indicated that the interpolation error could be reduced by the ordinary cokriging fusion process (Setiyoko et al., 2019).

2.3.9 Modified k-means clustering fusion

The main objective of the modified k-means clustering technique is to fuse DEMs without any initial knowledge of the errors in the DEMs. The technique is made up of (1) slope and elevation thresholding, (2) k-means clustering and (3) adaptive mean and Gaussian filtering (Fuss et al., 2016).

The slope thresholding process removes attributes of DEM surfaces that are different from other DEM surfaces in the same location. Elevation thresholding removes elevations that are different from other elevations in the same location. The k- means clustering isolates groups of elevation that are similar. Adaptive mean filters compare the mean and standard deviation of neighbouring cells with the centre value based on a moving window. If the value in the center of the window is greater than the calculated threshold value, the centre value is replaced by the mean of the neighbouring values (Fuss et al., 2016). Gaussian filtering smooths the DEM and reduces the short-scale variance that resulted from k-means clustering.

Fuss et al. (2016) tested the modified k-means clustering technique using 12 DEMs from Synthetic Aperture Radar (SAR) imagery in Southern Ontario, Canada, Northwest of the city of Guelph. The site had an area of 316 km^2, elevation ranges from 310 to 443 m above mean sea level with a post-glacial landscape that is mostly moderately sloping with some hillocky topography present. According to Fuss et al. (2016), the final DEM product from the fusion was more accurate and precise than a simple averaging of DEMs. The fusion step that included slope and elevation thresholding was effective in increasing the accuracy and precision of the final DEM product. The overall accuracy of the final DEM product was also impacted by the k-means clustering of the elevations as this reduced the precision

of the estimates, but the erroneous elevation estimates were removed in the final step of the fusion using the adaptive mean and Gaussian filtering (Fuss et al., 2016).

2.3.10 Self-consistency fusion

The self-consistency fusion detects and removes errors from the tiles, then produces a low noise fused DEM by averaging the different clean tile elevations. The method is based on the expectation that reversing the reference and target images will produce similar (or self-consistent) results when the image matching algorithm finds the correct match, and if the algorithm fails, different results will be produced (Schultz et al., 2002).

Schultz et al. (2002) tested self-consistency fusion on two data sets. The first dataset was a set of four high elevation images covering the same area captured over a desert environment, and the second dataset was a set of photo-realistic simulated images generated from a known DEM and ortho-image. The results from the fusion showed that the method can generate a fused DEM that is almost 'error-free' (Schultz et al., 2002).

2.4 Digital elevation models in South Africa

In this section several types of popular DEMs in South Africa are presented together with related challenges or problems.

2.4.1 Ground based digital elevation models and other elevation sources in South Africa

CD: NGI 25 m DEM: This DEM is generated from a stereo pair of photogrammetric images or from contour data sets at 25 m resolution and is accurate to 3 m at 95% confidence level and covers approximately 66% of the area of South Africa (Verhulp, 2015).

GISCOE 20 m DEM: GISCOE was previously known as GIMS. In 2000 they created a 20 m DEM based on contours, spot heights, and trigonometrical beacons digitized from the 1:50 000 map series. No accuracy statement is available for the product (Verhulp, 2015).

DEMSA: The digital elevation model of South Africa (DEMSA) was generated from 0.5 m resolution stereo aerial or satellite imagery and has a resolution of approximately 2 m. The product is available as a Digital Surface Model (DSM) and as a Digital Terrain Model (DTM). The DEM has a mean vertical error of 35 cm and is available for the whole of South Africa at a cost, depending on the size and product level (van Niekerk, 2021). There is not much information about the validation data for this DEM.

CD: NGI contours and spot heights: The contours (20 m vertical interval) and spot heights depicted on the 1:50 000 South African topographical maps are primary sources of elevation data in South Africa. These sources of elevation data were digitized by the Chief Directorate: National Geospatial Information (CD: NGI) and are available for use by the public for free. The contours are accurate to 11 m at a 95% confidence level (Verhulp, 2015). CD: NGI also provides free 1:10 000 contours and spot heights to the public that are derived from 1:10 000 orthophoto maps, and no accuracy statement is available for these products.

2.4.2 Fused digital elevation models in South Africa

SUDEM: The Stellenbosch University Digital Elevation Model (SUDEM) is a 5 m resolution DEM created by combining multiple sources of elevation data, namely large scale (1:10 000 and 1:50 000) contours and spot heights, and 1-arc-second SRTM. The SUDEM has three product levels, at levels 1 and 2, the resolution is 5 m, with an RMSE of 10.1 and 10.2 m, respectively. An estimated absolute accuracy of less than 1 m is achieved using the Level 3 DSM (van Niekerk, 2015). The level 1 SUDEM product was utilised in filling up any voids present in the SRTM, after which the two DEMs were fused using a patented weighting scheme that favours the SRTM in areas where contour and spot heights densities are low (van Niekerk, 2021). The SUDEM is assessed using high accurate surveyed reference points obtained from the City of Cape Town (van Niekerk, 2015). The SUDEM is available at a cost and has a vertical accuracy of 2 to 15 m depending on the area (van Niekerk, 2021).

SANSA 20 m DEM: Originally acquired through ComputaMaps in 2000, the DEM is primarily used as a reference for automated image processing (orthorectification) and hydrological modeling, as well as DEM derivatives. Interpolated from contour vector lines and spot heights of 1:50 000 (20 m) and patched using SRTM (90 m). Limitations such as a wide range of artifacts caused by incorrectly assigned contour heights, and the elevation accuracy is unknown (Verhulp, 2015).

2.5 Problems with existing digital elevation models over South Africa

The CD: NGI free contours and spot heights provide valuable information about elevation over South Africa. However, contours are not ideal for interpolating DEMs because their densities are affected by slope gradients. Low-relief areas are particularly problematic because contours are often spaced far apart (horizontally), reducing the efficiency of interpolation. Contour DEMs can be improved by incorporating the spot heights in the interpolation process. However, the product is still insufficient to represent subtle changes in terrain. The CD: NGI free 25 m resolution DEM does not provide the full coverage of the country, and from a preliminary assessment and analysis conducted, some tiles contain pixels with incorrect or abnormally high or low height information. Access to products such as LiDAR data, SUDEM, and various large-scale DEMs that were generated for specific projects is restricted as these are available to the public at high costs.

On the other hand, the satellite-based DEMs over South Africa provide an accurate surface replication but are associated with errors such as speckle noise, strip noise, and vegetation error, limiting their applications (Yamazaki et al., 2017). Some of the satellite-based DEMs contain voids and abnormally high or low height information, relatively low resolution (30m or less) and poor quality, which make them unsuitable for some applications (e.g., flood modelling, geomorphometry, civil engineering) (van Niekerk, 2015). High-resolution and quality satellite-based DEMs are also available to the public at high costs.

Due to the less accuracy and limited coverage of South African free local DEMs and the high cost of accurate DEMs, this project will provide the public with the ability to access an accurate DEM at no cost, reflecting current topography and land cover for the entire country.

2.6 Chapter conclusion

Different high-resolution global DEMs described above include SRTM, ASTER, AW3D30, TanDEM-X, and MERIT. The case studies indicate that AW3D30 is the most reliable DEM available in comparison to the SRTM (30 m), ASTER (30 m), TanDEM-X (90 m), NASADEM (30 m), and MERIT (90 m). Due to TanDEM-X (30 m) not being accessible to the public for free, no large-scale comparison of its performance with AW3D30 has been conducted yet. In comparison to SRTM (30 m), TanDEM-X (30 m) performs better. The ASTER (30 m) DEM shows the worst performance compared to all the free high-resolution DEM's. It was found that slope was the most significant factor affecting DEM accuracy, while aspect had no significant effect. Change in land cover also affects the vertical accuracy of DEMs.

In the studies, DEM accuracy is evaluated using two methods. One method is to compare the DEM with more accurate points (point-based), such as GPS data and elevation controls collected from large-scale topographic maps. The other way to compare the DEM is by comparing it with higher-accuracy DEMs (surface-based), such as large-scale topographic maps, LiDAR DEMs, and other high-accuracy DEMs. The regressions (linear and multiple linear), and adaptive terrain-dependent methods have been shown to deliver reliable results. There are various fusion techniques described, including sparse representation, weighted averaging, linear combination, frequency domain, multi-scale, active surface, ordinary cokriging, modified k-means clustering, and self-consistency averaging of DEMs. According to Schindler et al. (2011), fusion techniques perform the same way.

Among the different techniques described in section (2.3), the DEM fusion by weighted averaging is the most applied fusion algorithm. To accomplish the fusion, height error maps need to be available for weights derivation (Papasaika et al., 2011; Schindler et al., 2011). Height error maps are provided by DEM providers but in most cases, they are not available. Therefore, data-driven strategies to find weight maps based on geomorphological characteristics are used (Papasaika et al., 2011). Weights can also be generated using a specially trained artificial neural network (Bagheri et al., 2018). There are several DEMs and other elevation sources in South Africa, including CD: NGI 25 m DEM, GISCOE 20 m DEM, DEMSA, SUDEM, SANSA 20 m DEM, NGI contours, and spot heights. A lot of inconsistencies exist in the publicly available DEMs, including missing pixels. Obtaining local DEMs with full national coverage and reducing anomalies in satellite-based DEMs can be costly.

This study aims at developing an optimal digital elevation model over South Africa by using freely available satellite-based DEMs with high resolution and ground levelling data. In the literature, the DEMs were assessed vertically over small areas with a less spatially distributed ground control network. This research will therefore evaluate vertical accuracy of the satellite-based DEMs implied on a larger scale against a more spatially distributed ground control network. Also, satellite-based DEMs will be compared with high-accuracy DEM (i.e., LiDAR). Candidate DEMs from the assessment that show results of being most reliable will be modelled using all the correction models described above, then fused using the fusion methods (weighed averaging fusion, linear combinations, and simple averaging). The modelling and fusion algorithms will be implemented using MATLAB, ESRI ARC/GIS, GRASS, and EViews software.

Chapter Three: EMPIRICAL INVESTIGATIONS FOR DEVELOPMENT OF ACCURATE DIGITAL ELEVATION MODEL FROM GROUND AND SATELLITE DATA OVER SOUTH AFRICA

3.1 Preparation of satellite-based digital elevation models over South Africa

This section shows the methodology of how the datasets are acquired and processed to achieve the objectives. The research is divided into four phases: preparation of satellite-based DEMs, assessment of the satellite-based DEMs, selection of DEMs for fusion and error modelling, and DEM fusion over South Africa. Figure 2 shows a flowchart of the processes towards the development of an accurate digital elevation model from ground and satellite data over South Africa. The first top row indicates the data sources, the second row indicates the data supplied by the sources, followed by data processing flowcharts to achieve different objectives.

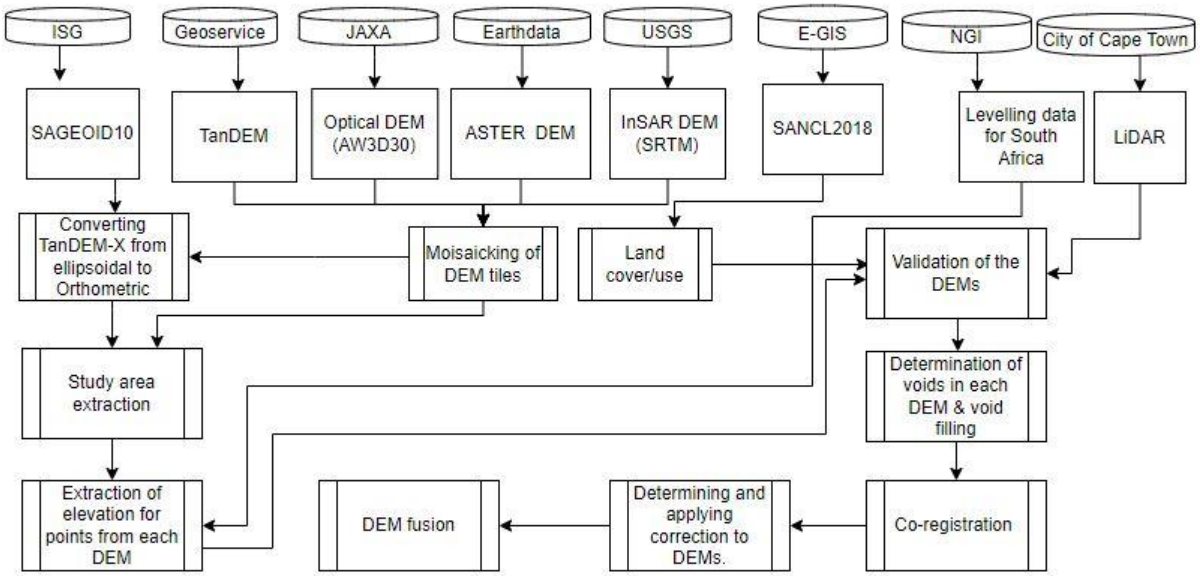

Figure 2: Flowchart for Methodology process

3.1.1 Introduction

To prepare the data for processing, all tiles of the DEMs over the whole of South Africa need to be first merged. Uniform horizontal and vertical datums among the DEMs is very critical in understanding the data before doing any further assessment or application. Void presence needs to be checked, and any voids available in the DEMs need to be filled.

3.1.2 Data and methods

Table 1 shows the data prepared, sources, spatial resolution, and accuracy. The ASTER, AW3D30, MERIT, SRTM, and TanDEM-X are satellite-based DEMs. The absolute vertical accuracy specification for the MERIT and AW3D30 is based on the results of tests conducted by different authors. The

absolute vertical accuracy specifications for the SRTM, ASTER, and TanDEM-X are provided by the data producers. However, the relative vertical accuracy specifications are based on the results of tests conducted by different authors.

Table 1: DEM types, sources, spatial resolution, and accuracies

Dataset	Spatial resolution	Source	Vertical Accuracy specifications
SRTM	30 m	USGS (https://www.usgs.gov/)	< ±16 m absolute & < ±6 m relative.
ASTER	30 m	Earthdata(NASA) (https://search.earthdata.nasa.gov/search)	< ±16 m absolute & < ±6 m relative.
AW3D30	30 m	JAXA (https://eorc.jaxa.jp/ALOS/en/aw3d30/data/index.htm)	< ±5 m absolute
TanDEM-X	30 m	Geoservice (https://download.geoservice.dlr.de/TDM90/)	< ±10 m absolute
MERIT	90 m	Yamazakilab (http://hydro.iis.utokyo.ac.jp/~yamadai/MERIT_DEM/)	< ±12 m absolute

In addition, SAGEOID10 was also used for converting ellipsoidal heights to spheroidal orthometric heights. The collected SAGEOID10 is a 2½' x 2½' final hybrid geoid model and covers the whole of South Africa between 22°S and 35°S latitude and 16°E and 33°E longitude. The data is downloaded as an ASCII data file containing 128,017 geoidal height points. The SAGEOID10 model is estimated to have an accuracy of better than 10 cm and was developed using satellite altimetry, global DEM, land-based gravity measurements, the Earth Gravity Model 2008, and GPS/levelling. The data source is the International Service for the Geoid (ISG) (https://www.isgeoid.polimi.it/Geoid/geoid_rep.html).

3.1.2.1 Merging the DEM tiles

Each freely available DEM comes in several raster tiles. Therefore, a mosaic of the raster data tiles is done. Mosaicking of tiles combines all the raster tiles to produce one continuous raster.

3.1.2.2 Unifying horizontal and vertical datums among the DEMs

All the DEMs are collected in a GeoTIFF format in a geographic coordinate system and based on WGS84 ellipsoid for horizontal datum. The AW3D30, SRTM, ASTER, and MERIT heights are orthometric and based on EGM96 as the reference vertical datum, while the TanDEM-X heights are ellipsoidal heights and based on the WGS84. A conversion of TanDEM-X heights from ellipsoidal to spheroidal orthometric is done before further application using height anomaly as follows,

$$H = h - N \tag{3.1}$$

where, H is the spheroidal orthometric height, h is the ellipsoidal height (TanDEM-X heights) and N represents the geoidal heights (in this case SAGEOID10 heights were used). A total of 128,017 geoidal height points from SAGEOID10 are used in interpolating a 30 m resolution raster surface using the inverse distance weighted (IDW) technique.

3.1.2.3 Voids in DEMs

According to Qiu et al. (2019), the voids in DEMs are normally found in rugged topography, and DEMs such as the SRTM, ASTER, and TanDEM-X are affected by many voids. Many spatial analysis processes such as orthorectification, viewshed generation, slope, and aspect generation fail because of voids that are present in some areas of DEMs (Kroenung et al., 2006). Some of the causes of the presence of voids in satellite-based DEMs are topographic shadowing and the complex nature of Interferometric Synthetic Aperture Radar (IFSAR) technology (Kroenung et al., 2006).

Before the DEMs implied can be used for further applications, a check for the void presence needs to be done, and present voids must be filled (Qiu et al., 2019). Locations in DEM with voids contain pixel values with no data. To determine the presence of voids for each satellite-based DEM in this study, a conditional map algebra expression is used in classifying the data into two classes. The expression classifies the raster pixels that have a value into one class and pixels with no data into another class.

Many studies usually propose general interpolation methods to fill the voids in the DEMs, and these interpolation methods include kriging, spline, and inverse distance weighting (IDW). Due to the limitation of interpolation methods, which only use neighboring elevations for filling voids, these methods can sometimes produce less accurate geomorphological features (Qiu et al., 2019). Methods such as Delta Surface Fill, multi-source fusion, and fill and feather can be used to fill large voids (Qiu et al., 2019).

This study uses the Arc GIS Elevation Void Fill function to fill voids using an interpolation method. The function creates pixels in DEMs where holes exist by using the Plane Fitting/ IDW method to fill the voids. The method first calculates the value of the missing pixel by taking the average of the eight neighboring values, then applies the plane fitting method, and if the error of the plane fitting method is too large, an inverse distance weighted (IDW) algorithm is applied.

3.1.3 Results and discussion

The results and discussion based on the merging DEM tiles, voids detected and filled are presented.

3.1.3.1 Merged DEM tiles

The result for merged raster tiles for each satellite-based DEM are shown in Figure 3.

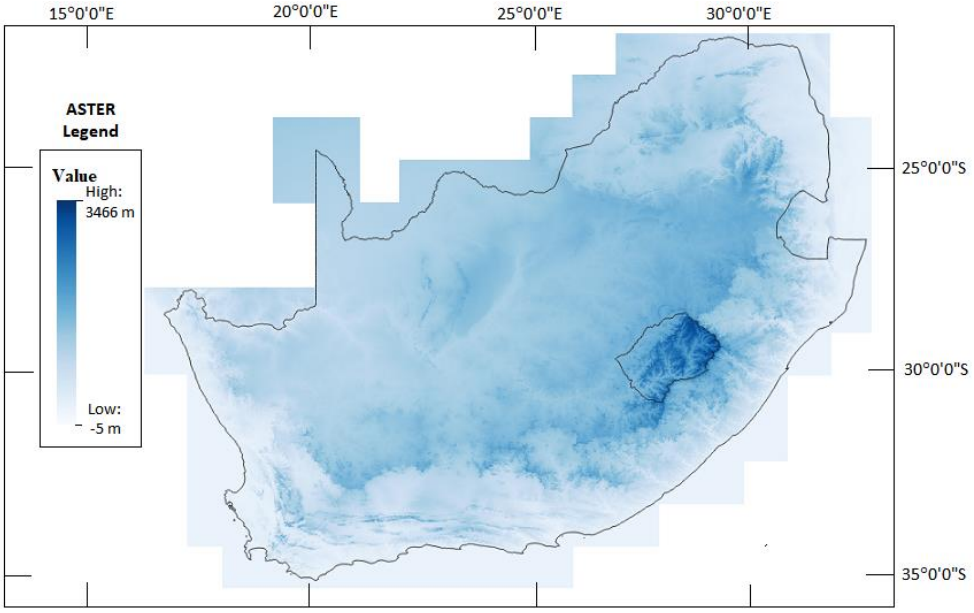

(a) ASTER DEM

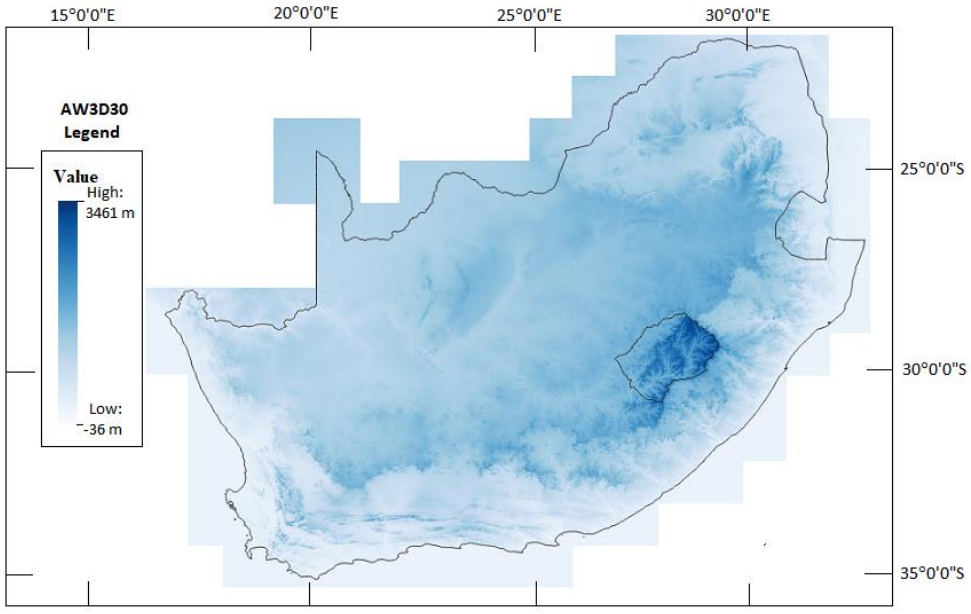

(b) AW3D30 DEM

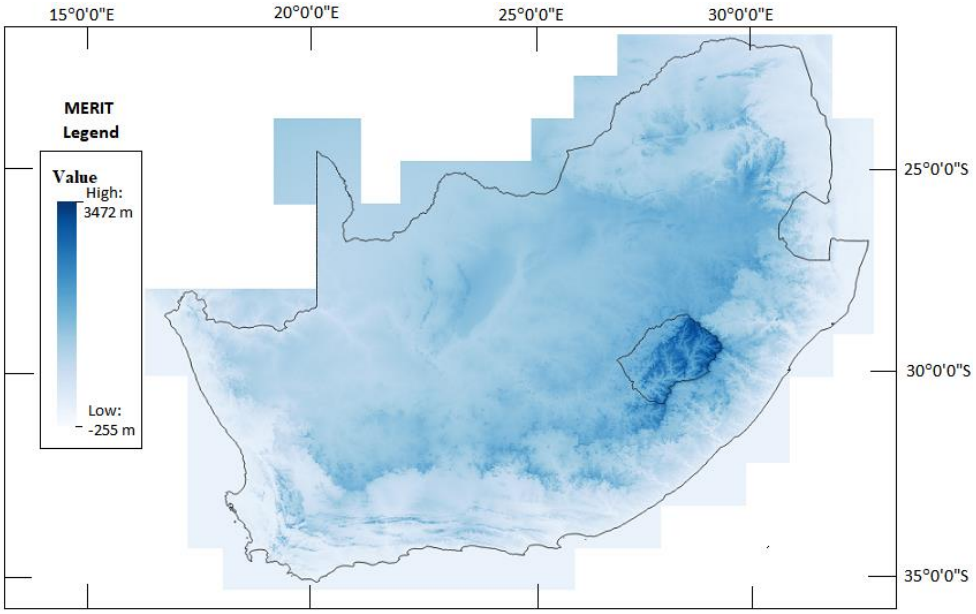

(c) MERIT DEM

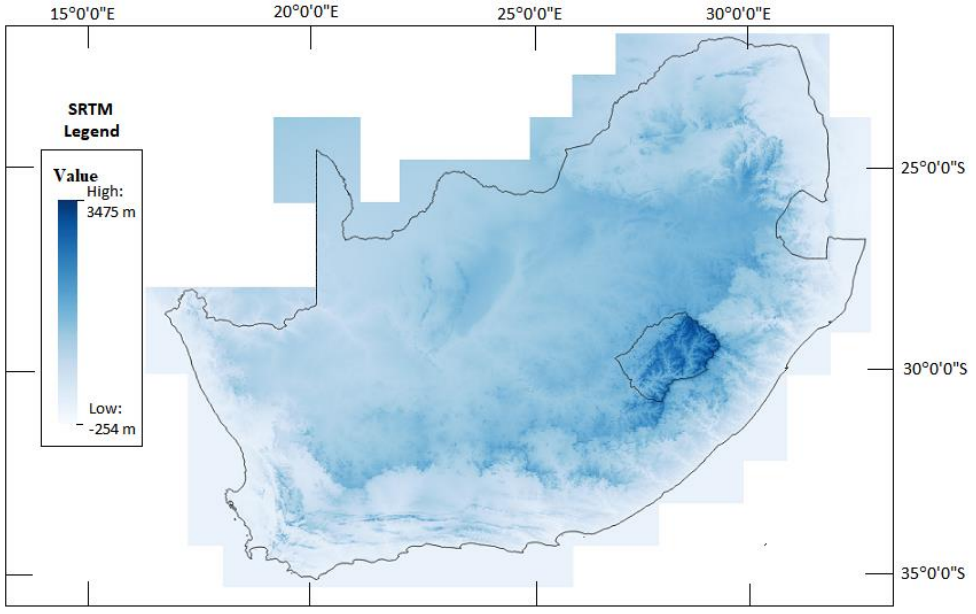

(d) SRTM DEM

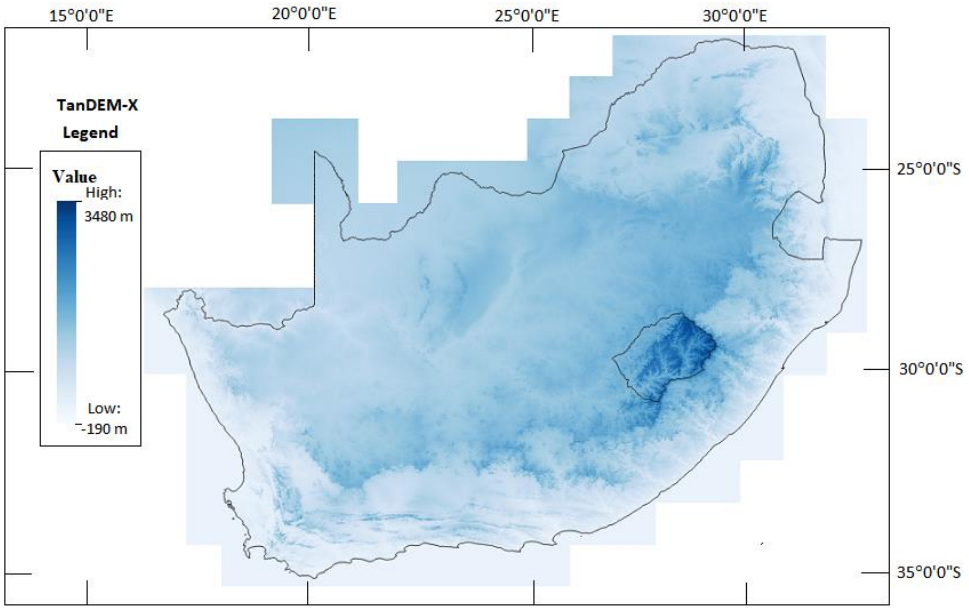

(e) TanDEM-X DEM (after converting ellipsoidal to orthometric heights)

Figure 3: Satellite-based DEMs after merging the raster tiles over South Africa (units are in m)

All the merged satellite-based DEMs provide full coverage of South Africa and fair surface replication. The satellite-based DEMs (ASTER, AW3D30, MERIT, SRTM, and TanDEM-X) have maximum elevation values of 3466, 3461, 3472, 3475, and 3480 m, respectively. The satellite-based DEMs have minimum elevation values of -5, -36, -255, -254, and -190 m, respectively. The negative elevation values are located over mines and waterbodies.

3.1.3.2 DEM voids detected and filled

Over South Africa, the pixels with no data values were found only in the SRTM. There were no voids in the AW3D30, TanDEM-X, MERIT, and ASTER though Qiu et al. (2019) observed that TanDEM-X and ASTER are also usually affected by voids. For the MERIT DEM, no voids were expected as this DEM is produced by removing major error components from existing satellite-based DEMs (SRTM3 v2.1 and AW3D30). SRTM DEM and Hillshade before and after the voids have been filled are shown in Figure 4.

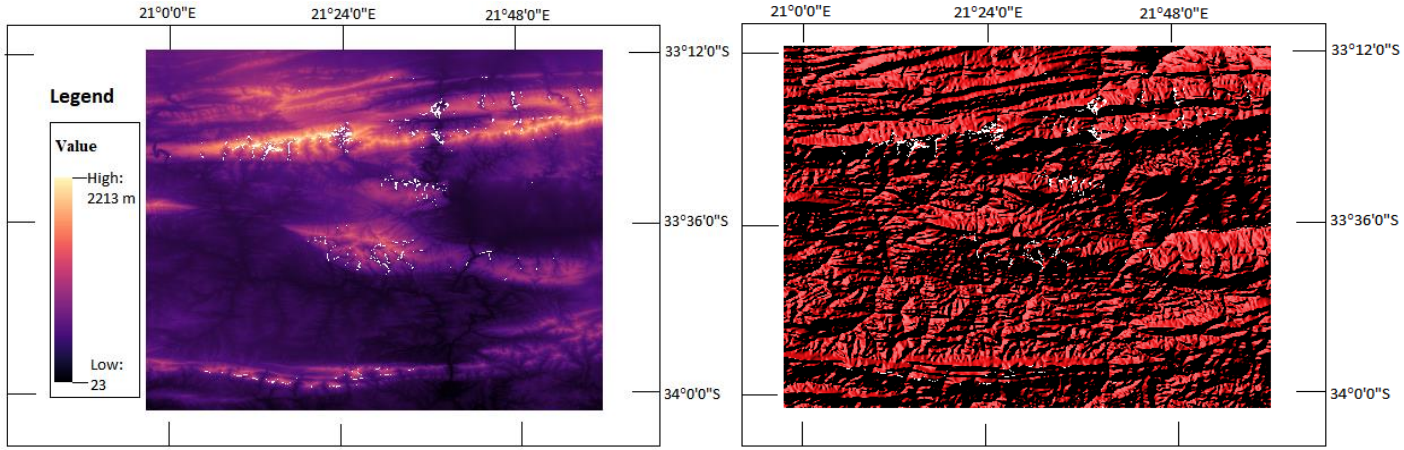

SRTM DEM (left) and Hillshade (right) before void filling

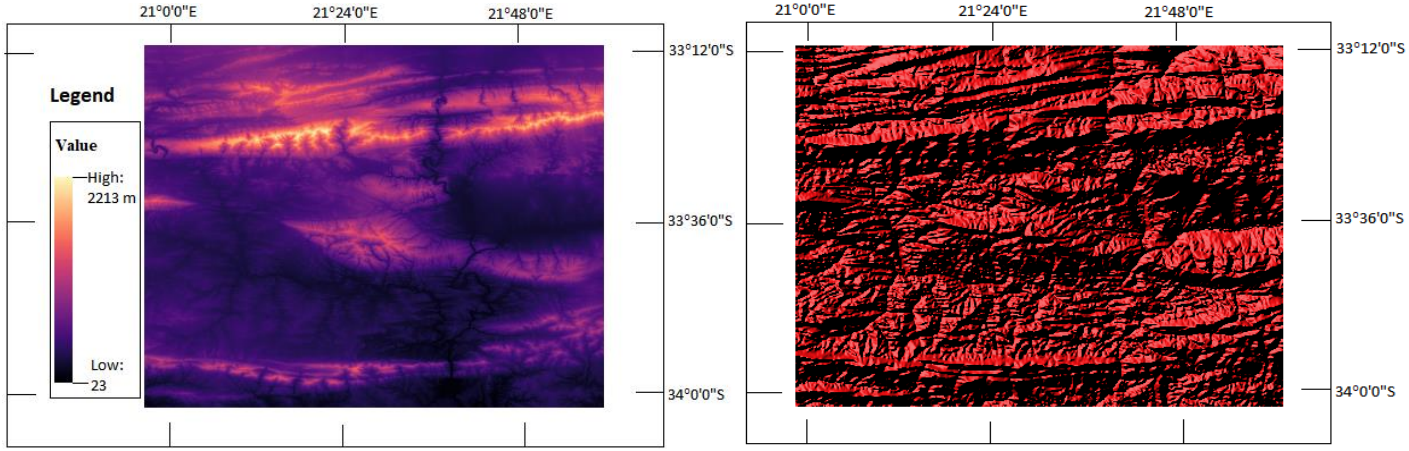

SRTM DEM (left) and Hillshade (right) after void filling

Figure 4: SRTM DEM (left) and Hillshade(right) before and after void filling

All the present voids in the locations identified in the SRTM vary from large to small and are in higher elevations. The maximum and minimum void have an area of approximately 4.3 km^2 and 542.10 m^2, respectively. Because of the size of the voids, other void filling techniques such as multi-source fusion needs to be considered once the assessment of the DEMs has been done. However, in this case, the voids are present in areas where there is no reference data to assess the improvement. The void filling technique has filled all the voids in the SRTM as shown in Figure 4 and the results indicate a fair surface replication.

3.2 Assessment of satellite-based digital elevation models using ground levelling data over South Africa

3.2.1 Introduction

The point-based approach is used in the assessment of the satellite-based DEMs over South Africa. The vertical accuracy of the DEMs is assessed against ground levelling data. This process includes extracting the elevations from DEMs corresponding to the ground levelling data, validating the heights of the DEMs, and studying the Influences of elevation, slope, and land use/cover on height differences.

3.2.2 Data and methods

The datasets used are all the DEMs in Figure 3, the ground levelling (trigonometrical beacon) data described in section (2.1.1) is used as reference. Spatial distribution of the ground levelling is shown in Figure 5. The ground levelling data position (latitude, longitude) were used to extract elevation from the DEMs to facilitate assessment of vertical accuracy. The AW3D30, SRTM, ASTER, TanDEM-X, and MERIT elevations corresponding to a total of 27,350 ground levelling data points were extracted. To do the process, a spatial analysis extraction tool is used to extract multi-raster values to points.

In addition, a SANCL 2018 (South African National Land Cover 2018) is also used in the assessment. The data has a 20 m resolution and covers the full extent of South Africa. The Land Cover dataset is generated from multi-seasonal 20 m resolution Sentinel 2 satellite imagery. The imagery used represents the complete temporal range of accessible imagery attained by Sentinel 2 through the period 01 January 2018 to 31 December 2018. The data is downloaded in a GeoTIFF raster format in geographic coordinate system and in Albers Equal Area projection. The data source is the E-GIS (https://www.environment.gov.za/mapsgraphics).

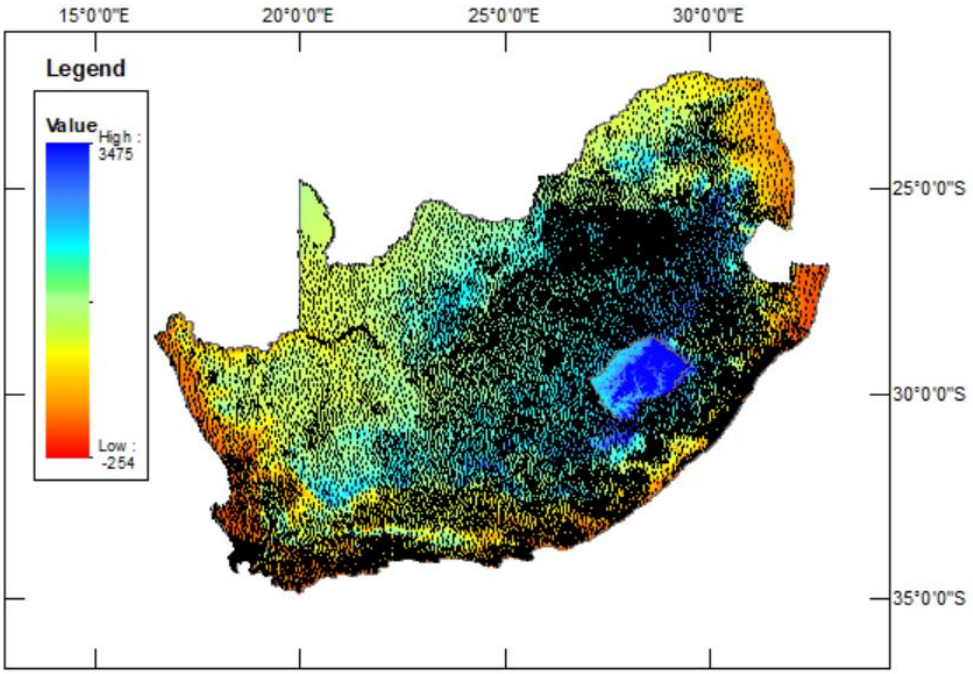

Figure 5: Distribution of ground levelling data points, with black dots representing ground levelling data points

3.2.2.1 Validation of vertical accuracy of the satellite-based DEMs over South Africa

The validation of the vertical accuracy of DEMs over South Africa includes the determination of the absolute differences in heights between the DEMs and ground levelling data and determining the relative differences between the DEMs. Outliers present in height differences are removed for each DEM, and statistical analysis of the height differences is done. The influence that elevation, slope, and land use/cover change have on height differences is assessed. The absolute height differences between the DEMs heights corresponding to 27,350 ground levelling data are determined as follows,

$$\Delta \mathrm{H}_{Trig-DEM} = \mathrm{H}^{Trig} - \mathrm{H}^{DEM} \tag{3.2}$$

where, $\Delta H_{Trig-DEM}$ are differences in heights between trigonometrical beacons and AW3D, SRTM, ASTER, TanDEM-X, and MERIT heights, respectively. H^{Trig} and H^{DEM} represent trigonometrical beacon heights and corresponding extracted heights on the DEMs. A total of 27,350 successfully extracted points from the DEMs were used in evaluating the relative differences in heights between the DEMs, as follows,

$$\Delta \mathrm{H}_{DEM_1-DEM_2} = \mathrm{H}^{DEM_1} - \mathrm{H}^{DEM_2} \tag{3.3}$$

where, $\Delta H_{DEM_1-DEM_2}$ are differences in heights among the AW3D, SRTM, ASTER, TanDEM-X, and MERIT, respectively. H^{DEM_1} and H^{DEM_2} represent DEM heights. The statistical parameters computed include the minimum, maximum, mean, and standard deviation. The statistical parameters are computed for the absolute height difference, and for the relative differences between DEMs. The minimum and maximum values are the lowest and highest values from the 27,350 height differences

dataset. The equations (3.4) and (3.5) below represent the formulas used in the computation of the mean and standard deviation for the height differences, respectively.

$$\overline{\Delta \mathrm{H}_i} = \frac{\sum_{i=0}^{n} \Delta \mathrm{H}_i}{n} \tag{3.4}$$

$$SD = \frac{1}{n-1}\sqrt{\sum_{i=0}^{n}\left(\Delta \mathrm{H}_i - \overline{\Delta \mathrm{H}_i}\right)^2} \tag{3.5}$$

where, ΔH_i, is the height differences between a satellite-based DEM and ground levelling data for point i , n is the number of ground levelling test data points, $\overline{\Delta H_i}$ is the mean of the height differences between a satellite-based DEM and ground levelling data. Outliers are removed using a method as shown in equation (3.6) that focuses on a percentage of differences with respect to orthometric ground levelling data heights (taking > 3% to be outliers). This method is a more thorough approach to identifying outliers because it can identify outliers that cannot be visually identified by plotting data and using common sense. The method also ensures that elevation data in high areas that are normally less accurate on DEMs are not arbitrarily removed, while errors in more accurate elevation data in lower areas are detected and removed.

$$\mathrm{H}_{outlier} \geq \frac{\left|\Delta \mathrm{H}_i\right| \times 100}{\mathrm{H}^{Trig}} \tag{3.6}$$

$$\text{where, } \Delta \mathrm{H}_i = \mathrm{H}^{Trig} - \mathrm{H}^{DEM}$$

Several tests were conducted using different percentages before arriving at 3% for application in this research. The method is applied to each DEM, then the remaining points and outliers are plotted to check spatial variations in the differences for each DEM. Height differences with values corresponding to more than 3% are considered outliers and are removed. The statistical parameters of the height differences of the remaining points are computed for each DEM.

3.2.2.2 Assessment of the influence of elevation, slope, and land use/cover on heights differences

First, the influences of slope and elevation changes on height differences are assessed, then secondly, the influence the change in land use/cover has on height differences and lastly, incorporating the assessment of slope and elevation change over each land use/cover. The slope ***S***, can mathematically be defined as a function of gradients at x and y direction at a given point on a surface $[z = f(x, y)]$ as follows,

$$S(x,y) = \tan^{-1}\sqrt{f_x^2 + f_y^2} \tag{3.7}$$

where, $S(x,y)$ is the slope and f_x and f_y are gradients in $x-$ and $y-$ directions. A geodesic slope raster in degrees is generated for the full extent of South Africa using the SRTM. The slope map is shown in Figure 6, and it was reclassified into ranges with an interval of 10° to get well-defined areas for testing the effect of slope change on the DEM's. The reclassified slope over South Africa using SRTM is shown in Figure 7.

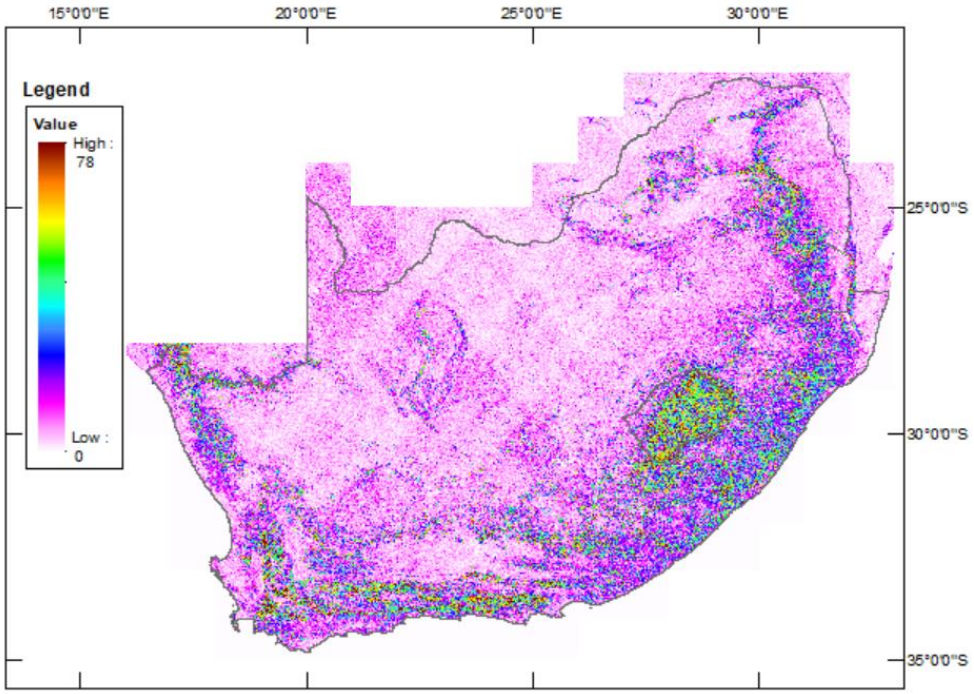

Figure 6: Un-ccategorised slope representation over South Africa based on SRTM data (units are in degrees)

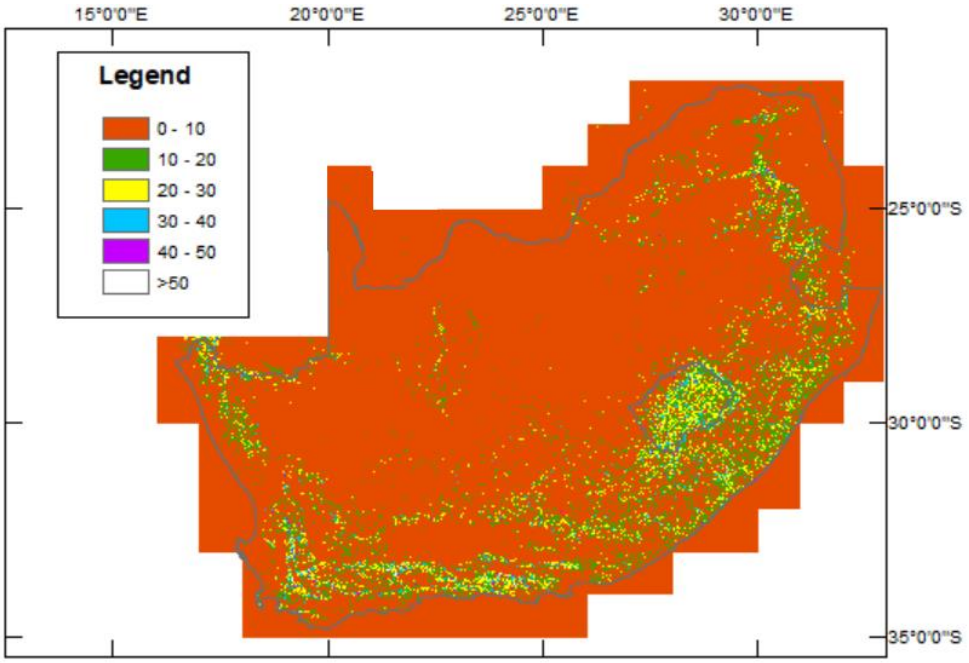

Figure 7: Categorised slope representation over South Africa based on SRTM data (units are in degrees)

Regarding land use/cover, the South African National land use/cover includes 9 features (bare land, grassland, shrub-land, water bodies, wetlands, cultivated land, forestland, built up, and mines & quarries) as is shown in Figure 8. Image reclassification of the 9 classes into 3 classes of land use/cover (low, medium, and high) is done, and the corresponding categorised land use/cover is shown in Figure 9. The low land use/cover is composed of bare land, grassland, shrub-land, water bodies, and wetlands. Medium land use/cover is composed of cultivated land. High land use/cover is composed of forestland and built-up areas.

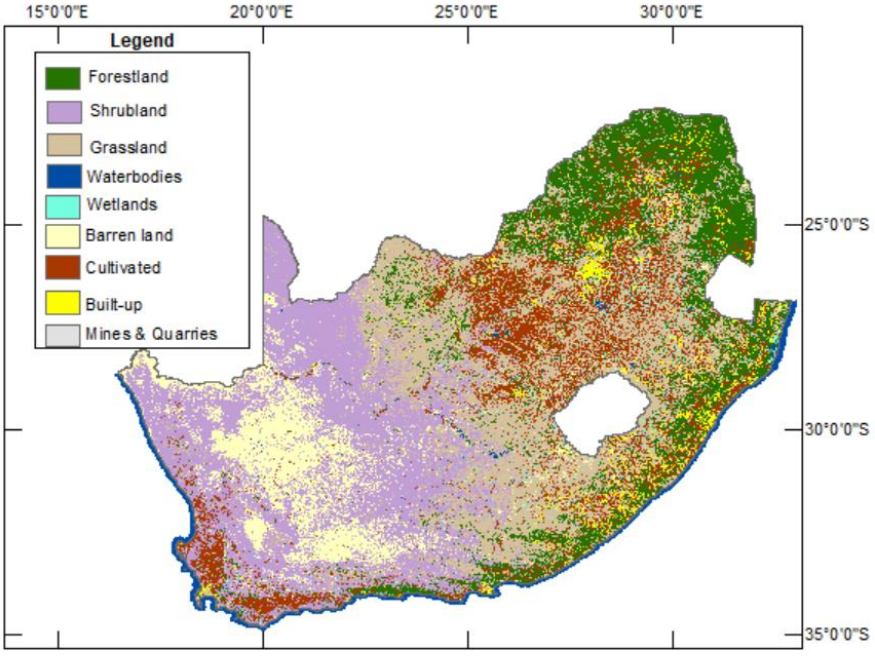

Figure 8: South African National Land use/cover before categorisation

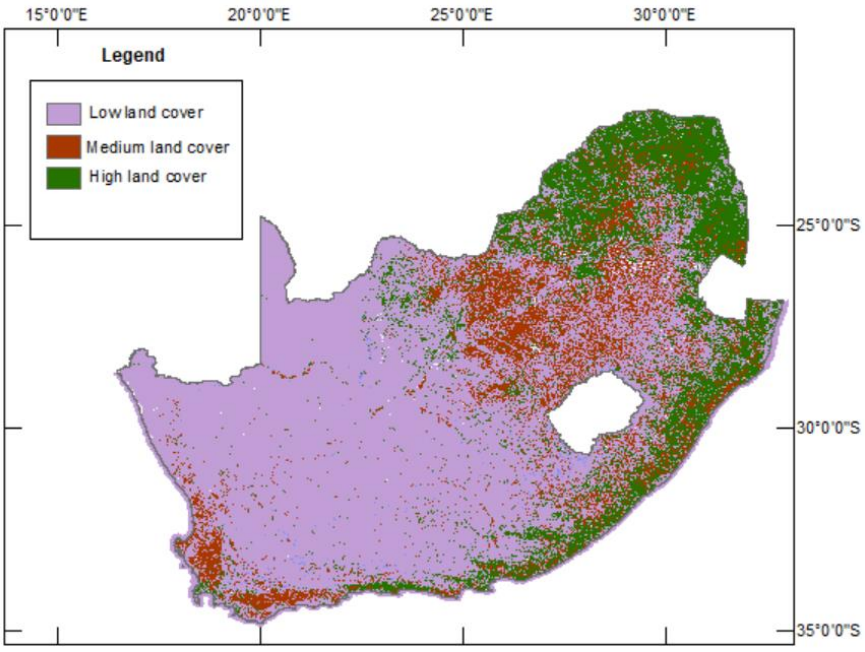

Figure 9: South African National Land use/cover after categorisation

Extracted elevation and slopes corresponding to the ground levelling data are divided into different ranges, and statistical parameters for the height differences in each range are computed to assess the vertical accuracy. To determine the influence of land use/cover on height variation, the land use/cover corresponding to the ground levelling data points is extracted, differences in heights in each land use/cover are determined, and statistical parameters for the height differences are computed. The influence of elevation and slope change on the vertical accuracy of each DEM over each land use/cover is assessed.

Out of 27,350 ground levelling data points before outlier removal, only a total of 27,120 were classified into different land use/cover classes, and 230 levelling data points were unclassified. The unclassified points either fell in the mines & quarries class or were part of an originally unclassified area. A total of 18,962 levelling data points fell in low land use/cover areas, 2678 in medium land use/cover areas, and 5480 in high land use/cover areas.

3.2.3 Results and discussion

The results and discussions of vertical accuracies of the DEMs before and after outliers are removed are first presented, then followed by the influences of elevation, slope, and land use/cover on the vertical accuracy of each DEM.

3.2.3.1 Height differences before removing outliers

Statistical results for the absolute height difference between the DEMs and the ground levelling data before removing outliers are presented in Table 2, while scatter plots of the height differences are given in Figure 10.

Table 2: Absolute height difference between the DEMs and ground levelling

	AW3D30	SRTM	ASTER	TanDEM-X	Merit
N	27350	27350	27350	27350	27350
Min(m)	-987.70	-982.70	-989.70	-990.26	-977.99
Max(m)	243.10	298.00	300.00	400.70	318.36
Mean (m)	3.44	4.69	10.70	5.33	9.30
STDV (±m)	9.52	11.24	12.92	12.85	12.56

In Table 2, the overall height differences between the DEMs (AW3D30, SRTM, ASTER, TanDEM-X, and MERIT) and the ground levelling data have standard deviations of ±9.52, ±11.24, ±12.92, ±12.85, and ±12.56 m, respectively with mean values of 3.44, 4.69, 10.70, 5.33, and 9.30 m. The statistical parameters indicate that the AW3D30 achieves better absolute vertical accuracy compared to all other DEMs, followed by the SRTM, MERIT, TanDEM-X, and ASTER, respectively.

Although the statistical results indicate that the AW3D30 achieves better vertical accuracy compared to all other DEMs, the original specification of better than ±5 m is not met over South Africa. The TanDEM-X and MERIT vertical accuracy specifications of better than ±10 and ±12 m, respectively, are also not met over South Africa. The SRTM and ASTER vertical accuracy specifications of better than ±16 m are met over South Africa.

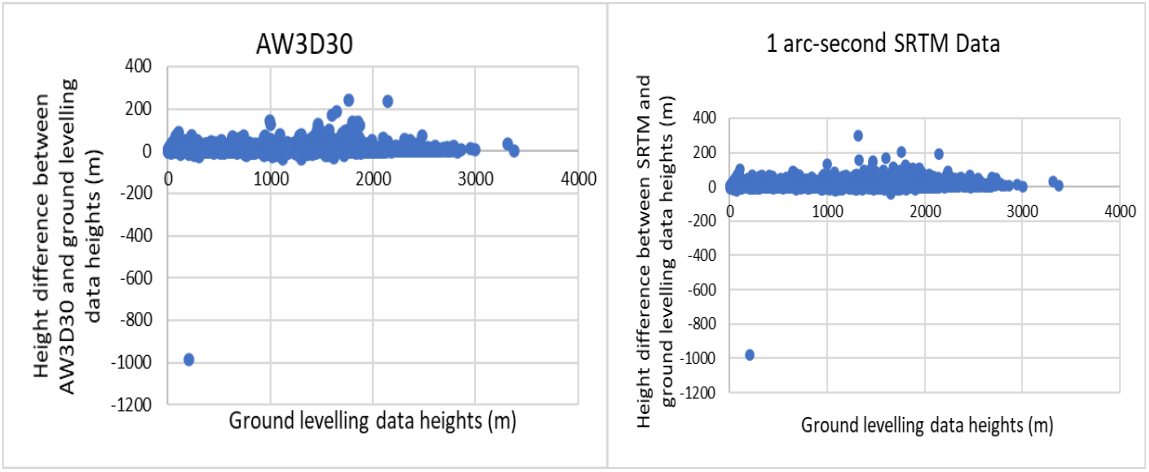

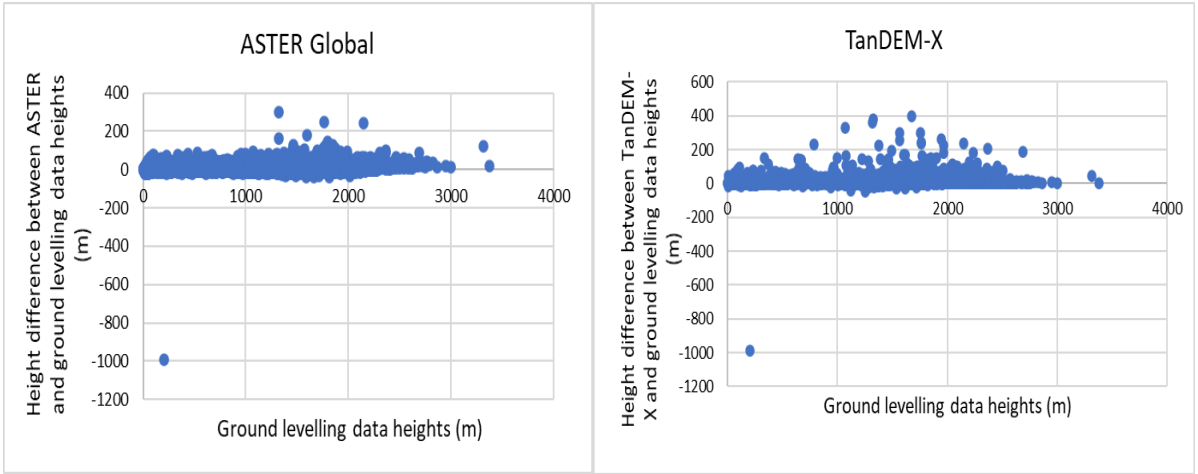

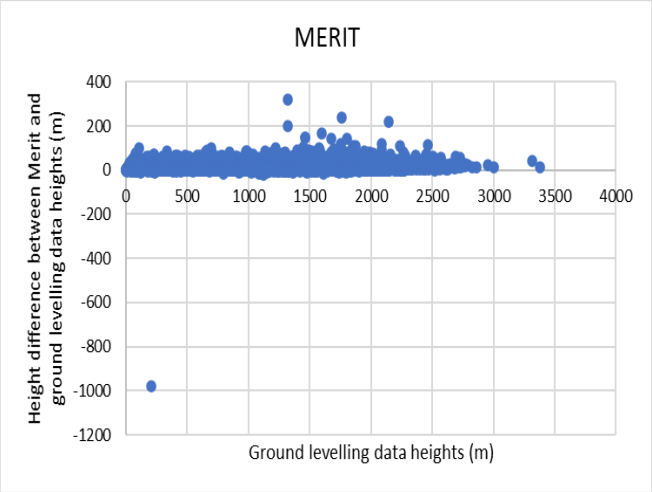

Figure 10: Scatter plots for height differences between ground levelling and satellite-based DEM heights before removing outliers

In the scatter plots in Figure 10, outliers can be visually identified. In Table 2, the maximum and minimum height differences indicated a difference in the satellite-based DEMs from ground levelling heights by more than ±100 m, and this is another general indication of outlier presence in the data. According to Figure 10, outliers are distributed in almost all elevation ranges, so applying a threshold of removing height differences of more than ±100 m would not be an effective way to remove outliers. Because elevation data in high areas that are normally less accurate on DEMs are arbitrarily removed, while errors in more accurate elevation data in low areas are not detected and removed. Therefore, the method in equation (3.6) was applied. The statistical results for the differences in heights between the DEMs are illustrated in Table 3.

Table 3: Relative height differences among the DEMs

	N	Min(m)	Max(m)	Mean (m)	STDV (±m)
AW3D30 & SRTM	27350	-174.00	277.00	1.26	6.71
AW3D30 & ASTER	27350	-147.00	279.00	7.27	9.42
AW3D30 & TanDEM-X	27350	-99.18	387.30	1.89	8.96
AW3D30 & MERIT	27350	-169.27	297.36	5.86	8.43
SRTM & ASTER	27350	-100.00	97.00	6.01	8.81
SRTM & TanDEM-X	27350	-87.74	334.30	0.64	8.05
SRTM & MERIT	27350	-94.00	98.15	4.61	5.16
ASTER & TanDEM-X	27350	-80.47	344.30	-5.38	10.83
ASTER & MERIT	27350	-114.12	131.35	-1.41	9.58
TanDEM-X & MERIT	27350	-322.61	119.09	3.97	9.64

In Table 3, statistical results indicate that discrepancies between the DEMs exist and that larger discrepancies exist between the ASTER and TanDEM-X while smaller discrepancies are observed between the SRTM and MERIT.

3.2.3.2 Height differences after removing outliers

From the 27, 350 height differences, there were 3.6% outliers for AW3D30, 5.9% for SRTM, 13.1% for ASTER, 5.1% for TanDEM-X, and 10.5% for MERIT. Spatial distribution of the ground levelling data points used to extract corresponding AW3D30, SRTM, ASTER, TandDEM-X, and MERIT heights over South Africa after taking > 3% to be outliers are given in Figures 11 to 15.

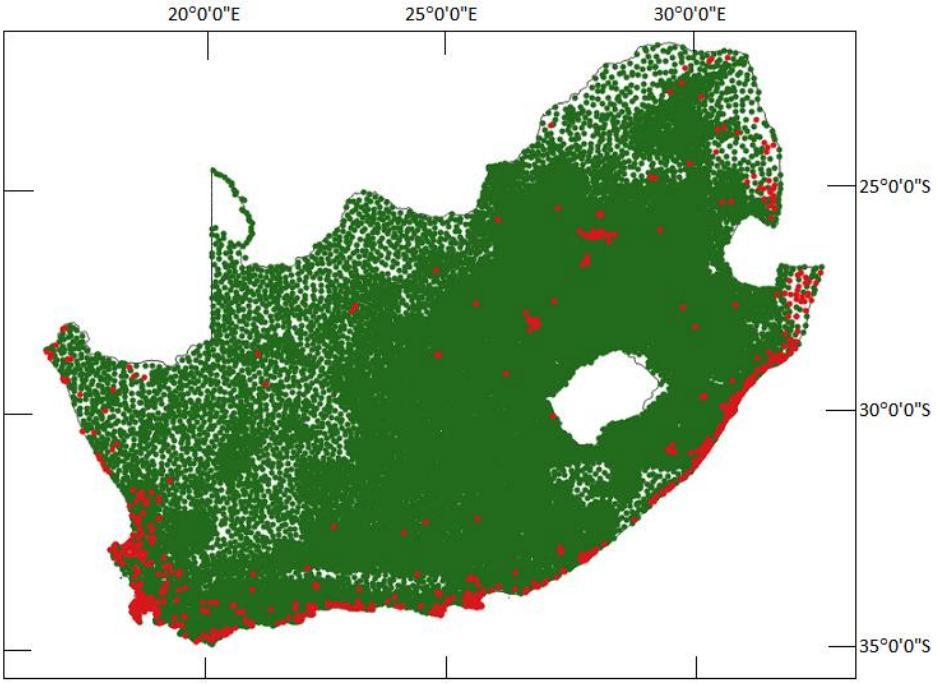

Figure 11: Distribution of selected ground levelling points (green dots) and outlier points (red) based on AW3D30 DEM

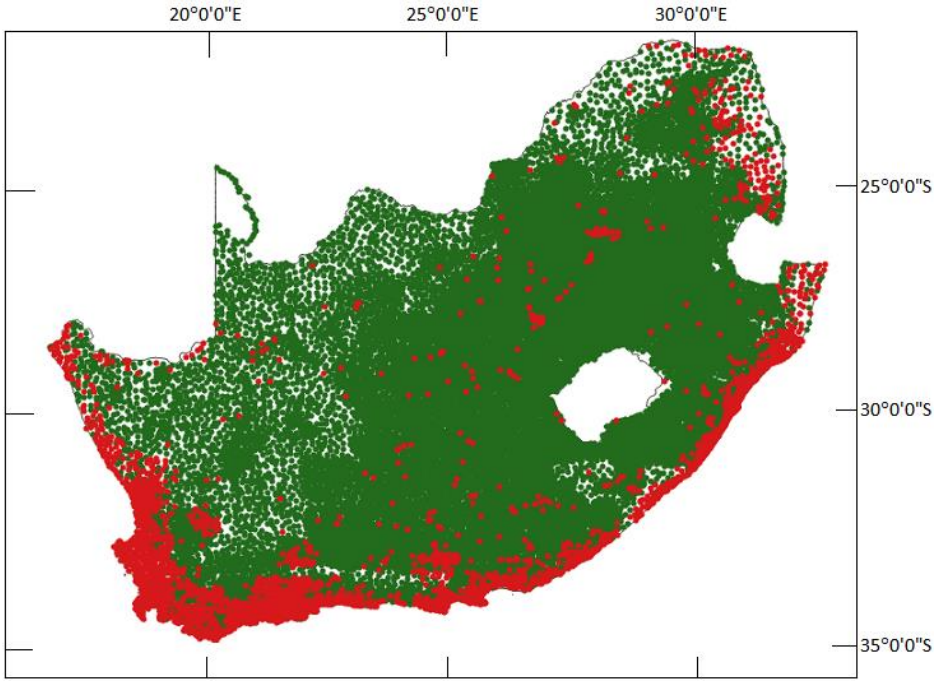

Figure 12: Distribution of selected ground levelling points (green dots) and outlier points (red) based on ASTER DEM

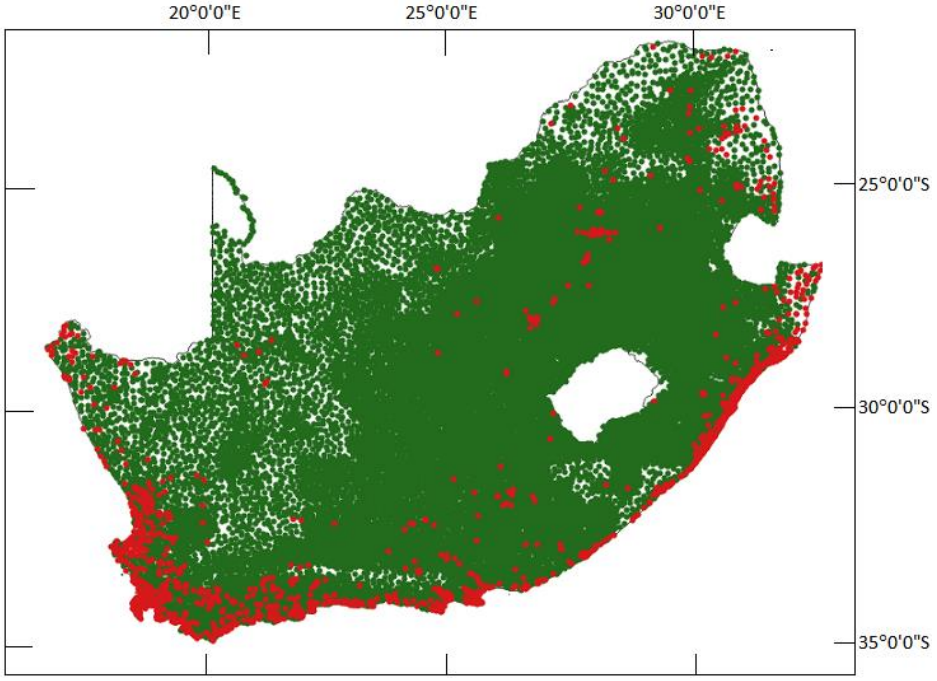

Figure 13: Distribution of selected ground levelling points (green dots) and outlier points (red) based on SRTM DEM

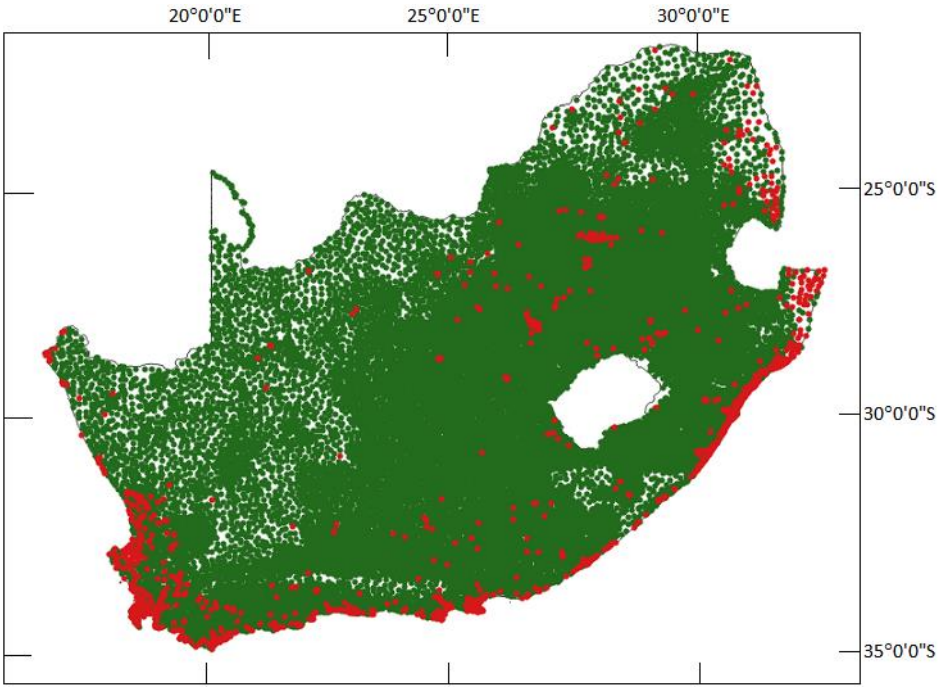

Figure 14: Distribution of selected ground levelling points (green dots) and outlier points (red) based on TanDEM-X DEM

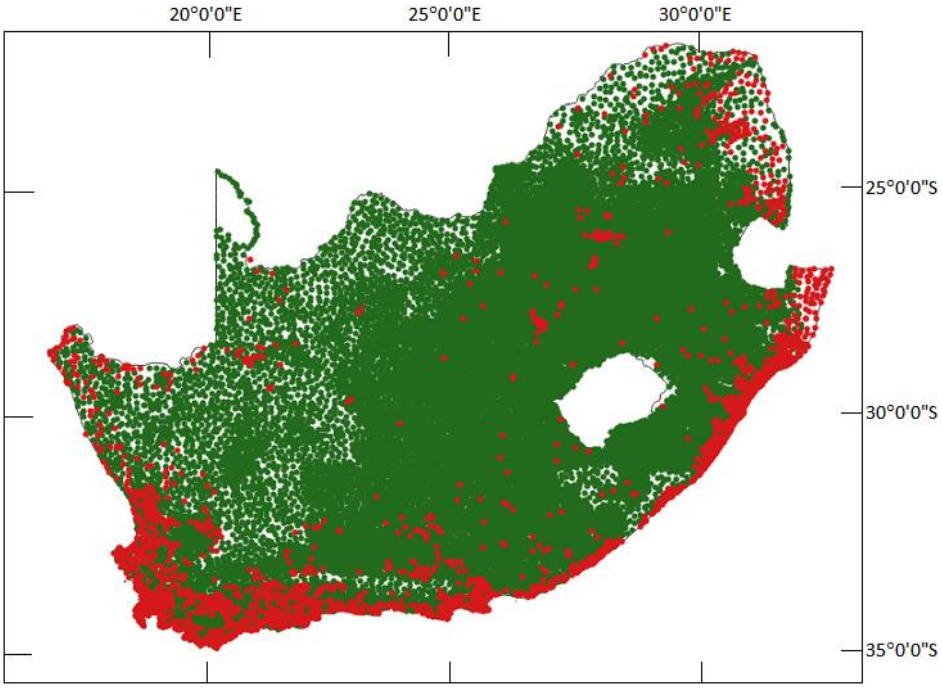

Figure 15: Distribution of selected ground levelling points (green dots) and outlier points (red) based on MERIT DEM

Most outliers are spatially distributed around locations with medium and high land use/cover. It is possible that this is due to the low penetration capacity of SRTM and TanDEM-X radar signals in dense vegetation and the canopy sensitivity of the optical images used to generate ASTER GDEM and AW3D30. Fewer outliers are spatially distributed over the low land use/cover locations, which typically are areas where radar signals can penetrate well and where no canopy has an effect on vegetation reflectance on satellite images. ASTER has a large distribution of outliers, followed by MERIT, SRTM, TanDEM-X, and AW3D30, respectively. Statistical results for the absolute height difference between the DEMs and the ground levelling data after removing outliers are illustrated in Table 4, while corresponding scatter plots of the height differences after removing outliers are given in Figure 16.

Table 4: Absolute height difference between the DEMs and ground levelling over South Africa

	AW3D30	SRTM	ASTER	TanDEM-X	MERIT
N	26364	25727	23773	25962	24485
Min (m)	-34.90	-37.80	-40.70	-28.83	-18.62
Max (m)	74.30	66.20	63.20	73.95	72.29
Mean (m)	2.94	3.81	9.35	4.27	7.91
STDV (±m)	5.09	7.03	9.20	4.99	8.36

In Table 4, the absolute height differences after removing outliers between the DEMs (AW3D30, SRTM, ASTER, TanDEM-X, and MERIT) and ground levelling data have standard deviations of ±5.09, ±7.03, ±9.20, ±4.99, and ±8.36m, respectively with mean values of 2.94, 3.81, 9.35, 4.27, and 7.91 m, respectively. The results indicate that the TanDEM-X achieves better absolute vertical accuracy compared to all other DEMs followed by the AW3D30, SRTM, MERIT, and ASTER, respectively. The TanDEM-X and MERIT standard deviations are within the vertical accuracy specifications of better than

±10 and ±12 m, respectively. The SRTM and ASTER vertical accuracy specifications of better than ±16 m is met and the AW3D30 original specification of better than ±5 m is marginally met.

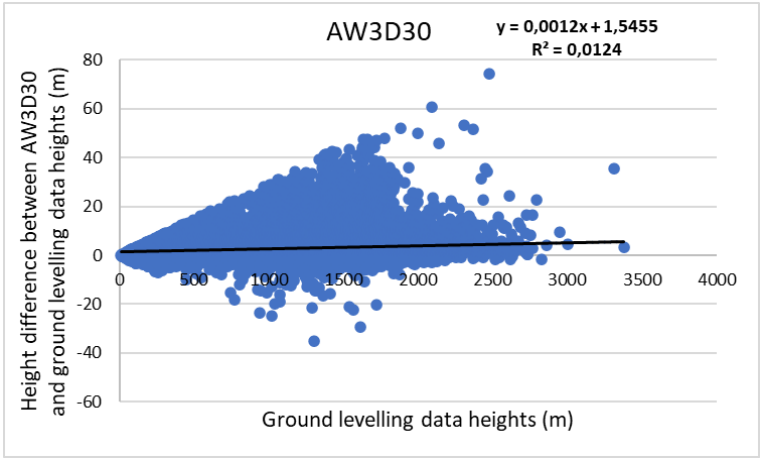

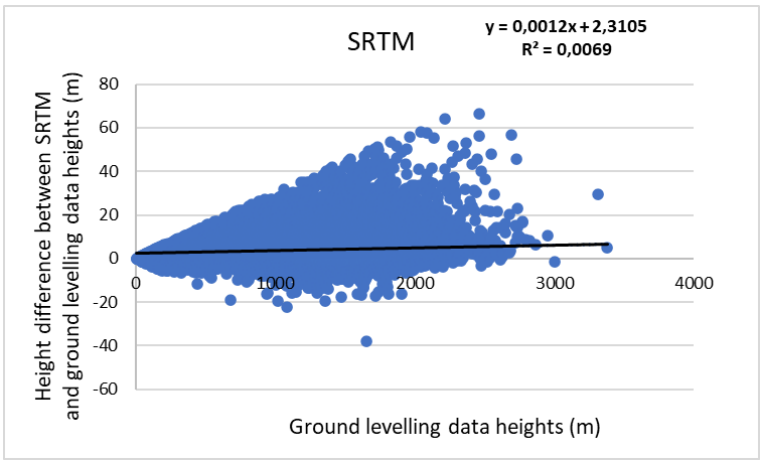

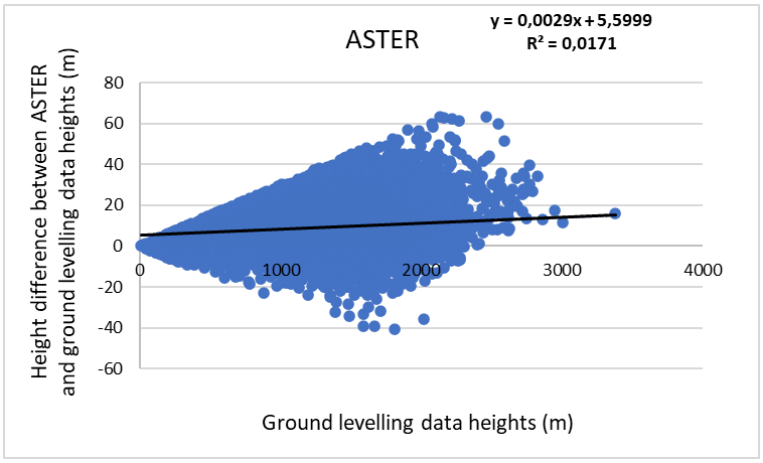

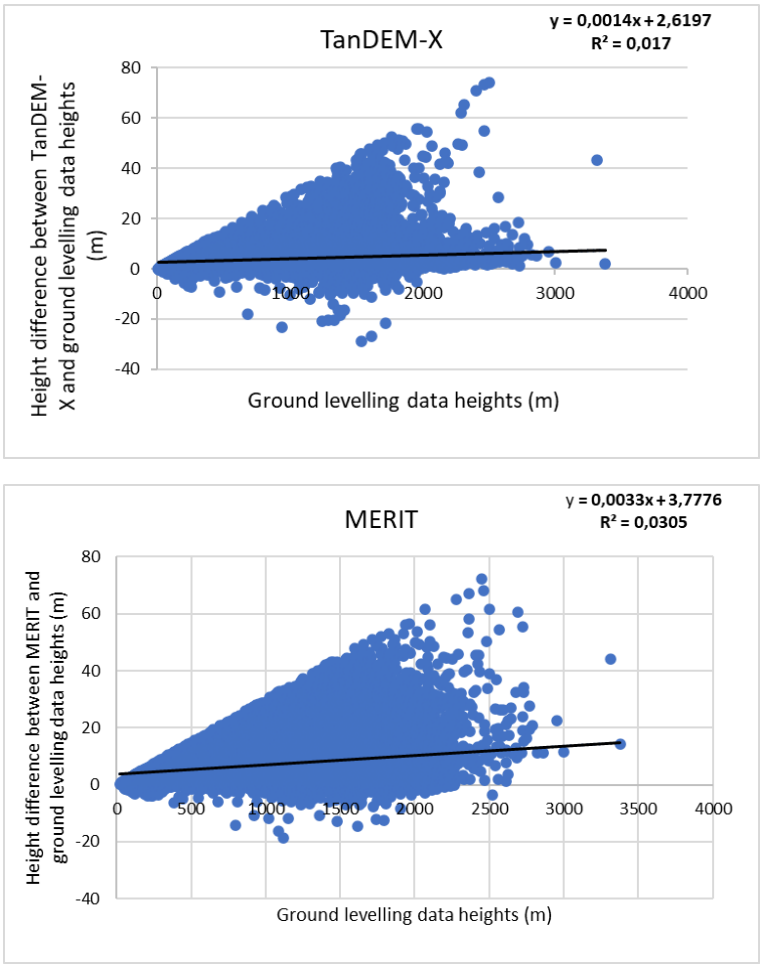

Figure 16: Scatter plots for height differences between ground levelling and satellite-based DEM heights after removing outliers

In Figure 16, the minimum and maximum height differences improved after outlier removal and are less than ±100 m. The coefficients of determination between ground levelling data and height differences for the DEMs (AW3D30, SRTM, ASTER, TanDEM-X, and MERIT) are 0.0124, 0.0069, 0.0171, 0.017, and 0.0305, respectively. Based on these results, there is a very weak linear (positive) correlation between the ground levelling data heights and height differences for all DEMs. On the other hand, if we look at the absolute height differences and visually at sub-figures in Figure 16, we can see that there is a high correlation. As elevation increases, absolute height differences also increase. This indicates a decrease in the vertical accuracies of the satellite-based DEMs, indicating that high areas are less accurate compared to low areas.

3.2.3.3 Influences of elevation, slope, and land use/cover on heights variation

Variation of standard deviation with elevation change

Table 5: Variation of standard deviation of the differences between ground levelling and satellite-based DEM heights with elevation over South Africa

	Height range (m)	0 - 500	500 - 1000	1000 - 1500	1500 - 2000	2000 - 2500	2500 - 3000	> 3000	**R^2**
AW3D30	Number of points	3184	4629	10854	7105	540	49	3	0.0124
	STDV (±m)	2.63	4.04	5.19	5.99	7.01	6.15	15.05	
SRTM	Number of points	2722	4516	10818	7082	537	49	3	0.0069
	STDV (±m)	3.09	5.45	6.84	8.30	11.44	12.16	13.44	
ASTER	Number of points	1200	4209	10709	7069	536	48	2	0.0171
	STDV (±m)	4.79	7.15	8.75	10.51	13.24	10.50	2.40	
TanDEM-X	Number of points	2943	4603	10781	7065	519	48	3	0.017
	STDV (±m)	2.15	3.32	4.54	6.42	9.67	10.79	19.39	
MERIT	Number of points	1923	4197	10710	7073	530	49	3	0.0305
	STDV (±m)	3.16	6.02	8.02	9.78	12.95	14.32	14.85	

In Table 5, there is a relationship between the standard deviation of the height differences and elevation range. As the elevation increases, the standard deviation also increases. The lowest standard deviations for all the DEMs were found in the height range (0 to 500 m). The highest standard deviation for AW3D30, SRTM, TanDEM-X, and MERIT are found in the height range greater than 3000 m. Although the standard deviations depict a relationship, Table 5 indicates a very weak linear (positive) correlation between the elevation and height differences for all DEM's. From these results, it can be drawn that these DEM's vertical accuracy degrade with an increase in elevation. It can also be deduced that it is more likely for higher areas to have lower vertical accuracy compared to lower areas.

Variation of standard deviation with slope

Table 6: Variation of standard deviation of the differences between ground levelling and satellite-based DEM heights with slope over South Africa

	Slope range	0° - 2°	2° - 4°	4° - 6°	6° - 8°	8° - 10°	> 10°	**R^2**
AW3D30	Number of points	9433	7121	3245	1927	1332	3306	0.0524
	STDV (±m)	4.54	5.14	5.02	4.90	4.63	5.84	
SRTM	Number of points	9371	7033	3171	1856	1266	3030	0.3024
	STDV (±m)	4.97	5.83	6.20	6.29	6.06	8.75	
ASTER	Number of points	8669	6427	2893	1728	1186	2870	0.1118
	STDV (±m)	7.82	8.39	9.15	9.09	9.38	10.55	
TanDEM-X	Number of points	9342	7038	3201	1892	1307	3182	0.1053
	STDV (±m)	4.34	4.76	4.49	4.45	3.55	6.79	
MERIT	Number of points	9145	6745	2961	1718	1165	2751	0.3223
	STDV (±m)	5.21	6.48	7.21	7.56	7.97	10.27	

In Table 6, as the slope increases, the standard deviation also increases, meaning deterioration in the vertical accuracy. All the DEMs have the lowest standard deviations in areas with the slope range (0° to 2°). The highest standard deviations for all the DEMs are found in the slope range greater than 10°. Although the standard deviations depict a relationship, the coefficients of determination in Table 6 indicate a very weak linear (positive) correlation between the slope and height differences for the AW3D30, ASTER, and TanDEM-X, and a moderate positive correlation for the SRTM and MERIT. From these results, it can be drawn that these DEM's vertical accuracies degrade with an increase in slope. It can also be deduced that it is more likely for steeper areas to have lower vertical accuracies compared to gentle areas.

Land use/cover verses elevation

Variation of standard deviation with elevation in low land use/cover

Table 7: Variation of standard deviation of the height differences with elevation in low land use/cover areas over South Africa

	Height range (m)	0 - 250	250 - 500	500 - 750	750 - 1000	1000 - 1250	1250 - 1500	1500 - 1750	1750 - 2000	>2000	**R^2**
AW3D30	Number of points	689	898	1117	2258	3120	4512	4014	1368	580	0.0055
	STDV (±m)	1.78	3.06	3.58	3.65	4.08	4.41	4.82	5.24	7.06	
SRTM	Number of points	541	756	1051	2222	3108	4495	3999	1356	577	0.0061
	STDV (±m)	2.00	3.57	5.15	5.51	5.99	6.91	7.39	8.69	11.60	
ASTER	Number of points	137	364	887	2156	3075	4455	3995	1357	574	0.0107
	STDV (±m)	3.19	4.91	6.16	7.19	7.71	9.07	9.73	11.13	13.25	
TanDEM-X	Number of points	585	874	1104	2256	3115	4484	3999	1351	558	0.0109
	STDV (±m)	1.34	2.37	2.97	3.25	3.53	4.00	4.94	6.44	9.92	
MERIT	Number of points	363	579	925	2115	3060	4464	3993	1359	570	0.0352
	STDV (±m)	1.90	3.28	5.24	6.48	7.25	8.48	9.07	10.69	13.20	

In Table 7, it can be observed that as the elevation increases, there is also an increase in standard deviations. In all DEMs, areas with a height range (0 to 250 m) have the lowest standard deviations, and areas with a height range greater than 2000 m have the highest standard deviations. Although Table 7 standard deviations depict a relationship, the coefficient of determination indicates a very weak linear (positive) correlation between the elevation change and height differences for all DEMs.

Variation of standard deviation with elevation in medium land use/cover

Table 8: Variation of standard deviation of the height differences with elevation in medium land use/cover areas over South Africa

	Height range (m)	0 - 250	250 - 500	500 - 750	750 - 1000	1000 - 1250	1250 - 1500	1500 - 1750	>1750	**R^2**
AW3D30	Number of points	409	252	116	96	161	760	751	78	0.00001
	STDV (±m)	1.63	2.10	2.13	2.86	3.88	2.76	2.61	1.86	
SRTM	Number of points	357	249	115	96	161	760	751	78	0.1645
	STDV (±m)	1.91	2.74	3.57	3.21	4.46	2.50	2.67	2.14	
ASTER	Number of points	99	132	111	96	161	759	750	78	0.0016
	STDV (±m)	2.81	4.62	6.24	6.95	6.90	7.30	8.25	7.93	
TanDEM-X	Number of points	377	251	116	96	161	760	751	78	0.0012
	STDV (±m)	1.01	1.47	1.62	2.27	3.20	1.87	2.10	1.48	
MERIT	Number of points	290	221	109	95	161	760	751	78	0.0568
	STDV (±m)	1.62	3.12	3.37	3.59	5.13	2.68	2.74	2.60	

In Table 8, the AW3D30, SRTM, TanDEM-X, and MERIT standard deviations increase with an increase in elevation from height range (0 to 1250 m). These height ranges are also areas where the lowest and highest standard deviations for these DEMs are found. The standard deviations of the DEMs implied above decrease from a height range greater than 1250 m. The ASTER standard deviation increases with an increase in elevation from height range (0 to 1750 m) and decreases from height range greater than 1750 m. In ASTER, areas with a height range (0 to 250 m) have the lowest standard deviation, and (1500 to 1750 m) have the highest standard deviations. The coefficients of determination in Table 8 indicate a weak linear (positive) correlation between the elevation and height differences for the AW3D30, ASTER, TanDEM-X, and MERIT and a moderate positive correlation for the SRTM.

Variation of standard deviation with elevation in high land use/cover

Table 9: Variation of standard deviation of the height differences with elevation in high land use/cover areas over South Africa

	Height range (m)	0 - 250	250 - 500	500 - 750	750 - 1000	1000 - 1250	1250 - 1500	1500 - 1750	>1750	**R^2**
AW3D30	Number of points	473	454	484	532	1008	1207	719	123	0.074
	STDV (±m)	1.89	3.43	4.50	5.75	6.10	7.78	10.02	11.84	
SRTM	Number of points	370	439	476	530	1000	1201	719	120	0.0304
	STDV (±m)	2.27	3.65	5.28	5.85	6.25	8.58	11.02	12.91	
ASTER	Number of points	177	287	422	511	995	1180	715	122	0.0694
	STDV (±m)	2.96	4.91	6.89	8.00	8.54	10.05	12.01	14.38	
TanDEM-X	Number of points	405	442	479	526	999	1186	717	119	0.0684
	STDV (±m)	1.77	2.92	3.44	4.13	5.46	7.21	11.02	12.69	
MERIT	Number of points	167	298	410	530	998	1190	714	122	0.0553
	STDV (±m)	2.23	3.53	5.06	6.43	7.53	8.88	11.46	12.84	

In Table 9, as the elevation increases, there is also an increase in standard deviations for the height differences. In all DEMs, areas with a height range (0 to 250 m) have the lowest standard deviation, and areas with a height range greater than 1750 m have the highest standard deviations. As the Table 9 standard deviations indicate a strong relationship, the coefficient of determination also indicates a weak linear (positive) correlation between the elevation and height differences for all DEM's.

Table 7 shows a similar trend in results to those in Table 9. In all the results, the standard deviations for the height differences increase with an increase in elevation, meaning deterioration in the vertical accuracy. From these results, it can be drawn that these DEM's vertical accuracies degrade with an increase in elevation in low and high land use/cover. From the results in Table 8 it is deduced that in medium land use/cover, AW3D30, SRTM, TanDEM-X, and MERIT vertical accuracies degrade with an increase in elevation in range (0 to 1250 m). The ASTER vertical accuracy in medium land use/cover degrades with an increase in all elevation ranges.

Land use/cover verses slope

Variation of standard deviation with slope in low land use/cover

Table 10: Variation of standard deviation of the height differences with slope in low land use/cover areas over South Africa

	Slope range	0° - 2°	2° - 4°	4° - 6°	6° - 8°	8° - 10°	> 10°	**R^2**
AW3D30	Number of points	5973	4933	2350	1468	1054	2778	0.091
	STDV (±m)	3.66	4.06	4.04	3.82	4.24	5.71	
SRTM	Number of points	5930	4895	2310	1428	1004	2538	0.3764
	STDV (±m)	4.40	5.06	5.58	5.68	5.95	8.90	
ASTER	Number of points	5566	4560	2151	1342	959	2422	0.1304
	STDV (±m)	7.34	7.88	8.81	8.85	9.31	10.59	
TanDEM-X	Number of points	5923	4899	2337	1459	1035	2673	0.1924
	STDV (±m)	3.34	3.43	3.63	3.52	3.47	7.08	
MERIT	Number of points	5829	4772	2210	1350	940	2327	0.3619
	STDV (±m)	4.80	5.98	6.92	7.32	7.95	10.36	

In Table 10, as the slope increases, the standard deviations of the DEMs also increases. In all DEMs, areas with a slope range (0° to 2°) have the lowest standard deviations, and areas with a slope range greater than 10° have the highest standard deviations. The coefficients of determination in Table 10, indicate a weak linear correlation between the slope and height differences for the AW3D30 and ASTER, moderate positive correlation for the TanDEM-X, and a strong positive correlation for the SRTM and MERIT.

Variation of standard deviation with slope in medium land use/cover

Table 11: Variation of standard deviation of the height differences with slope in medium land use/ cover areas over South Africa

	Slope range	0° - 2°	2° - 4°	4° - 6°	6° - 8°	8° - 10°	> 10°	**R^2**
AW3D30	Number of points	1683	716	129	49	24	22	0.0151
	STDV (±m)	2.41	2.76	3.08	4.65	2.67	2.82	
SRTM	Number of points	1676	686	118	45	20	22	0.1988
	STDV (±m)	2.48	3.14	4.11	3.32	4.87	4.77	
ASTER	Number of points	1473	551	91	36	15	20	0.0132
	STDV (±m)	7.28	7.58	8.99	7.99	7.40	8.70	
TanDEM-X	Number of points	1678	698	125	44	23	22	0.0146
	STDV (±m)	1.71	2.33	2.37	2.01	1.73	1.62	

MERIT	Number of points	1651	648	98	36	16	16	0.2371
	STDV (±m)	2.26	3.29	4.38	4.55	5.26	9.83	

The only consistent trend in Table 11 is the variation of standard deviations of SRTM and MERIT with slope range. It can be observed that as the slope increases, the standard deviations of the SRTM and MERIT also increase, and there is a moderate positive correlation between these DEM height differences and slope. In the SRTM, ASTER, and MERIT, areas with a slope range (0° to 2°) have the lowest standard deviation, and with a slope range greater than 8° have the highest standard deviation. For the AW3D30, ASTER, and TanDEM-X, there is variation in standard deviations as slope increases. However, for AW3D30 and TanDEM-X, low standard deviations are in areas with slope range (0° to 2°) and (>10°), respectively. In slope range (6° to 8°), the AW3D30 has the highest standard deviations, and the TanDEM-X has the highest standard deviation in slope range (4° to 6°). Table 11 also indicates a weak linear correlation between the slope and height differences for the AW3D30, ASTER, and TanDEM-X.

Variation of standard deviation with slope in high land use/cover

Table 12: Variation of standard deviation of the height differences with slope in high land use/cover areas over South Africa

	Slope range	0° - 2°	2° - 4°	4° - 6°	6° - 8°	8° - 10°	> 10°	**R^2**
AW3D30	Number of points	1698	1421	742	403	248	488	0.0017
	STDV (±m)	7.03	7.74	6.91	7.13	5.99	6.46	
SRTM	Number of points	1683	1396	715	376	236	449	0.0731
	STDV (±m)	6.99	7.93	7.56	8.08	6.33	7.38	
ASTER	Number of points	1552	1270	628	343	206	410	0.028
	STDV (±m)	9.19	9.94	9.60	9.38	9.20	9.73	
TanDEM-X	Number of points	1662	1394	718	384	243	472	0.0009
	STDV (±m)	7.10	7.96	6.70	6.89	3.84	4.48	
MERIT	Number of points	1589	1282	637	328	204	389	0.1199
	STDV (±m)	7.14	8.30	8.13	8.40	7.89	9.39	

In Table 12, there is a variation in the standard deviations of the DEMs as the slope increases. However, for AW3D30 and TanDEM-X, the lowest standard deviations are found in slope ranges (>10°) and higher standard deviations in slope ranges (2°- 4°). Table 12 also indicates a weak linear correlation between the height differences of these DEMs and the slope.

From the results in Table 10, it can also be deduced that in all the DEMs in low land use/cover it is more likely for steeper areas to have lower vertical accuracies compared to flat areas. In Table 11, for the SRTM and MERIT in medium land use/cover, it is more likely for steeper areas to have lower vertical accuracies compared to flat areas. However, for AW3D30, TanDEM-X, and ASTER, this is not

the case as there is an unclear variation in vertical accuracies as slope changes. For AW3D30 and TanDEM-X in high land use/cover, it is more likely for steeper areas to have higher vertical accuracies compared to flat areas. For the MERIT, SRTM, and ASTER, in high land use/cover it is more likely for steeper areas to have lower vertical accuracies compared to flat areas.

In all the evaluations of the satellite-based DEMs against ground levelling data, the ASTER shows the lowest vertical accuracy, followed by the MERIT and SRTM. These DEMs also provide very low accuracies in areas with the highest elevations and slopes. The AW3D30 and TanDEM-X provide relatively high vertical accuracies in most elevation and slope ranges. Therefore, they (AW3D30 and TanDEM-X) are candidate DEMs suitable for fusion over South Africa and this is only based on the DEMs evaluated in this study.

3.3 Assessment of satellite-based digital elevation models using ground levelling data and LiDAR data over a portion of western part of South Africa

3.3.1 Introduction

The point and surface-based approach is used in the assessment of the satellite-based DEMs over a portion of the western part of South Africa. The vertical accuracy of the DEMs is assessed against ground levelling and reference surface data (LiDAR DEM). This process included extracting the elevations from DEMs corresponding to the data, validating the heights of the DEMs, and studying the Influences of geomorphological factors and semantic information on height differences.

3.3.2 Data and methods

The datasets used are all the DEMs in Table 1, the ground levelling (trigonometrical beacon) data described in section (2.1.1) and LiDAR data are used as references. The LiDAR comes in a point cloud and has a density of 2 to 3 points per m^2 at a vertical accuracy of 0.1 m. The LiDAR is provided by the City of Cape Town, captured in the years 2011 to 2015 and updated annually.

3.3.2.1 Preparation of the collected LiDAR Data

The LiDAR data collected for the City of Cape Town region had 150 different LAS datasets. The LAS datasets act as a simple container definition of one or more LiDAR (LAS) files that present a single unit. The LAS dataset also allows the storage and display of the LiDAR data and surface measurements, making it possible to process large volumes of LiDAR data. The LAS data points were collected in geographic coordinate system and based on WGS84 transverse Mercator, with horizontal datum as Hartebeesthoek 94.

Data processing steps include generating a LAS dataset, calculating statistics, generating a layer from the LAS dataset, and converting the LAS dataset to raster format. By creating a new LAS dataset, all the collected LAS files were combined into one LAS file. The LAS dataset's statistics were calculated through the computation and updating of all missing file statistics as this is essential for understanding the dataset. Creating a layer from a LAS dataset was done by filtering the LAS dataset generated using the last return values as the filtering points. To generate a DEM from the LiDAR (LAS) file, a conversion of the LAS file to a raster surface was done using elevation values stored in the LiDAR points. The resulting raster had a spatial resolution of 1 m.

3.3.2.2 Selected area for LiDAR reference

Getting a high-quality ground truth reference surface that covers the whole country was a challenge because high-quality reference DEMs from sources such as LiDAR are limited to small areas as a result of high costs. From the LiDAR data, a region (A) as shown in Figure 17, with elevation and slope variation was identified. The area was used as a reference for assessing the satellite-based DEMs. Region (A) had an area of approximately 406.239 km^2 and is characterized mostly by flat surfaces with an elevation range of approximately 514 m. Spatial distribution of ground levelling data over area A (DEM and Slope) are shown in Figures 18 and 19.

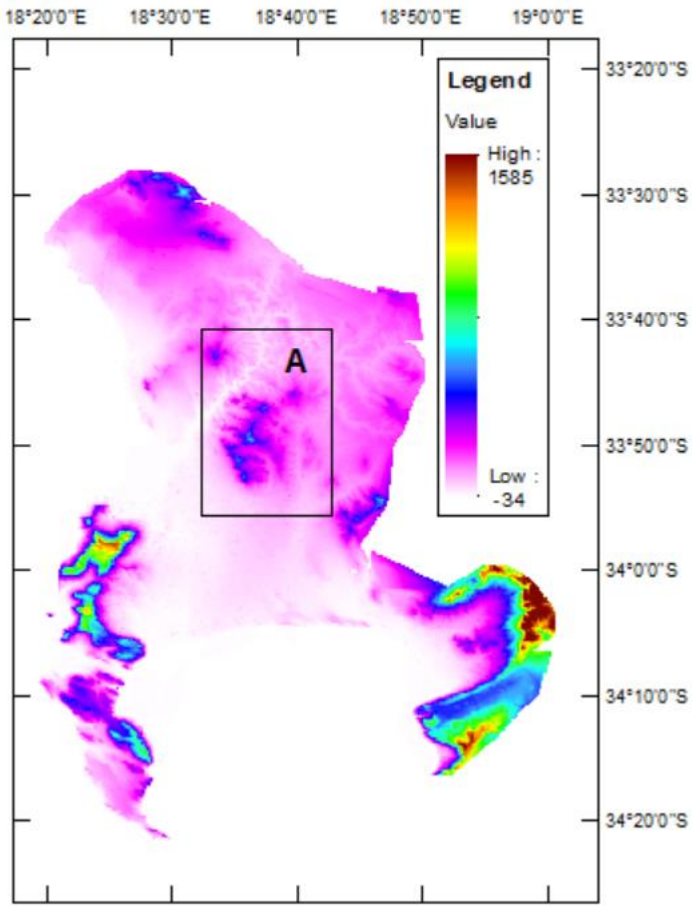

Figure 17: LiDAR DEM for the City of Cape Town (units are in m)

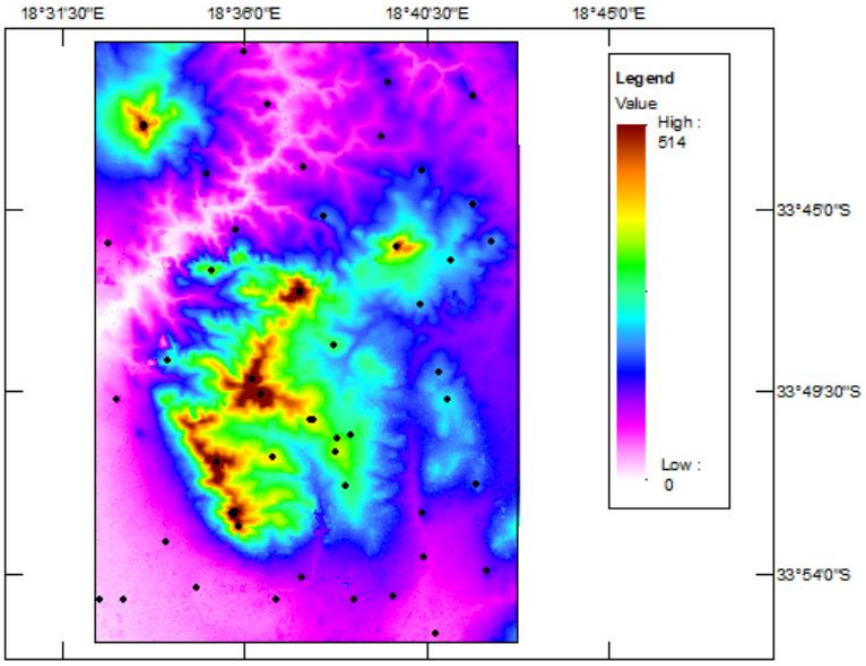

Figure 18: Distribution of ground levelling data points, with black dots representing ground levelling data points over LiDAR DEM in area (A)

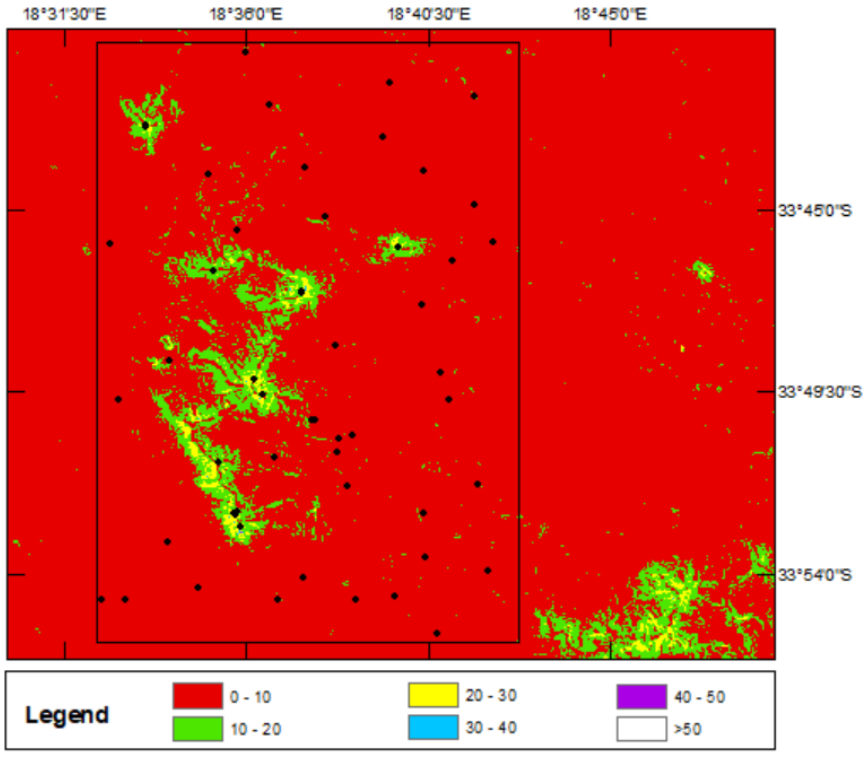

Figure 19: Categorised slope representation over area (A) based on SRTM data (units are in degrees)

3.3.2.3 Validation of the vertical accuracies of the DEMs over area (A)

The quality of the DEMs in area (A) is assessed using two methods: (1) comparison using ground levelling height data as reference (absolute) and (2) using LiDAR DEM as reference (relative). Absolute height differences are obtained by comparing trigonometrical beacon heights data against LiDAR and the satellite-based DEMs (AW3D30, SRTM, TanDEM-X, ASTER, and MERIT). Relative height differences are obtained by comparing LiDAR and satellite-based DEMs for area (A) at each pixel (grid) and in each land use/cover.

LiDAR DEM is in a raster format, and point features are needed. Therefore, a 90 × 90 m polygon sampling grid of points (fishnet) was generated. A total of 42,160 sampling grid points were generated for area (A). Coordinates for each output sampling grid point feature class were calculated. The point's coordinates were referenced on WGS 84. The elevations for the DEMs (LiDAR, AW3D30, SRTM, TanDEM-X, ASTER, and MERIT) on the grids were extracted. The height differences between the LiDAR and satellite-based DEMs corresponding to sampling grid points are determined as follows,

$$\Delta \mathrm{H}_{LiDAR-DEM} = \mathrm{H}^{LiDAR} - \mathrm{H}^{DEM} \tag{3.8}$$

where, $\Delta H_{liDAR-DEM}$ are differences in heights between LiDAR and AW3D, SRTM, ASTER, TanDEM-X, and MERIT heights, respectively. H^{LiDAR} and H^{DEM}represent LiDAR heights and corresponding extracted heights on the DEMs.

3.3.2.4 Assessment of the influence of geomorphological factors and semantic information on height differences

The evaluation process includes looking at the influence that geomorphological factors have on height differences in different categories, and this is done using the 90 × 90 m sampling grid data points. This is essential in studying the correlation of height errors with geomorphological parameters (slope, elevation, aspect, and surface roughness) as it helps in selecting better candidate DEMs for fusion over South Africa. The generation of slope and land use/cover over South Africa is already discussed in section (3.2.2.2).

According to Papasaika et al. (2009), the aspect is opposite to the direction of the gradient; it is the direction perpendicular to the contour lines. The aspect **A** can mathematically be defined as a function of gradients at x and y direction at a given point on a surface $z = f(x, y)$ as,

$$A(x, y) = 270^{\circ} + \tan^{-1}\left(\frac{f_x}{f_y}\right) - 90^{\circ}\frac{f_x}{|f_x|} \tag{3.9}$$

where, $A(x, y)$ is the Aspect and f_x and f_y are gradients in $x-$ and $y-$ direction. The geodesic aspect is generated, and the process involves the aspect derivation from each cell of the DEM by identifying the compass direction that the downhill slope faces for each location. The aspect over South Africa using SRTM is shown in Figure 20. The aspect over area (A) is shown in Figure 21.

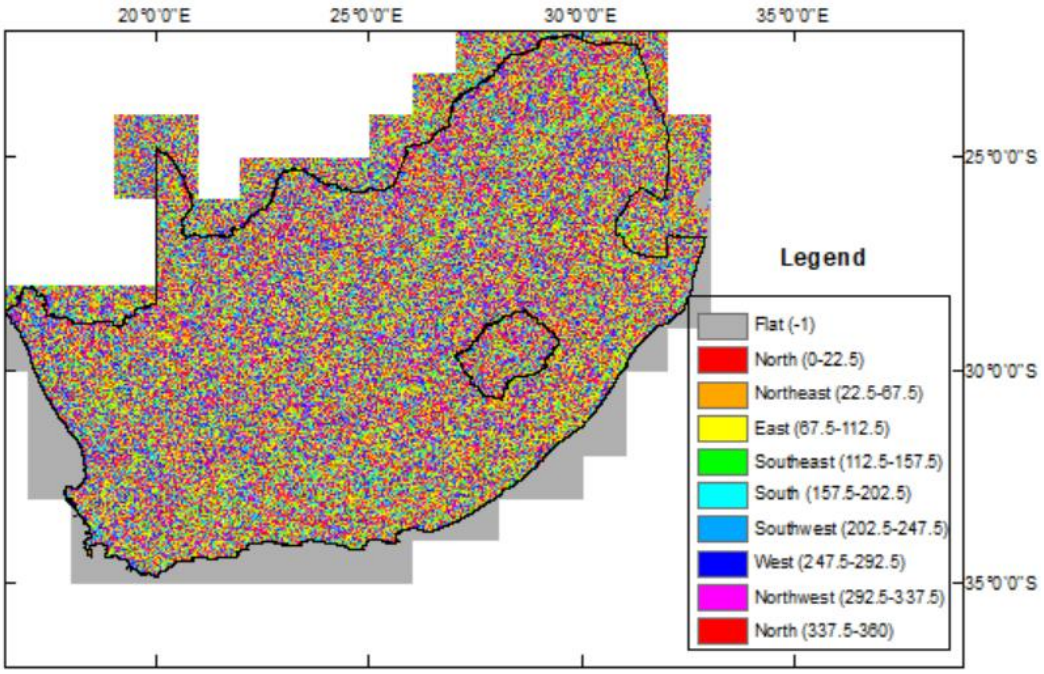

Figure 20: Aspect representation over South Africa based on SRTM data (units are in degrees)

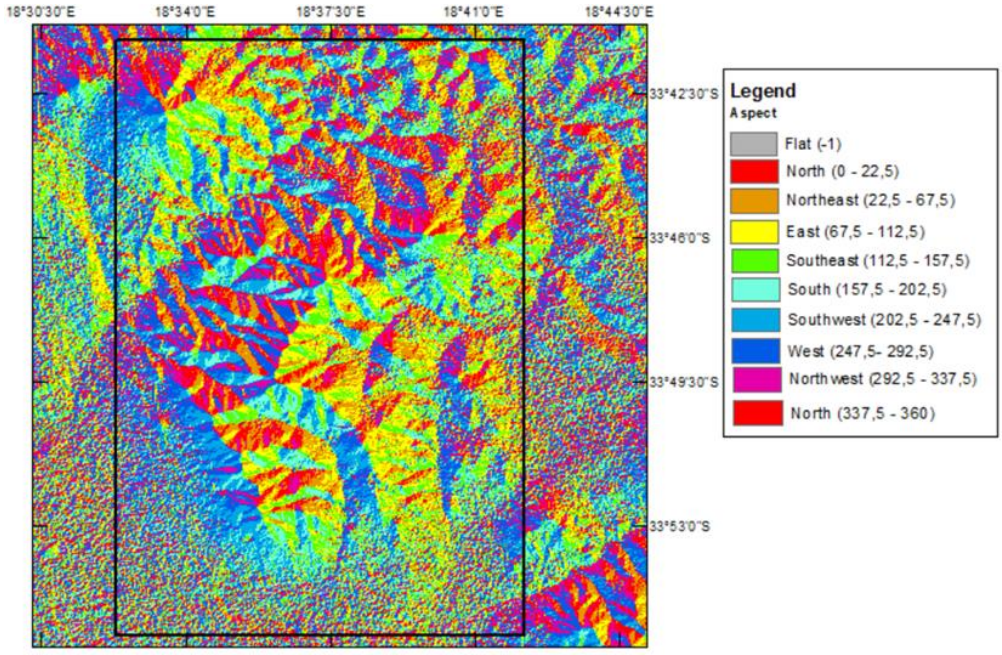

Figure 21: Aspect representation over area (A) based on SRTM data (units are in degrees)

The surface roughness is generated using a focal statistics tool, which calculates a statistic of the values within a specified neighborhood for each input cell location. In the focal statistic tool, the surface roughness is generated by assuming that it is approximately the standard deviation of the DEM, and the output surface roughness is shown in Figure 22. The surface roughness over area (A) is shown in Figure 23.

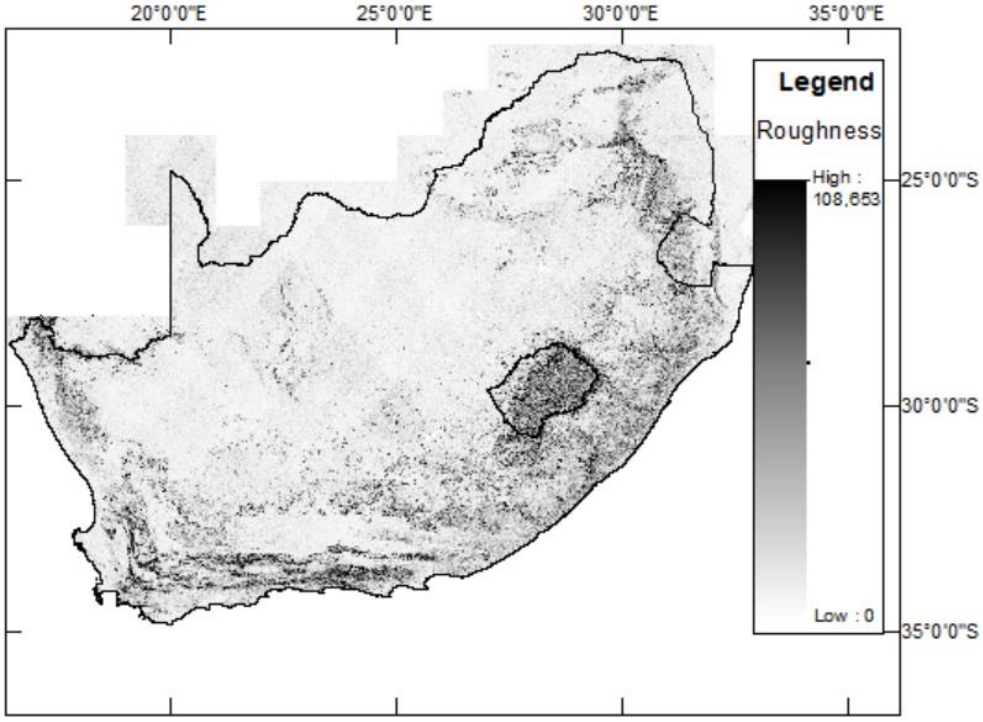

Figure 22: Surface Roughness representation over South Africa based on SRTM data (±m)

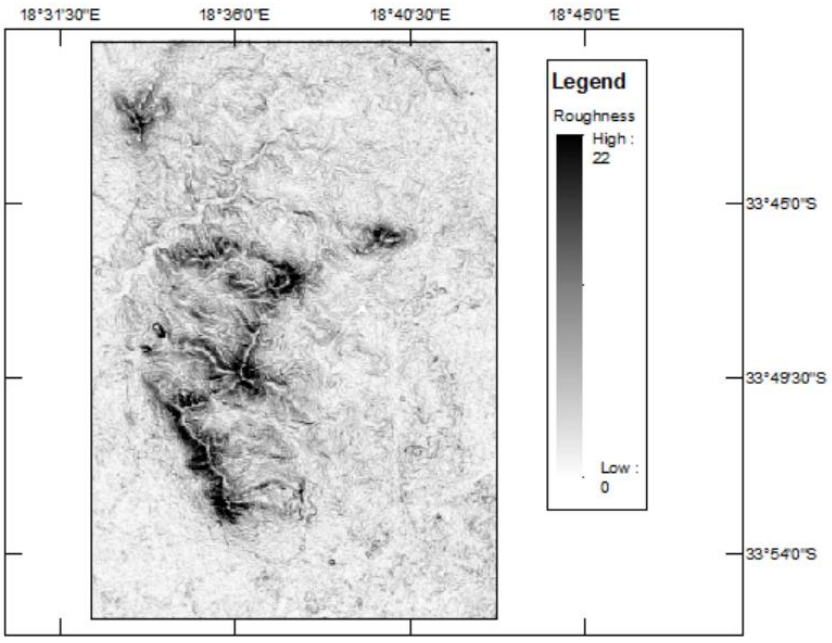

Figure 23: Surface Roughness representation over area (A) based on SRTM data (±m)

Regarding land use/cover, from the 42,160 grid points in the region (A), 354 points were unclassified, and 41,806 were classified into three different classes. From the classified grid points, a total of 9,091 were in low land use/cover, 19,116 in medium land use/cover, and 13,599 in high land use/cover. The categorized land use/cover over area (A) is shown in Figure 24.

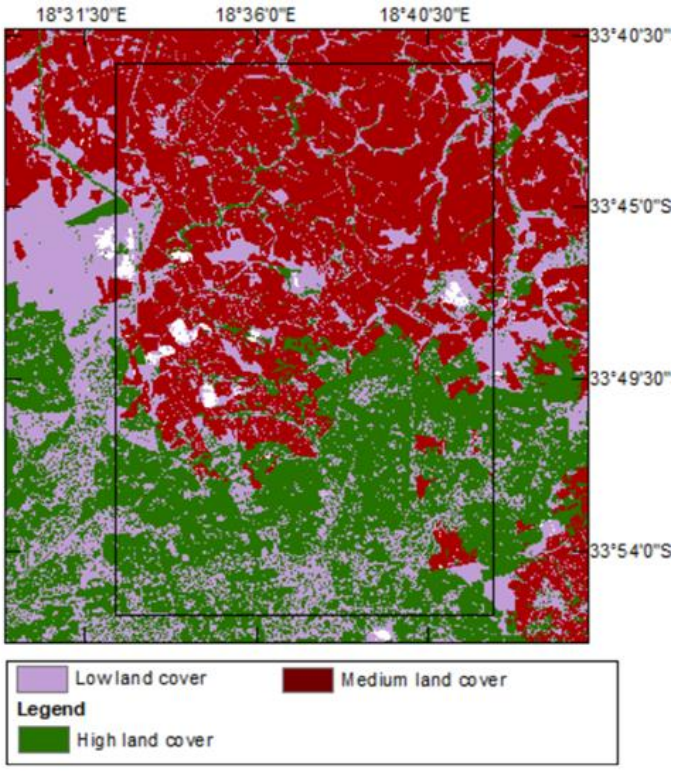

Figure 24: Land use/cover over area (A)

Extracted sampling grids, elevation, slopes, surface roughness, and aspect over area (A) are divided into different ranges. However, for aspect the 9 campus directions are used to segment the data. Statistical parameters for the height differences in each range are computed to assess the vertical accuracies. To determine the influence of land use/cover on height variation, the land use/cover corresponding to the grid points is extracted, differences in heights in each land use/cover are determined, and statistical parameters for the height differences are computed. The influence the change in the geomorphological factors (slope, elevation, aspect, and surface roughness) has on the vertical accuracy of each DEM over each land use/cover is also assessed.

3.3.3 Results and discussion

The results and discussions of vertical accuracies of the satellite-based DEMs in area (A) are presented, followed by the influences of geomorphological parameters, and land use/cover on the vertical accuracy of each DEM.

3.3.3.1 Relative height differences in area (A)

Statistics of the relative height differences between LiDAR and satellite-based DEMs at 42,160 grid points (90 by 90 m) over area (A) are presented in Table 13, while scatter plots of elevation change and height differences are given in Figures 25 and 26, respectively.

Table 13: Relative height difference over area (A)

	AW3D30	SRTM	ASTER	TanDEM-X	MERIT
N	42160	42160	42160	42160	42160
Min (m)	-36.00	-54.00	-48.00	-73.12	-54.22
Max (m)	41.00	53.00	63.00	61.82	57.01
Mean (m)	-1.79	-1.22	7.31	0.37	-0.68
STDV (±m)	2.27	3.10	4.94	2.32	3.71

In Table 13, the height differences between the DEMs (AW3D30, SRTM, ASTER, TanDEM-X, and MERIT) and the LiDAR data heights have standard deviations of ±2.27, ±3.10, ±4.94, ±2.32, and ±3.71 m respectively, with mean values of -1.79, -1.22, 7.31, 0.37, and -0.68 m. The statistical parameters indicate that the AW3D30 achieves better relative vertical accuracy compared to all other DEMs, followed by the TanDEM-X, SRTM, MERIT, and ASTER, respectively, in that order. The original ±6 m relative accuracy specifications of the SRTM and ASTER are met.

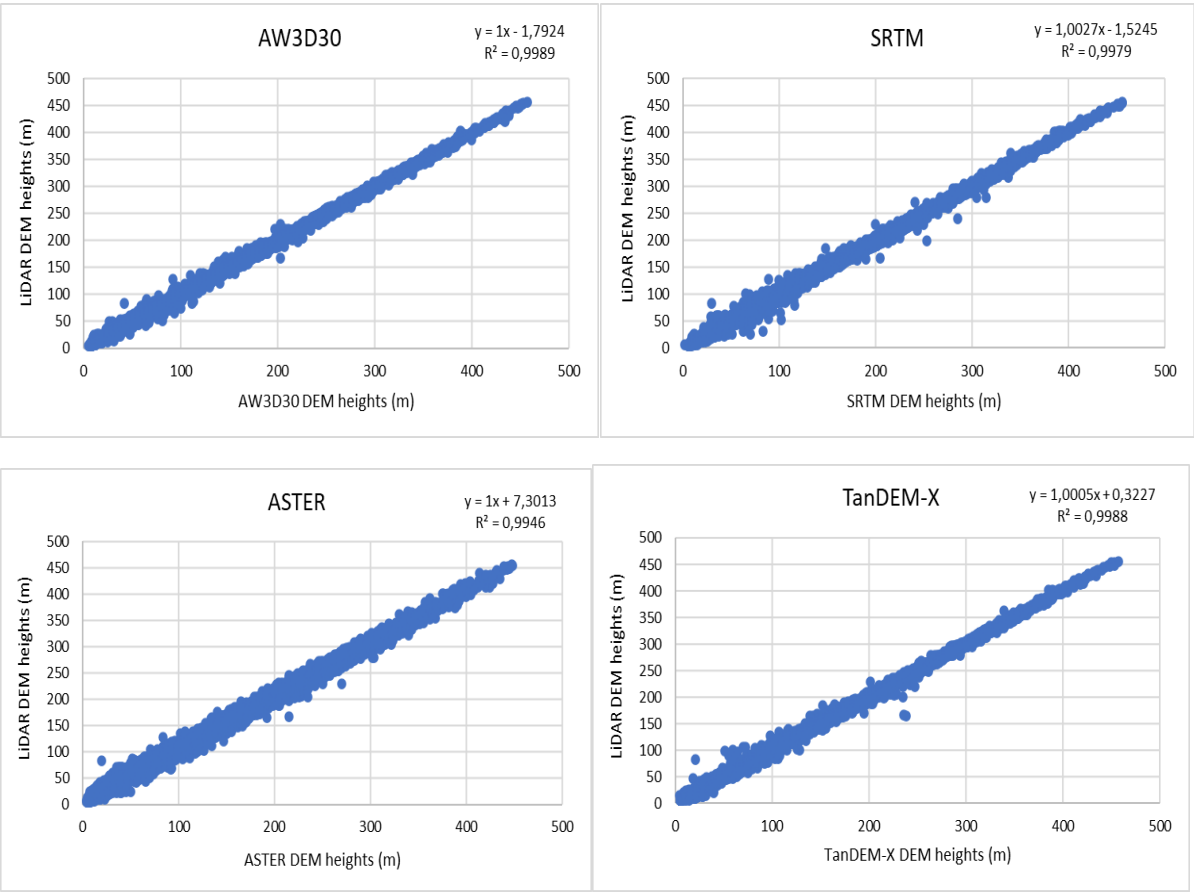

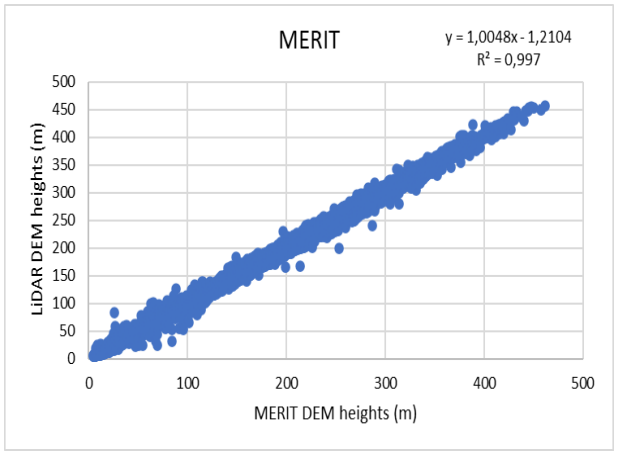

Figure 25: Scatter plots of LiDAR against satellite-based DEM heights over area (A)

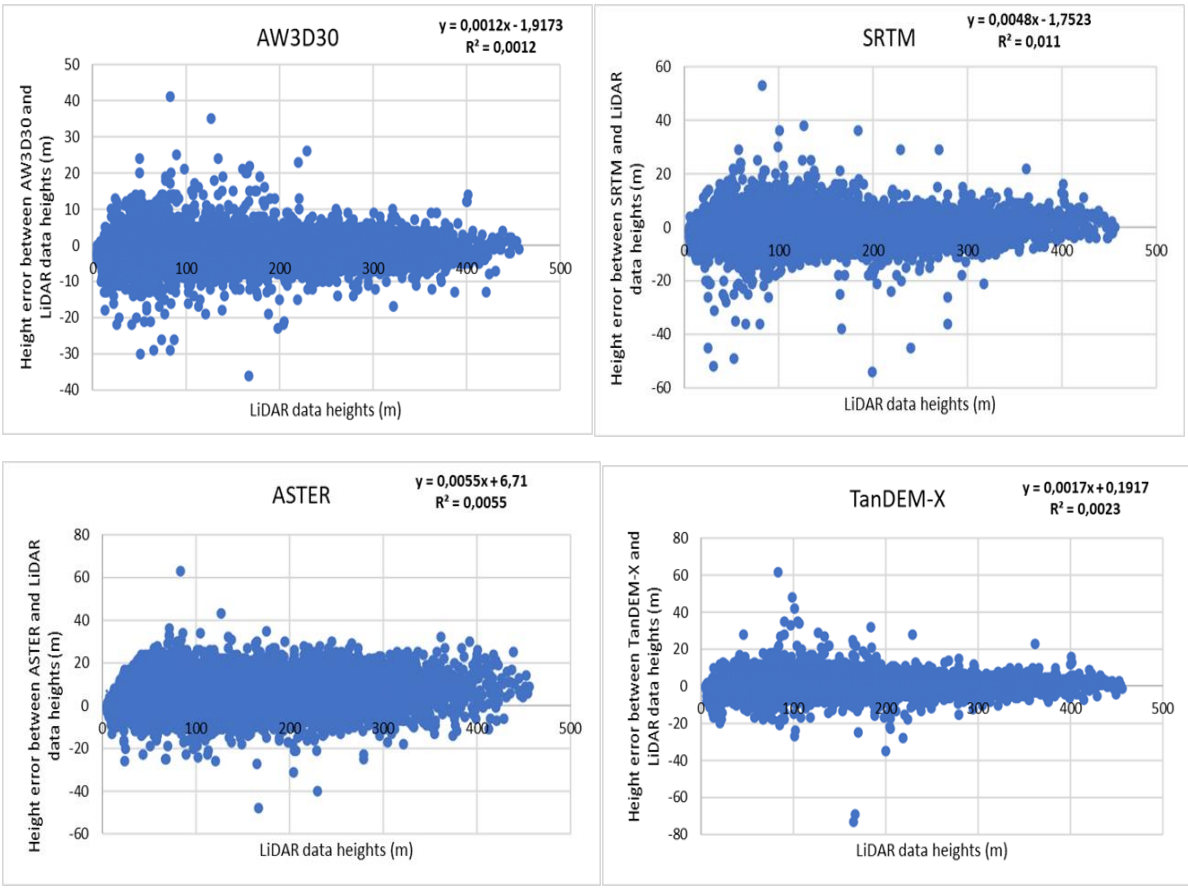

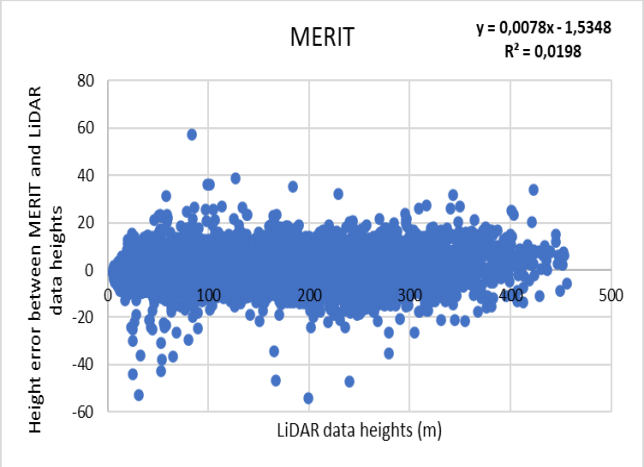

Figure 26: Scatter plots of heigh errors against LiDAR DEM heights over area (A)

In all the scatter plots in Figure 25, $R^2 > 0.99$, this indicates that there is approximately 99% correlation between the heights of the satellite-based DEMs with those of LiDAR DEM. Based on the coefficient of determination, there is a very strong positive correlation. Satellite-based DEM heights increase as LiDAR heights increase. It can be seen, however, from the figure, that the DEMs do not coincide when replicating the terrain.

In the scatter plots in Figure 26, the coefficients of determination between LiDAR data heights and height differences for the satellite-based DEMs (AW3D30, SRTM, ASTER, TanDEM-X, and MERIT) are 0.0012, 0.011, 0.0055, 0.0023, and 0.0198, respectively. Based on these results, there are very weak linear correlations between the LiDAR data heights and height differences for all DEMs implied. A satellite-based DEM's vertical accuracy is usually affected by elevation, with high areas being less accurate than low areas. However, LiDAR elevations do not have a systematic effect on DEM performance in the sub-figures of Figure 26. The weak linear correlation is due to the extreme influence of overrepresented height.

3.3.3.2 Absolute height differences in area (A)

Statistical results for the height difference between the DEMs heights and the ground levelling data heights in the area (A) are presented in Table 14, while scatter plots of elevation changes are given in Figure 27.

Table 14: Absolute height difference over area (A)

	LiDAR	AW3D30	SRTM	ASTER	TanDEM-X	MERIT
N	53	53	53	53	53	53
Min (m)	-5.10	-5.10	-4.90	3.90	-7.16	-2.2
Max (m)	25.70	67.10	64.10	75.10	70.92	66.11
Mean (m)	2.18	4.50	7.60	15.62	8.19	9.48
STDV (±m)	4.37	11.15	12.14	11.59	13.16	11.86

The statistical parameters in Table 14 indicate that the LiDAR achieves better absolute vertical accuracy compared to all other DEMs and is followed by the AW3D30, ASTER, MERIT, SRTM, and TanDEM-X, respectively. From these results, all the satellite-based DEMs show the worst performance.

The original absolute vertical accuracy specification of the SRTM, ASTER, and MERIT is also within the expected vertical accuracy. The TanDEM-X and AW3D30 results are beyond the vertical accuracy specifications. The few numbers of ground levelling data points covering area (A) have resulted in poor statistics for all the DEMS, especially the TanDEM-X.

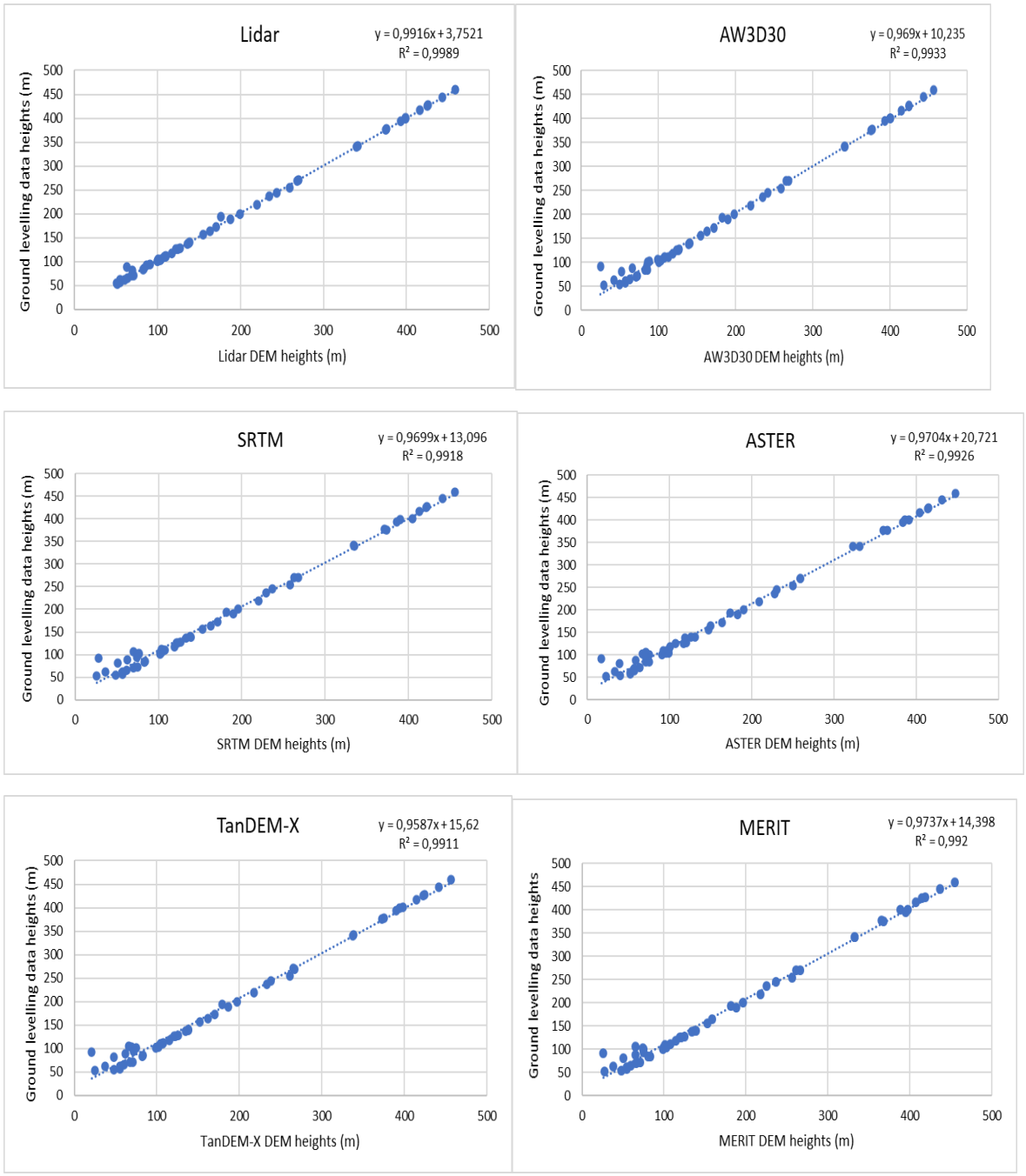

Figure 27: Scatter plots of ground levelling data heights against satellite-based DEM heights in area (A)

In all the scatter plots in Figure 27, $R^2 > 0.99$, and this indicates that there is approximately 99% correlation between the heights of DEMs with those of ground levelling. Based on the coefficient of determination, there is a very strong positive correlation. The DEM heights increase as LiDAR heights

increase. It can be seen, however, from the figure that the DEM which replicates the bare earth with better accuracy is the LiDAR.

3.3.3.3 Relative height differences in each land use/cover in area (A)

The statistical results for the height difference in low land use/cover between the satellite-based DEMs and the LiDAR DEM grid points heights in the area (A) are presented in Table 15. In low land use/cover, the AW3D30 still achieves better relative vertical accuracy compared to all other DEMs, followed by the TanDEM-X, SRTM, MERIT, and ASTER, respectively.

Table 15: Relative height difference in low land use/cover over area (A)

	AW3D30	SRTM	ASTER	TanDEM-X	MERIT
N	9091	9091	9091	9091	9091
Min (m)	-36.00	-52.00	-48.00	-69.12	-52.95
Max (m)	41.00	53.00	63.00	61.82	57.01
Mean (m)	-1.94	-1.34	6.77	0.26	-0.87
STDV (±m)	2.67	3.70	5.49	2.95	4.44

The statistical results for the height difference in medium land use/cover between the satellite-based DEMs and the LiDAR DEM grid points heights in the area (A) are presented in Table 16. In medium land use/cover, the TanDEM-X achieves better relative vertical accuracy compared to all other DEMs, followed by the AW3D30, SRTM, MERIT, and ASTER, respectively.

Table 16: Relative height difference in medium land use/cover over area (A)

	AW3D30	SRTM	ASTER	TanDEM-X	MERIT
N	19116	19116	19116	19116	19116
Min (m)	-18.00	-15.00	-26.00	-17.04	-21.19
Max (m)	21.00	16.00	31.00	18.02	18.71
Mean (m)	-1.58	-1.33	8.08	0.42	-0.44
STDV (±m)	1.52	2.16	4.65	1.21	2.98

The statistical results for the height difference in high land use/cover between the satellite-based DEMs and the LiDAR DEM grid points heights in the area (A) are presented in Table 17. In high land use/cover, the AW3D30 achieves better relative vertical accuracy compared to all other DEMs, and is followed by the TanDEM-X, SRTM, MERIT, and ASTER, respectively.

Table 17: Relative height difference in high land use/cover over area (A)

	AW3D30	SRTM	ASTER	TanDEM-X	MERIT
N	13599	13599	13599	13599	13599
Min (m)	-26.00	-25.00	-27.00	-73.12	-34.22
Max (m)	26.00	36.00	35.00	47.88	35.94
Mean (m)	-2.00	-0.96	6.60	0.37	-0.88
STDV (±m)	2.70	3.40	4.64	2.91	3.76

3.3.3.4 Influences of elevation, slope, aspect, and surface roughness change on heights errors over area (A)

Height error correlation with elevation

The variation of the standard deviation of the differences between LiDAR and satellite-based DEM heights with the elevation over the area (A) are presented in Figure 28, while scatter plots of mean values are given in Figure 29. In Figure 28, an increase in the elevation results in an increase in the standard deviations of all the DEM's. From these results, it can be deduced that the vertical accuracies of these DEMs relative to the LiDAR decreases with an increase in elevation. The ASTER has the lowest vertical accuracy compared to all the DEMs in the range (< 236 m), followed by the SRTM in elevation (5 – 28 m) and MERIT in the range (28 -236 m). At elevations (> 236 m), the MERIT has very low accuracy compared to all other DEMs.

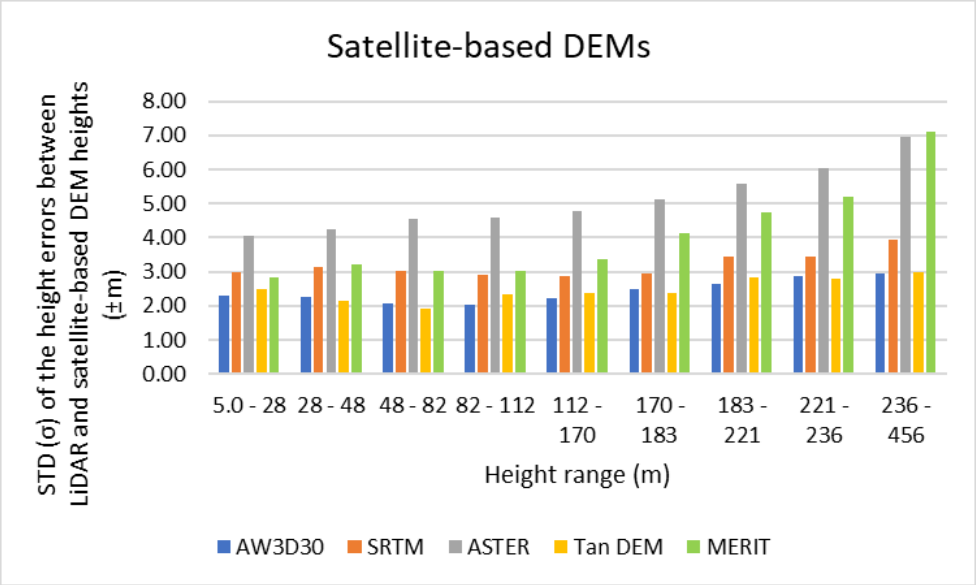

Figure 28: Variation of standard deviation of the height errors between LiDAR and DEMs heights with elevation change (m) over area (A)

In all the scatter plots in Figure 29, the ASTER has the highest mean height differences in all elevation ranges compared to all other DEMs, which indicates that in area (A), ASTER has the largest offsets from LiDAR. The offsets are positive, indicating that ASTER generally underestimates LiDAR heights. The AW3D30 and SRTM show negative offsets in all ranges, indicating an overestimation of LiDAR heights. TanDEM-X offsets are significantly smaller than the offsets of AW3D30, SRTM, and MERIT in elevation ranges (5 - 221 m) and (> 236 m). In elevation ranges (< 28 m), the TanDEM-X overestimates LiDAR heights, and in elevation ranges (> 28 m), it underestimates. The MERIT overestimates LiDAR heights at elevations (< 236 m); for values above (> 236 m) it underestimates.

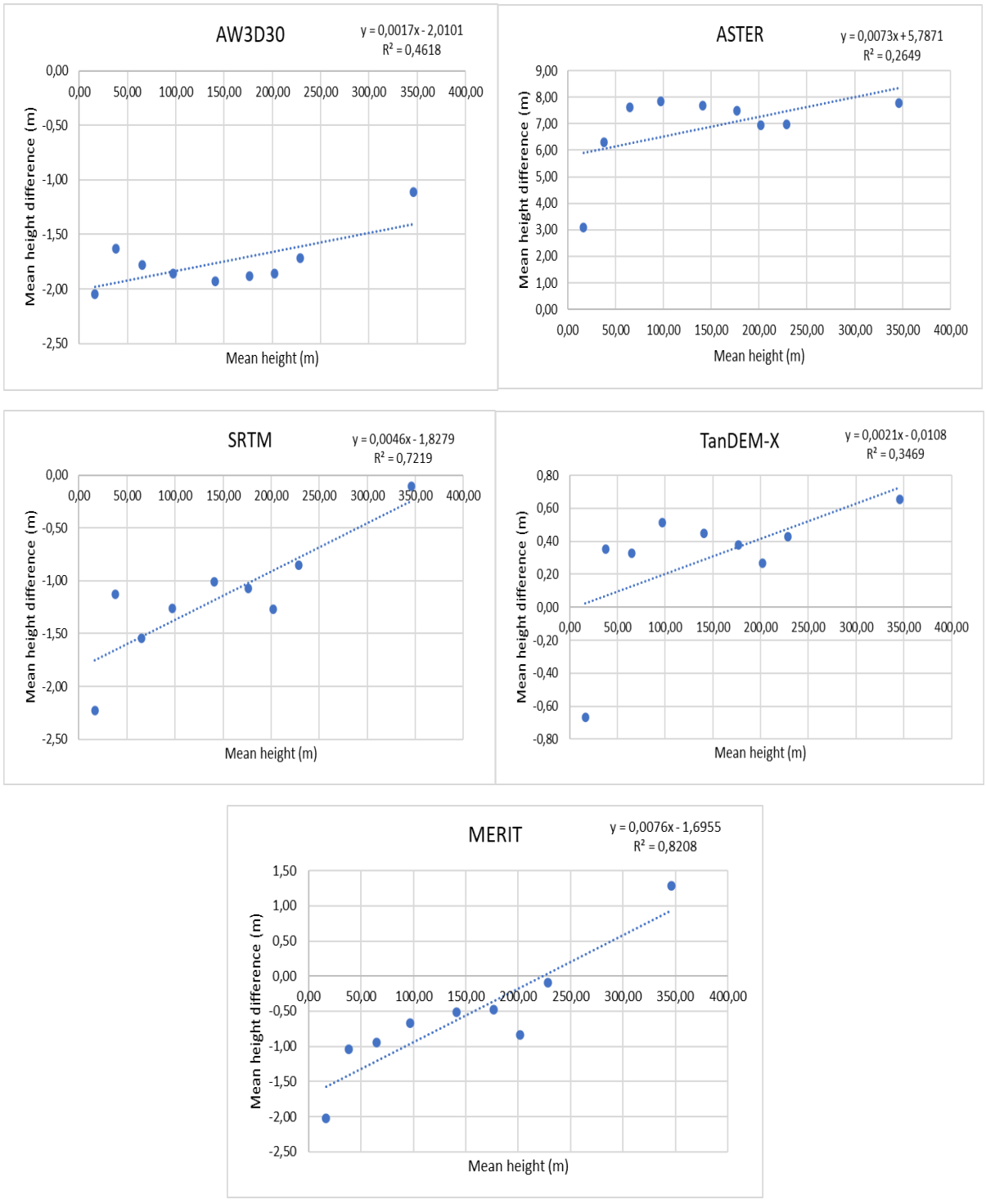

Figure 29: Scatter plots for mean height differences against mean of the height (m) over area (A)

Height error correlation with slope

The variation of the standard deviation of the differences between LiDAR and satellite-based DEM heights with slope over the area(A) are presented in Figure 30, while scatter plots of mean values are given in Figure 31. In Figure 30, an increase in slope results in an increase in the standard deviations of all the DEMs. From these results, it can be deduced that the vertical accuracies of these DEMs relative to the LiDAR decreases with an increase in slope. The ASTER has the lowest vertical accuracy

compared to all the DEMs in all ranges, followed by the SRTM in slope (0° - 3.9°) and MERIT in slope (> 3.9°).

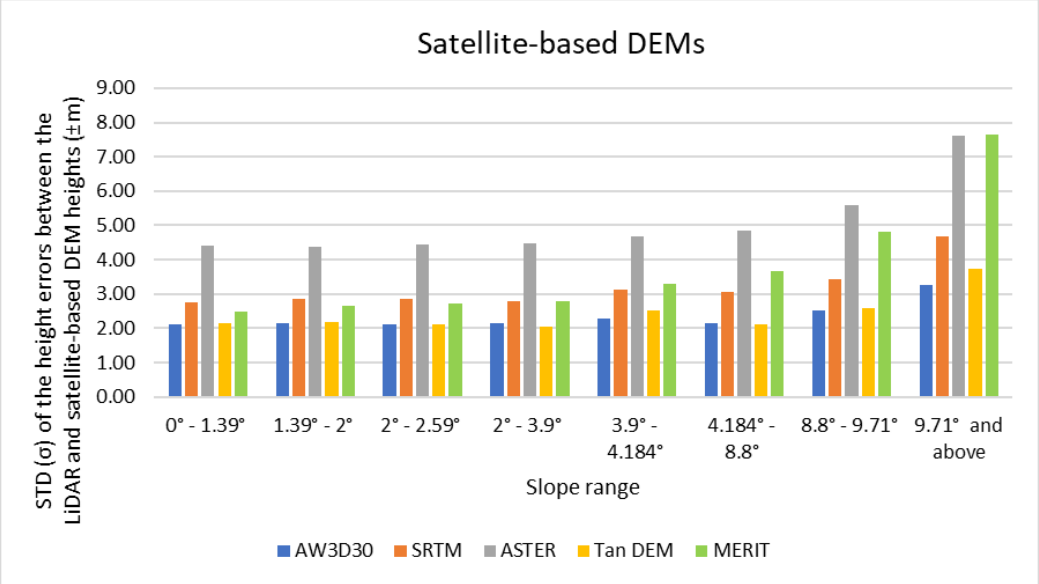

Figure 30: Variation of standard deviation of the height errors between LiDAR and DEMs heights with slope (°) over area (A)

In all the scatter plots in Figure 31, the ASTER has the highest mean height differences in all slope ranges compared to all other DEMs, which indicates that in area (A), ASTER has the largest offsets from LiDAR. The offsets are positive, indicating that ASTER underestimates LiDAR heights. The AW3D30 and SRTM show negative offsets in all ranges, indicating an overestimation of LiDAR heights. The TanDEM-X underestimates LiDAR heights in all ranges. The MERIT overestimates LiDAR heights at slope (< 9.71°); for values (> 9.71°) it underestimates. The TanDEM-X offsets are significantly smaller than the offsets of AW3D30, SRTM, and MERIT in range (< 9.71°).

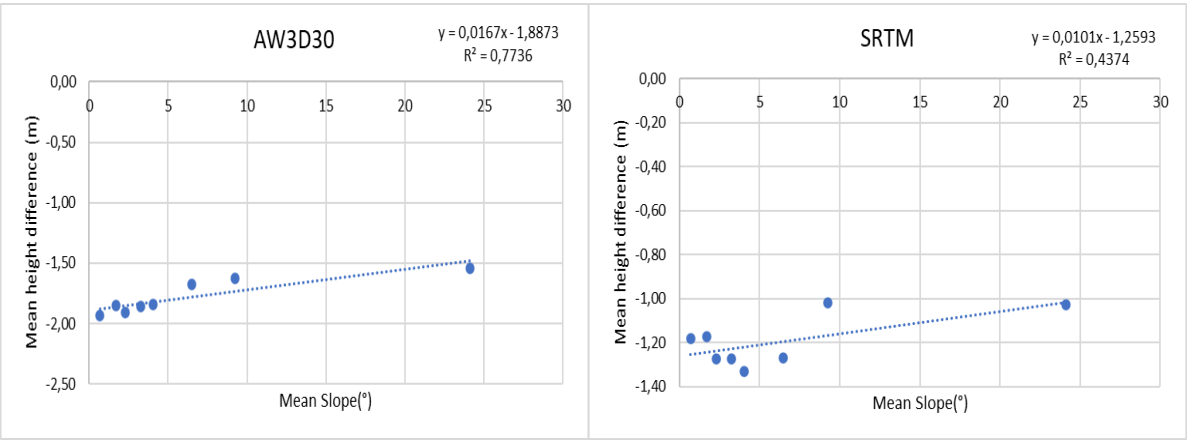

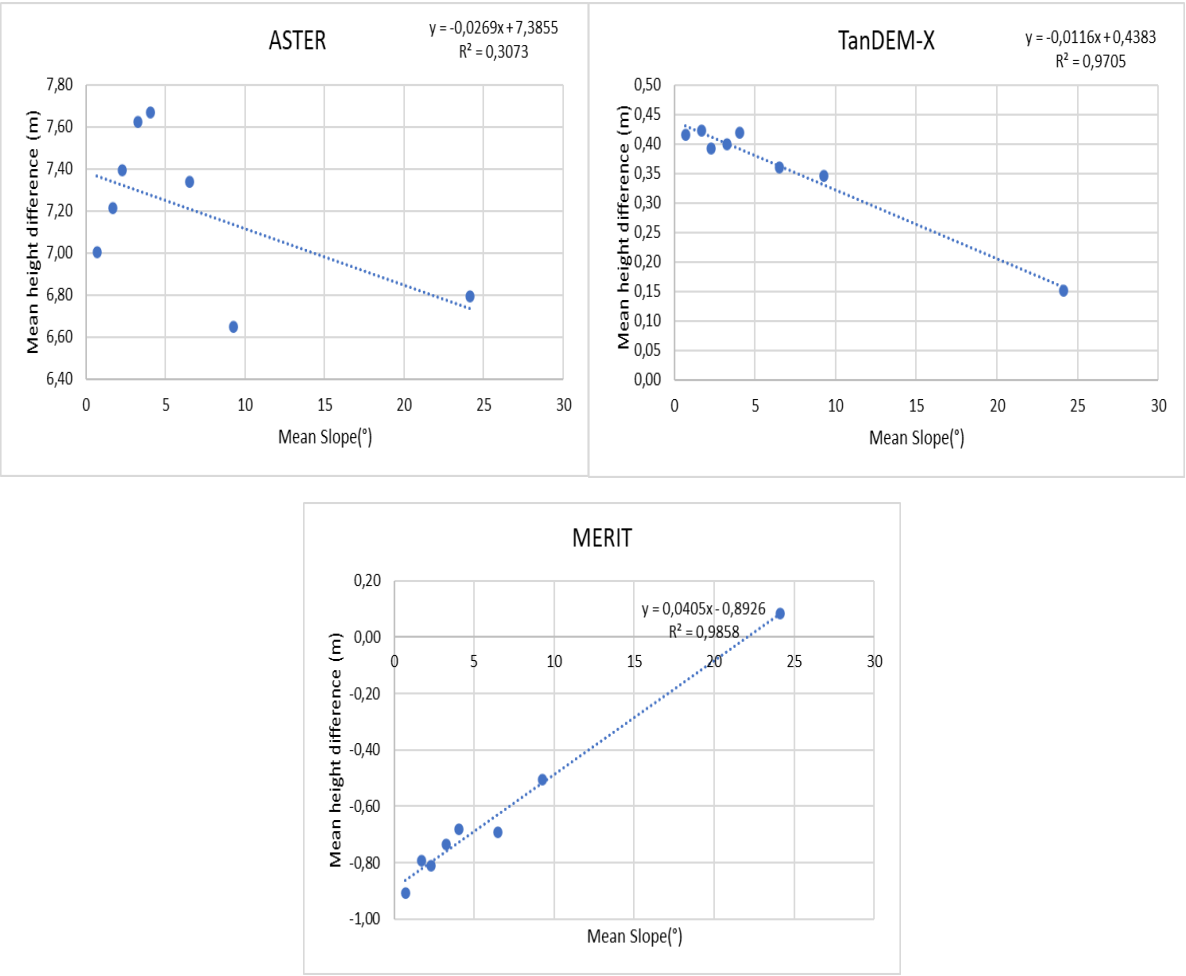

Figure 31: Scatter plots for mean height differences against mean slope (°) over area (A)

Height error correlation with surface roughness

The variation of standard deviation of the differences between LiDAR and satellite-based DEM heights with surface roughness over area(A) are presented in Figure 32 while scatter plots of mean values are given in Figure 33. In Figure 32, an increase in surface roughness results in an increase in the standard deviations of all the DEM's. From these results, it can be deduced that the vertical accuracies of these DEMs relative to the LiDAR decreases with an increase in surface roughness. The ASTER has the lowest vertical accuracy compared to all the DEMs in the range (0 - 4.807), followed by the SRTM in the range (0 - 1.523) and MERIT in (> 1.523).

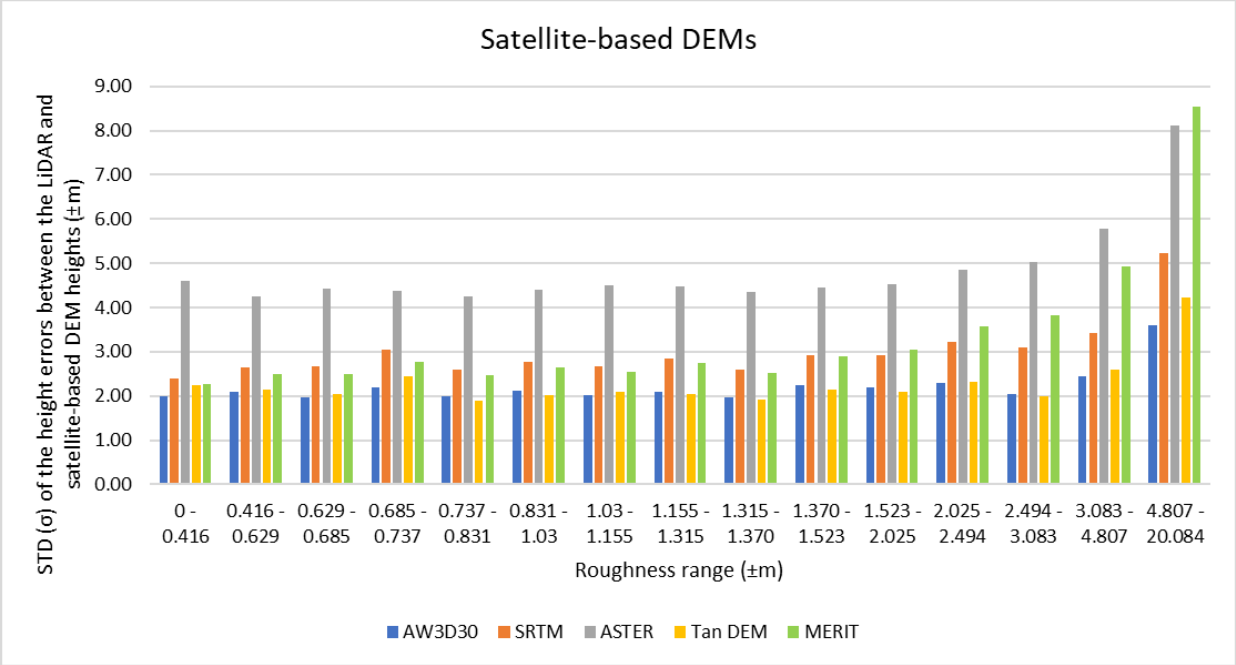

Figure 32: Variation of standard deviation of the height errors between LiDAR and DEMs heights with roughness (± m) over area (A)

In all the scatter plots in Figure 33, the ASTER has the highest mean height differences in all surface roughness ranges compared to all other DEMs, which indicates that in area (A), ASTER has the largest offsets from LiDAR. The offsets are positive, indicating that ASTER generally underestimates LiDAR heights. The AW3D30 and SRTM show negative offsets in all the ranges, indicating an overestimation of LiDAR heights. The TanDEM-X underestimates LiDAR heights in all ranges. The MERIT overestimates LiDAR heights at surface roughness (< 4.807); for values (> 4.807) it underestimates. The TanDEM-X offsets are significantly smaller than the offsets of the AW3D30, SRTM, and MERIT in ranges (0 – 3,083) and (> 4.807).

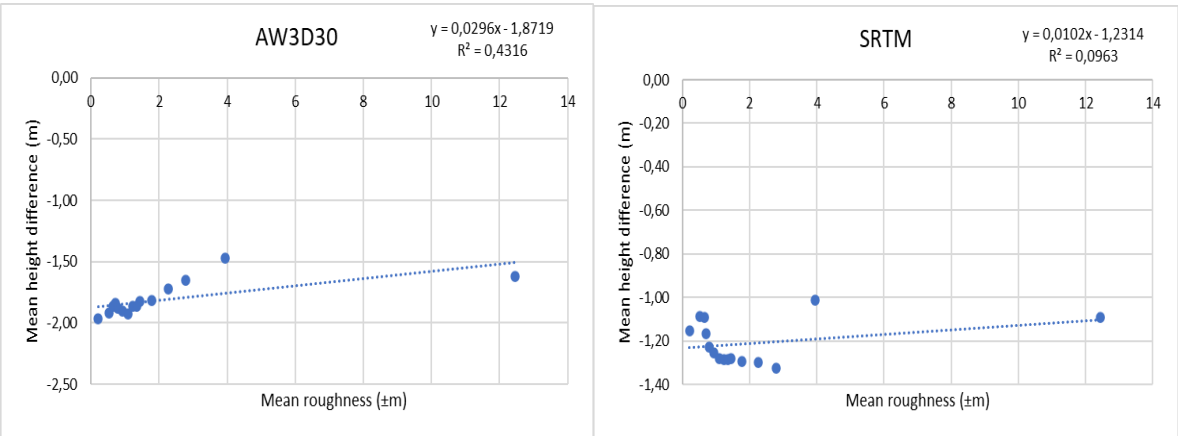

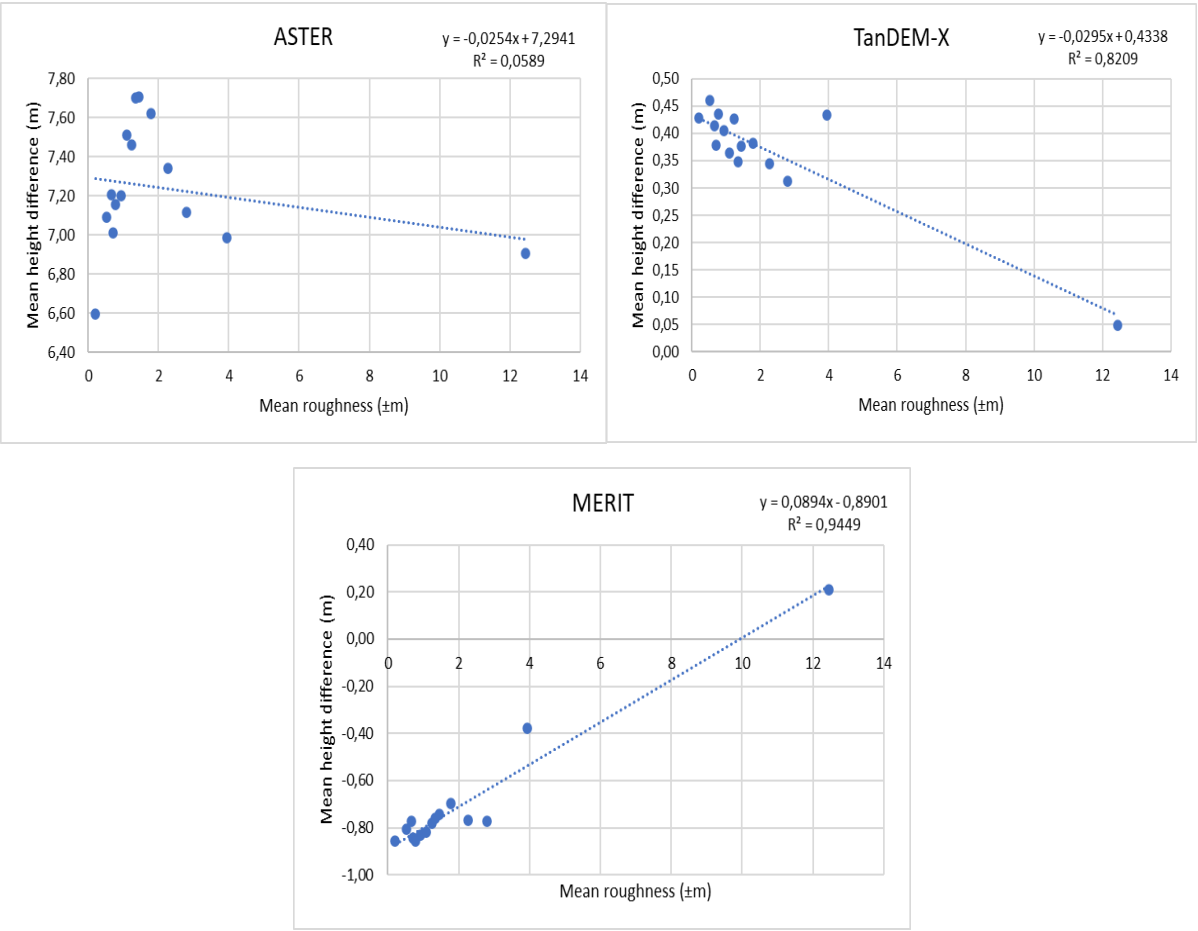

Figure 33: Scatter plots for mean height differences against mean roughness (± m) area (A)

Height error correlation with aspect

The variation of the standard deviation of the differences between LiDAR and satellite-based DEM heights with aspect over the area(A) are presented in Figure 34 while scatter plots of mean values are given in Figure 35. In Figure 34, it can be observed that a change in aspect does not provide a clear pattern to indicate what happens in the standard deviations of the DEM's height differences. However, the more an area is flat, the better the vertical accuracies of the AW3D30, MERIT, and SRTM and this can also be observed in the aspect range (-1– 0), which is classified as flat. The ASTER has the lowest vertical accuracy compared to all the DEMs in all ranges, followed by the MERIT and SRTM.

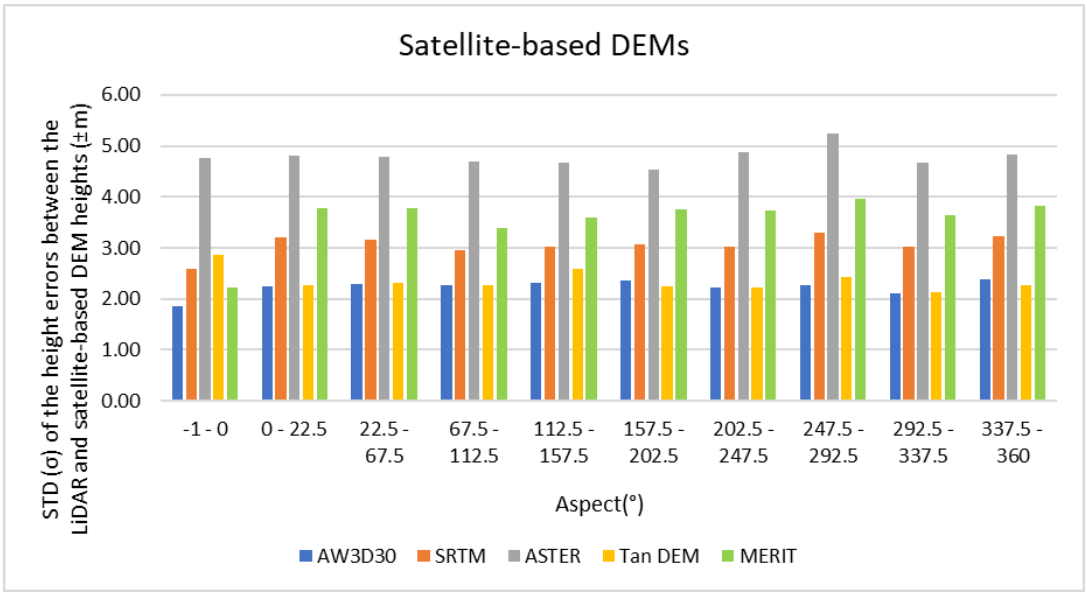

Figure 34: Variation of standard deviation of the height errors between LiDAR and DEMs heights with aspect (°) over area(A)

In all the scatter plots in Figure 35, the ASTER has the highest mean height differences in all aspect ranges compared to all other DEMs, which indicates that in area (A), ASTER has the largest offsets from LiDAR. The offsets are positive, indicating that ASTER generally underestimates LiDAR heights. The AW3D30, SRTM, and MERIT show negative offsets in all the ranges, indicating a general overestimation of LiDAR heights. The TanDEM-X underestimates LiDAR heights in all ranges. The TanDEM-X offsets are significantly smaller relative to the AW3D30, SRTM, and MERIT offsets.

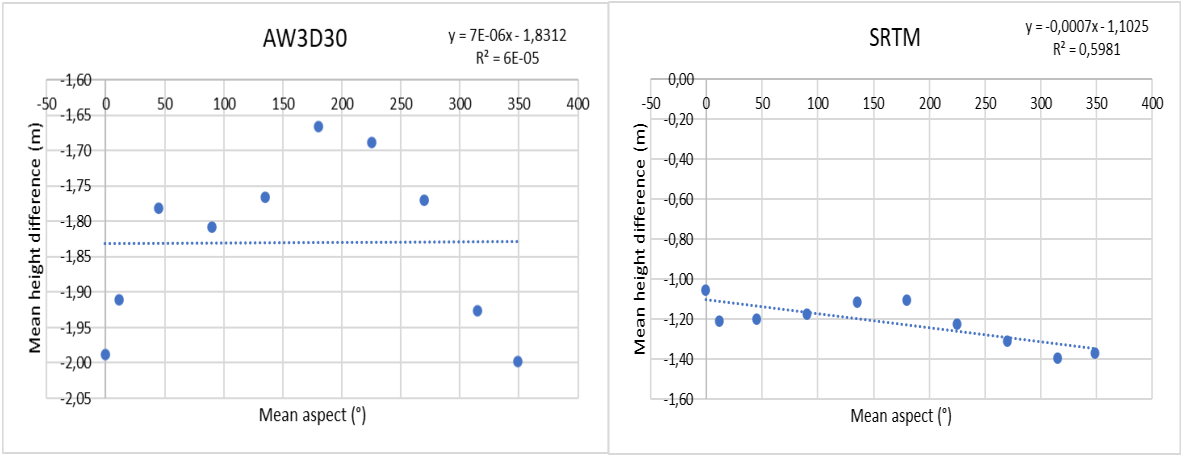

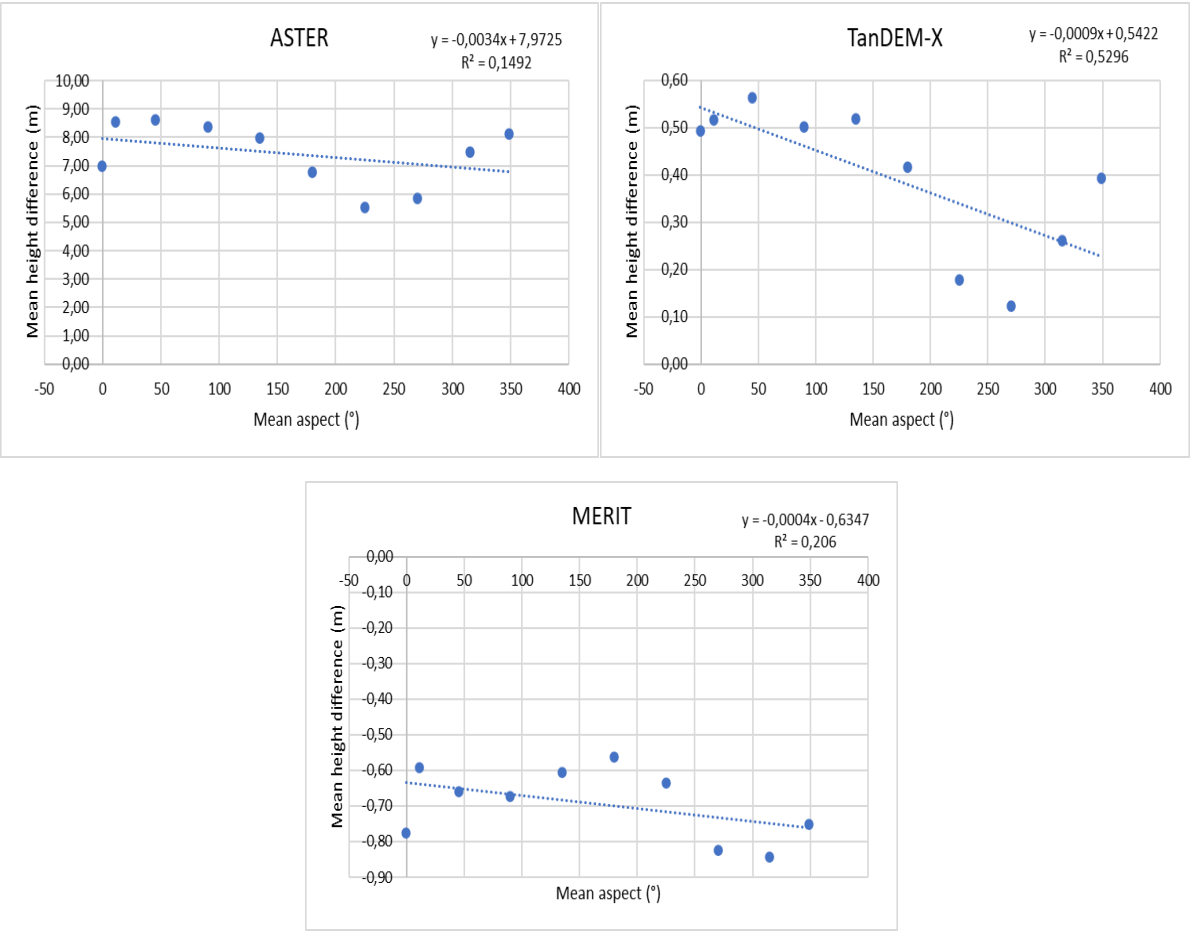

Figure 35: Scatter plots for mean height differences against mean aspect (°) over area (A)

Coefficients of correlation for the geomorphological factors

The coefficients of correlation for the geomorphological factors over area (A) from Figures 29, 31, 33, and 35 are summarised in Table 18.

Table 18: Coefficients of correlation for the geomorphological factors in % over area (A)

	LiDAR			
	mean height	mean slope	mean roughness	mean aspect
AW3D30	67.96	87.95	65.70	-0.77
SRTM	84.96	66.14	31.03	-77.34
ASTER	51.47	-55.43	-24.27	-38.63
TanDEM-X	58.90	-98.51	-90.60	-72.77
MERIT	90.60	99.29	97.21	-45.39

The mean aspect against the mean height difference shows a relatively weaker (negative) linear correlation for the AW3D30 and ASTER while the MERIT shows a moderate(negative) correlation. The mean roughness against the mean height difference for SRTM and ASTER shows a weak (positive) and weak(negative) correlation, respectively. The mean height against the mean height difference for ASTER and TanDEM-X shows a moderate (positive) correlation. The rest of the correlation coefficients range from strong to very strong.

3.3.3.5 Influence of elevation, slope, aspect, and surface roughness on heights errors in different land use/cover over area (A)

Height error correlation with elevation, slope, aspect, and surface roughness in low land use/cover over area (A)

The results for variation of standard deviations of the differences between LiDAR and satellite-based DEM heights with elevation over area (A) in low land use/cover are presented in Figure 36, while scatter plots of mean values are given in Figure 37. In Figure 36, an increase in the elevation results in an increase in the standard deviations of the ASTER and MERIT. From these results, it can be deduced that the vertical accuracies of these DEMs relative to the LiDAR decreases with an increase in elevation in low land use/cover. The TanDEM-X, SRTM, and AW3D30 indicate a variation as elevation increases. The ASTER, MERIT, and SRTM indicate very low accuracies in all the ranges compared to the AW3D30 and TanDEM-X.

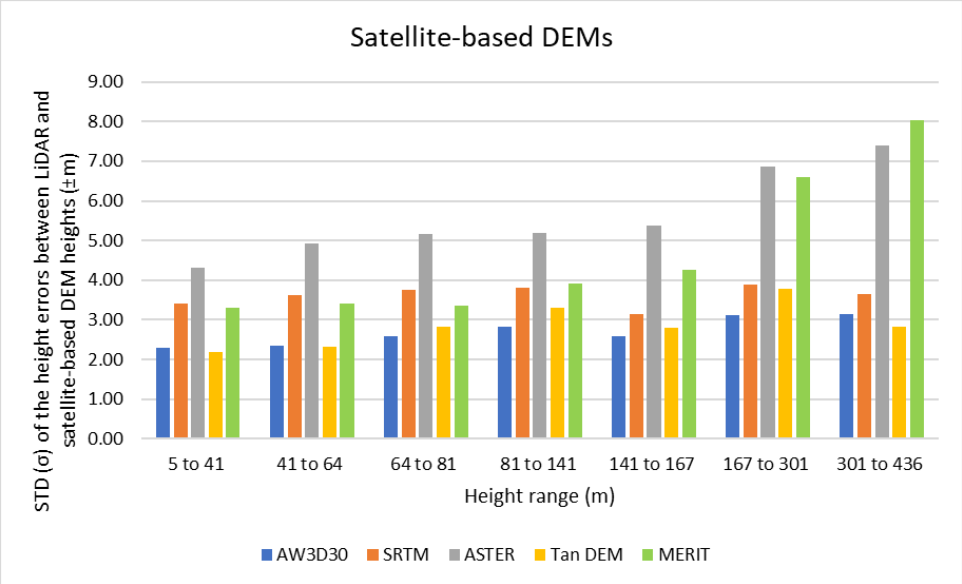

Figure 36: Variation of standard deviation of the height errors between LiDAR and DEMs heights with elevation (m) in low land use/cover over area (A)

In all the scatter plots in Figure 37, the ASTER has the highest mean height differences in all elevation ranges compared to all other DEMs, which indicates that in low land use/cover of area (A), ASTER has the largest offsets from LiDAR. The offsets are positive, indicating that ASTER generally underestimates LiDAR heights. The AW3D30 shows negative offsets in all ranges, indicating an overestimation of LiDAR heights. In elevation ranges (< 41 m), the TanDEM-X overestimates LiDAR heights, and in elevation ranges (> 41 m), it underestimates. The MERIT and SRTM overestimate LiDAR heights at elevations (< 301 m); for values (> 301 m) they underestimate. TanDEM-X offsets are significantly smaller relative to the AW3D30, SRTM, and MERIT offsets in all ranges.

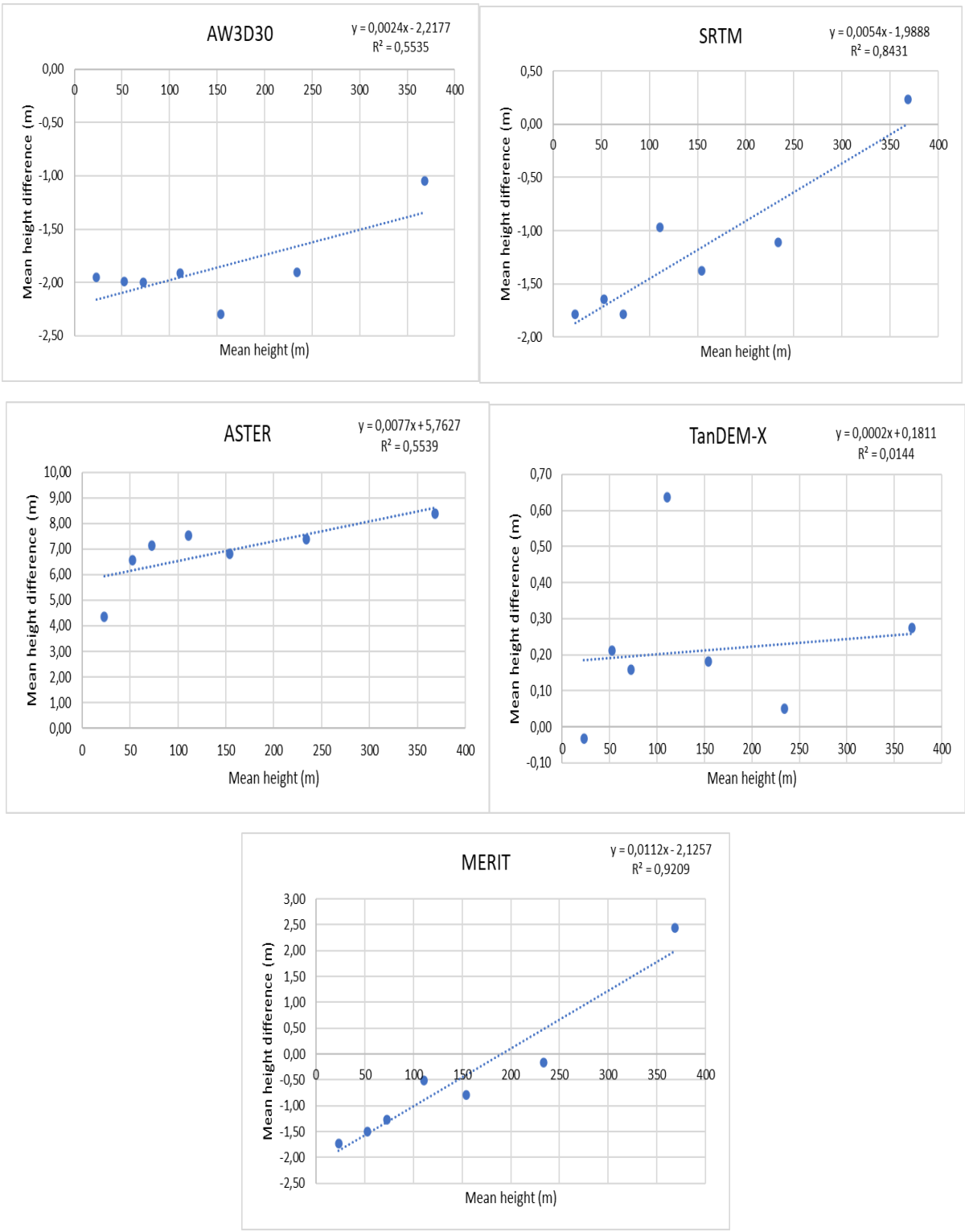

Figure 37: Scatter plots for mean height differences against mean height (m) in low land use/cover over area (A)

The results for variation of the standard deviations of the differences between LiDAR and satellite-based DEM heights with slope over the area (A) in low land use/cover are presented in Figure 38, while scatter plots of mean values are given in Figure 39. In Figure 38, an increase in the slope results in an increase in the standard deviations of the ASTER, SRTM, and MERIT. From these results, it can be deduced that the vertical accuracies of these DEMs relative to the LiDAR decreases with an increase

in slope in low land use/cover. The TanDEM-X and AW3D30 indicate a variation as the slope increases. The ASTER, MERIT, and SRTM indicate very low accuracies in all the ranges compared to the AW3D30 and TanDEM-X.

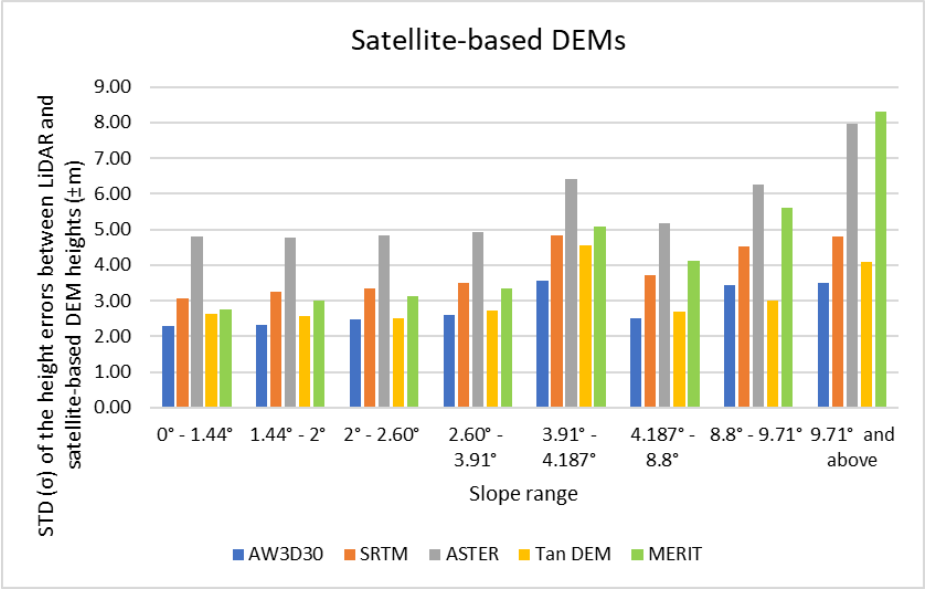

Figure 38: Variation of standard deviation of the height errors between LiDAR and DEMs heights with slope (°) in low land use/cover over area (A)

In all the scatter plots in Figure 39, the ASTER has the highest mean height differences in all slope ranges compared to all other DEMs, which indicates that in low land use/cover of area (A), ASTER has the largest offsets from LiDAR. The offsets are positive, indicating that ASTER generally underestimates LiDAR heights. The AW3D30 and SRTM show negative offsets in all ranges, indicating a general overestimation of LiDAR heights. In slope ranges (< 9.71°), the TanDEM-X underestimates LiDAR heights, and at slope ranges (> 9.71°) it overestimates. The MERIT overestimates LiDAR heights at slope (< 9.71°); for values (> 9.71°) it underestimates. TanDEM-X offsets are significantly smaller relative to the AW3D30, SRTM, and MERIT offsets in all ranges.

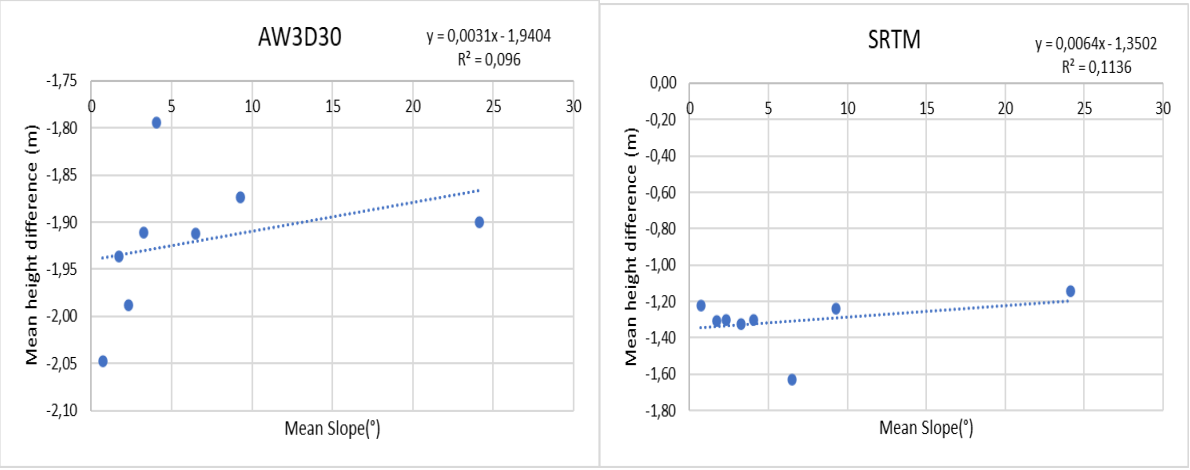

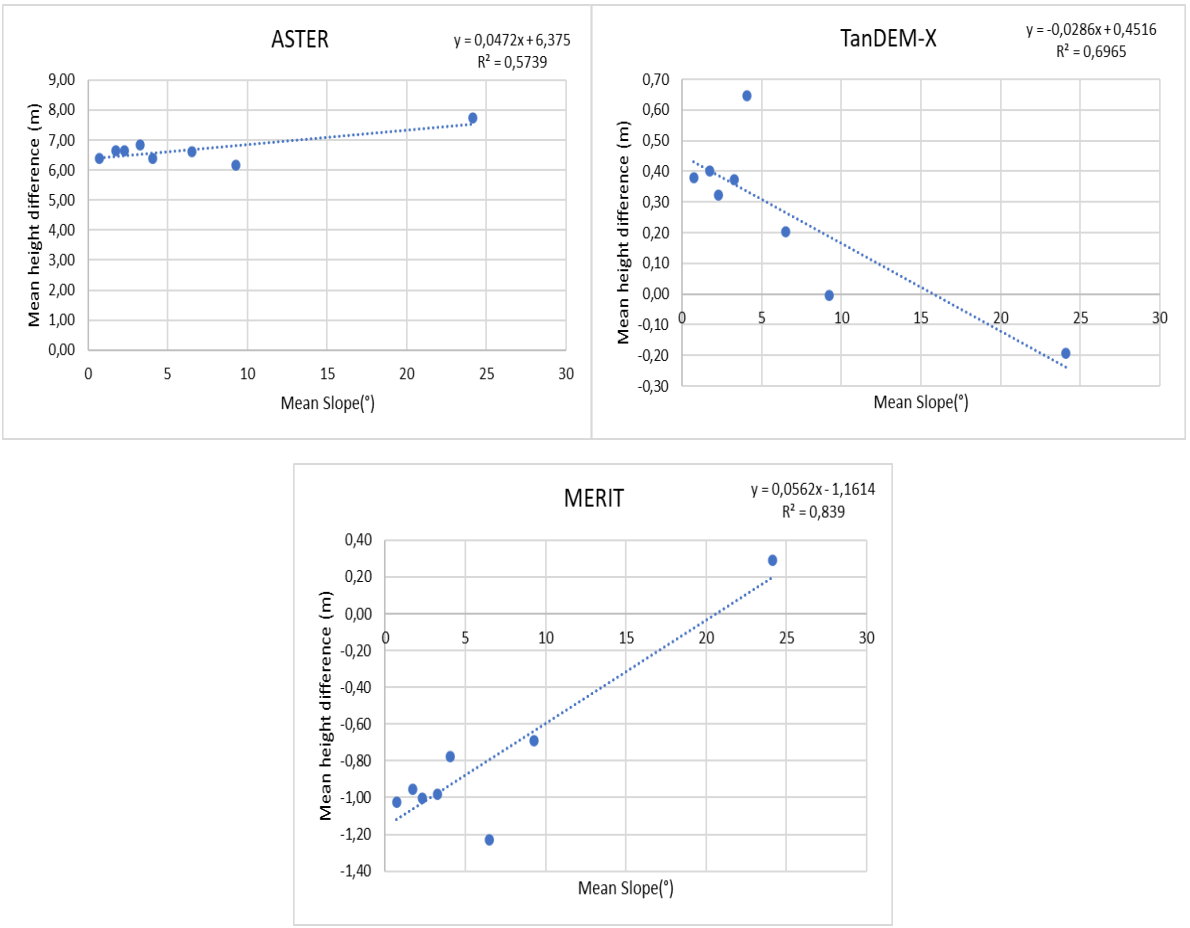

Figure 39: Scatter plots for mean height differences against mean slope (°) in low land use/cover over area (A)

The results for variation of the standard deviations of the differences between LiDAR and satellite-based DEM heights with surface roughness over the area (A) in low land use/cover are presented in Figure 40, while scatter plots of mean values are given in Figure 41. In Figure 40, all the DEMs have the largest standard deviations when the surface roughness (> 4.807). From these results, it can be deduced that the vertical accuracies of these DEMs relative to the LiDAR in areas with higher surface roughness in low land use/cover is very low. The ASTER, MERIT, and SRTM still indicate very low accuracies compared to the AW3D30 and TanDEM-X in almost all ranges.

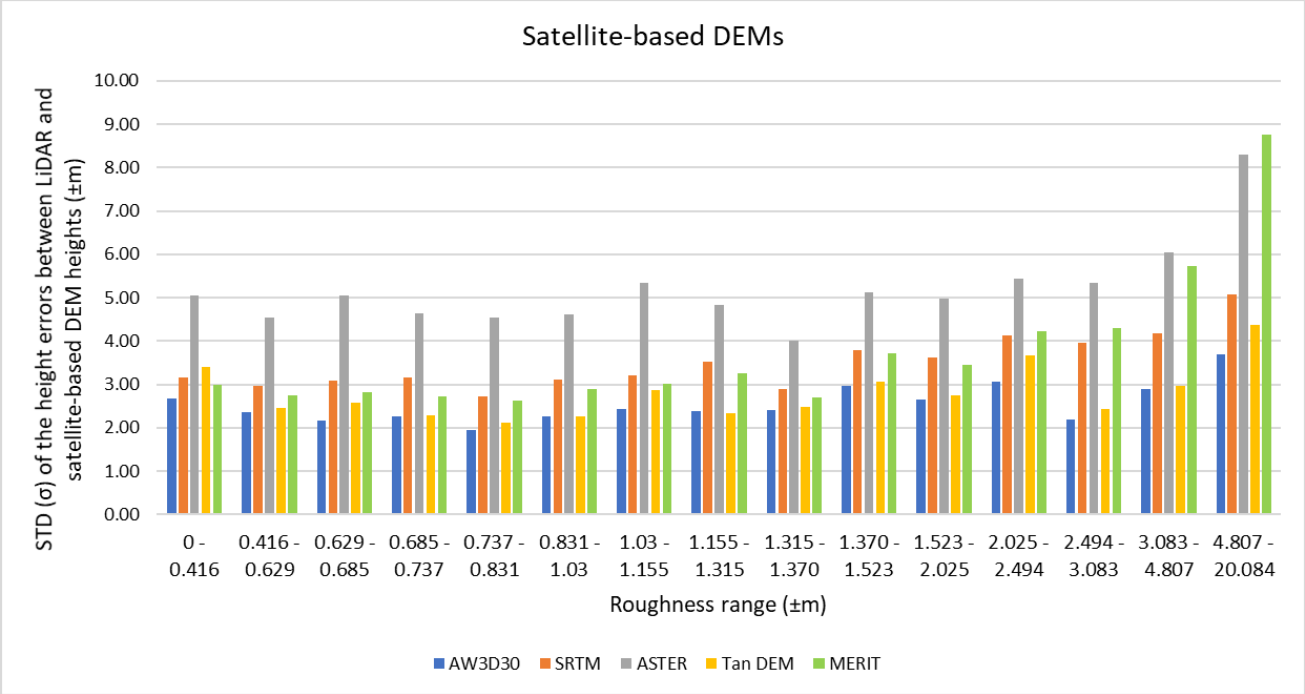

Figure 40: Variation of standard deviation of the height errors between LiDAR and DEMs heights with roughness (±m) in low land use/cover over area (A)

In all the scatter plots in Figure 41, the ASTER has the highest mean height differences in all surface roughness ranges compared to all other DEMs, which indicates that in low land use/cover of area (A), ASTER has the largest offsets from LiDAR. The offsets are positive, indicating that ASTER generally underestimates LiDAR heights. The AW3D30 and SRTM show negative offsets in all ranges, indicating a general overestimation of LiDAR heights. In ranges (< 4.807), the TanDEM-X underestimates LiDAR heights, and in ranges (> 4.807) it overestimates. The MERIT overestimates LiDAR heights at surface roughness (< 4.807); for values (> 4.807) it underestimates. TanDEM-X offsets are significantly smaller relative to the AW3D30, SRTM, and MERIT offsets in all ranges.

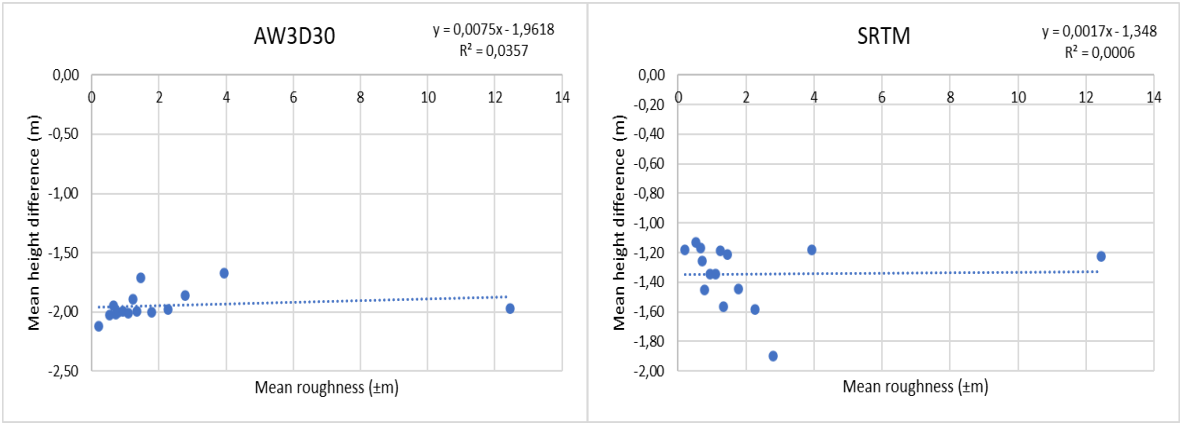

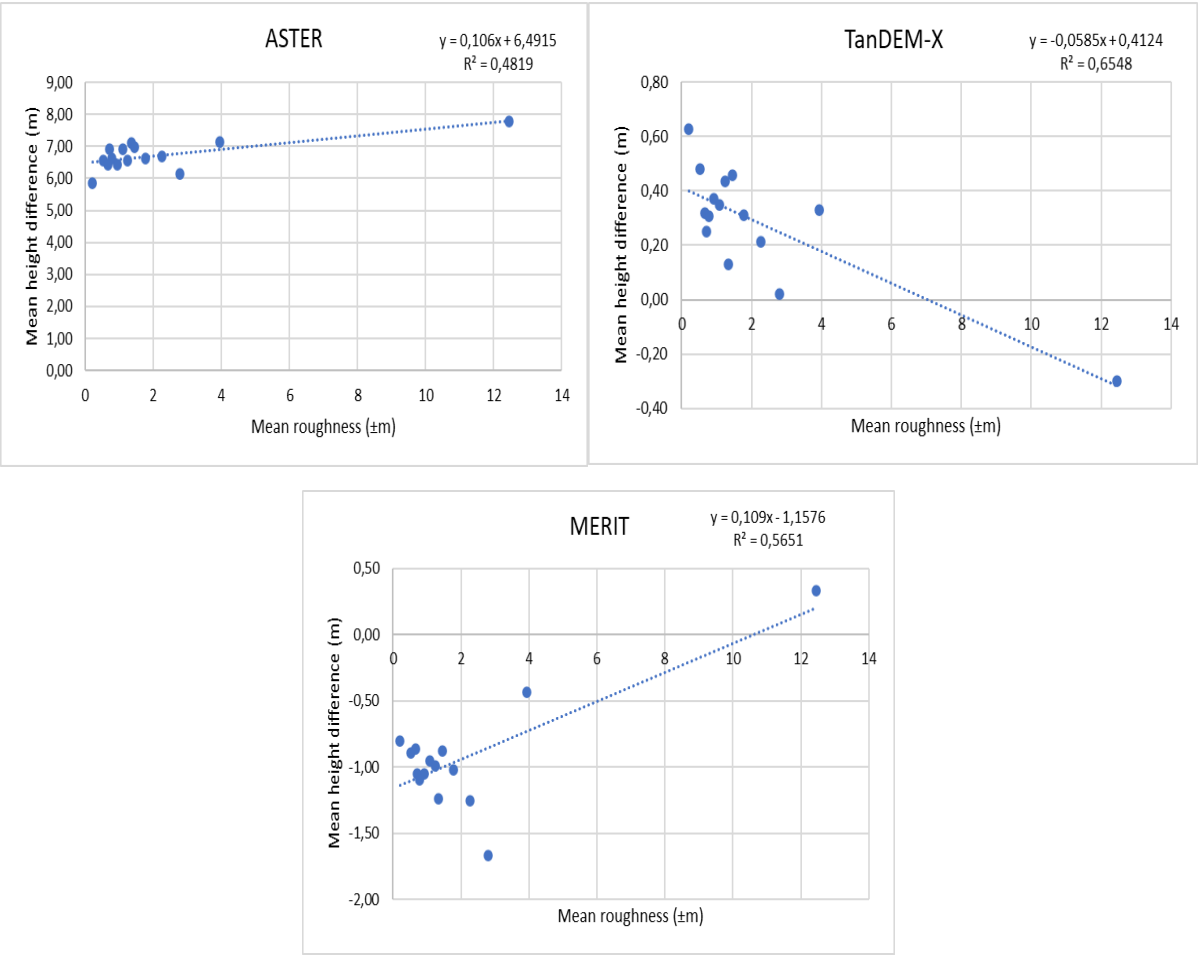

Figure 41: Scatter plots for mean height differences against mean roughness (±m) in low land use/cover over area (A)

The results for variation of the standard deviations of the differences between LiDAR and satellite-based DEM heights with aspect over the area (A) in low land use/cover are presented in Figure 42, while scatter plots of mean values are given in Figure 43. In Figure 42, as aspect changes, there is a variation in standard deviations of the DEM's. However, the more an area is flat, the better the vertical accuracies of the AW3D30, MERIT, SRTM, and ASTER. This can also be observed in the (-1 – 0) aspect range, which is classified as flat. The ASTER, MERIT, and SRTM still indicate very low accuracies compared to the AW3D30 and TanDEM-X, in almost all ranges.

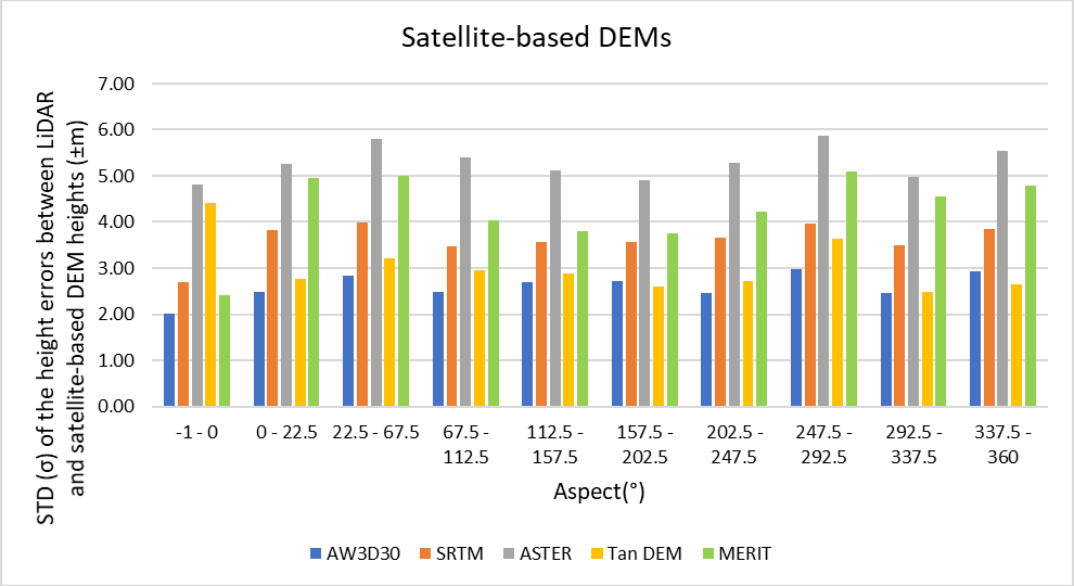

Figure 42: Variation of standard deviation of the height errors between LiDAR and DEMs heights with aspect (°) in low land use/cover over area (A)

In all the scatter plots in Figure 43, the ASTER has the highest mean height differences in all aspect ranges compared to all other DEMs, which indicates that in low land use/cover of area (A), ASTER has the largest offsets from LiDAR. The offsets are positive, indicating that ASTER generally underestimates LiDAR heights. The AW3D30, SRTM, and MERIT show negative offsets in all ranges, indicating a general overestimation of LiDAR heights. In ranges (< 247.5° and > 292.5°), the TanDEM-X underestimates LiDAR heights, and in ranges (247.5° - 292.5°) it overestimates. The TanDEM-X offsets are significantly smaller than the offsets of the AW3D30, SRTM, and MERIT in range (> 0°).

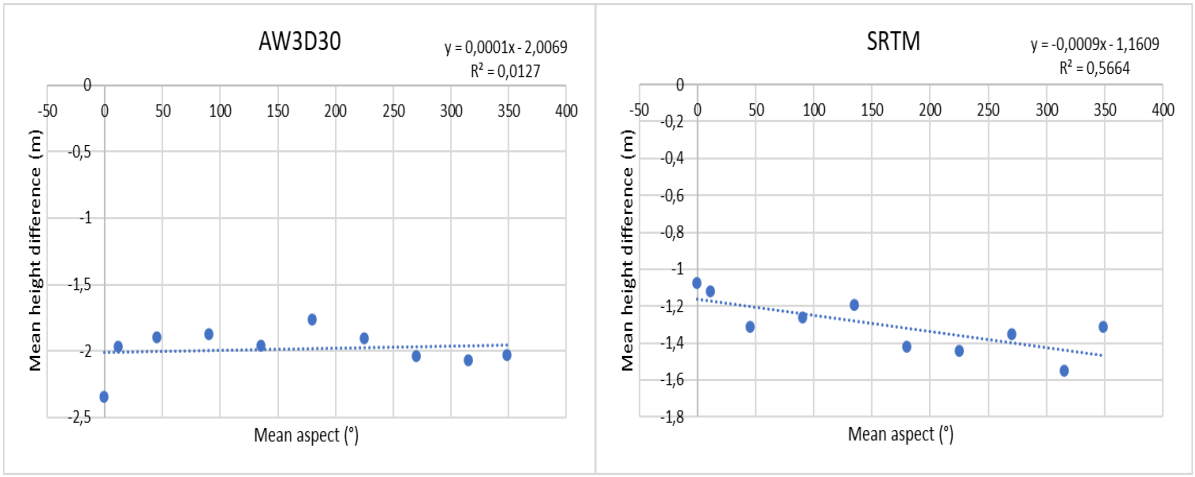

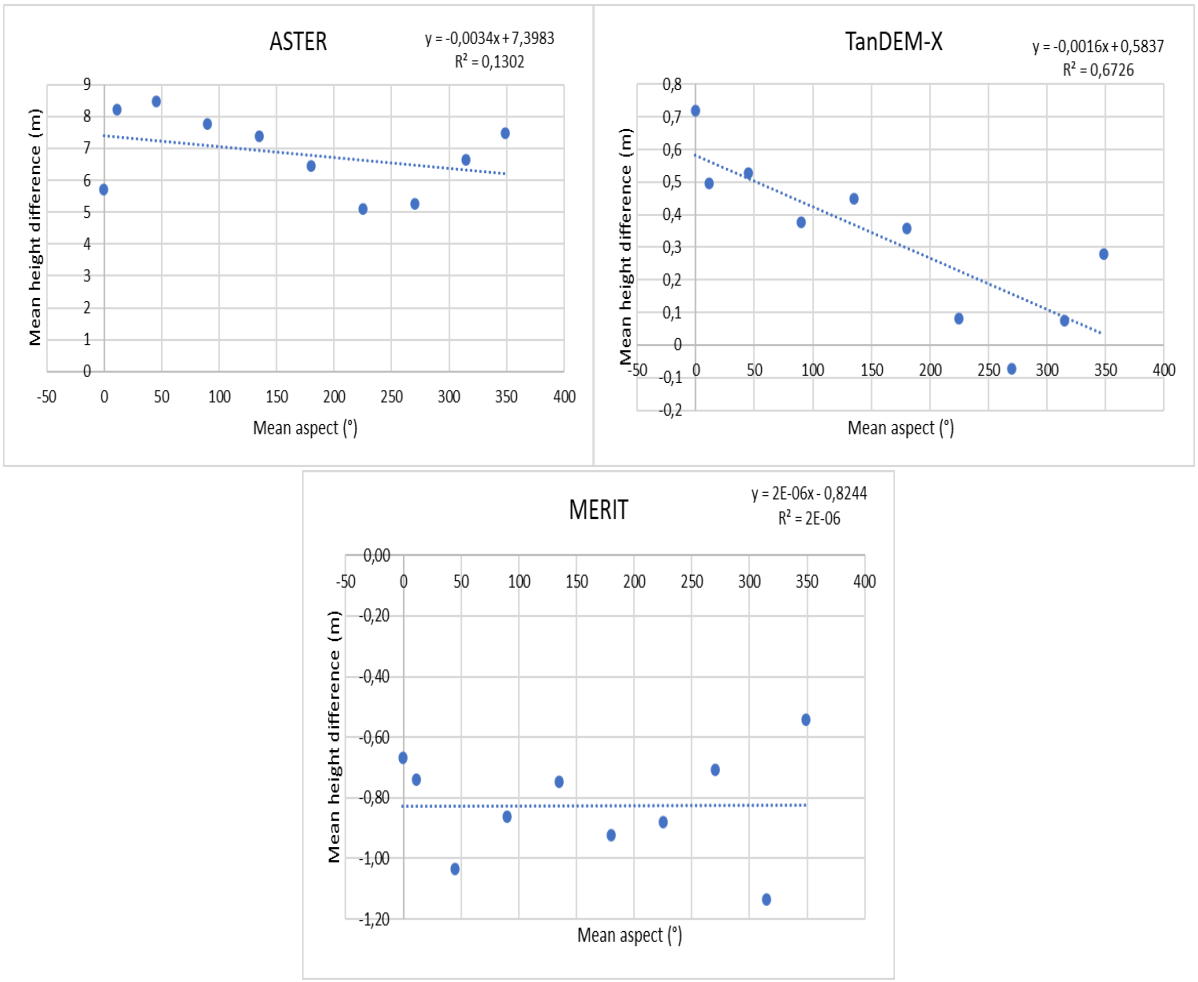

Figure 43: Scatter plots for mean height differences against mean aspect (°) in low land use/cover over area (A)

The coefficients of correlation for the geomorphological factors in low land use/cover over area (A) from Figures 37, 39, 41, and 43 are summarised in Table 19.

Table 19: Coefficients of correlation for the geomorphological factors in % over area (A) in low land use/cover

	Lidar in low land use/cover			
	mean height	mean slope	mean roughness	mean aspect
AW3D30	74.40	30.98	18.89	11.27
SRTM	91.82	33.70	2.45	-75.26
ASTER	74.42	75.76	69.42	-36.08
TanDEM-X	12.00	-83.46	-80.92	-82.01
MERIT	95.96	91.60	75.17	0.14

The mean aspect against the mean height difference shows a weak(positive) linear correlation for the AW3D30 and MERIT, while the ASTER shows a weak(negative) correlation. The mean roughness against the mean height difference for SRTM and AW3D30 shows a weak(positive) correlation. The

mean slope against the mean height difference for AW3D30 and SRTM shows a weak(positive) linear correlation. The mean height against the mean height difference for TanDEM-X shows a weak(positive) correlation. The rest of the correlation coefficients range from strong to very strong.

Height error correlation with elevation, slope, aspect, and surface roughness in medium land use/cover over area (A)

The results for variation of the standard deviation of the differences between LiDAR and satellite-based DEM heights with an elevation over the area (A) in medium land use/cover are presented in Figure 44, while scatter plots of mean values are given in Figure 45. In Figure 44, an increase in the elevation results in an increase in the standard deviations of all the DEMs. From these results, it can be deduced that the vertical accuracies of these DEMs relative to the LiDAR decreases with an increase in elevation in medium land use/cover. The ASTER, SRTM, and MERIT have low vertical accuracies compared to the AW3D30 and TanDEM-X in all ranges.

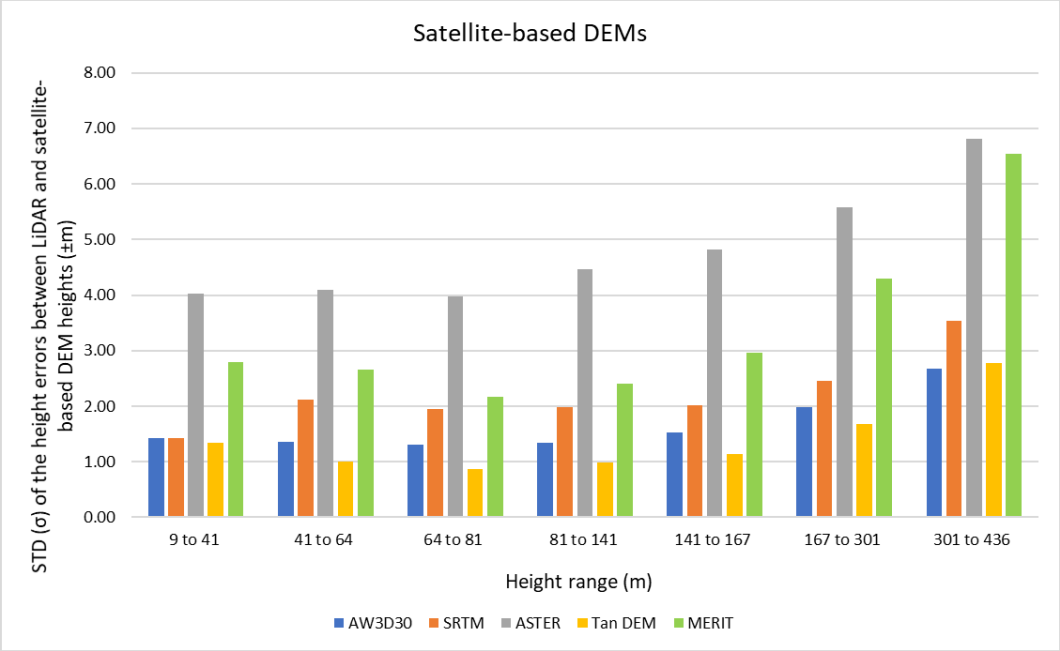

Figure 44: Variation of standard deviation of the height errors between LiDAR and DEMs heights with elevation (m) in medium land use/cover over area (A)

In all the scatter plots in Figure 45, the ASTER has the highest mean height differences in all elevation ranges compared to all other DEMs, which indicates that in medium land use/cover of area (A), ASTER has the largest offsets from LiDAR. The offsets are positive, indicating that ASTER generally underestimates LiDAR heights. The AW3D30 shows negative offsets in all ranges, indicating a general overestimation of LiDAR heights. The TanDEM-X underestimates LiDAR heights in all ranges. The MERIT and SRTM overestimate LiDAR heights at elevations (< 301 m); for values (> 301 m) they underestimate. In range (> 301 m), AW3D30 offsets are significantly smaller relative to the TanDEM-X, SRTM, and MERIT offsets. The ranges (9 – 41 m) and (64–167 m), TanDEM-X offsets are significantly smaller relative to the AW3D30, SRTM, and MERIT offsets. The ranges (41 – 64 m) and (167 – 301 m), MERIT offsets are significantly smaller relative to the TanDEM-X, AW3D30, and SRTM offsets.

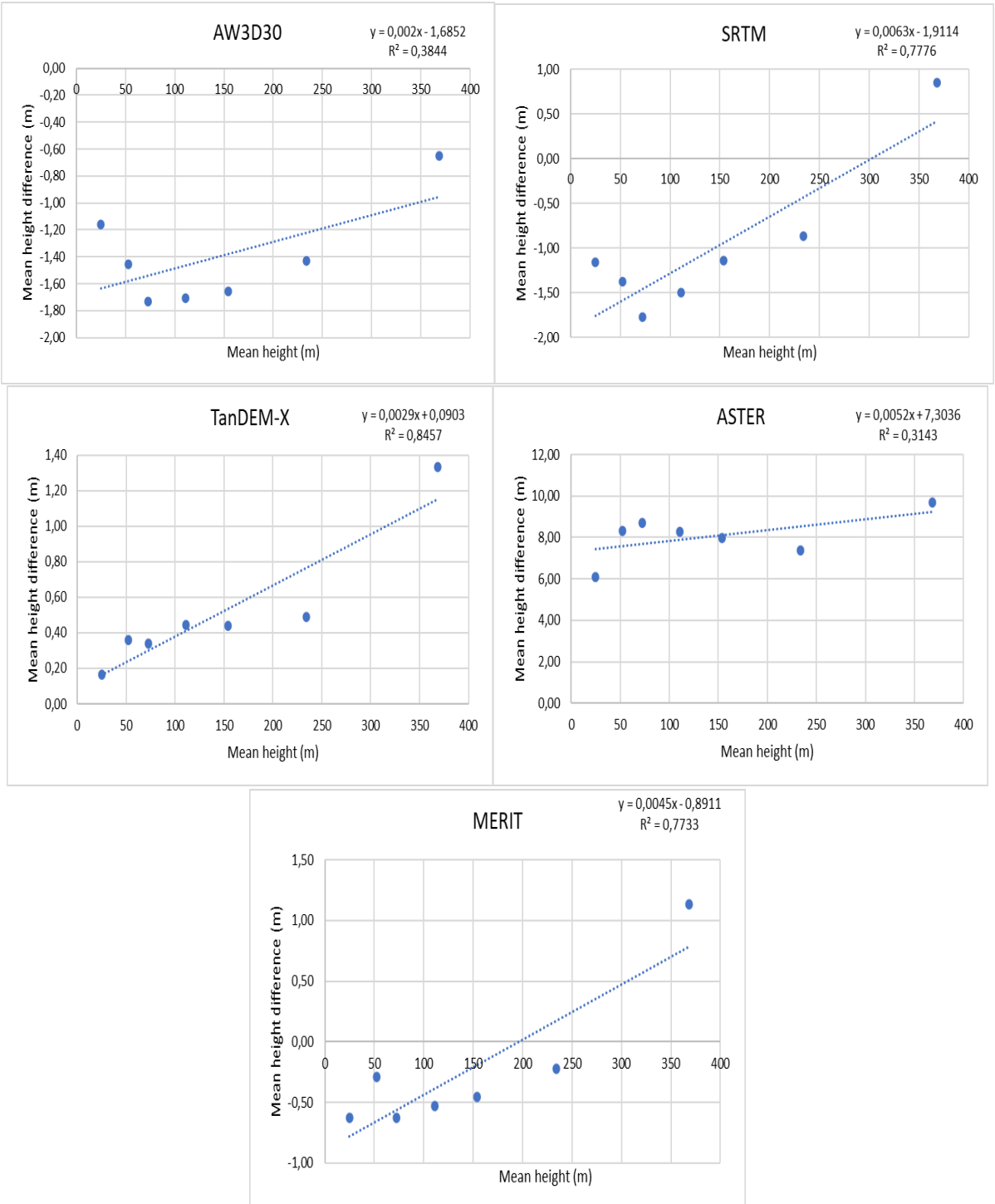

Figure 45: Scatter plots for mean height differences against mean height (m) in medium land use/cover over area(A)

The results for variation of the standard deviation of the differences between LiDAR and satellite-based DEM heights with slope over the area (A) in medium land use/cover are presented in Figure 46, while scatter plots of mean values are given in Figure 47. In Figure 46, an increase in the slope results in an increase in the standard deviations of all the DEMs. From these results, it can be deduced that the vertical accuracies of these DEMs relative to the LiDAR decreases with an increase in slope in medium land use/cover. The ASTER, SRTM, and MERIT have the lowest vertical accuracies compared to the AW3D30 and TanDEM-X in all ranges.

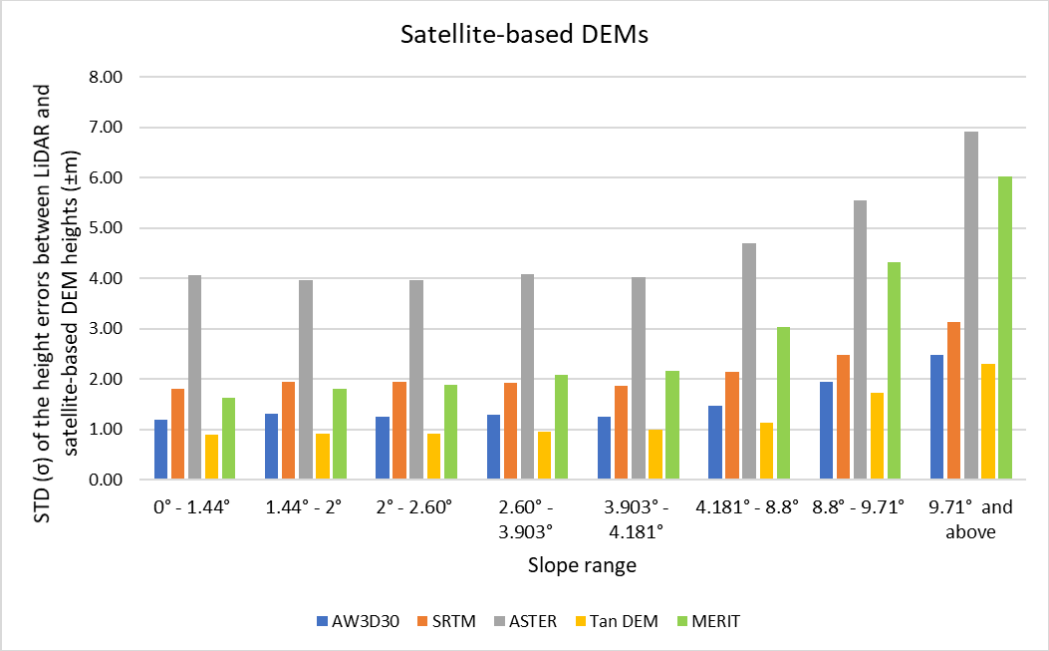

Figure 46: Variation of standard deviation of the height errors between LiDAR and DEMs heights with slope (°) in medium land use/cover over area (A)

In all the scatter plots in Figure 47, the ASTER has the highest mean height differences in all slope ranges compared to all other DEMs, which indicates that in medium land use/cover of area (A), ASTER has the largest offsets from LiDAR. The offsets are positive, indicating that ASTER generally underestimates LiDAR heights. The AW3D30 and SRTM show negative offsets in all ranges, indicating a general overestimation of LiDAR heights. The TanDEM-X underestimates LiDAR heights in all ranges. The MERIT overestimates LiDAR heights at slope (< 9.71°); for values (> 9.71°) it underestimates. In range (< 4.181°), TanDEM-X offsets are significantly smaller relative to the AW3D30, SRTM, and MERIT offsets. In ranges (> 4.181°), MERIT offsets are significantly smaller relative to the TanDEM-X, AW3D30, and SRTM offsets.

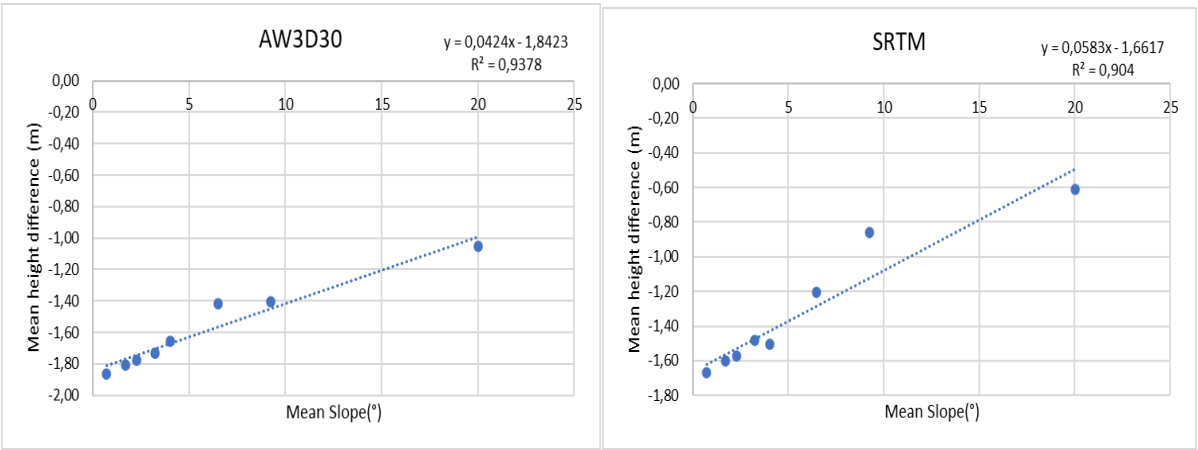

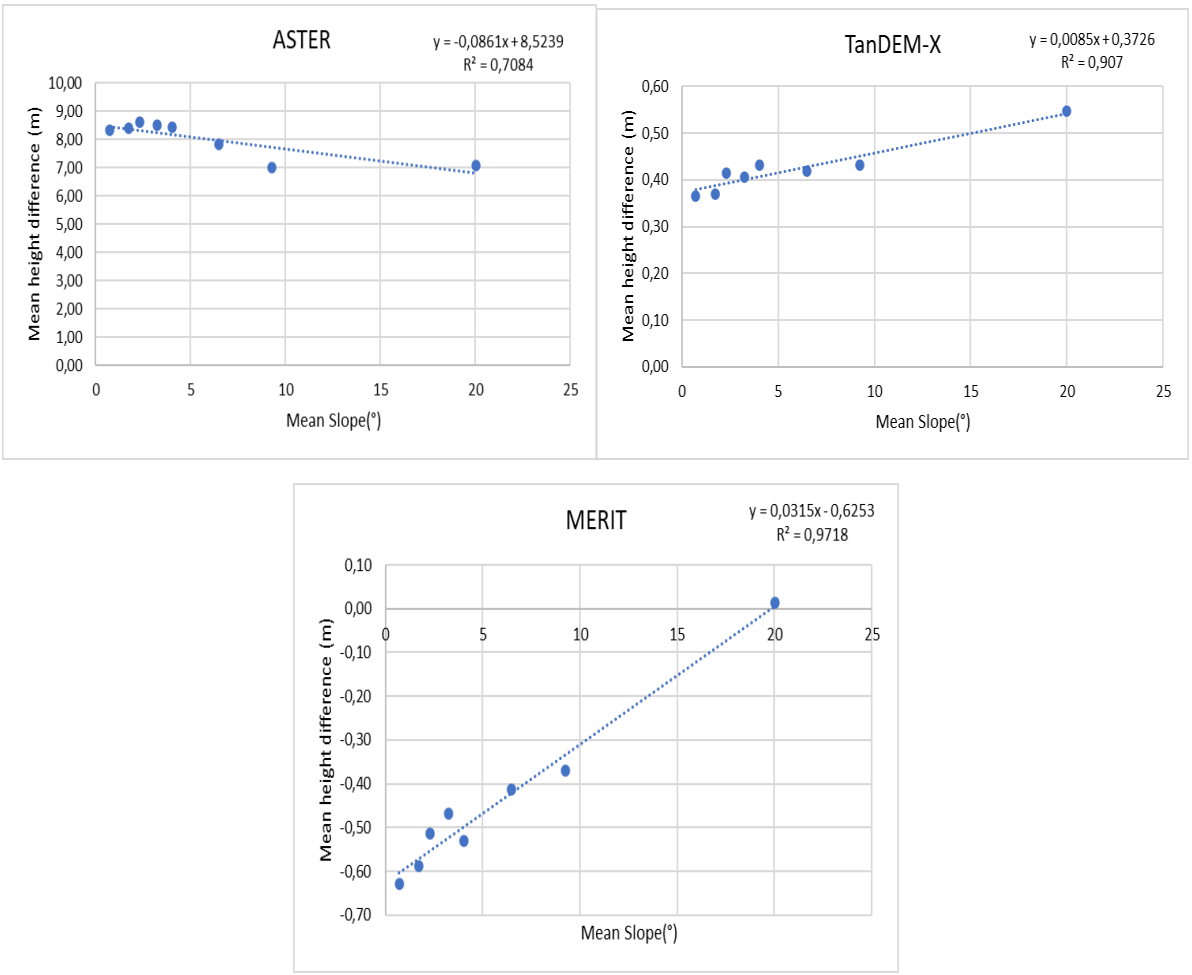

Figure 47: Scatter plots for mean height differences against mean slope (°) in medium land use/cover over area (A)

The results for variation of the standard deviation of the differences between LiDAR and satellite-based DEM heights with surface roughness over the area (A) in medium land use/cover are presented in Figure 48, while scatter plots of mean values are given in Figure 49. In Figure 48, an increase in the surface roughness results in an increase in the standard deviations of all the DEMs. From these results, it can be deduced that the vertical accuracies of these DEMs relative to the LiDAR decreases with an increase in surface roughness in medium land use/cover. The ASTER, SRTM, and MERIT have the lowest vertical accuracies compared to AW3D30 and TanDEM-X in all ranges.

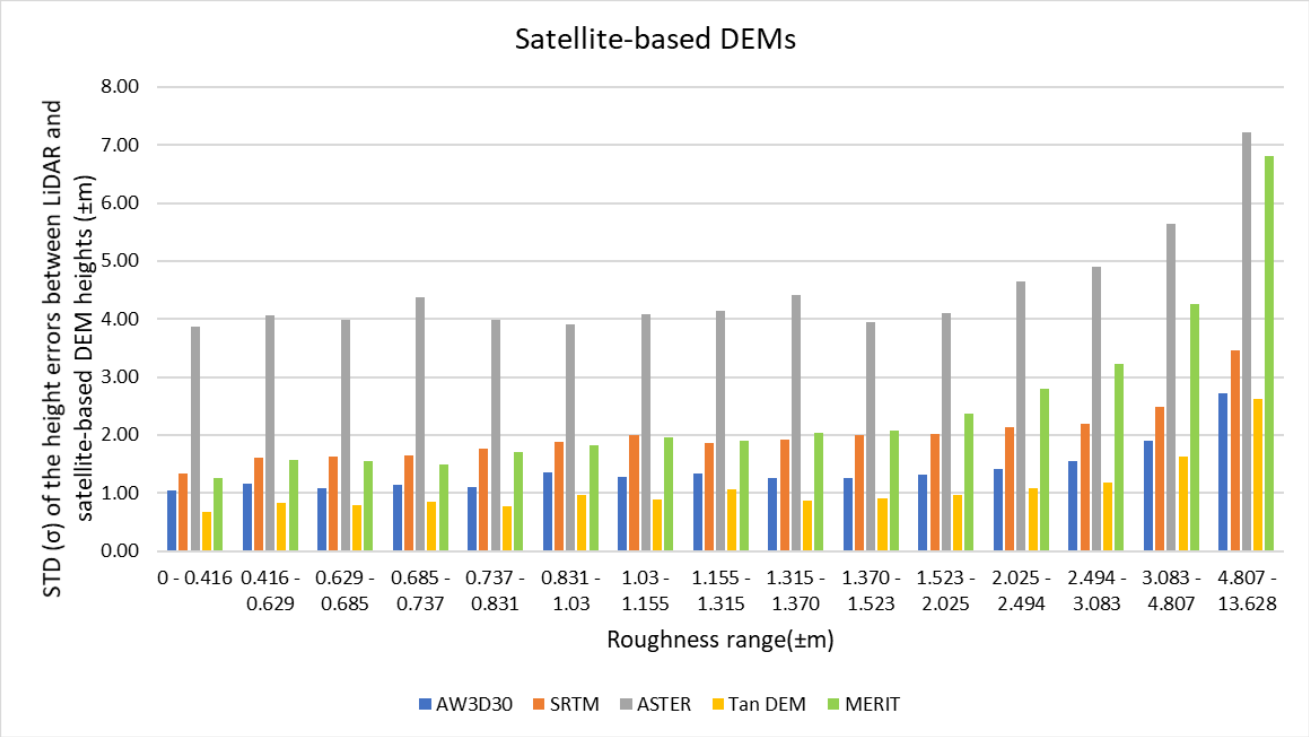

Figure 48: Variation of standard deviation of the height errors between LiDAR and DEMs heights with roughness (±m) in medium land use/cover over area (A)

In all the scatter plots in Figure 49, the ASTER has the highest mean height differences in all surface roughness ranges compared to all other DEMs, which indicates that in medium land use/cover of area (A), ASTER has the largest offsets from LiDAR. The offsets are positive, indicating that ASTER underestimates LiDAR heights. The AW3D30 and SRTM show negative offsets in all ranges, indicating an overestimation of LiDAR heights. The TanDEM-X underestimates LiDAR heights in all ranges. The MERIT overestimates LiDAR heights at surface roughness (< 4.807); for values (> 4.807) it underestimates. In range (< 2.494), TanDEM-X offsets are significantly smaller relative to the AW3D30, SRTM, and MERIT offsets. In range (> 2.494), MERIT offsets are significantly smaller relative to the TanDEM-X, AW3D30, and SRTM offsets.

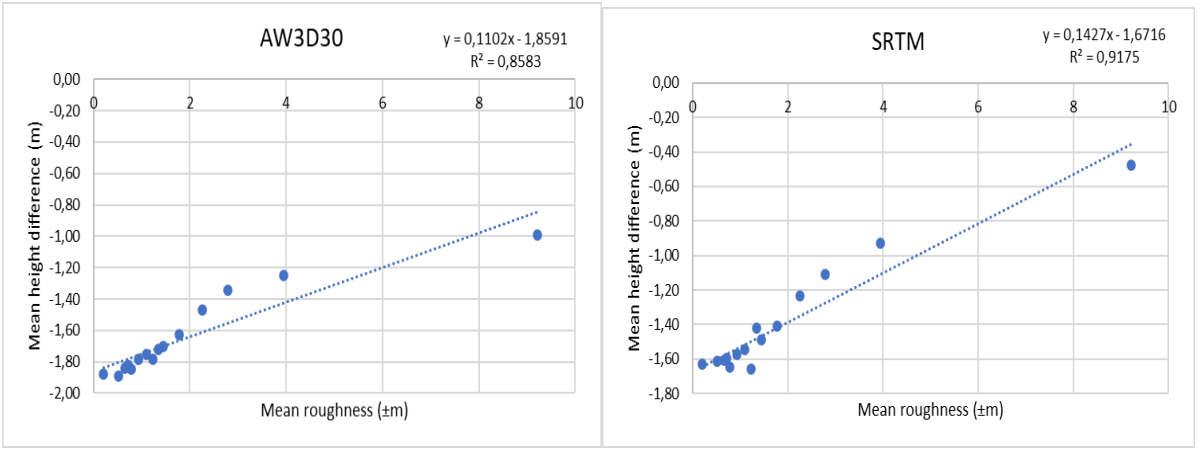

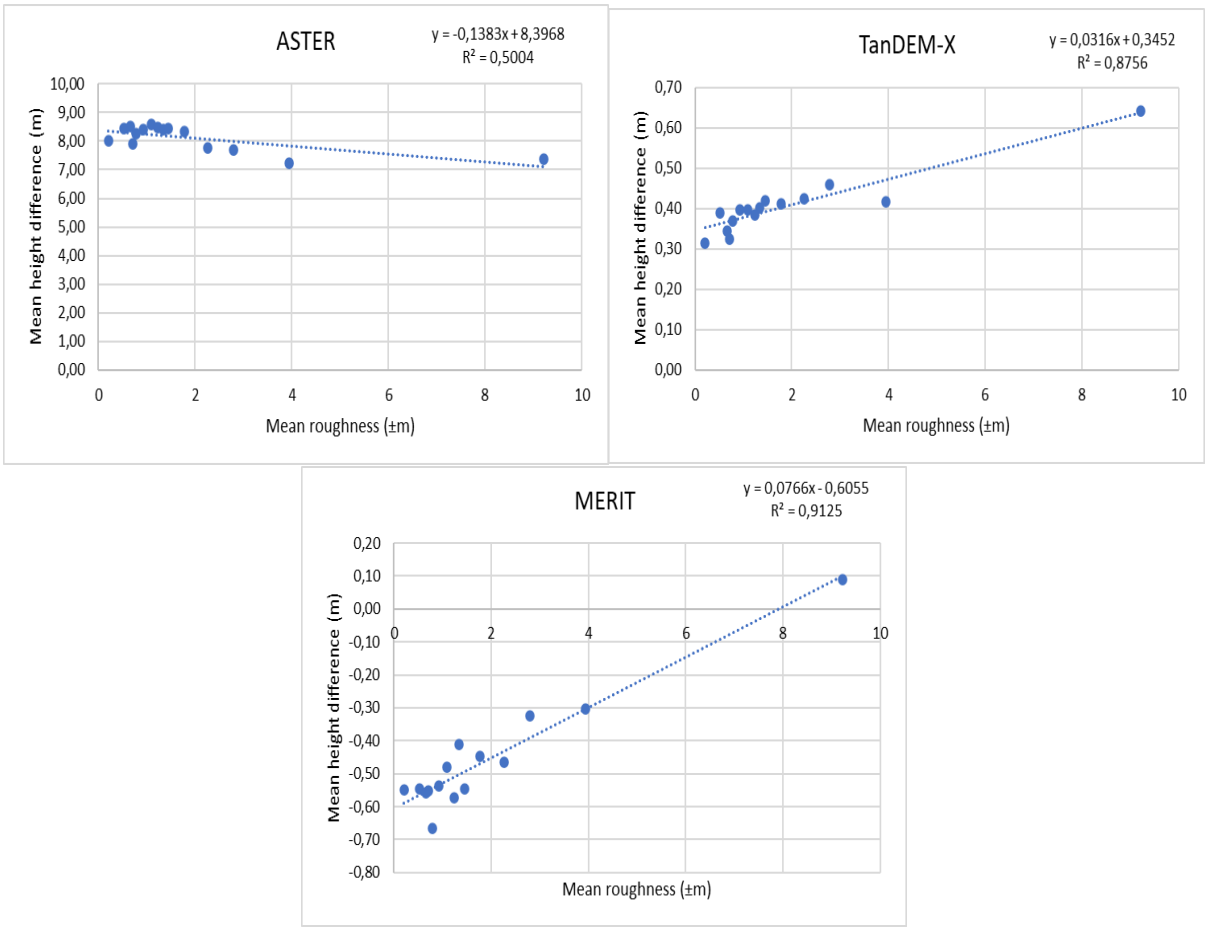

Figure 49: Scatter plots for mean height differences against mean roughness (±m) in medium land use/cover over area (A)

The results for variation of the standard deviation of the differences between LiDAR and satellite-based DEM heights with aspect over the area (A) in medium land use/cover are presented in Figure 50, while scatter plots of mean values are given in Figure 51. In Figure 50, as aspect changes, there is a variation in standard deviations of the DEM's. However, the more an area is flat, the better the vertical accuracies of the AW3D30, MERIT, SRTM, and TanDEM-X. This can also be observed in the (-1 – 0) aspect range, which is classified as flat. The ASTER, MERIT, and SRTM still indicate very low accuracies compared to the AW3D30 and TanDEM-X in all ranges.

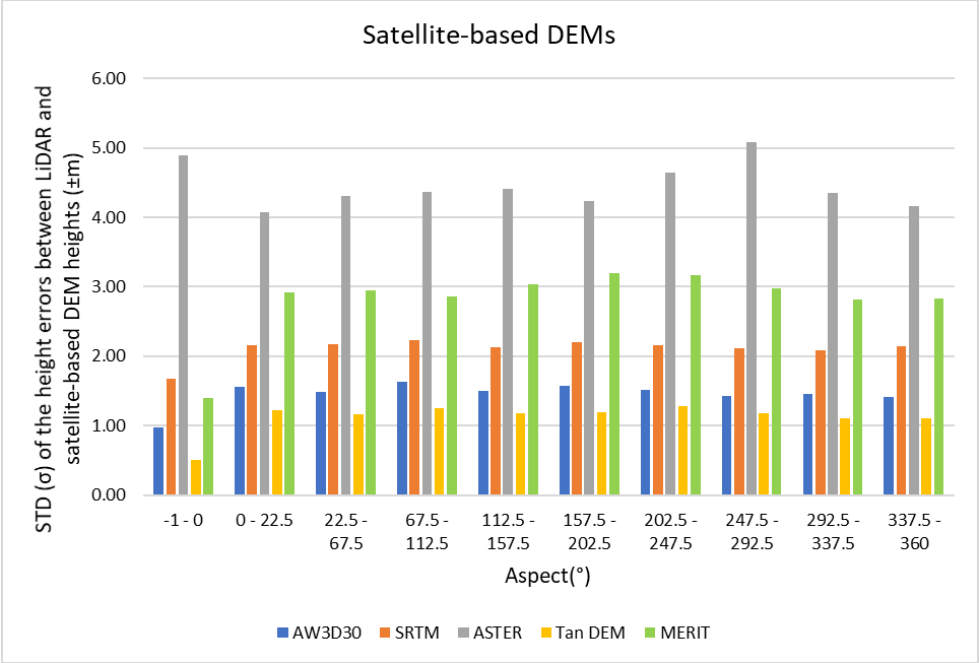

Figure 50: Variation of standard deviation of the height errors between LiDAR and DEMs heights with aspect (°) in medium land use/cover over area (A)

In all the scatter plots in Figure 51, the ASTER has the highest mean height differences in all aspect ranges compared to all other DEMs, which indicates that in medium land use/cover of area (A), ASTER has the largest offsets from LiDAR. The offsets are positive, indicating that ASTER generally underestimates LiDAR heights. The AW3D30, SRTM, and MERIT show negative offsets in all ranges, indicating a general overestimation of LiDAR heights. The TanDEM-X underestimates LiDAR heights in all ranges. The ranges (-1– 0°) and (> 247.5°), TanDEM-X offsets are significantly smaller relative to the AW3D30, SRTM, and MERIT offsets. In ranges (0° - 247.5°), MERIT offsets are significantly smaller relative to the TanDEM-X, AW3D30, and SRTM offsets.

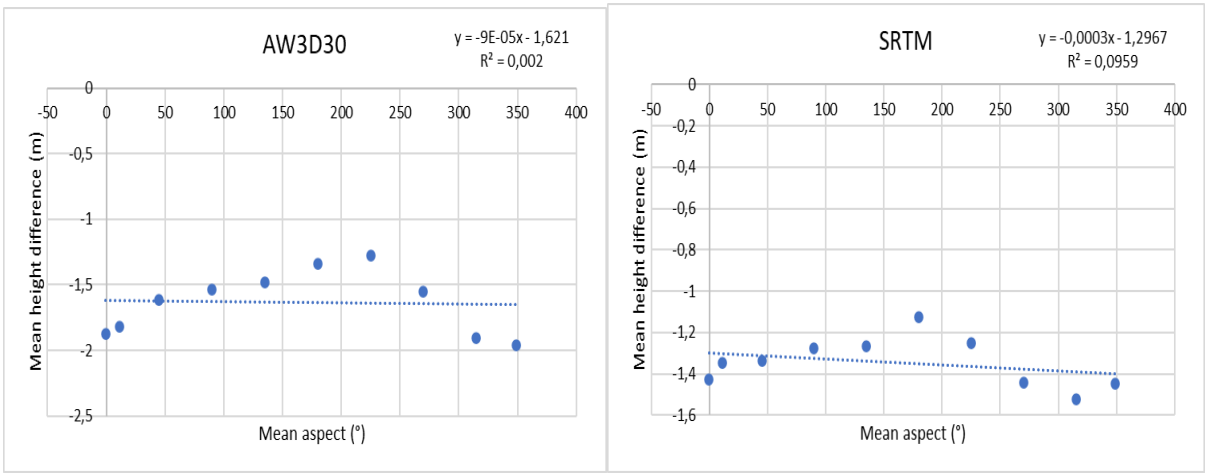

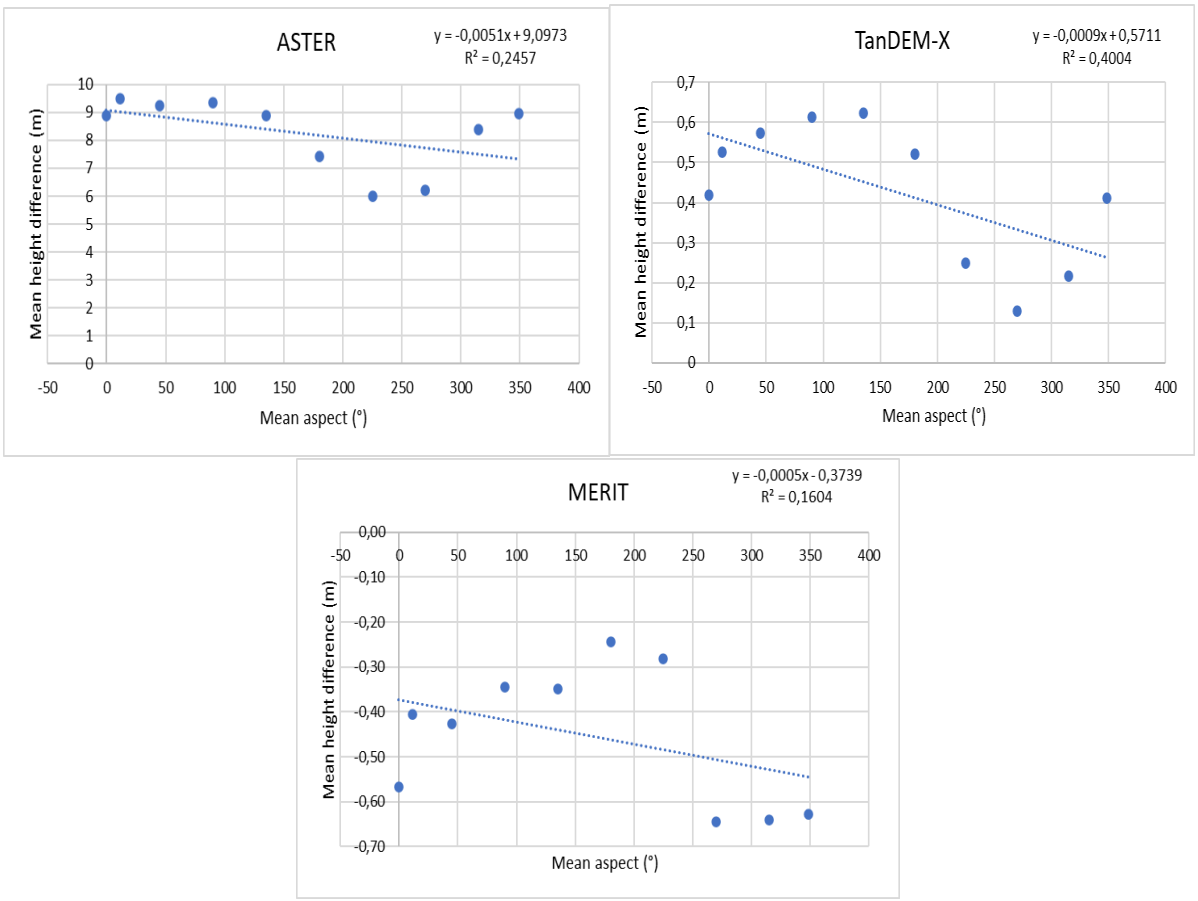

Figure 51: Scatter plots for mean height differences against mean aspect (°) in medium land use/cover over area (A)

The coefficients of correlation for the geomorphological factors in medium land use/cover over area (A) from Figures 45, 47, 49, and 51 are summarised in Table 20.

Table 20: Coefficients of correlation for the geomorphological factors in % over area (A) in medium land use/cover

	Lidar in medium land use/cover			
	mean height	mean slope	mean roughness	mean aspect
AW3D30	62.00	96.84	92.64	-4.47
SRTM	88.18	95.08	95.79	-30.97
ASTER	56.06	-84.17	-70.74	-49.57
TanDEM-X	91.96	95.24	93.57	-63.28
MERIT	87.94	98.58	95.52	-40.05

The mean aspect against the mean height difference shows weak(negative) linear correlation for AW3D30 and SRTM, and moderate (negative) correlation for ASTER and MERIT. The mean height against the mean height difference for ASTER shows a moderate (positive) correlation. The rest of the correlation coefficients range from strong to very strong.

Height error correlation with elevation, slope, aspect, and surface roughness in high land use/cover over area (A)

The results for variation of the standard deviation of the differences between LiDAR and satellite-based DEM heights with an elevation over the area (A) in high land use/cover are presented in Figure 52, while scatter plots of mean values are given in Figure 53. In Figure 52, an increase in the elevation results in an increase in the standard deviations of all the DEMs. From these results, it can be deduced that the vertical accuracies of these DEMs relative to the LiDAR decreases with an increase in elevation in high land use/cover. The ASTER, SRTM, and MERIT have the lowest vertical accuracies compared to AW3D30 and TanDEM-X, in almost all ranges.

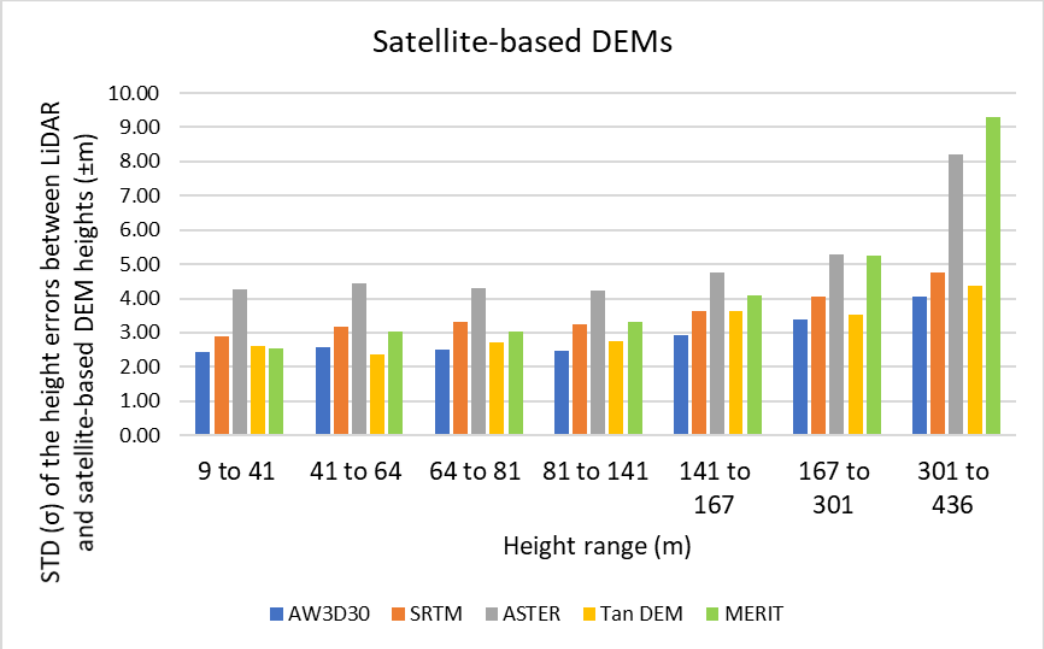

Figure 52: Variation of standard deviation of the height errors between LiDAR and DEMs heights with elevation (m) in high land use/cover over area (A)

In all the scatter plots in Figure 53, the ASTER has the highest mean height differences in all elevation ranges compared to all other DEMs, which indicates that in high land use/cover of area (A), ASTER has the largest offsets from LiDAR. The offsets are positive, indicating that ASTER underestimates LiDAR heights. The AW3D30 shows negative offsets in all ranges, indicating overestimation of LiDAR heights. The MERIT and SRTM overestimate LiDAR heights at elevations (< 301 m); for values (> 301 m) they underestimate. The TanDEM-X overestimates the LiDAR heights in elevations (< 41 m); for values (> 41 m) it underestimates. In ranges (< 167 and > 301 m), TanDEM-X offsets are significantly smaller relative to the AW3D30, SRTM, and MERIT offsets. In range (167 - 301 m), MERIT offsets are significantly smaller relative to the TanDEM-X, SRTM, and AW3D30 offsets.

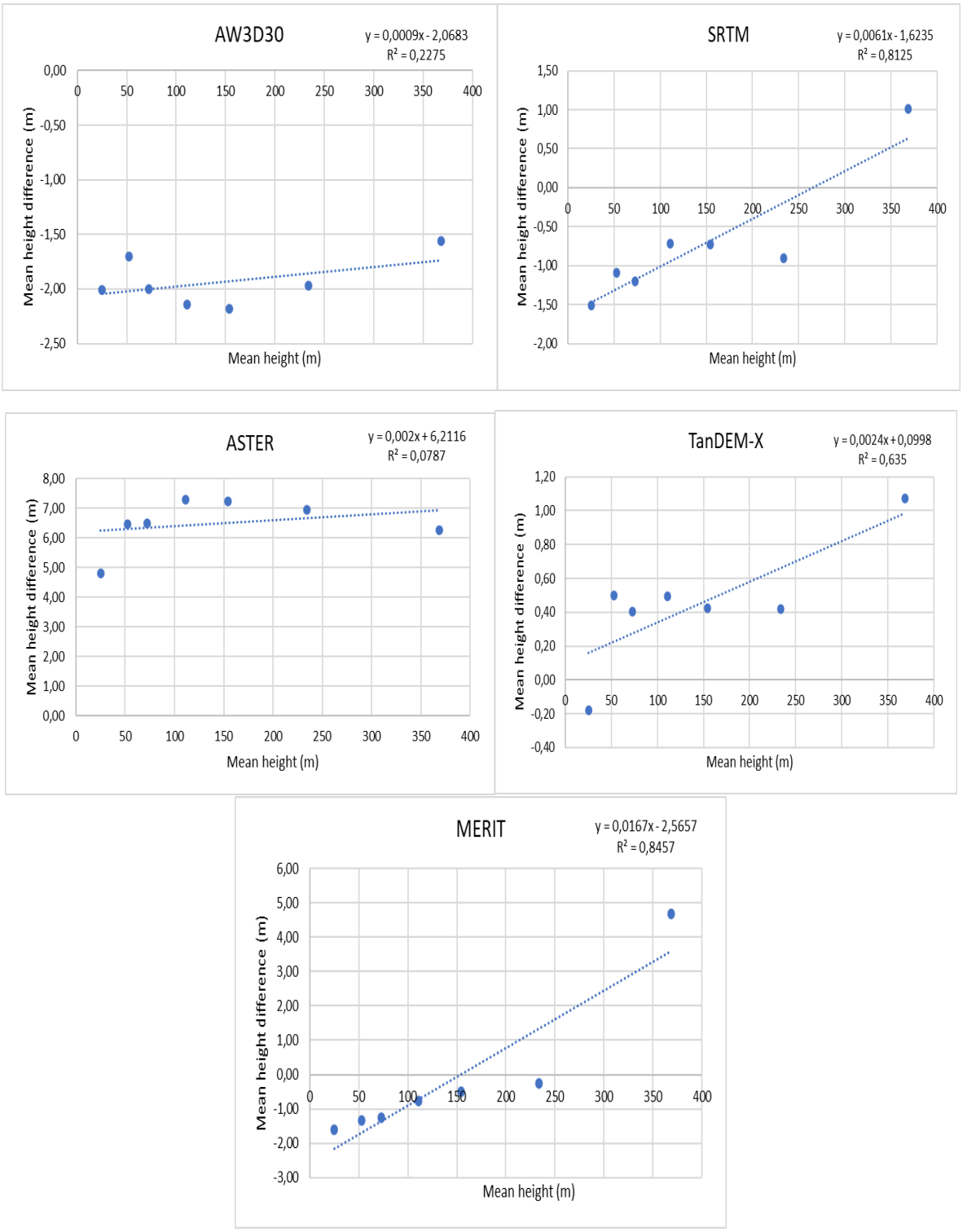

Figure 53: Scatter plots for mean height differences against mean height in high land use/cover over area (A)

The results for variation of the standard deviation of the differences between LiDAR and satellite-based DEM heights with slope over the area (A) in high land use/cover are presented below in Figure 54, while scatter plots of mean values are given in Figure 55. In Figure 54, an increase in the slope results in an increase in the standard deviations of all the DEMs. From these results, it can be deduced that the vertical accuracies of these DEMs relative to the LiDAR decreases with an increase in slope in

high land use/cover. The ASTER, SRTM, and MERIT have the lowest vertical accuracies compared to the AW3D30 and TanDEM-X in all ranges.

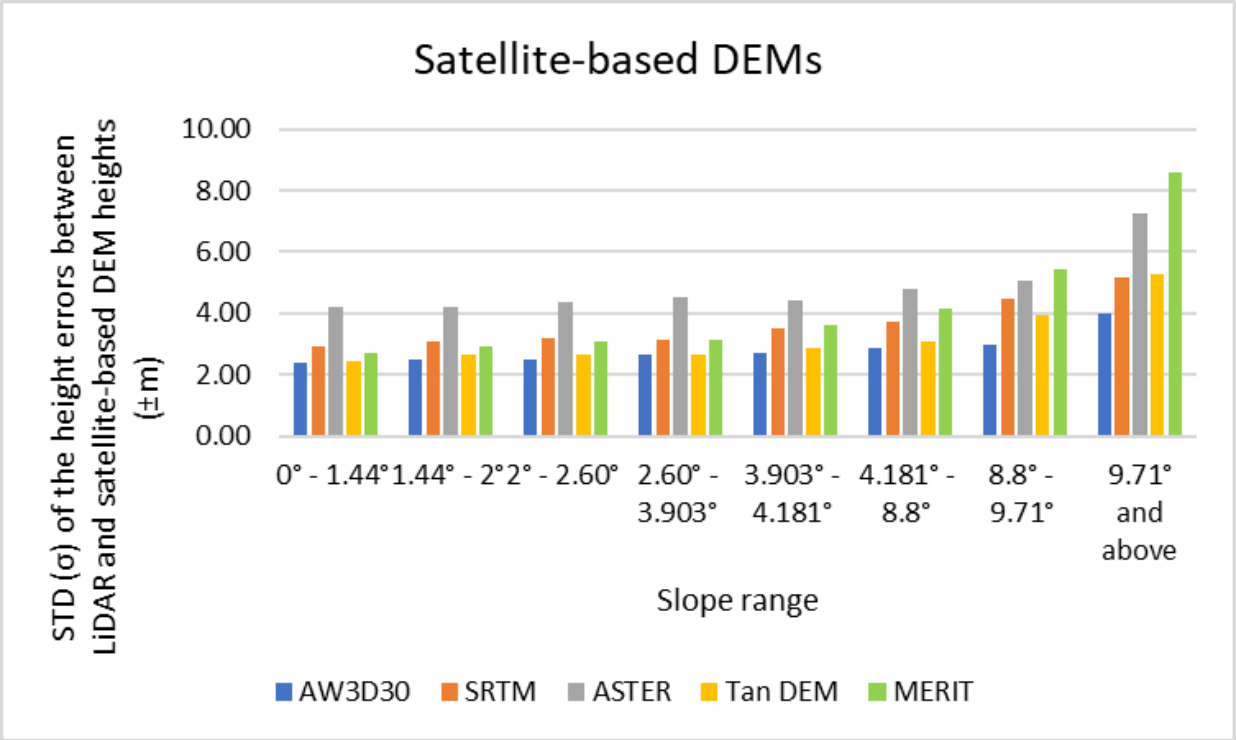

Figure 54: Variation of standard deviation of the height errors between LiDAR and DEMs heights with slope (°) in high land use/cover over area (A)

In all the scatter plots in Figure 55, the ASTER has the highest mean height differences in all slope ranges compared to all other DEMs, which indicates that in high land use/cover of area (A), ASTER has the largest offsets from LiDAR. The offsets are positive, indicating that ASTER underestimates LiDAR heights. The AW3D30 and SRTM show negative offsets in all ranges, indicating overestimation of LiDAR heights. The MERIT overestimates LiDAR heights at slope (< 9.71°); for values (> 9.71°) it underestimates. The TanDEM-X underestimates the LiDAR heights in slope (< 9.71°); for values (> 9.71°) it overestimates. The TanDEM-X offsets are significantly smaller relative to the AW3D30, SRTM, and MERIT offsets in all ranges.

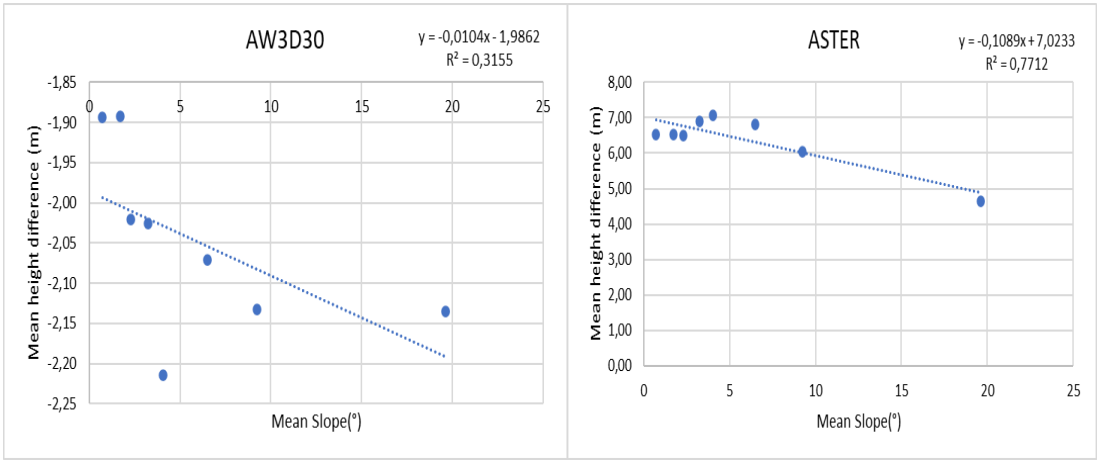

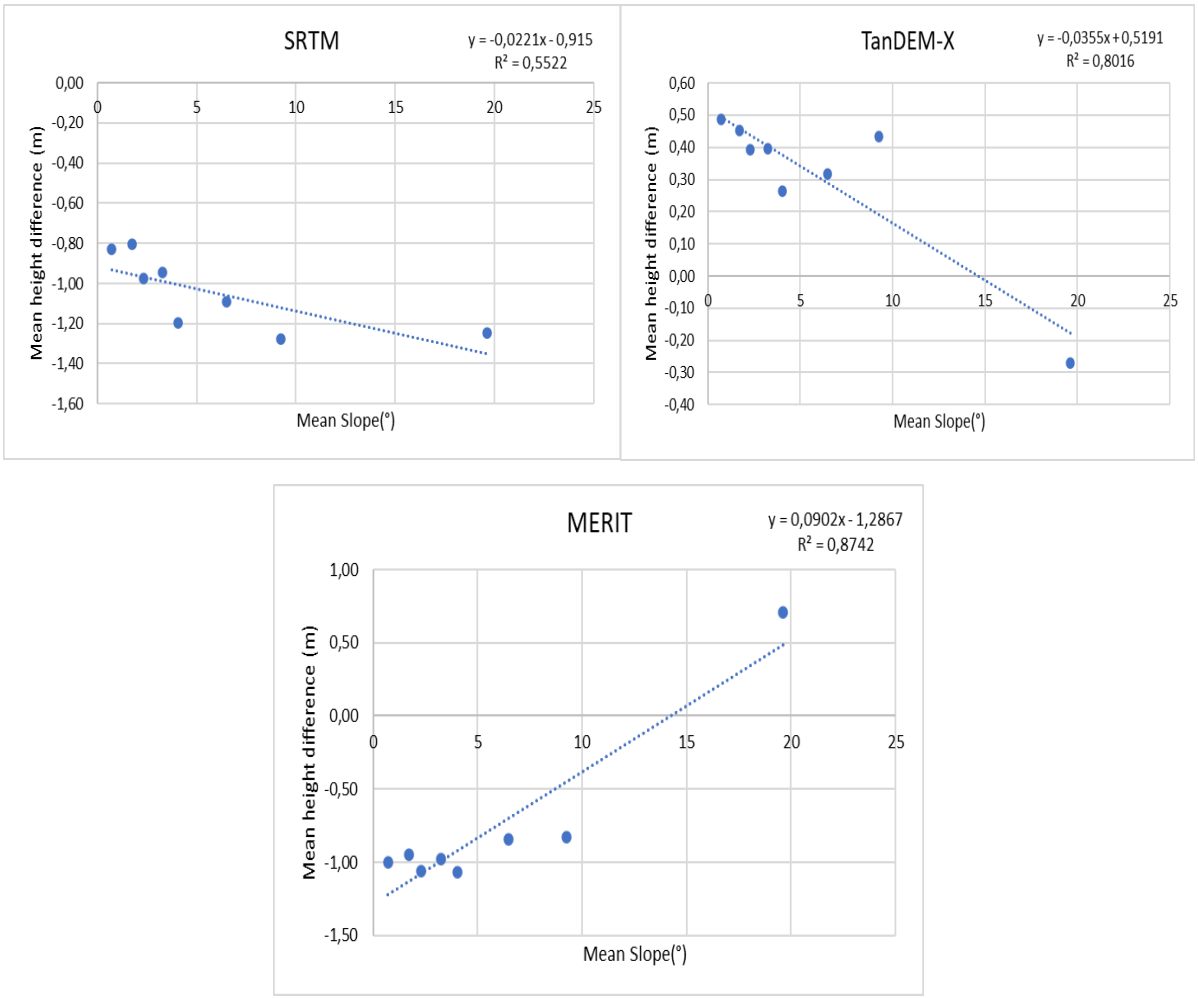

Figure 55: Scatter plots for mean height differences against mean slope (°) in high land use/cover over area (A)

The results for variation of the standard deviation of the differences between LiDAR and satellite-based DEM heights with surface roughness over the area (A) in high land use/cover are presented in Figure 56, while scatter plots of mean values are given in Figure 57. In Figure 56, an increase in the surface roughness results in an increase in the standard deviations of all the DEMs. From these results, it can be deduced that the vertical accuracies of these DEMs relative to the LiDAR decreases with an increase in surface roughness in high land use/cover. The ASTER, SRTM, and MERIT have the lowest vertical accuracies compared to AW3D30 and TanDEM-X in almost all ranges.

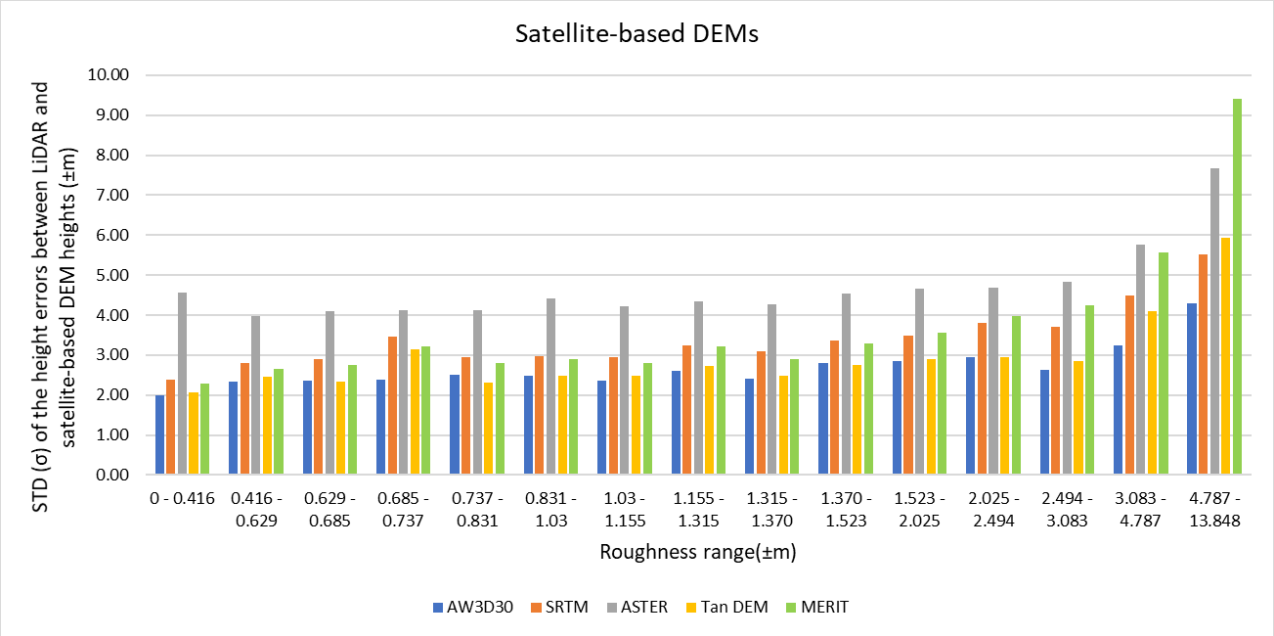

Figure 56: Variation of standard deviation of the height errors between LiDAR and DEMs heights with roughness (±m) in high land use/cover over area (A)

In all the scatter plots in Figure 57, the ASTER has the highest mean height differences in all surface roughness ranges compared to all other DEMs, which indicates that in high land use/cover of area (A), ASTER has the largest offsets from LiDAR. The offsets are positive, indicating that ASTER underestimates LiDAR heights. The AW3D30 and SRTM show negative offsets in all ranges, indicating overestimation of LiDAR heights. The MERIT overestimates LiDAR heights at surface roughness (< 4.787); for values (> 4.787) it underestimates. The TanDEM-X underestimates the LiDAR heights at surface roughness (< 4.787); for values (> 4.787) it overestimates. In ranges (< 3.083 and > 4.787), the TanDEM-X offsets are significantly smaller relative to the AW3D30, SRTM, and MERIT offsets. In range (3.083 - 4.787), the MERIT offsets are significantly smaller relative to the AW3D30, SRTM, and TanDEM-X offsets.

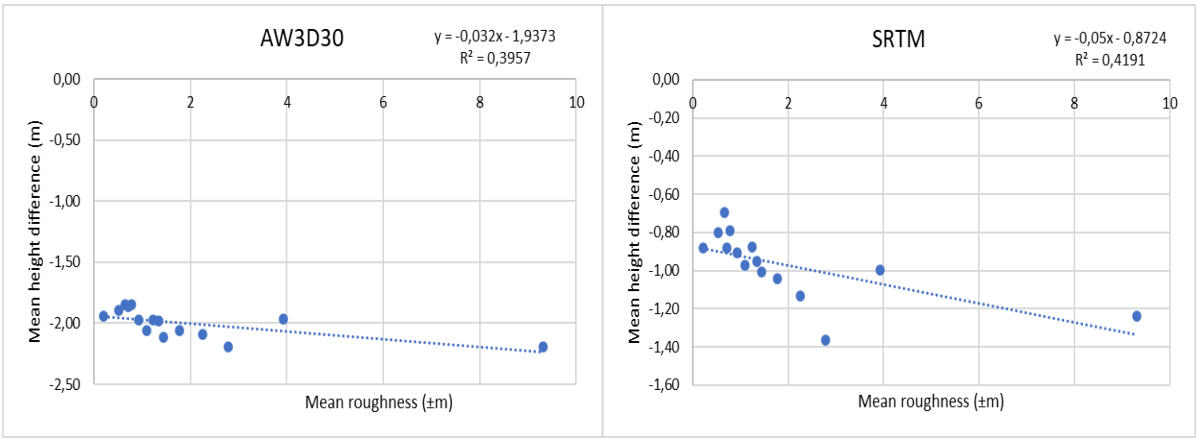

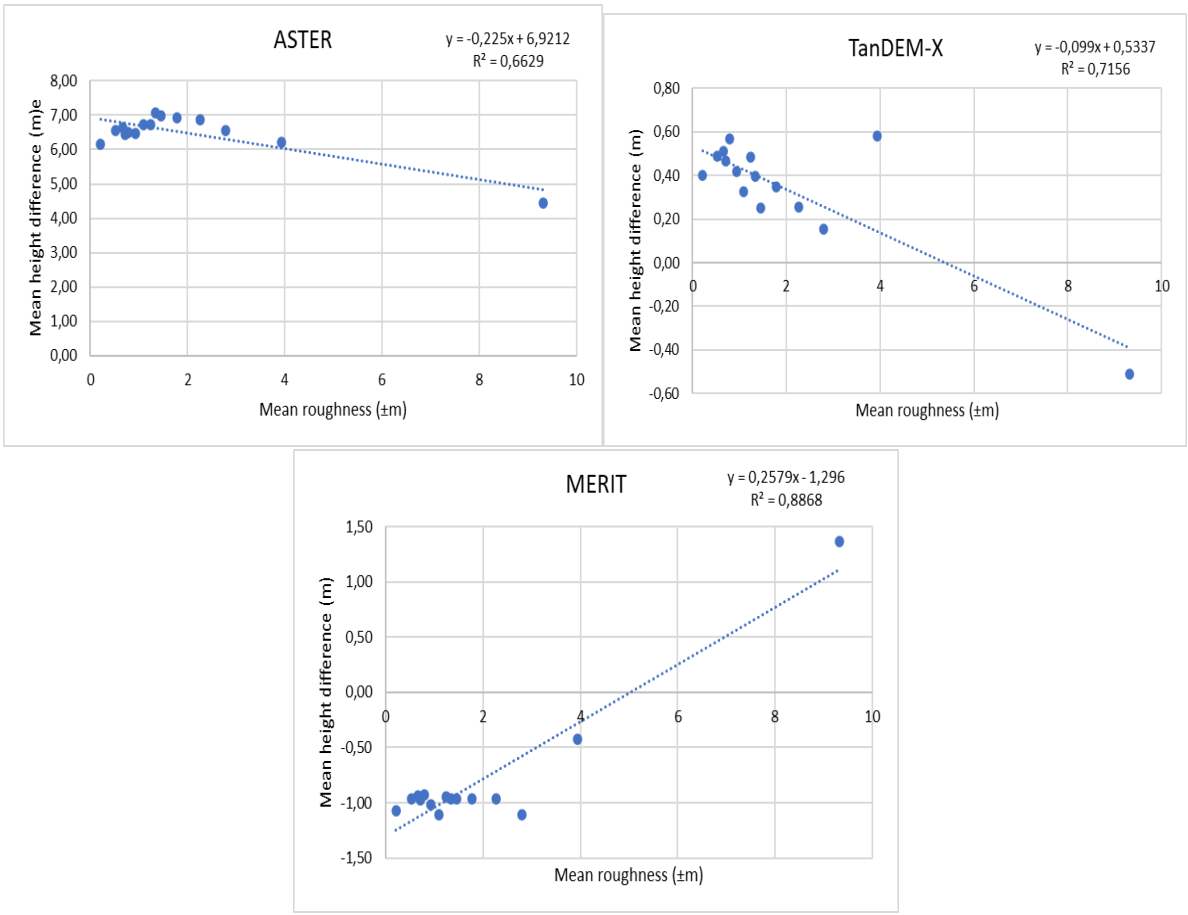

Figure 57: Scatter plots for mean height differences against mean roughness (±m) in high land use/cover over area (A)

The results for variation of the standard deviation of the differences between LiDAR and satellite-based DEM heights with aspect over the area (A) in high land use/cover are presented in Figure 58, while scatter plots of mean values are given in Figure 59. In Figure 58, as aspect changes, there is a variation in standard deviations of the DEM's. However, the more an area is flat, the better the vertical accuracies of all the DEMs. This can also be observed in the (-1 – 0) aspect range, which is classified as flat. The ASTER, MERIT, and SRTM still indicate very low accuracies compared to the AW3D30 and TanDEM-X in all ranges.

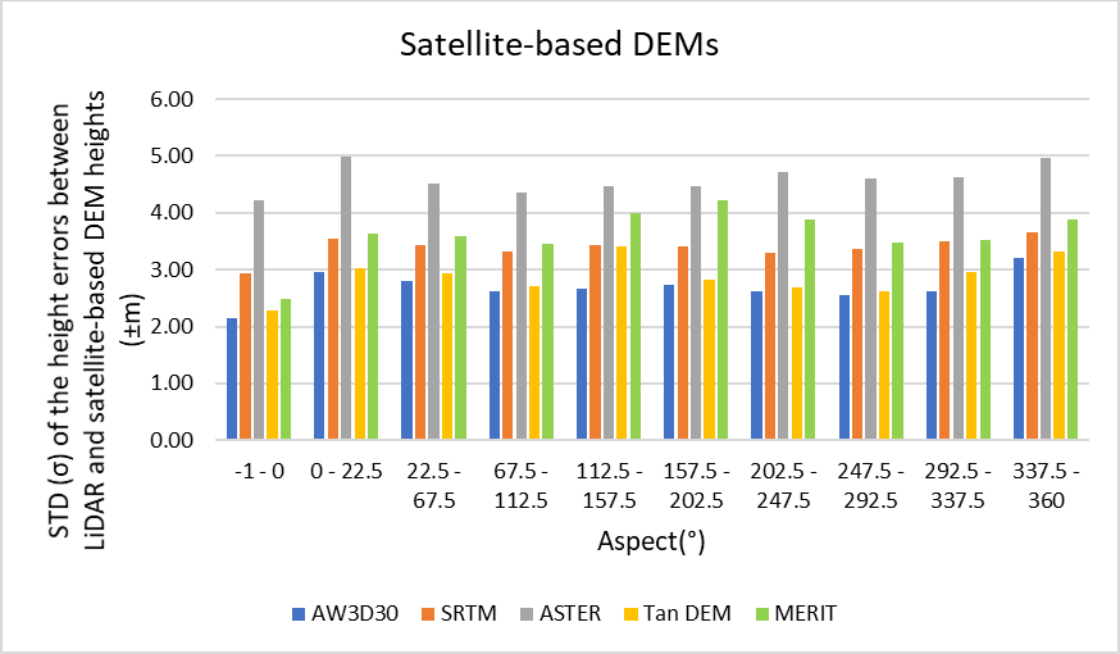

Figure 58: Variation of standard deviation of the height errors between LiDAR and DEMs heights with aspect (°) in high land use/cover over area (A)

In all the scatter plots in Figure 59, the ASTER has the highest mean height differences in all aspect ranges compared to all other DEMs, which indicates that in high land use/cover of area (A), ASTER has the largest offsets from LiDAR. The offsets are positive, indicating that ASTER generally underestimates LiDAR heights. The AW3D30, SRTM, and MERIT show negative offsets in all ranges, indicating overestimation of LiDAR heights. The TanDEM-X underestimates the LiDAR heights in all ranges. The TanDEM-X offsets are significantly smaller relative to the AW3D30, SRTM, and MERIT offsets in all ranges.

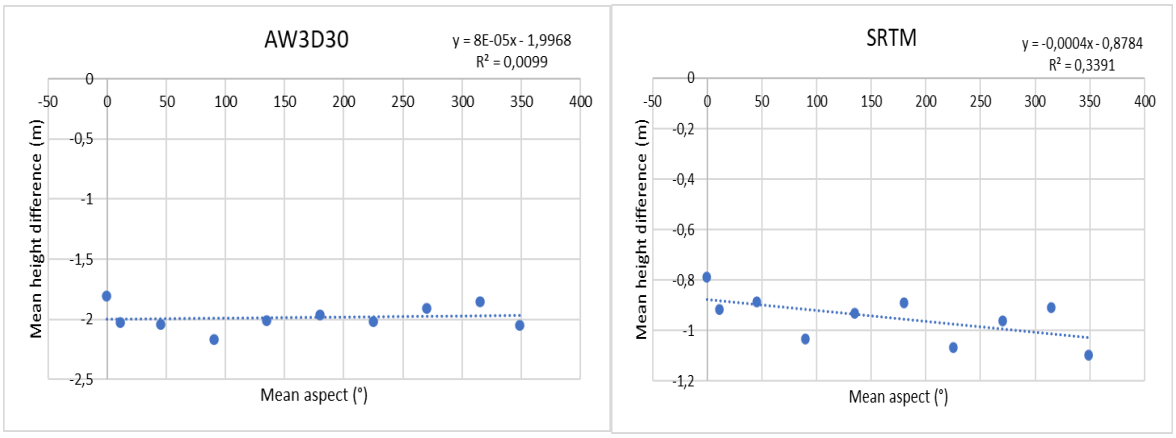

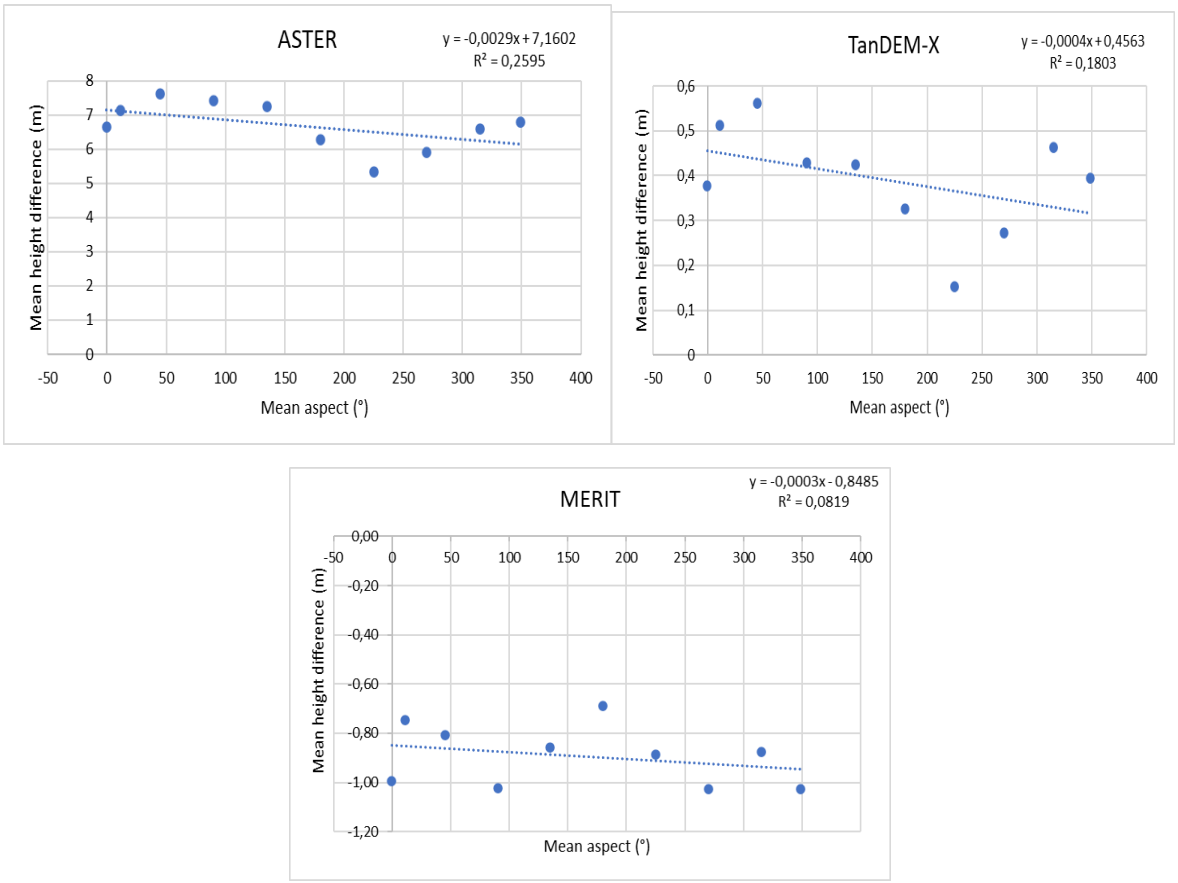

Figure 59: Scatter plots for mean height differences against mean aspect (°) in high land use/cover over area (A)

The coefficients of correlation for the geomorphological factors in high land use/cover over area (A) from Figures 53, 55, 57, and 59 are summarised in Table 21.

Table 21: Coefficients of correlation for the geomorphological factors in % over area (A) in high land use/cover

	Lidar in high land use/cover			
	mean height	mean slope	mean roughness	mean aspect
AW3D30	47.70	-56.17	-62.90	9.95
SRTM	90.14	-74.31	-64.74	-58.23
ASTER	28.05	-87.82	-81.42	-50.94
TanDEM-X	79.69	-89.53	-84.59	-42.46
MERIT	91.96	93.50	94.17	-28.62

For the mean aspect against the mean height difference, the AW3D30 shows a weak(positive) linear correlation, while the MERIT shows a weak (negative) linear correlation. The TanDEM-X, ASTER, and SRTM shows a moderate (negative) linear correlation. For the mean height against the mean height difference, the ASTER shows a weak(positive) correlation, while the AW3D30 shows a moderate (positive) linear correlation. The mean slope against the mean height difference for AW3D30 shows a moderate (negative) correlation. The rest of the correlation coefficients range from strong to very strong.

In all the evaluations of the satellite-based DEMs against LiDAR, the ASTER shows the lowest vertical accuracy, followed by the MERIT and SRTM. These DEMs also provide very low accuracies in the highest geomorphological (elevation, slope, and surface roughness) areas. The DEMs performance was not systematically affected by aspect, which is consistent with previous studies. The AW3D30 and TanDEM-X provide high vertical accuracies in most geomorphological areas compared to the implied DEMs. Therefore, they (AW3D30 and TanDEM-X) are candidate DEMs suitable for fusion over South Africa. This is only based on the DEMs evaluated in this study.

3.4 Error modelling strategies for developing accurate digital elevation model over South Africa

3.4.1 Introduction

The errors in the candidate DEMs are modelled using different strategies. The process involves co-registration of the DEMs, derivation of parameters for modelling the DEMs using the ground levelling data. The error modelling strategies applied include the regression and adaptive terrain dependent method. The modelled DEMs are evaluated using ground levelling data.

3.4.2 Data and methods

The dataset used is the AW3D30 and TanDEM-X in Figure 3, and the geomorphological parameters (slope, aspect, and surface roughness) generated in sections (3.2.2.2 and 3.3.2.4). The ground levelling (trigonometrical beacon) data described in section (2.1.1) is used as a reference and for the derivation of the model parameters.

3.4.2.1 Co-registration of DEMs

Since the geomorphological parameters to be used in the error modelling strategies were from an SRTM DEM, pixel alignment was necessary before the derivation. According to Jing et al. (2013), horizontal shifts, which are sometimes referred to as geo-location errors or horizontal errors, can exist among global DEMs. These shifts may come from erroneous georeferencing inherent in the DEM observations and can be encountered in practice by ambiguous or changing definitions of the position to which elevation refers (Jing et al., 2013). Figure 60 shows the investigation of pixel misalignment between the DEMs (AW3D30, SRTM, ASTER, and TanDEM-X).

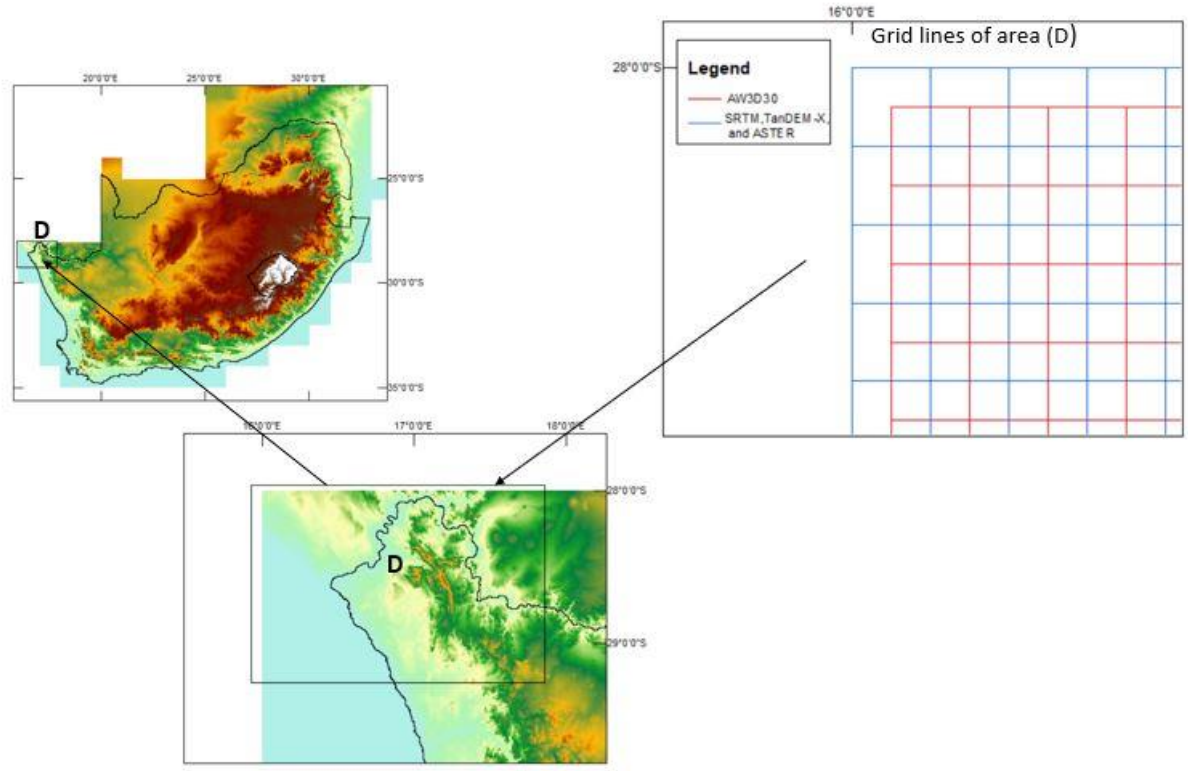

Figure 60: Pixel misalignment in AW3D30 relative to the SRTM, TanDEM-X, and ASTER

The area (D) inside the rectangle shown in Figure 60 was used to investigate pixel alignment between the 1 arc-second DEMs (AW3D30, SRTM, ASTER, and TanDEM-X). The area was chosen because it contained the original tiles from the producer for all DEMs, and all the tiles do not have null values. From this area, the raster tiles were converted to grid lines, and it was observed that superimposing the SRTM on the TanDEM-X and ASTER, the pixels aligned. When superimposing the AW3D30 on the DEMs (ASTER, TanDEM-X, and SRTM), there was a pixel misalignment in the AW3D30 relative to those DEMs. It can be observed in Figure 60 that there is an obvious ½ grid pixel shift in the northwest direction. A ½ grid shift of the AW3D30 relative to the DEM's (SRTM, ASTER, and TanDEM-X) in different directions (northwest, northeast, southeast, and southwest) was compensated and validation of the AW3D30 vertical accuracy using ground levelling was done.

3.4.2.2 Methods for modelling DEM errors

The improvement on the candidate DEMs was done using models with parameters derived using ground levelling data. Since the candidate DEMs (AW3D30 and TanDEM-X) had larger errors in high slope (>20°) relative to smaller errors in low slope areas, the regional corrections were considered throughout South Africa to try and model areas with slopes greater than 20° effectively. The six regions were chosen such that when a sample of models and test points is selected, areas with slopes greater than 20° will be modelled effectively. A sample of 66.67% of ground levelling data points from each region were chosen using random sampling. The remaining 33.33% of data points that were not part of the sample were used to test the derived correction models.

Nine different correction models were derived. These correction models include the simple linear regressions, multiple linear regressions, and the adaptive terrain-dependent method with parameters determined using Ordinary Least Squares (OLS) and Robust least squares (M-estimator) and these are discussed under section (2.2.4). The simple linear regression was used to estimate the relationship

between the geomorphological factors (slope, aspect, and surface roughness) and height errors. The simple linear regression was also used to estimate the relationship between the geomorphological factors (slope, aspect, and surface roughness) and absolute height errors. Multiple regression as a function of (slope, aspect, and surface roughness) to predict height errors was used.

Based on the slope ranges (0° – 2.5°, 2.5° – 5.5°, 5.5° – 7.5°, 7.5° – 10°, 10° – 20°, >20°), a selection of different methods that have high effect in improving the vertical accuracy of the DEMs in each slope range was done. The selected methods for each range were combined and used to generate final models that are applied to the candidate DEMs. The six regions for correction derivation are shown in Figure 61, and the number of ground levelling models and test points used are shown in Figures 62 to 73.

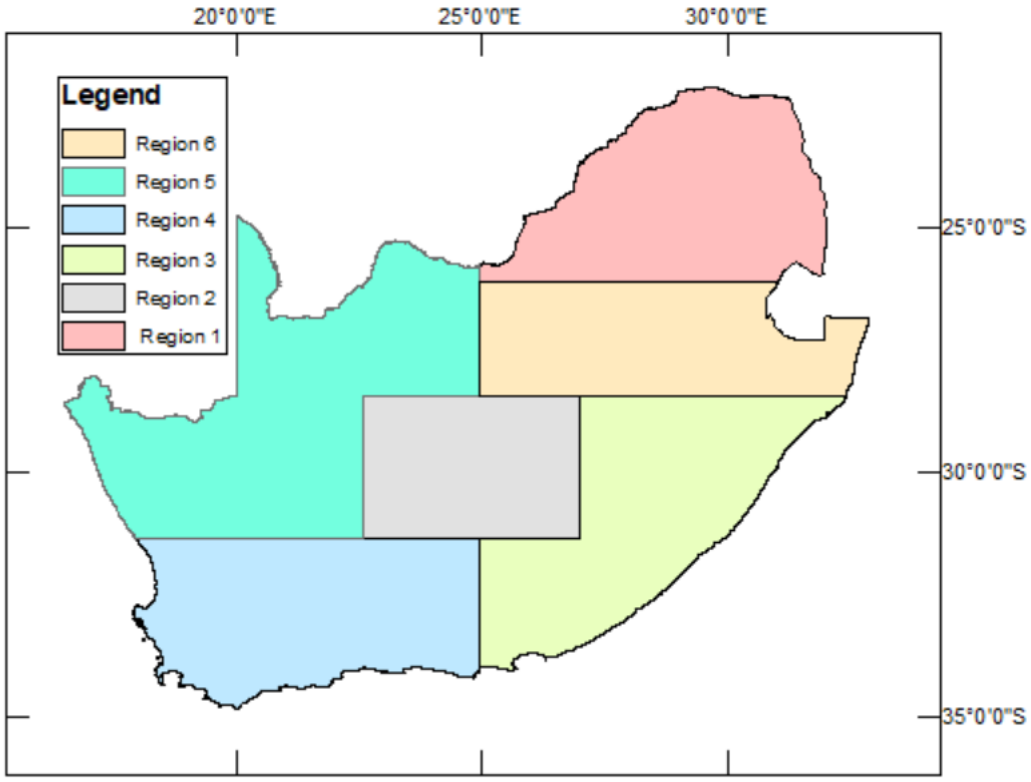

Figure 61: Different regions for correction model generation

In region 1, out of 3,656 points of height differences between ground levelling and each of the DEMs, 2,437 points were randomly selected for the model derivation. The remaining 1,219 points were used in the validation of each of the applied corrections.

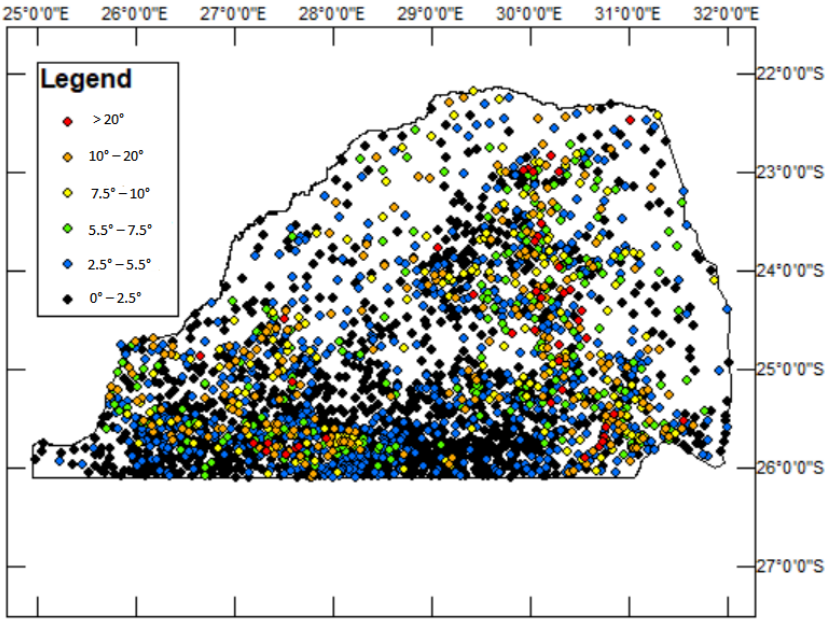

Figure 62: Spatial distribution of model points falling in different slope ranges over region 1

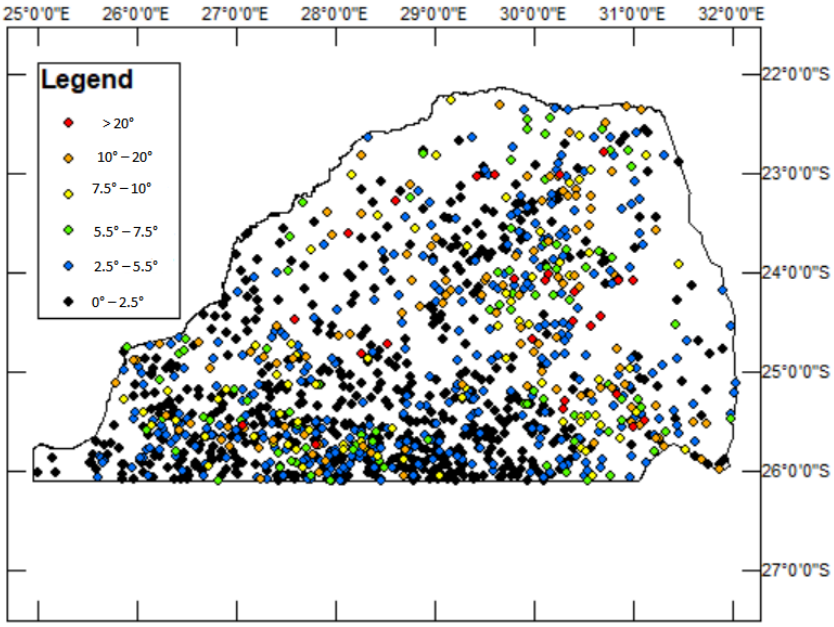

Figure 63: Spatial distribution of test points falling in different slope ranges over region 1

In region 2, out of 3,286 points of height differences between the ground levelling and each of the DEMs, 2,191 points were randomly selected for the model derivation. The remaining 1,095 points were used in the validation of each of the applied corrections.

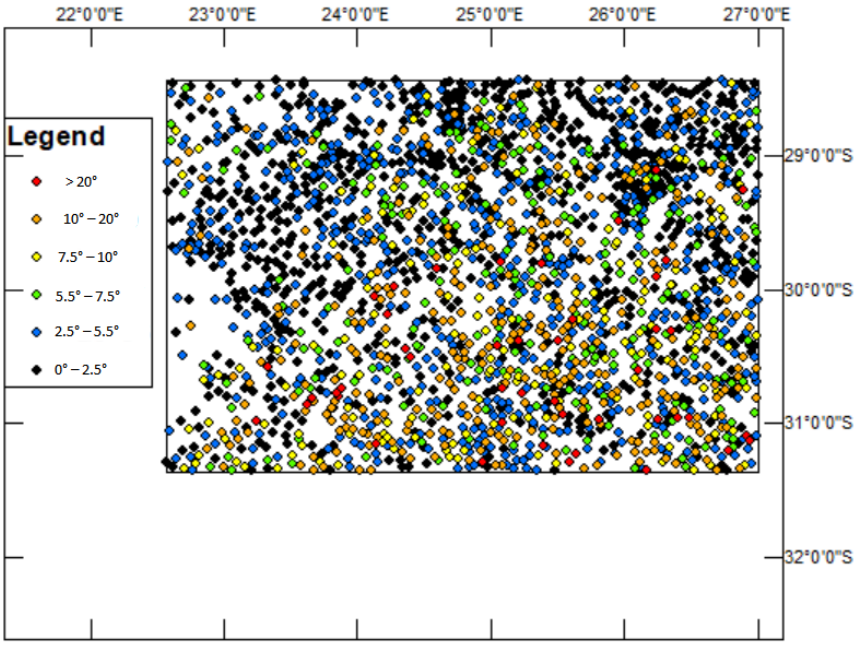

Figure 64: Spatial distribution of model points falling in different slope ranges over region 2

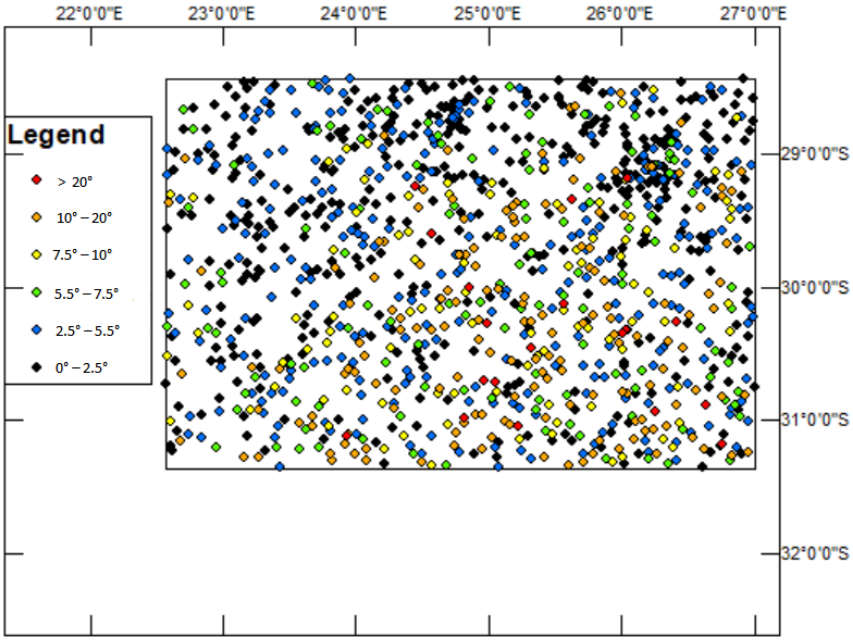

Figure 65: Spatial distribution of test points falling in different slope ranges over region 2

In region 3, out of 5,702 points of height differences between the ground levelling and each of the DEMs, 3,801 points were randomly selected for the model derivation. The remaining 1,901 points were used in the validation of each of the applied corrections.

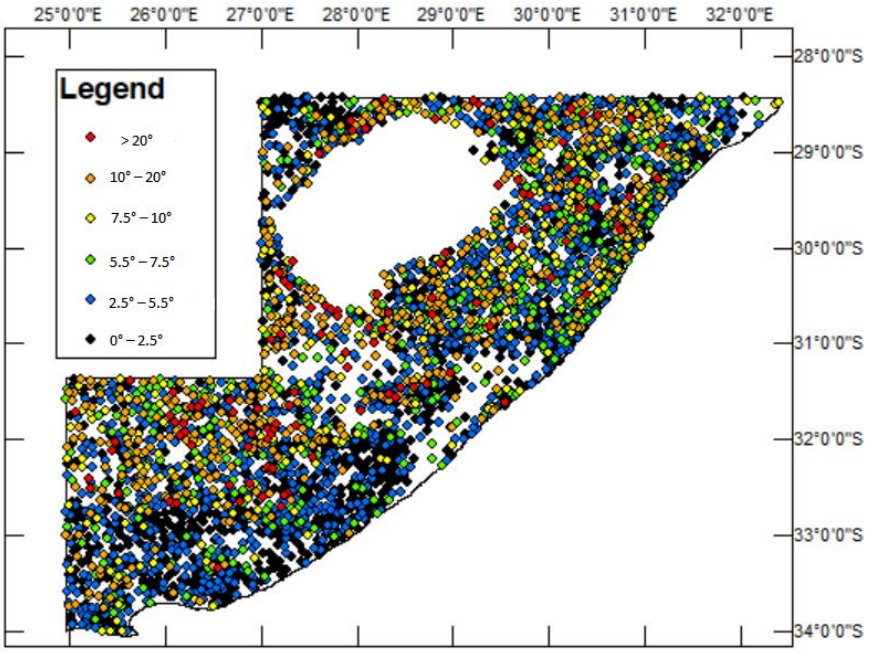

Figure 66: Spatial distribution of model points falling in different slope ranges over region 3

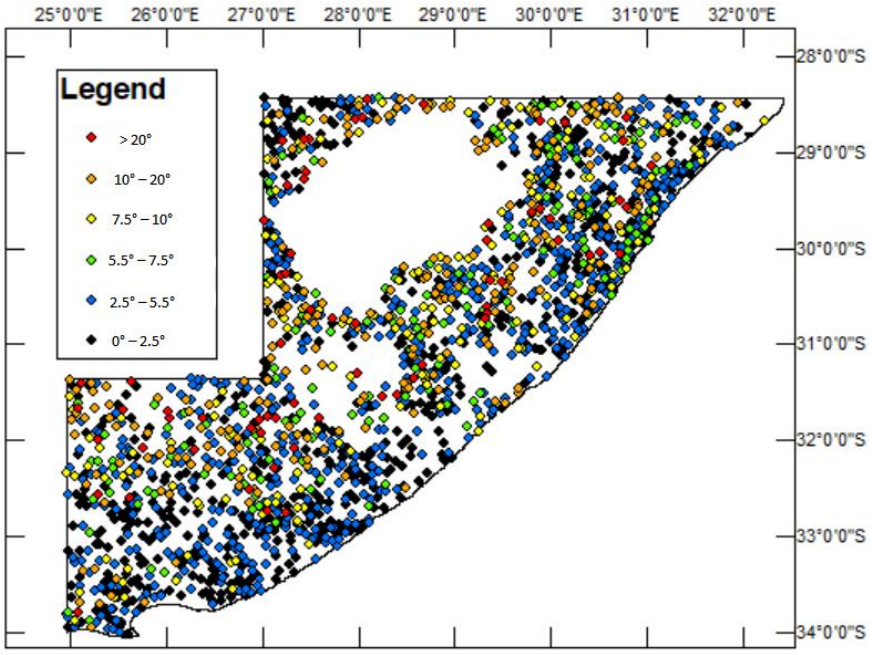

Figure 67: Spatial distribution of test points falling in different slope ranges over region 3

In region 4, out of 4,499 points of height differences between the ground levelling and each of the DEMs, 2,999 points were randomly selected for the model derivation. The remaining 1,500 points were used in the validation of each of the applied corrections.

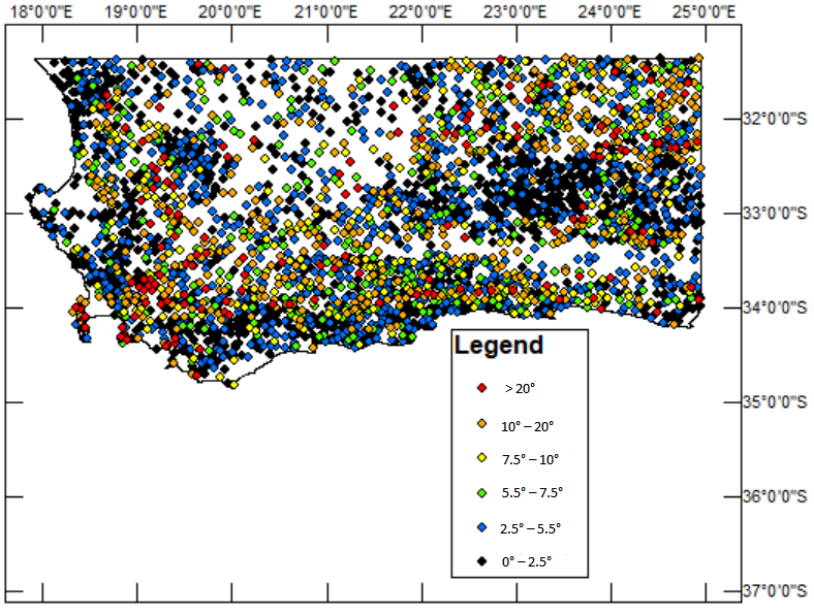

Figure 68: Spatial distribution of model points falling in different slope ranges over region 4

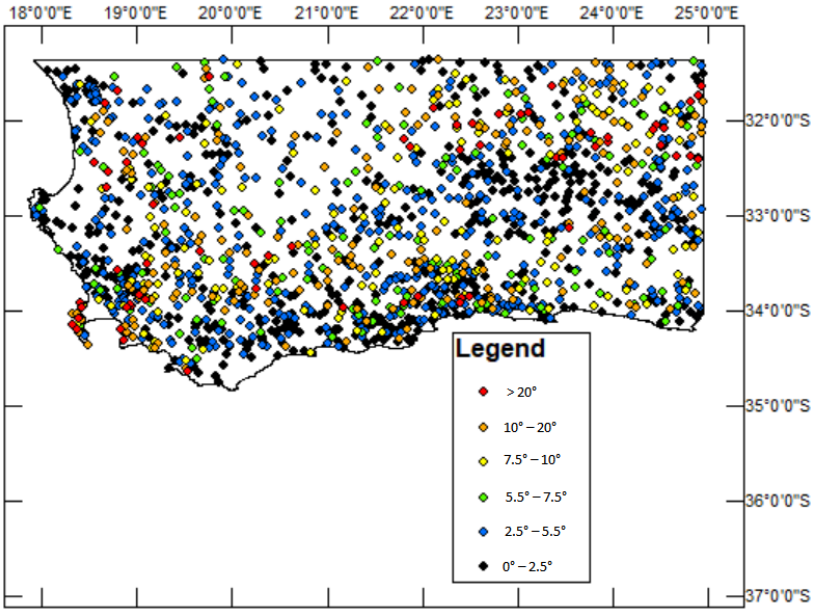

Figure 69: Spatial distribution of test points falling in different slope ranges over region 4

In region 5, out of 2,894 points of height differences between ground levelling and each of the DEMs, 1,929 points were randomly selected for the model derivation. The remaining 2,894 points were used in the validation of each of the applied corrections.

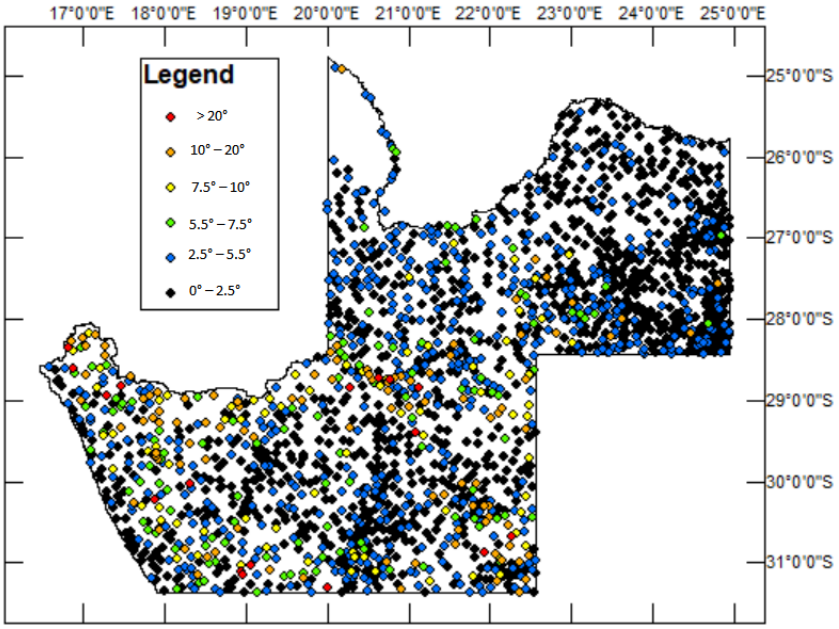

Figure 70: Spatial distribution of model points falling in different slope ranges over region 5

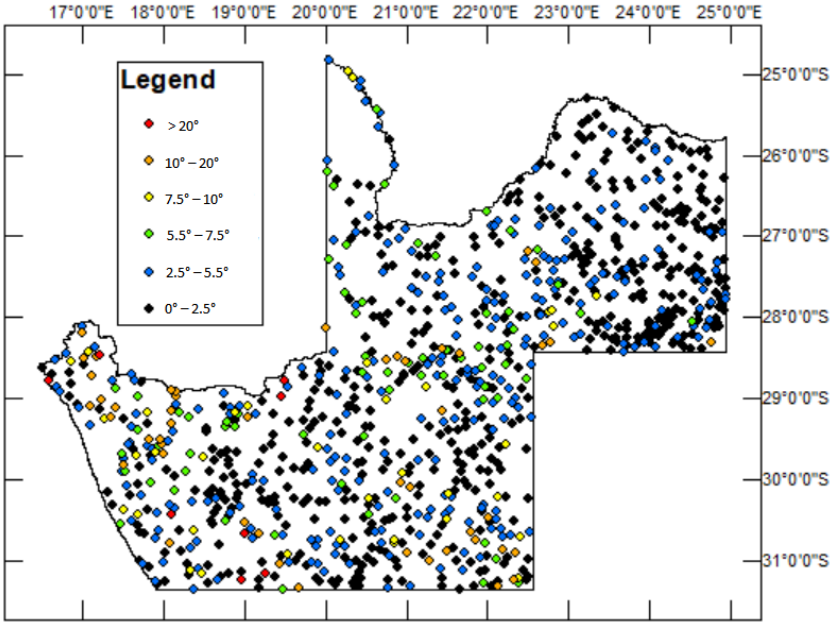

Figure 71: Spatial distribution of test points falling in different slope ranges over region 5

In region 6, out of 5,927 points of height differences between ground levelling and each of the DEMs, 3,950 points were randomly selected for the model derivation. The remaining 1,977 points were used in the validation of each of the applied corrections.

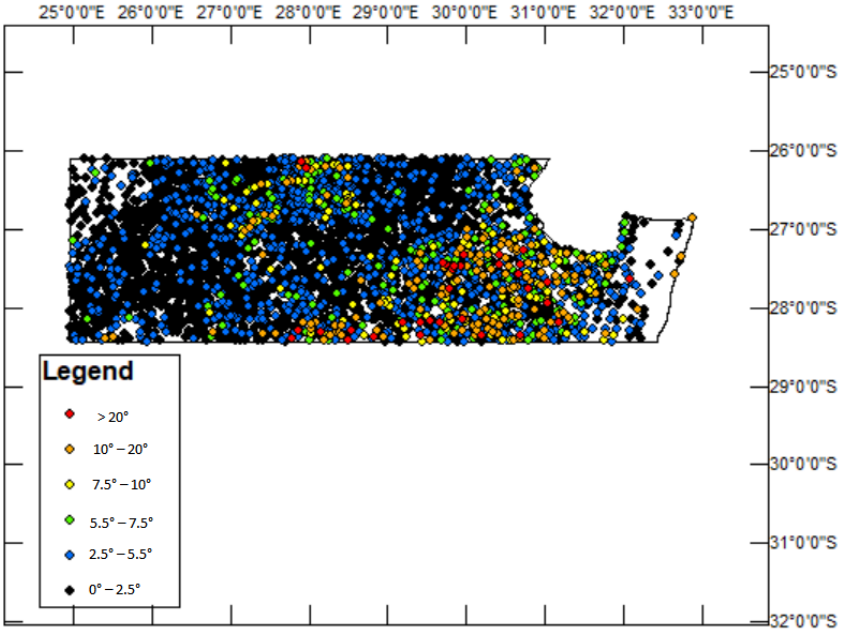

Figure 72: Spatial distribution of model points falling in different slope ranges over region 6

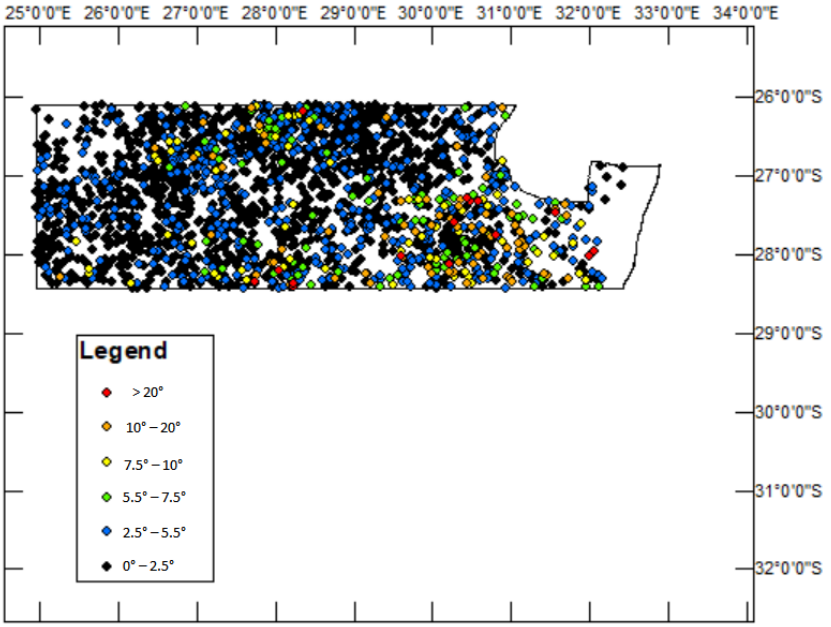

Figure 73: Spatial distribution of test points falling in different slope ranges over region 6

The validation of the corrected DEMs vertical accuracies was done using the combination of the whole test points from each region. The process included finding the height differences between the ground levelling test points and the corrected DEMs, then determining the statistical parameters as described in section (3.2.2.1). The validation of the vertical accuracies was also done for slope ranges (0° – 2.5°, 2.5° – 5.5°, 5.5° – 7.5°, 7.5° – 10°, 10° – 20°, >20°).

Other methods tested using the 41,260 LiDAR sampling grid of the area (A) are given as follows:

(i) Fitting different simple curves in the mean and actual data

For fitting different simple curves in the mean and actual data method, the process takes the correlation coefficient of the height error against each geomorphological factor data for each DEM into account. The geomorphological factors with the highest correlation coefficient against the height differences are chosen, and simple linear or exponential models are fitted. The method was tested using ground levelling over the whole of South Africa.

(ii) Using multiple trends for different geomorphological factor sections

The derivation of a correction model based on multiple trends for different sections includes looking at the trends that exist in a data, then fitting different simple curves for each data section. The method was tested using ground levelling over the whole of South Africa.

(iii) Using linear, multiple regression modelling, and adaptive terrain-dependent methods

The adaptive terrain-dependent, linear, and multiple regression methods are discussed in section (2.2.4).

(iv) Using the mean geomorphological (slope, aspect, and surface roughness) factors and semantic information errors to model DEM errors

The correction model based on geomorphological factors and semantic information errors involves the derivation of corrections based on the mean values of geomorphological parameters, height errors, and corresponding weights. This is done by fitting different models (polynomial, Gaussian, power functions, exponential, the sum of sines, Fourier series, and rational) for each DEM data. The method was tested using ground levelling and LiDAR over the area (A).

3.4.3 Results and discussion

The results and discussions of vertical accuracies of the co-registered AW3D30 are presented, followed by the vertical accuracies of the modelled DEMs.

3.4.3.1 Validation of co-registered AW3D30

The statistical results for the validation of co-registered AW3D30 in different directions, using ground levelling test data, are shown in Tables 22 and 23.

Table 22: Absolute height differences of co-registered AW3D30 on TanDEM-X grid

	AW3D30 Original	AW3D30 NW	AW3D30 NE	AW3D30 SE	AW3D30 SW
N	8657	8657	8657	8657	8657
Min(m)	-34.90	-34.90	-23.40	-24.70	-23.40
Max(m)	66.00	62.20	62.20	66.00	52.80
Mean (m)	2.768	3.867	3.626	3.370	3.619
STDV (±m)	4.784	5.745	5.609	5.414	5.562

Table 23: Absolute height differences of co-registered AW3D30 on TanDEM-X grid

	AW3D30 Original	AW3D30 NE	AW3D30 NE	AW3D30 SE	AW3D30 SW
0 < Slope < 2.5					
N	3920	3920	3920	3920	3920
Min(m)	-16.40	-15.40	-16.40	-16.40	-15.40
Max(m)	48.10	48.10	48.10	47.10	48.10
Mean (m)	1.878	2.222	2.080	2.022	2.134
STDV (±m)	4.357	4.580	4.505	4.461	4.522
2.5 < Slope < 5.5					
N	2448	2448	2448	2448	2448
Min(m)	-34.90	-34.90	-20.90	-24.70	-21.50
Max(m)	47.50	46.50	44.40	45.50	47.50
Mean (m)	2.768	3.698	3.437	3.225	3.450
STDV (±m)	5.015	5.416	5.220	5.179	5.298
5.5 < Slope < 7.5					
N	666	666	666	666	666
Min(m)	-23.40	-23.40	-23.40	-23.40	-23.40
Max(m)	31.80	33.80	48.80	39.80	31.80
Mean (m)	3.654	5.265	4.696	4.127	4.762
STDV (±m)	4.410	5.304	5.080	4.841	4.992
7.5 < Slope < 10					
N	593	593	593	593	593
Min(m)	-4.80	-5.60	-6.00	-6.60	-8.60
Max(m)	38.50	34.10	38.50	36.10	43.90
Mean (m)	3.698	5.689	5.286	5.064	5.463
STDV (±m)	4.303	5.169	4.843	5.226	5.566
10<Slope<20					
N	824	824	824	824	824
Min(m)	-4.60	-4.60	-8.10	-7.00	-4.30
Max(m)	60.60	60.60	60.60	46.60	36.60
Mean (m)	4.779	7.702	7.391	6.658	7.130
STDV (±m)	4.847	6.514	6.515	6.115	6.081
Slope > 20					
N	206	206	206	206	206
Min(m)	-2.70	-2.60	-2.90	-3.30	-2.30
Max(m)	66.00	62.20	62.20	66.00	52.80
Mean (m)	6.136	12.087	12.015	10.277	10.816
STDV (±m)	6.641	10.369	10.334	9.718	10.110

In Tables 22 and 23, there is an increase in the standard deviations and mean values in every direction the DEM is co-registered. In Table 23, the southeast shows the least standard deviation compared to other directions, and it is followed by the southwest, northeast, and northwest, respectively. From the results in these tables, co-registration of the AW3D30 on the grids of the DEMs (ASTER, SRTM, and TanDEM-X) decreases the vertical accuracy of the original DEM and the direction with better vertical accuracy is the southeast. However, based on the area (D) in Figure 61, a shift in the northwest direction was adopted for subsequent analysis and this was because of an obvious visible ½ grid pixel shift in the northwest direction.

3.4.3.2 Improvement on candidate DEMs

Tables 24 to 47 shows the statistical results for the six different regions before and after applying various models.

Region 1

Table 24: Absolute height difference in region 1 between the AW3D30 and ground levelling test data before and after applying different correction models

	Original AW3D30	Slope_corr	Aspect_corr	Roughness_corr	abs(Slope_corr)	abs(Aspect_corr)	abs(Roughness_corr)	Multiple linear reg_ corr	ATDM_corr(OLS)	ATDM_corr(M-estimator)
N	1219	1219	1219	1219	1219	1219	1219	1219	1219	1219
Min(m)	-23.40	-29.83	-29.14	-29.37	-30.17	-29.53	-29.73	-29.60	-32.46	-31.11
Max(m)	37.80	33.59	31.73	33.94	33.14	31.36	33.47	33.40	34.25	35.26
Mean (m)	5.308	-0.022	0.019	-0.023	-0.415	-0.386	-0.416	0.005	-0.007	0.934
STDV (±m)	6.195	5.906	6.194	5.872	5.895	6.194	5.857	5.868	5.768	5.839

Table 25: Comparison of the different correction methods in different slope ranges, using the ground levelling test data for AW3D30 in region 1

	Original AW3D30	Slope_corr	Aspect_corr	Roughness_corr	abs(Slope_corr)	abs(Aspect_corr)	abs(Roughness_corr)	Multiple linear reg_ corr	ATDM_corr(OLS)	ATDM_corr(M-estimator)
0 < Slope < 2.5										
N	571	571	571	571	571	571	571	571	571	571
Min(m)	-4.90	-8.94	-9.65	-8.76	-9.39	-10.08	-9.23	-8.32	-9.42	-8.93
Max(m)	37.80	33.59	31.73	33.94	33.14	31.36	33.47	33.40	34.25	35.26
Mean (m)	3.874	0.103	-1.413	0.097	-0.364	-1.819	-0.378	0.097	0.152	0.987
STDV (±m)	5.151	5.154	5.200	5.071	5.154	5.196	5.074	5.095	5.083	5.053
2.5 < Slope < 5.5										
N	350	350	350	350	350	350	350	350	350	350
Min(m)	-20.50	-26.00	-26.18	-25.41	-26.39	-26.57	-25.83	-25.60	-27.33	-25.49
Max(m)	34.30	28.82	29.43	29.39	28.44	29.01	28.97	29.81	29.99	30.80
Mean (m)	5.202	0.250	-0.084	0.244	-0.161	-0.489	-0.168	0.267	0.183	1.002
STDV (±m)	6.105	6.067	6.091	5.965	6.068	6.091	5.968	5.948	6.022	6.026
5.5 < Slope < 7.5										
N	88	88	88	88	88	88	88	88	88	88
Min(m)	-23.40	-29.83	-29.14	-29.37	-30.17	-29.53	-29.73	-29.60	-32.46	-31.11
Max(m)	33.80	27.30	29.00	27.83	26.96	28.57	27.47	28.32	29.64	29.88
Mean (m)	6.186	-0.177	0.863	-0.211	-0.520	0.459	-0.547	-0.194	-0.231	0.621
STDV (±m)	6.557	6.547	6.649	6.400	6.547	6.644	6.406	6.454	6.727	6.763
7.5 < Slope < 10										
N	73	73	73	73	73	73	73	73	73	73
Min(m)	-5.00	-12.38	-10.45	-12.02	-12.68	-10.85	-12.32	-12.03	-13.27	-10.88
Max(m)	30.50	22.52	24.54	23.48	22.25	24.16	23.18	23.17	22.85	24.73
Mean (m)	6.886	-0.577	1.660	-0.407	-0.868	1.252	-0.696	-0.270	-0.699	0.442
STDV (±m)	5.573	5.514	5.402	5.510	5.516	5.408	5.511	5.372	5.236	5.610
10<Slope<20										
N	110	110	110	110	110	110	110	110	110	110
Min(m)	-4.60	-15.37	-9.27	-14.78	-15.51	-9.70	-14.92	-14.11	-11.80	-11.11
Max(m)	31.70	21.77	26.56	21.52	21.59	26.13	21.38	21.50	26.39	27.87
Mean (m)	9.648	0.052	4.366	0.216	-0.137	3.961	0.040	0.350	0.205	1.383
STDV (±m)	7.549	7.672	7.506	7.520	7.662	7.507	7.515	7.467	7.157	7.550
Slope > 20										
N	27	27	27	27	27	27	27	27	27	27
Min(m)	1.40	-15.72	-3.43	-25.73	-14.90	-3.86	-24.25	-26.03	-13.82	-14.79
Max(m)	25.30	11.81	19.56	13.01	11.81	19.17	12.99	13.01	7.59	20.60
Mean (m)	12.185	-4.494	6.744	-5.367	-4.345	6.345	-5.114	-5.358	-4.096	-0.564
STDV (±m)	7.432	7.198	7.191	8.679	7.160	7.201	8.511	8.703	5.974	7.604

Table 26: Absolute height difference in region 1 between the TanDEM-X and ground levelling test data before and after applying different correction models

	Original TanDEM-X	Slope_corr	Aspect_corr	Roughness_corr	abs(Slope_corr)	abs(Aspect_corr)	abs(Roughness_corr)	Multiple linear reg_ corr	ATDM_corr(OLS)	ATDM_corr(M-estimator)
N	1219	1219	1219	1219	1219	1219	1219	1219	1219	1219
Min(m)	-23.08	-28.64	-28.30	-28.43	-28.71	-28.37	-28.51	-28.53	-29.63	-29.33
Max(m)	50.07	43.84	44.78	44.26	43.79	44.71	44.20	44.12	43.44	45.27
Mean (m)	5.057	-0.027	-0.022	-0.028	-0.113	-0.094	-0.114	-0.019	-0.015	0.882
STDV (±m)	5.146	5.045	5.148	5.052	5.044	5.148	5.051	5.053	4.989	5.009

Table 27: Comparison of the different correction methods in different slope ranges, using the ground levelling test data for TanDEM-X in region 1

	Original TanDEM-X	Slope_corr	Aspect_corr	Roughness_corr	abs(Slope_corr)	abs(Aspect_corr)	abs(Roughness_corr)	Multiple linear reg_ corr	ATDM_corr(OLS)	ATDM_corr(M-estimator)
0 < Slope < 2.5										
N	571	571	571	571	571	571	571	571	571	571
Min(m)	-5.07	-9.40	-10.02	-9.08	-9.51	-10.09	-9.20	-8.98	-9.18	-8.43
Max(m)	39.88	35.28	34.55	35.42	35.18	34.48	35.32	35.25	35.19	36.68
Mean (m)	4.518	0.107	-0.561	0.097	0.001	-0.632	-0.011	0.104	0.112	1.087
STDV (±m)	4.774	4.774	4.782	4.761	4.774	4.782	4.761	4.767	4.683	4.674
2.5 < Slope < 5.5										
N	350	350	350	350	350	350	350	350	350	350
Min(m)	-20.54	-25.70	-25.74	-25.45	-25.78	-25.81	-25.54	-25.53	-25.60	-24.59
Max(m)	34.61	29.46	29.67	29.70	29.38	29.59	29.61	29.81	29.69	30.96
Mean (m)	4.743	-0.178	-0.335	-0.182	-0.269	-0.407	-0.274	-0.174	-0.199	0.689
STDV (±m)	5.074	5.072	5.077	5.081	5.072	5.077	5.080	5.083	5.034	5.052
5.5 < Slope < 7.5										
N	88	88	88	88	88	88	88	88	88	88
Min(m)	-23.08	-28.64	-28.30	-28.43	-28.71	-28.37	-28.51	-28.53	-29.63	-29.33
Max(m)	47.85	42.26	42.93	42.49	42.19	42.86	42.42	42.61	42.58	43.88
Mean (m)	5.127	-0.403	0.037	-0.413	-0.476	-0.034	-0.484	-0.410	-0.524	0.310
STDV (±m)	6.107	6.104	6.129	6.081	6.104	6.129	6.081	6.096	6.123	6.205
7.5 < Slope < 10										
N	73	73	73	73	73	73	73	73	73	73
Min(m)	-7.90	-13.87	-13.03	-13.71	-13.93	-13.10	-13.77	-13.73	-12.38	-11.63
Max(m)	50.07	43.84	44.78	44.26	43.79	44.71	44.20	44.12	43.44	45.27
Mean (m)	6.175	0.170	1.116	0.252	0.111	1.044	0.194	0.278	0.215	0.962
STDV (±m)	6.344	6.310	6.305	6.332	6.311	6.305	6.333	6.303	6.179	6.309
10<Slope<20										
N	110	110	110	110	110	110	110	110	110	110
Min(m)	-0.57	-8.01	-5.45	-7.73	-8.02	-5.52	-7.74	-7.57	-7.66	-7.35
Max(m)	35.57	28.10	30.39	27.07	28.08	30.31	27.09	27.02	28.85	29.57
Mean (m)	6.995	0.070	1.918	0.159	0.038	1.847	0.131	0.176	0.159	0.818
STDV (±m)	4.316	4.255	4.311	4.202	4.256	4.311	4.205	4.199	4.413	4.389
Slope > 20										
N	27	27	27	27	27	27	27	27	27	27
Min(m)	1.05	-10.46	-4.07	-14.62	-10.23	-4.14	-14.21	-14.37	-7.26	-6.57
Max(m)	22.73	10.79	17.50	10.17	10.91	17.43	10.33	10.12	9.89	12.27
Mean (m)	9.367	-0.617	4.239	-0.937	-0.558	4.168	-0.851	-0.939	0.021	0.947
STDV (±m)	5.399	5.393	5.364	5.934	5.386	5.364	5.899	5.899	4.998	5.058

In Table 25, the correction model for the AW3D30 is a combination of the adaptive terrain-dependent method with parameters determined using Robust least squares (M-estimator) for slope less than 2.5°, multiple regression as a function of (slope, aspect, and surface roughness) for slope 2.5° to 7.5°, and adaptive terrain-dependent method with parameters determined using Ordinary Least Squares for slope greater than 7.5°. In Table 27, the correction model for the TanDEM-X is a combination of the adaptive terrain-dependent method with parameters determined using Robust least squares (M-estimator) for slope less than 2.5° and greater than 20°, adaptive terrain-dependent method with parameters determined using Ordinary Least Squares for slope 2.5° to 5.5° and 7.5° to 10°, simple linear regression as a function of surface roughness for slope 5.5° to 7.5°, and multiple regression as a function of (slope, aspect, and surface roughness) for slope 10° to 20°. The models are adopted because, after being applied to these DEMs, there is a remarkable decrease in standard deviations in those slope ranges, meaning an improvement in vertical accuracy.

Region 2

Table 28: Absolute height difference in region 2 between the AW3D30 and ground levelling test data before and after applying different correction models

	Original AW3D30	Slope_corr	Aspect_corr	Roughness_corr	abs(Slope_corr)	abs(Aspect_corr)	abs(Roughness_corr)	Multiple linear reg_ corr	ATDM_corr(OLS)	ATDM_corr(M-estimator)
N	1095	1095	1095	1095	1095	1095	1095	1095	1095	1095
Min(m)	-3.90	-14.05	-8.56	-15.84	-13.96	-8.81	-15.62	-17.83	-12.17	-8.81
Max(m)	39.50	30.23	35.08	29.38	30.21	34.82	29.43	29.31	29.69	30.51
Mean (m)	4.114	-0.348	-0.371	-0.317	-0.607	-0.629	-0.578	-0.317	-0.360	0.632
STDV (±m)	5.107	4.782	5.097	4.736	4.785	5.097	4.739	4.715	4.409	4.494

Table 29: Comparison of the different correction methods in different slope ranges, using the ground levelling test data for AW3D30 in region 2

	Original AW3D30	Slope_corr	Aspect_corr	Roughness_corr	abs(Slope_corr)	abs(Aspect_corr)	abs(Roughness_corr)	Multiple linear reg_ corr	ATDM_corr(OLS)	ATDM_corr(M-estimator)
0 < Slope < 2.5										
N	413	413	413	413	413	413	413	413	413	413
Min(m)	-3.90	-7.02	-8.56	-7.01	-7.35	-8.81	-7.34	-7.27	-7.52	-6.16
Max(m)	31.80	28.90	28.05	28.69	28.56	27.78	28.36	29.31	29.69	30.51
Mean (m)	2.210	-0.917	-2.295	-0.870	-1.244	-2.553	-1.204	-0.942	-0.550	0.476
STDV (±m)	3.983	3.986	4.038	3.916	3.986	4.036	3.918	3.970	4.046	4.013
2.5 < Slope < 5.5										
N	283	283	283	283	283	283	283	283	283	283
Min(m)	-2.70	-6.47	-7.94	-6.59	-6.76	-8.19	-6.88	-7.57	-7.81	-6.11
Max(m)	22.90	18.79	19.31	19.01	18.52	19.04	18.72	20.13	20.13	20.79
Mean (m)	3.789	-0.078	-0.669	0.014	-0.367	-0.928	-0.282	0.056	-0.125	0.759
STDV (±m)	4.477	4.451	4.459	4.324	4.452	4.459	4.331	4.248	4.365	4.415
5.5 < Slope < 7.5										
N	122	122	122	122	122	122	122	122	122	122
Min(m)	-3.00	-7.49	-8.36	-7.67	-7.75	-8.60	-7.91	-8.77	-8.62	-7.35
Max(m)	24.90	19.93	20.90	19.45	19.70	20.64	19.25	19.72	20.05	20.16
Mean (m)	5.189	0.406	0.710	0.382	0.163	0.452	0.141	0.372	-0.072	0.761
STDV (±m)	4.974	4.951	4.966	4.908	4.952	4.965	4.911	4.882	4.876	4.811
7.5 < Slope < 10										
N	95	95	95	95	95	95	95	95	95	95
Min(m)	-3.00	-8.84	-6.93	-8.45	-9.03	-7.20	-8.65	-7.54	-9.17	-8.50
Max(m)	17.20	11.72	12.20	11.75	11.51	11.95	11.55	11.22	9.28	10.73
Mean (m)	6.187	0.650	1.606	0.603	0.446	1.350	0.404	0.496	0.032	0.783
STDV (±m)	4.356	4.381	4.301	4.413	4.379	4.302	4.408	4.388	3.949	4.062
10<Slope<20										
N	163	163	163	163	163	163	163	163	163	163
Min(m)	-1.90	-10.58	-6.26	-10.72	-10.61	-6.50	-10.67	-12.37	-11.98	-8.81
Max(m)	27.60	20.66	23.03	20.60	20.53	22.77	20.48	20.55	16.64	18.63
Mean (m)	6.844	-0.453	2.424	-0.461	-0.568	2.165	-0.566	-0.282	-0.918	0.369
STDV (±m)	5.681	5.711	5.565	5.748	5.706	5.566	5.740	5.644	4.418	4.747
Slope > 20										
N	19.00	19.00	19.00	19.00	19.00	19.00	19.00	19.00	19.00	19.00
Min(m)	-2.60	-14.05	-8.16	-15.84	-13.96	-8.40	-15.62	-17.83	-12.17	-6.12
Max(m)	39.500	30.226	35.075	29.380	30.212	34.817	29.428	29.135	27.280	29.349
Mean (m)	9.679	-0.914	5.097	-1.097	-0.861	4.840	-1.014	-1.060	1.245	2.793
STDV (±m)	11.191	11.282	11.162	11.348	11.274	11.162	11.333	11.385	8.634	9.631

Table 30: Absolute height difference in region 2 between the TanDEM-X and ground levelling test data before and after applying different correction models

	Original TanDEM-X	Slope_corr	Aspect_corr	Roughness_corr	abs(Slope_corr)	abs(Aspect_corr)	abs(Roughness_corr)	Multiple linear reg_ corr	ATDM_corr(OLS)	ATDM_corr(M-estimator)
N	1095	1095	1095	1095	1095	1095	1095	1095	1095	1095
Min(m)	-1.49	-6.50	-5.60	-6.66	-6.50	-5.60	-6.65	-7.34	-8.59	-4.87
Max(m)	33.29	30.01	29.17	29.85	30.01	29.17	29.84	30.12	30.22	31.19
Mean (m)	4.106	-0.263	-0.278	-0.242	-0.267	-0.280	-0.247	-0.245	-0.272	0.677
STDV (±m)	3.674	3.496	3.674	3.472	3.496	3.674	3.472	3.469	3.484	3.493

Table 31: Comparison of the different correction methods in different slope ranges, using the ground levelling test data for TanDEM-X in region 2

	Original TanDEM-X	Slope_corr	Aspect_corr	Roughness_corr	abs(Slope_corr)	abs(Aspect_corr)	abs(Roughness_corr)	Multiple linear reg_ corr	ATDM_corr(OLS)	ATDM_corr(M-estimator)
0 < Slope < 2.5										
N	413	413	413	413	413	413	413	413	413	413
Min(m)	-1.49	-5.05	-5.60	-4.93	-5.05	-5.60	-4.94	-4.57	-4.81	-3.80
Max(m)	33.29	30.01	29.17	29.85	30.01	29.17	29.84	30.12	30.22	31.19
Mean (m)	3.017	-0.417	-1.374	-0.407	-0.424	-1.377	-0.413	-0.430	-0.380	0.539
STDV (±m)	3.791	3.793	3.797	3.764	3.793	3.797	3.764	3.771	3.815	3.797
2.5 < Slope < 5.5										
N	283	283	283	283	283	283	283	283	283	283
Min(m)	-0.44	-4.13	-5.19	-3.88	-4.14	-5.20	-3.89	-4.30	-4.27	-3.08
Max(m)	32.28	28.16	28.22	28.30	28.16	28.22	28.30	28.74	28.60	29.55
Mean (m)	3.896	-0.055	-0.477	-0.002	-0.061	-0.479	-0.007	0.012	-0.048	0.772
STDV (±m)	3.715	3.706	3.711	3.658	3.706	3.711	3.658	3.646	3.728	3.727
5.5 < Slope < 7.5										
N	122	122	122	122	122	122	122	122	122	122
Min(m)	0.63	-4.07	-3.84	-4.00	-4.08	-3.84	-4.00	-4.37	-4.42	-3.49
Max(m)	20.99	16.29	16.87	16.48	16.28	16.87	16.48	16.86	17.19	17.57
Mean (m)	4.546	-0.047	0.165	-0.059	-0.051	0.163	-0.062	-0.064	-0.123	0.727
STDV (±m)	3.096	3.089	3.091	3.054	3.089	3.091	3.054	3.041	3.144	3.078
7.5 < Slope < 10										
N	95	95	95	95	95	95	95	95	95	95
Min(m)	1.68	-3.61	-2.85	-3.36	-3.61	-2.85	-3.36	-3.54	-3.56	-2.91
Max(m)	10.98	6.12	6.46	5.41	6.12	6.45	5.40	5.43	5.77	6.45
Mean (m)	5.047	-0.075	0.629	-0.090	-0.078	0.626	-0.092	-0.139	-0.124	0.684
STDV (±m)	2.150	2.207	2.167	2.173	2.206	2.167	2.173	2.192	2.245	2.221
10<Slope<20										
N	163	163	163	163	163	163	163	163	163	163
Min(m)	1.18	-5.74	-3.49	-6.25	-5.74	-3.49	-6.24	-6.45	-7.67	-4.87
Max(m)	17.27	10.46	12.74	10.63	10.46	12.74	10.63	10.55	8.82	11.53
Mean (m)	5.940	-0.414	1.580	-0.374	-0.414	1.578	-0.373	-0.325	-0.549	0.729
STDV (±m)	3.146	3.087	3.129	3.100	3.087	3.129	3.100	3.082	2.955	3.042
Slope > 20										
N	19	19	19	19	19	19	19	19	19	19
Min(m)	2.65	-6.50	-1.55	-6.66	-6.50	-1.56	-6.65	-7.34	-8.59	-3.48
Max(m)	19.43	9.60	14.92	9.59	9.61	14.92	9.60	9.47	6.08	13.43
Mean (m)	7.628	-1.034	3.209	-1.060	-1.029	3.207	-1.054	-1.081	-0.607	1.439
STDV (±m)	4.121	4.172	4.096	4.333	4.172	4.096	4.333	4.359	3.223	4.121

In Table 29, the correction model for the AW3D30 is a combination of the simple linear regression as a function of surface roughness for slope less than 2.5°, multiple regression as a function of (slope, aspect, and surface roughness) for slope 2.5° to 7.5°, and adaptive terrain-dependent method with parameters determined using Ordinary Least Squares for slope greater than 7.5°. In Table 31, the correction model for the TanDEM-X is a combination of the simple linear regression as a function of surface roughness for slope less than 2.5°, multiple regression as a function of (slope, aspect, and surface roughness) for slope 2.5° to 7.5°, original TanDEM-X for slope 7.5° to 10°, and adaptive terrain-dependent method with parameters determined using Ordinary Least Squares for slope greater than 10°. The models are adopted because, after being applied to these DEMs, there is a remarkable decrease in standard deviations in those slope ranges, meaning an improvement in vertical accuracy.

Region 3

Table 32: *Absolute height difference in region 3 between the AW3D30 and ground levelling test data before and after applying different correction models*

	Original AW3D30	Slope_corr	Aspect_corr	Roughness_corr	abs(Slope_corr)	abs(Aspect_corr)	abs(Roughness_corr)	Multiple linear reg_ corr	ATDM_corr(OLS)	ATDM_corr(M-estimator)
N	1901	1901	1901	1901	1901	1901	1901	1901	1901	1901
Min(m)	-34.90	-37.27	-38.90	-37.77	-37.95	-39.48	-38.42	-38.21	-38.22	-37.57
Max(m)	62.20	54.36	58.49	53.76	53.94	57.91	53.41	53.34	50.28	53.82
Mean (m)	3.444	-0.337	-0.346	-0.358	-0.919	-0.926	-0.938	-0.366	-0.299	0.571
STDV (±m)	5.746	5.062	5.727	5.014	5.065	5.727	5.014	4.993	4.756	4.946

Table 33: Comparison of the different correction methods in different slope ranges, using the ground levelling test data for AW3D30 in region 3

	Original AW3D30	Slope_corr	Aspect_corr	Roughness_corr	abs(Slope_corr)	abs(Aspect_corr)	abs(Roughness_corr)	Multiple linear reg_ corr	ATDM_corr(OLS)	ATDM_corr(M-estimator)
0 < Slope < 2.5										
N	638	638	638	638	638	638	638	638	638	638
Min(m)	-13.30	-15.13	-16.73	-15.18	-15.85	-17.31	-15.90	-14.90	-15.31	-15.09
Max(m)	29.80	27.93	25.56	27.92	27.22	24.98	27.20	27.52	26.58	28.63
Mean (m)	1.404	-0.437	-2.408	-0.514	-1.151	-2.988	-1.234	-0.632	-0.148	0.276
STDV (±m)	3.632	3.635	3.626	3.515	3.634	3.626	3.520	3.481	3.623	3.616
2.5 < Slope < 5.5										
N	617	617	617	617	617	617	617	617	617	617
Min(m)	-34.90	-37.27	-38.90	-37.77	-37.95	-39.48	-38.42	-38.21	-38.22	-37.57
Max(m)	23.60	21.14	19.27	19.62	20.46	18.69	18.90	19.12	20.18	21.08
Mean (m)	2.324	-0.565	-1.449	-0.552	-1.208	-2.029	-1.201	-0.562	-0.501	0.039
STDV (±m)	4.023	4.011	4.025	3.834	4.011	4.025	3.844	3.790	3.999	3.986
5.5 < Slope < 7.5										
N	161	161	161	161	161	161	161	161	161	161
Min(m)	-12.30	-16.00	-16.56	-16.16	-16.59	-17.15	-16.74	-16.70	-16.40	-15.95
Max(m)	27.50	22.96	23.61	20.66	22.43	23.03	20.31	19.81	20.51	22.60
Mean (m)	4.109	0.006	0.292	-0.005	-0.554	-0.289	-0.562	-0.027	-0.384	0.511
STDV (±m)	4.725	4.707	4.709	4.546	4.707	4.709	4.557	4.486	4.649	4.658
7.5 < Slope < 10										
N	178	178	178	178	178	178	178	178	178	178
Min(m)	-3.40	-8.16	-6.53	-8.25	-8.67	-7.11	-8.76	-7.59	-9.25	-7.51
Max(m)	19.80	14.53	16.00	13.45	14.05	15.41	13.03	13.45	13.78	14.62
Mean (m)	4.724	-0.305	0.979	-0.247	-0.801	0.399	-0.741	-0.138	-0.547	0.395
STDV (±m)	4.628	4.625	4.562	4.507	4.624	4.562	4.512	4.421	4.250	4.387
10<Slope<20										
N	236	236	236	236	236	236	236	236	236	236
Min(m)	-4.60	-10.98	-8.31	-11.81	-11.33	-8.89	-11.95	-11.47	-12.18	-9.03
Max(m)	60.60	54.36	56.52	53.76	53.94	55.94	53.41	53.34	50.28	53.82
Mean (m)	7.617	0.317	3.825	0.498	-0.024	3.245	0.163	0.681	-0.110	1.689
STDV (±m)	7.323	7.278	7.251	7.300	7.274	7.251	7.294	7.249	6.550	6.733
Slope > 20										
N	71.00	71.00	71.00	71.00	71.00	71.00	71.00	71.00	71.00	71.00
Min(m)	-1.20	-16.62	-4.39	-20.19	-16.02	-4.97	-19.23	-20.77	-22.02	-10.96
Max(m)	62.200	51.039	58.485	50.405	50.961	57.905	50.414	50.494	48.539	52.237
Mean (m)	12.910	-0.499	9.135	-1.190	-0.423	8.555	-1.010	-1.106	0.300	4.724
STDV (±m)	11.898	12.052	11.838	12.469	12.012	11.838	12.355	12.604	10.514	11.253

Table 34: Absolute height difference in region 3 between the TanDEM-X and ground levelling test data before and after applying different correction models

	Original TanDEM-X	Slope_corr	Aspect_corr	Roughness_corr	abs(Slope_corr)	abs(Aspect_corr)	abs(Roughness_corr)	Multiple linear reg_ corr	ATDM_corr(OLS)	ATDM_corr(M-estimator)
N	1901	1901	1901	1901	1901	1901	1901	1901	1901	1901
Min(m)	-7.24	-12.58	-11.03	-18.56	-12.53	-11.18	-18.36	-19.55	-17.94	-13.31
Max(m)	73.32	63.46	69.54	63.01	63.39	69.41	62.97	63.02	63.37	67.73
Mean (m)	3.763	-0.013	-0.020	-0.030	-0.162	-0.157	-0.178	-0.034	0.013	0.812
STDV (±m)	5.277	4.557	5.277	4.463	4.560	5.277	4.468	4.457	4.499	4.874

Table 35: Comparison of the different correction methods in different slope ranges, using the ground levelling test data for TanDEM-X in region 3

	Original TanDEM-X	Slope_corr	Aspect_corr	Roughness_corr	abs(Slope_corr)	abs(Aspect_corr)	abs(Roughness_corr)	Multiple linear reg_ corr	ATDM_corr(OLS)	ATDM_corr(M-estimator)
0 < Slope < 2.5										
N	638	638	638	638	638	638	638	638	638	638
Min(m)	-7.24	-9.57	-11.03	-9.46	-9.74	-11.18	-9.64	-9.48	-9.54	-9.40
Max(m)	30.16	27.96	26.34	27.94	27.79	26.17	27.76	27.87	25.77	28.04
Mean (m)	2.453	0.278	-1.330	0.197	0.106	-1.468	0.021	0.153	0.070	0.357
STDV (±m)	2.956	2.970	2.955	2.921	2.970	2.953	2.921	2.917	2.952	2.962
2.5 < Slope < 5.5										
N	617	617	617	617	617	617	617	617	617	617
Min(m)	-6.44	-9.45	-10.22	-9.47	-9.61	-10.35	-9.63	-9.48	-9.16	-8.97
Max(m)	17.72	14.29	13.95	12.63	14.13	13.83	12.47	12.67	13.54	14.72
Mean (m)	2.833	-0.207	-0.949	-0.205	-0.367	-1.085	-0.367	-0.216	-0.164	0.258
STDV (±m)	2.165	2.170	2.166	2.049	2.170	2.167	2.049	2.040	2.179	2.161
5.5 < Slope < 7.5										
N	161	161	161	161	161	161	161	161	161	161
Min(m)	-4.06	-7.88	-7.82	-7.90	-8.03	-7.93	-8.05	-7.88	-7.63	-7.08
Max(m)	22.71	19.00	18.92	19.68	18.85	18.77	19.52	19.80	18.72	19.76
Mean (m)	3.684	-0.358	-0.100	-0.364	-0.503	-0.238	-0.508	-0.363	-0.204	0.567
STDV (±m)	2.918	2.929	2.917	2.818	2.929	2.917	2.819	2.803	2.872	2.905
7.5 < Slope < 10										
N	178	178	178	178	178	178	178	178	178	178
Min(m)	-4.75	-10.07	-8.50	-10.21	-10.19	-8.60	-10.33	-10.17	-11.64	-8.50
Max(m)	49.10	44.50	45.35	42.83	44.37	45.24	42.73	42.54	43.08	45.51
Mean (m)	4.242	-0.562	0.462	-0.504	-0.697	0.327	-0.635	-0.474	-0.277	0.701
STDV (±m)	4.291	4.304	4.292	4.146	4.303	4.294	4.148	4.122	4.181	4.272
10<Slope<20										
N	236	236	236	236	236	236	236	236	236	236
Min(m)	-4.97	-10.84	-8.76	-10.43	-10.96	-8.91	-10.55	-10.33	-9.80	-9.01
Max(m)	30.64	24.72	26.86	24.37	24.60	26.72	24.27	24.33	25.37	26.52
Mean (m)	5.770	-0.909	1.987	-0.729	-1.017	1.850	-0.830	-0.647	-0.608	1.200
STDV (±m)	4.386	4.362	4.386	4.339	4.360	4.386	4.338	4.341	4.396	4.338
Slope > 20										
N	71	71	71	71	71	71	71	71	71	71
Min(m)	1.63	-12.58	-2.16	-18.56	-12.53	-2.30	-18.36	-19.55	-17.94	-13.31
Max(m)	73.32	63.46	69.54	63.01	63.39	69.41	62.97	63.02	63.37	67.73
Mean (m)	15.915	4.195	12.133	3.721	4.160	11.997	3.720	3.752	4.314	9.252
STDV (±m)	17.674	16.858	17.673	16.713	16.867	17.672	16.721	16.708	16.591	17.688

In Table 33, the correction model for the AW3D30 is a combination of multiple regression as a function of (slope, aspect, and surface roughness) for slope less than 7.5°, and an adaptive terrain-dependent method with parameters determined using Ordinary Least Squares for slopes greater than 7.5°. In Table 35, the correction model for the TanDEM-X is a combination of multiple regression as a function of (slope, aspect, and surface roughness) for slope less than 10°, simple linear regression as a function

of surface roughness and absolute height errors for slope 10° to 20°, and adaptive terrain-dependent method with parameters determined using Ordinary Least Squares for slope greater than 20°. The models are adopted because, after being applied to these DEMs, there is a remarkable decrease in standard deviations in those slope ranges, meaning an improvement in vertical accuracy.

Region 4

Table 36: Absolute height difference in region 4 between the AW3D30 and ground levelling test data before and after applying different correction models

	Original AW3D30	Slope_corr	Aspect_corr	Roughness_corr	abs(Slope_corr)	abs(Aspect_corr)	abs(Roughness_corr)	Multiple linear reg_ corr	ATDM_corr(OLS)	ATDM_corr(M-estimator)
N	1500	1500	1500	1500	1500	1500	1500	1500	1500	1500
Min(m)	-7.80	-21.33	-12.51	-25.65	-20.86	-12.74	-24.57	-26.87	-16.10	-10.97
Max(m)	40.00	27.72	35.53	28.42	27.44	35.30	28.12	28.65	26.31	28.19
Mean (m)	4.354	-0.067	-0.134	-0.094	-0.296	-0.370	-0.322	-0.122	-0.037	0.638
STDV (±m)	5.125	4.558	5.116	4.531	4.552	5.116	4.522	4.515	4.068	4.274

Table 37: Comparison of the different correction methods in different slope ranges, using the ground levelling test data for AW3D30 in region 4

	Original AW3D30	Slope_corr	Aspect_corr	Roughness_corr	abs(Slope_corr)	abs(Aspect_corr)	abs(Roughness_corr)	Multiple linear reg_ corr	ATDM_corr(OLS)	ATDM_corr(M-estimator)
0 < Slope < 2.5										
N	500	500	500	500	500	500	500	500	500	500
Min(m)	-3.50	-6.15	-8.20	-6.18	-6.44	-8.43	-6.48	-6.66	-6.85	-5.83
Max(m)	16.70	13.96	12.78	13.23	13.66	12.54	12.96	13.96	14.75	15.41
Mean (m)	2.183	-0.410	-2.334	-0.551	-0.712	-2.570	-0.848	-0.638	0.105	0.468
STDV (±m)	2.863	2.831	2.879	2.639	2.832	2.879	2.646	2.665	2.727	2.732
2.5 < Slope < 5.5										
N	448	448	448	448	448	448	448	448	448	448
Min(m)	-7.80	-10.94	-12.51	-11.27	-11.22	-12.74	-11.54	-11.67	-11.26	-10.43
Max(m)	31.10	27.72	26.72	28.42	27.44	26.49	28.12	28.65	26.31	27.32
Mean (m)	3.493	0.023	-0.982	0.013	-0.243	-1.217	-0.253	0.008	0.072	0.453
STDV (±m)	4.104	4.052	4.100	3.826	4.054	4.100	3.835	3.812	3.879	3.904
5.5 < Slope < 7.5										
N	145	145	145	145	145	145	145	145	145	145
Min(m)	-2.20	-6.93	-6.75	-6.47	-7.15	-6.98	-6.70	-6.52	-7.88	-6.78
Max(m)	31.00	26.24	26.25	26.73	26.02	26.02	26.50	26.38	21.96	24.24
Mean (m)	5.386	0.904	0.941	0.862	0.678	0.705	0.637	0.896	0.179	0.918
STDV (±m)	4.922	4.916	4.881	4.803	4.916	4.881	4.806	4.736	4.507	4.672
7.5 < Slope < 10										
N	145	145	145	145	145	145	145	145	145	145
Min(m)	-5.60	-10.81	-9.98	-10.66	-11.01	-10.21	-10.86	-10.50	-11.12	-10.46
Max(m)	20.80	15.86	16.02	14.15	15.66	15.78	14.01	13.47	11.97	14.36
Mean (m)	5.433	0.081	0.905	0.048	-0.110	0.670	-0.142	-0.039	-0.564	-0.053
STDV (±m)	4.532	4.511	4.477	4.412	4.511	4.477	4.414	4.336	4.479	4.370
10<Slope<20										
N	196	196	196	196	196	196	196	196	196	196
Min(m)	-4.10	-10.56	-8.15	-11.03	-10.71	-8.39	-11.04	-11.96	-13.41	-10.97
Max(m)	32.70	26.30	28.31	26.84	26.15	28.07	26.67	27.03	24.17	25.46
Mean (m)	7.803	0.336	3.333	0.686	0.229	3.097	0.566	0.734	-0.518	0.618
STDV (±m)	5.602	5.723	5.556	5.655	5.714	5.556	5.648	5.603	4.978	5.159
Slope > 20										
N	66.00	66.00	66.00	66.00	66.00	66.00	66.00	66.00	66.00	66.00
Min(m)	-2.40	-21.33	-6.54	-25.65	-20.86	-6.77	-24.57	-26.87	-16.10	-9.16
Max(m)	40.000	26.250	35.532	26.782	26.322	35.296	26.834	26.790	23.098	28.190
Mean (m)	11.755	-1.736	7.346	-2.096	-1.602	7.110	-1.946	-2.043	0.259	4.139
STDV (±m)	9.658	9.926	9.579	10.794	9.889	9.579	10.692	10.810	7.321	8.499

Table 38: Absolute height difference in region 4 between the TanDEM-X and ground levelling test data before and after applying different correction models

	Original TanDEM-X	Slope_corr	Aspect_corr	Roughness_corr	abs(Slope_corr)	abs(Aspect_corr)	abs(Roughness_corr)	Multiple linear reg_ corr	ATDM_corr(OLS)	ATDM_corr(M-estimator)
N	1500	1500	1500	1500	1500	1500	1500	1500	1500	1500
Min(m)	-9.25	-16.97	-13.94	-28.86	-16.97	-13.98	-28.82	-31.94	-18.24	-13.57
Max(m)	48.32	33.60	43.70	32.55	33.58	43.66	32.53	32.33	30.83	43.80
Mean (m)	4.558	-0.053	-0.099	-0.080	-0.086	-0.136	-0.113	-0.093	-0.048	0.612
STDV (±m)	4.323	3.522	4.325	3.454	3.522	4.325	3.454	3.461	3.446	3.733

Table 39:Comparison of the different correction methods in different slope ranges, using the ground levelling test data for TanDEM-X in region 4

	Original TanDEM-X	Slope_corr	Aspect_corr	Roughness_corr	abs(Slope_corr)	abs(Aspect_corr)	abs(Roughness_corr)	Multiple linear reg_ corr	ATDM_corr(OLS)	ATDM_corr(M-estimator)
0 < Slope < 2.5										
N	500	500	500	500	500	500	500	500	500	500
Min(m)	-3.85	-6.97	-8.42	-7.50	-7.00	-8.46	-7.54	-7.76	-6.08	-6.22
Max(m)	16.81	13.87	12.26	12.35	13.83	12.22	12.32	11.76	12.55	13.47
Mean (m)	2.820	0.020	-1.827	-0.096	-0.017	-1.865	-0.133	-0.199	-0.008	0.305
STDV (±m)	1.786	1.777	1.788	1.595	1.777	1.788	1.595	1.569	1.766	1.731
2.5 < Slope < 5.5										
N	448	448	448	448	448	448	448	448	448	448
Min(m)	-3.56	-6.96	-8.31	-6.90	-6.99	-8.35	-6.93	-7.08	-6.38	-6.20
Max(m)	32.77	29.19	28.08	29.91	29.15	28.04	29.87	30.12	28.26	29.00
Mean (m)	3.639	-0.029	-1.022	-0.025	-0.064	-1.059	-0.060	-0.056	-0.056	0.222
STDV (±m)	2.754	2.702	2.754	2.526	2.702	2.754	2.526	2.502	2.606	2.611
5.5 < Slope < 7.5										
N	145	145	145	145	145	145	145	145	145	145
Min(m)	-0.65	-5.24	-5.26	-5.10	-5.28	-5.30	-5.14	-5.09	-4.43	-4.34
Max(m)	17.33	12.38	12.75	12.87	12.35	12.72	12.84	12.99	11.16	11.94
Mean (m)	4.742	0.069	0.072	0.027	0.036	0.035	-0.006	0.018	-0.035	0.372
STDV (±m)	2.914	2.916	2.926	2.780	2.916	2.926	2.781	2.751	2.716	2.782
7.5 < Slope < 10										
N	145	145	145	145	145	145	145	145	145	145
Min(m)	-9.25	-14.65	-13.94	-14.50	-14.68	-13.98	-14.53	-14.42	-13.34	-13.57
Max(m)	19.13	13.63	14.42	9.41	13.60	14.39	9.37	9.46	13.70	14.15
Mean (m)	5.534	0.000	0.890	-0.045	-0.031	0.853	-0.076	-0.043	0.011	0.403
STDV (±m)	3.468	3.452	3.484	3.139	3.452	3.484	3.140	3.071	3.537	3.434
10<Slope<20										
N	196	196	196	196	196	196	196	196	196	196
Min(m)	0.69	-6.88	-4.10	-7.46	-6.90	-4.14	-7.48	-7.59	-6.62	-5.24
Max(m)	41.80	33.50	37.20	32.55	33.47	37.16	32.53	32.33	30.83	34.19
Mean (m)	7.169	-0.462	2.507	-0.152	-0.490	2.470	-0.179	0.038	-0.254	0.754
STDV (±m)	4.369	4.350	4.376	4.166	4.350	4.376	4.166	4.122	4.253	4.313
Slope > 20										
N	66	66	66	66	66	66	66	66	66	66
Min(m)	2.94	-16.97	-1.80	-28.86	-16.97	-1.84	-28.82	-31.94	-18.24	-5.29
Max(m)	48.32	33.60	43.70	31.88	33.58	43.66	31.88	31.63	30.49	43.80
Mean (m)	13.661	0.061	8.980	-0.428	0.044	8.943	-0.439	-0.293	0.155	6.160
STDV (±m)	10.651	10.334	10.669	10.876	10.334	10.669	10.871	11.093	10.124	10.804

In Table 37, the correction model for the AW3D30 is a combination of the simple linear regression as a function of surface roughness for slope less than 2.5°, multiple regression as a function of (slope, aspect, and surface roughness) for slope 2.5° to 5.5° and 7.5° to 10°, and adaptive terrain-dependent method with parameters determined using Ordinary Least Squares for slope 5.5° to 7.5° and greater than 10°. In Table 39, the correction model for the TanDEM-X is a combination of multiple regression as a function of (slope, aspect, and surface roughness) for slope less than 5.5° and 7.5° to 20°, and an

adaptive terrain-dependent method with parameters determined using Ordinary Least Squares for slope 5.5° to 7.5° and greater than 20°. The models are adopted because, after being applied to these DEMs, there is a remarkable decrease in standard deviations in those slope ranges, meaning an improvement in vertical accuracy.

Region 5

Table 40: *Absolute height difference in region 5 between the AW3D30 and ground levelling test data before and after applying different correction models*

	Original AW3D30	Slope_corr	Aspect_corr	Roughness_corr	abs(Slope_corr)	abs(Aspect_corr)	abs(Roughness_corr)	Multiple linear reg_ corr	ATDM_corr(OLS)	ATDM_corr(M-estimator)
N	965	965	965	965	965	965	965	965	965	965
Min(m)	-7.60	-12.48	-12.74	-12.60	-12.61	-12.82	-12.72	-13.07	-13.43	-10.89
Max(m)	27.50	23.53	22.58	23.48	23.37	22.43	23.32	23.10	23.55	23.62
Mean (m)	4.768	0.012	0.023	0.002	-0.121	-0.103	-0.130	0.013	0.060	0.731
STDV (±m)	4.577	4.293	4.577	4.228	4.293	4.576	4.229	4.209	4.204	4.182

Table 41: Comparison of the different correction methods in different slope ranges, using the ground levelling test data for AW3D30 in region 5

	Original AW3D30	Slope_corr	Aspect_corr	Roughness_corr	abs(Slope_corr)	abs(Aspect_corr)	abs(Roughness_corr)	Multiple linear reg_ corr	ATDM_corr(OLS)	ATDM_corr(M-estimator)
0 < Slope < 2.5										
N	536	536	536	536	536	536	536	536	536	536
Min(m)	-4.10	-8.14	-8.53	-8.12	-8.29	-8.69	-8.28	-7.81	-6.62	-6.27
Max(m)	27.50	23.53	22.58	23.48	23.37	22.43	23.32	23.10	23.55	23.62
Mean (m)	3.558	-0.349	-1.197	-0.338	-0.507	-1.322	-0.496	-0.399	-0.098	0.406
STDV (±m)	3.688	3.687	3.690	3.638	3.687	3.689	3.639	3.640	3.627	3.601
2.5 < Slope < 5.5										
N	269	269	269	269	269	269	269	269	269	269
Min(m)	-7.60	-12.48	-12.74	-12.60	-12.61	-12.82	-12.72	-13.07	-11.17	-10.89
Max(m)	25.30	20.41	20.16	20.48	20.28	20.08	20.32	20.48	21.46	21.85
Mean (m)	5.103	0.259	0.346	0.303	0.129	0.221	0.172	0.344	0.067	0.733
STDV (±m)	4.517	4.500	4.511	4.439	4.500	4.511	4.440	4.420	4.478	4.442
5.5 < Slope < 7.5										
N	68	68	68	68	68	68	68	68	68	68
Min(m)	-0.20	-6.34	-4.70	-6.17	-6.43	-4.84	-6.27	-6.08	-5.75	-5.02
Max(m)	22.60	16.80	18.17	17.60	16.70	18.01	17.48	18.55	17.69	17.82
Mean (m)	7.194	1.222	2.477	0.991	1.127	2.348	0.902	1.005	0.824	1.677
STDV (±m)	5.063	5.088	5.084	4.996	5.087	5.081	4.996	4.981	5.376	5.320
7.5 < Slope < 10										
N	36	36	36	36	36	36	36	36	36	36
Min(m)	0.30	-6.76	-4.06	-6.65	-6.82	-4.23	-6.72	-5.94	-6.19	-4.51
Max(m)	22.50	15.94	17.54	15.55	15.86	17.44	15.48	15.26	14.62	16.24
Mean (m)	7.756	0.884	3.091	0.889	0.817	2.956	0.819	1.182	0.407	1.416
STDV (±m)	5.572	5.603	5.475	5.402	5.602	5.485	5.406	5.201	4.969	5.154
10<Slope<20										
N	48	48	48	48	48	48	48	48	48	48
Min(m)	-0.20	-8.10	-4.72	-8.45	-8.14	-4.87	-8.40	-7.92	-9.06	-6.79
Max(m)	26.90	18.87	21.99	18.98	18.83	21.88	18.94	19.17	14.79	17.42
Mean (m)	10.181	1.257	5.492	1.142	1.253	5.359	1.137	1.511	1.191	2.779
STDV (±m)	5.371	5.403	5.264	5.268	5.398	5.276	5.267	5.097	5.001	4.955
Slope > 20										
N	8.00	8.00	8.00	8.00	8.00	8.00	8.00	8.00	8.00	8.00
Min(m)	2.80	-11.04	-2.31	-11.74	-10.76	-2.39	-11.46	-10.83	-13.43	-7.47
Max(m)	18.500	4.304	13.899	3.754	4.463	13.757	3.920	4.414	6.299	9.850
Mean (m)	8.025	-5.834	3.371	-6.599	-5.685	3.235	-6.437	-6.158	-4.456	-0.945
STDV (±m)	4.613	4.927	4.661	4.811	4.908	4.655	4.795	4.761	5.861	4.994

Table 42: Absolute height difference in region 5 between the TanDEM-X and ground levelling test data before and after applying different correction models

	Original TanDEM-X	Slope_corr	Aspect_corr	Roughness_corr	abs(Slope_corr)	abs(Aspect_corr)	abs(Roughness_corr)	Multiple linear reg_corr	ATDM_corr(OLS)	ADTM_corr(M-estimator)
N	965	965	965	965	965	965	965	965	965	965
Min(m)	-0.87	-5.31	-5.81	-5.3	-5.31	-5.81	-5.31	-5.54	-8.25	-9.5
Max(m)	59.06	24.46	24.4	24.4	24.46	24.4	24.43	24.4	22.65	23.32
Mean(m)	4.813	0.078	0.087	0.074	0.073	0.084	0.069	0.080	0.157	0.769
STDV (±m)	3.881	3.803	3.885	3.797	3.803	3.885	3.797	3.802	3.452	3.447

Table 43: Comparison of the different correction methods in different slope ranges, using the ground levelling test data for TanDEM-X in region 5

	Original TanDEM-X	Slope_corr	Aspect_corr	Roughness_corr	abs(Slope_corr)	abs(Aspect_corr)	abs(Roughness_corr)	Multiple linear reg_ corr	ATDM_corr(OLS)	ATDM_corr(M-estimator)
0 < Slope < 2.5										
N	536	536	536	536	536	536	536	536	536	536
Min(m)	-0.87	-5.31	-5.81	-5.30	-5.31	-5.81	-5.31	-5.54	-7.65	-6.77
Max(m)	28.87	24.46	24.06	24.44	24.46	24.06	24.43	24.30	22.65	23.32
Mean (m)	4.373	-0.006	-0.358	-0.006	-0.012	-0.361	-0.012	-0.024	0.036	0.675
STDV (±m)	3.793	3.798	3.792	3.796	3.798	3.792	3.796	3.797	3.294	3.302
2.5 < Slope < 5.5										
N	269	269	269	269	269	269	269	269	269	269
Min(m)	-0.11	-4.71	-5.00	-4.54	-4.71	-5.01	-4.54	-4.64	-4.73	-4.09
Max(m)	29.06	24.14	24.44	24.23	24.13	24.44	24.22	24.40	22.02	22.86
Mean (m)	4.844	0.072	0.113	0.091	0.067	0.110	0.086	0.105	0.160	0.793
STDV (±m)	3.834	3.838	3.841	3.834	3.838	3.841	3.833	3.841	3.456	3.456
5.5 < Slope < 7.5										
N	68	68	68	68	68	68	68	68	68	68
Min(m)	0.90	-4.29	-3.71	-3.94	-4.29	-3.71	-3.94	-3.85	-3.70	-2.83
Max(m)	24.88	19.71	20.31	20.04	19.70	20.31	20.04	20.41	18.78	19.24
Mean (m)	5.314	0.068	0.602	-0.021	0.065	0.599	-0.024	-0.010	0.472	1.056
STDV (±m)	3.697	3.701	3.698	3.722	3.701	3.698	3.722	3.736	3.673	3.604
7.5 < Slope < 10										
N	36	36	36	36	36	36	36	36	36	36
Min(m)	1.65	-3.80	-2.95	-3.67	-3.80	-2.95	-3.68	-3.66	-4.60	-3.70
Max(m)	12.28	6.79	7.45	6.64	6.78	7.45	6.63	6.51	8.00	8.20
Mean (m)	5.847	0.223	1.160	0.236	0.223	1.157	0.234	0.346	0.678	1.199
STDV (±m)	2.921	2.945	2.893	2.844	2.945	2.893	2.844	2.771	3.136	3.131
10<Slope<20										
N	48	48	48	48	48	48	48	48	48	48
Min(m)	1.67	-4.67	-2.95	-4.85	-4.66	-2.95	-4.85	-4.63	-5.63	-5.05
Max(m)	19.41	13.51	14.89	12.96	13.51	14.89	12.96	13.00	14.09	14.47
Mean (m)	7.242	0.757	2.543	0.730	0.760	2.540	0.731	0.859	0.757	1.180
STDV (±m)	4.284	4.242	4.308	4.211	4.242	4.308	4.211	4.231	4.516	4.445
Slope > 20										
N	8	8	8	8	8	8	8	8	8	8
Min(m)	5.55	-4.72	0.92	-4.95	-4.70	0.92	-4.93	-4.61	-8.25	-9.50
Max(m)	17.91	9.21	13.25	9.03	9.22	13.25	9.04	9.27	7.74	7.41
Mean (m)	9.803	1.247	5.121	0.975	1.258	5.118	0.984	1.129	-0.518	-0.571
STDV (±m)	3.636	3.813	3.641	3.866	3.812	3.641	3.865	3.885	4.668	4.804

In Table 41, the correction model for the AW3D30 is a combination of the adaptive terrain-dependent method with parameters determined using Robust least squares (M-estimator) for slope less than 2.5° and 10° to 20°, multiple regression as a function of (slope, aspect, and surface roughness) for slope 2.5° to 7.5°, adaptive terrain-dependent method with parameters determined using Ordinary Least Squares for slope 7.5° to 10°, and original AW3D30 DEM for slope greater than 20°. In Table 43, the correction model for the TanDEM-X is a combination of the adaptive terrain-dependent method with parameters determined using Ordinary Least Squares for slope less than 5.5°, adaptive terrain-dependent method with parameters determined using Robust least squares (M-estimator) for slope

5.5° to 7.5°, multiple regression as a function of (slope, aspect, and surface roughness) for slope 7.5° to 10°, simple linear regression as a function of surface roughness for slope 10° to 20°, and original TanDEM-X DEM for slope greater than 20°. The models are adopted because, after being applied to these DEMs, there is a remarkable decrease in standard deviations in those slope ranges, meaning an improvement in vertical accuracy.

Region 6

Table 44: Absolute height difference in region 6 between the AW3D30 and ground levelling test data before and after applying different correction models

	Original AW3D30	Slope_corr	Aspect_corr	Roughness_corr	abs(Slope_corr)	abs(Aspect_corr)	abs(Roughness_corr)	Multiple linear reg_ corr	ATDM_corr(OLS)	ATDM_corr(M-estimator)
N	1977	1977	1977	1977	1977	1977	1977	1977	1977	1977
Min(m)	-15.40	-17.42	-18.52	-17.47	-18.47	-19.73	-18.50	-17.23	-17.53	-15.49
Max(m)	48.10	45.85	45.87	45.91	44.64	44.82	44.68	46.37	44.87	47.57
Mean (m)	2.440	-0.190	-0.203	-0.188	-1.320	-1.331	-1.319	-0.171	-0.171	1.249
STDV (±m)	6.357	6.146	6.353	6.133	6.166	6.353	6.155	6.128	6.003	6.092

Table 45: Comparison of the different correction methods in different slope ranges, using the ground levelling test data for AW3D30 in region 6

	Original AW3D30	Slope_corr	Aspect_corr	Roughness_corr	abs(Slope_corr)	abs(Aspect_corr)	abs(Roughness_corr)	Multiple linear reg_ corr	ATDM_corr(OLS)	ATDM_corr(M-estimator)
0 < Slope < 2.5										
N	1262	1262	1262	1262	1262	1262	1262	1262	1262	1262
Min(m)	-15.40	-16.85	-18.52	-16.71	-18.23	-19.73	-18.13	-17.19	-17.53	-15.49
Max(m)	48.10	45.85	45.87	45.91	44.64	44.82	44.68	46.37	44.87	47.57
Mean (m)	1.339	-0.656	-1.308	-0.695	-1.920	-2.436	-1.958	-0.687	-0.507	0.796
STDV (±m)	5.400	5.384	5.406	5.368	5.387	5.409	5.372	5.374	5.362	5.363
2.5 < Slope < 5.5										
N	481	481	481	481	481	481	481	481	481	481
Min(m)	-14.40	-17.42	-16.84	-17.47	-18.47	-17.92	-18.50	-17.23	-15.97	-15.46
Max(m)	46.50	43.62	44.25	43.43	42.54	43.19	42.40	43.85	43.15	45.53
Mean (m)	3.716	0.858	1.077	0.952	-0.225	-0.049	-0.150	0.983	0.699	2.237
STDV (±m)	7.571	7.542	7.561	7.521	7.547	7.560	7.528	7.510	7.421	7.549
5.5 < Slope < 7.5										
N	82	82	82	82	82	82	82	82	82	82
Min(m)	-1.50	-5.24	-3.72	-5.05	-6.09	-4.82	-5.89	-5.17	-6.88	-4.76
Max(m)	28.80	24.90	26.54	24.85	24.03	25.49	24.01	25.28	24.74	27.87
Mean (m)	4.846	0.833	2.186	0.779	-0.007	1.056	-0.033	0.779	0.318	2.002
STDV (±m)	5.550	5.552	5.588	5.533	5.551	5.597	5.534	5.572	5.681	5.696
7.5 < Slope < 10										
N	66	66	66	66	66	66	66	66	66	66
Min(m)	-3.50	-8.21	-5.74	-7.63	-8.79	-6.79	-8.29	-7.28	-8.77	-6.09
Max(m)	34.10	29.60	31.82	30.15	28.87	30.76	29.31	30.61	30.04	32.48
Mean (m)	5.687	0.830	3.084	0.899	0.168	1.965	0.247	0.972	0.437	2.343
STDV (±m)	7.191	7.268	7.125	7.221	7.251	7.114	7.210	7.154	6.906	7.192
10<Slope<20										
N	71	71	71	71	71	71	71	71	71	71
Min(m)	-3.00	-9.97	-6.11	-10.47	-10.18	-7.32	-10.53	-10.97	-10.04	-7.66
Max(m)	16.70	9.18	13.97	9.23	9.08	12.83	9.17	9.18	6.13	9.38
Mean (m)	4.987	-1.775	2.345	-1.601	-2.036	1.218	-1.854	-1.555	-2.001	-0.170
STDV (±m)	5.147	4.879	5.054	4.858	4.918	5.037	4.899	4.763	3.592	4.184
Slope > 20										
N	15.00	15.00	15.00	15.00	15.00	15.00	15.00	15.00	15.00	15.00
Min(m)	-0.30	-12.61	-2.64	-13.96	-11.16	-3.71	-12.07	-13.58	-7.00	-6.17
Max(m)	29.900	19.238	27.046	19.793	19.797	25.879	20.320	19.656	15.992	18.938
Mean (m)	14.700	2.868	12.054	2.599	3.673	10.926	3.569	2.622	3.458	5.447
STDV (±m)	10.006	10.840	9.869	10.950	10.644	9.843	10.696	10.821	7.175	8.491

Table 46: Absolute height difference in region 6 between the TanDEM-X and ground levelling test data before and after applying different correction models.

	Original TanDEM-X	Slope_corr	Aspect_corr	Roughness_corr	abs(Slope_corr)	abs(Aspect_corr)	abs(Roughness_corr)	Multiple linear reg_ corr	ATDM_corr(OLS)	ATDM_corr(M-estimator)
N	1977	1977	1977	1977	1977	1977	1977	1977	1977	1977
Min(m)	-16.49	-19.41	-20.62	-19.29	-19.60	-20.89	-19.49	-19.46	-20.67	-18.26
Max(m)	61.93	49.75	57.87	47.55	49.79	57.67	47.70	47.41	45.29	55.84
Mean (m)	3.792	-0.165	-0.195	-0.163	-0.332	-0.351	-0.330	-0.157	-0.132	1.395
STDV (±m)	6.283	6.141	6.284	6.123	6.142	6.285	6.125	6.124	6.063	6.182

Table 47: Comparison of the different correction methods in different slope ranges, using the ground levelling test data for TanDEM-X in region 6

	Original TanDEM-X	Slope_corr	Aspect_corr	Roughness_corr	abs(Slope_corr)	abs(Aspect_corr)	abs(Roughness_corr)	Multiple linear reg_ corr	ATDM_corr(OLS)	ATDM_corr(M-estimator)
0 < Slope < 2.5										
N	1262	1262	1262	1262	1262	1262	1262	1262	1262	1262
Min(m)	-16.49	-19.41	-20.62	-19.29	-19.60	-20.89	-19.49	-19.46	-20.49	-18.26
Max(m)	50.24	46.62	46.38	46.67	46.44	46.32	46.49	46.84	45.29	48.15
Mean (m)	3.036	-0.362	-0.952	-0.398	-0.543	-1.109	-0.581	-0.396	-0.478	0.938
STDV (±m)	5.052	5.044	5.055	5.038	5.044	5.058	5.038	5.041	5.031	5.030
2.5 < Slope < 5.5										
N	481	481	481	481	481	481	481	481	481	481
Min(m)	-9.11	-13.41	-13.03	-13.45	-13.57	-13.14	-13.61	-13.37	-11.89	-11.20
Max(m)	49.26	45.09	45.39	44.92	44.92	45.33	44.76	45.07	44.19	46.67
Mean (m)	4.705	0.548	0.719	0.631	0.386	0.565	0.467	0.642	0.774	2.194
STDV (±m)	7.785	7.769	7.785	7.767	7.770	7.785	7.767	7.766	7.633	7.776
5.5 < Slope < 7.5										
N	82	82	82	82	82	82	82	82	82	82
Min(m)	-0.75	-6.29	-4.74	-5.86	-6.42	-4.89	-6.00	-5.84	-5.76	-4.50
Max(m)	43.35	38.30	39.47	38.24	38.16	39.40	38.10	38.38	39.19	40.97
Mean (m)	5.018	-0.156	1.025	-0.199	-0.293	0.866	-0.328	-0.200	0.531	1.947
STDV (±m)	6.932	6.943	6.950	6.928	6.943	6.964	6.928	6.951	6.928	7.021
7.5 < Slope < 10										
N	66	66	66	66	66	66	66	66	66	66
Min(m)	1.43	-4.97	-2.68	-5.23	-5.07	-2.93	-5.31	-5.38	-5.87	-2.60
Max(m)	42.15	36.51	38.03	34.72	36.38	37.77	34.66	34.50	35.13	38.82
Mean (m)	5.780	-0.137	1.805	-0.070	-0.255	1.658	-0.180	-0.044	0.581	2.385
STDV (±m)	7.815	7.892	7.801	7.787	7.890	7.792	7.788	7.768	7.629	7.860
10<Slope<20										
N	71	71	71	71	71	71	71	71	71	71
Min(m)	0.47	-7.04	-3.50	-6.96	-7.12	-3.64	-7.02	-6.92	-8.71	-3.98
Max(m)	19.44	10.51	15.32	10.47	10.47	15.07	10.45	10.32	10.21	15.12
Mean (m)	4.808	-2.785	0.821	-2.621	-2.862	0.666	-2.683	-2.604	-2.163	0.490
STDV (±m)	3.046	2.801	3.032	2.753	2.804	3.024	2.756	2.739	3.170	2.962
Slope > 20										
N	15	15	15	15	15	15	15	15	15	15
Min(m)	2.68	-11.93	-1.22	-13.17	-11.81	-1.30	-12.95	-13.18	-20.67	-4.97
Max(m)	61.93	49.75	57.87	47.55	49.79	57.67	47.70	47.41	43.75	55.84
Mean (m)	17.850	5.795	13.862	5.585	5.829	13.706	5.669	5.593	2.813	11.125
STDV (±m)	15.309	15.249	15.275	14.857	15.249	15.250	14.866	14.798	14.570	15.637

In Table 45, the correction model for the AW3D30 is a combination of the adaptive terrain-dependent method with parameters determined using Ordinary Least Squares for slope less than 5.5° and greater than 7.5°, and simple linear regression as a function of surface roughness for slope 5.5° to 7.5°. In Table 47, the correction model for the TanDEM-X is a combination of the adaptive terrain-dependent method with parameters determined using Robust least squares (M-estimator) for slope less than 2.5°, adaptive terrain-dependent method with parameters determined using Ordinary Least Squares

for slope 2.5° to 10° and greater than 20°, and multiple regression as a function of (slope, aspect, and surface roughness) for slope 10° to 20°. The models are adopted because, after being applied to these DEMs, there is a remarkable decrease in standard deviations in those slope ranges, meaning an improvement in vertical accuracy.

3.4.3.3 Assessment of the final regional correction models over South Africa

The correction models used in modelling AW3D30, and TanDEM-X errors are shown in Figures 74 and 75. Tables 48 and 49 show the validation results of the vertical accuracies of the corrected/improved DEMs. According to Figures 74 and 75, large corrections were applied to areas with slopes greater than 10°. Areas with slope less than 10° had small corrections.

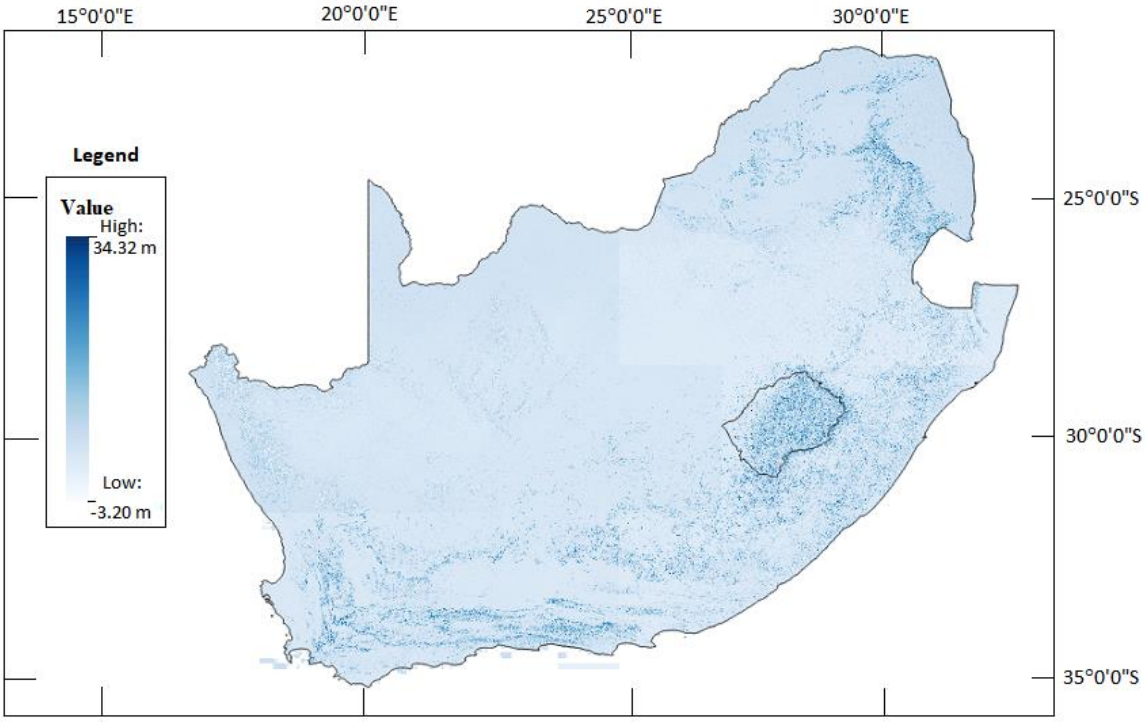

Figure 74: AW3D30 final corrections model over South Africa (units are in m)

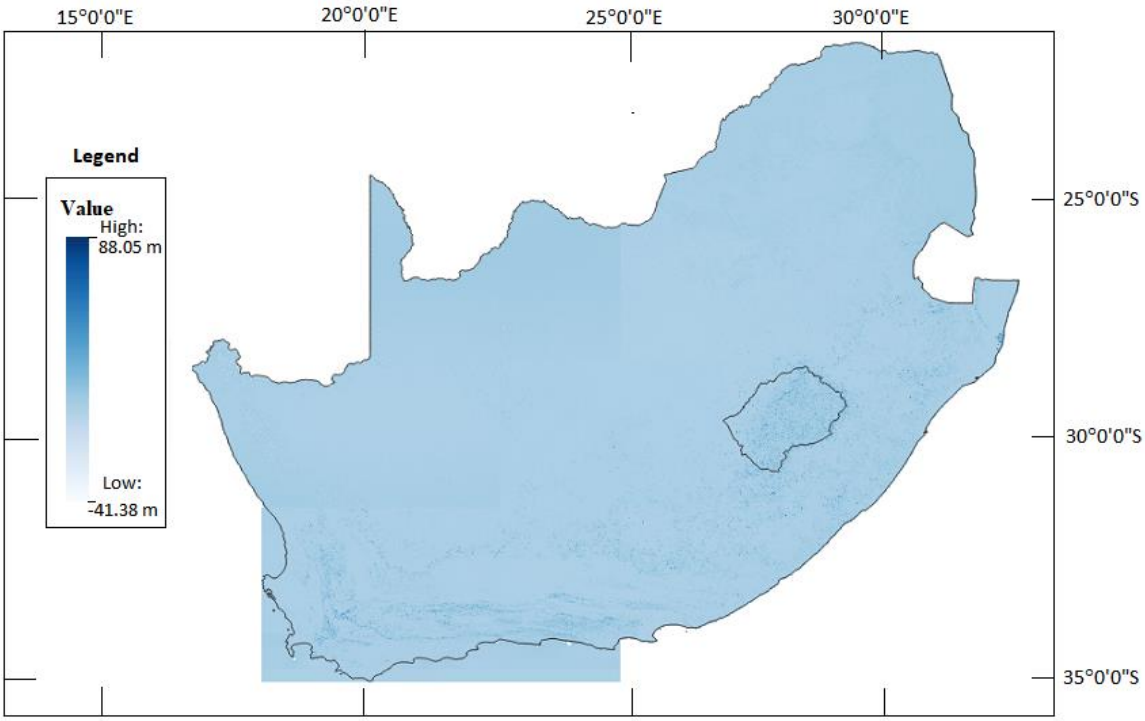

Figure 75: TanDEM-X final corrections model over South Africa (units are in m)

Table 48: Absolute height differences between the DEMs and ground levelling data for the test data before and after applying correction

	Original DEMs		**Corrected DEMs**	
	AW3D30	TanDEM-X	AW3D30	TanDEM-X
N	8657	8657	8657	8657
Min(m)	-34,900	-23,079	-37,954	-28,338
Max(m)	62,200	73,320	50,458	62,921
Mean (m)	3,867	4,250	-0,073	0,213
STDV (±m)	5,745	5,073	4,995	4,582

Table 49: Absolute height differences in different slope ranges between the DEMs and ground levelling data for the test data before and after applying correction

	Original DEMs		Corrected DEMs	
Slope ranges	AW3D30	TanDEM-X	AW3D30	TanDEM-X
0 < Slope < 2.5				
N	3920	3920	3920	3920
Min(m)	-15,40	-16,49	-17,016	-18,257
Max(m)	48,10	50,24	46,336	48,184
Mean (m)	2,22	3,31	-0,269	0,427
STDV (±m)	4,58	4,17	4,420	4,037
2.5 < Slope < 5.5				
N	2448	2448	2448	2448
Min(m)	-34,90	-20,54	-37,954	-25,559
Max(m)	46,50	49,26	43,167	44,198
Mean (m)	3,70	3,97	0,041	0,065
STDV (±m)	5,42	4,69	5,126	4,491
5.5 < Slope < 7.5				
N	666	666	666	666
Min(m)	-23,40	-23,08	-29,067	-28,338
Max(m)	33,80	47,85	28,800	42,401
Mean (m)	5,27	4,59	0,837	0,034
STDV (±m)	5,30	4,27	5,224	4,173
7.5 < Slope < 10				
N	593	593	593	593
Min(m)	-5,60	-9,25	-13,265	-14,226
Max(m)	34,10	50,07	30,052	43,460
Mean (m)	5,69	5,19	-0,173	-0,040
STDV (±m)	5,17	4,69	4,759	4,434
10<Slope<20				
N	824	824	824	824
Min(m)	-4,60	-4,97	-12,956	-10,249
Max(m)	60,60	41,80	50,458	31,974
Mean (m)	7,70	6,30	-0,241	-0,484
STDV (±m)	6,51	4,12	5,700	3,953
Slope > 20				
N	206,00	206,00	206,00	206,00
Min(m)	-2,60	1,05	-22,18	-21,94
Max(m)	62,200	73,320	48,563	62,921
Mean (m)	12,09	13,47	0,34	1,99
STDV (±m)	10,37	13,28	8,79	12,27

In Table 48, after the correction is applied to the AW3D30 and TanDEM-X, there is a remarkable decrease in mean values. A decrease in standard deviation was also observed. The AW3D30 before correction does not meet the absolute vertical accuracy specification, and this might be because of the DEM co-registration process, but the corrected AW3D30 has a standard deviation less than ±4.995 m, which is within the vertical accuracy specifications. The TanDEM-X before and after the correction has a standard deviation of ±5.073 and ±4.582 m, respectively and is within the expected ±10 m absolute vertical accuracy specifications.

In Table 49, after the correction is applied to the AW3D30 and TanDEM-X, the mean values decrease for all slope ranges. A decrease in standard deviation is also observed in all slope ranges. Steeper slopes experience higher standard deviations of the height errors for all the DEMs before and after correction, but there is a decrease for corrected compared to the original DEM's. The corrected

TanDEM-X has a better performance on slopes ranging from 0° - 20°. For slopes greater than 20°, the corrected AW3D30 has better performance. The vertical accuracy of all the corrected DEMs still decreases on steeper slopes.

3.5 Fusion strategies for developing an accurate digital elevation model over South Africa

3.5.1 Introduction

The DEM fusions are between the corrected (AW3D30 and TanDEM-X), using ground levelling to derive fusion parameters. The fusion methods applied include the linear combination, weighted averaging, averaging of the DEMs, and taking corrected TanDEM-X elevations for slope values less than 20° and corrected AW3D30 elevations for slope values greater than 20°. The fused DEM is evaluated using ground levelling data.

3.5.2 Data and methods

The datasets used are the DEMs (AW3D30 and TanDEM-X) improved in section (3.4), the ground levelling (trigonometrical beacon) data described in section (2.1.1) is used as a reference and for the derivation of fusion parameters.

The methods for fusing the improved DEMs (AW3D30 and TanDEM-X) included using the linear combination, weighted averaging, and averaging of the DEM's. These methods are described under section (2.3). The other fusion method that was used to fuse the DEMs but not described in section (2.3) involved the use of TanDEM-X data for the slope range 0° – 20° and AW3D30 data for slope > 20°, based on empirical investigation results. The results of DEM validation using ground levelling showed that the corrected TanDEM-X has better performance than the corrected AW3D30 in low slope ranges, while AW3D30 performs relatively better than TanDEM-X in high areas. Therefore, this information was used in deriving a fusion method as follows,

$$DEM\ fusion = \boldsymbol{if}(slope < 20°), Corrected\ TanDEM - X\ \boldsymbol{or\ else}\ Corrected\ AW3D30 \tag{3.10}$$

In this method, for slope values between 0° and 20°, the corrected TanDEM-X elevations are used, then for slope values greater than 20° the corrected AW3D30 elevations are used. The ground levelling data used for fusion parameter derivation is the same as those described under section (3.4.2.2). A sample of 66% of ground levelling data points from each of the regions in Figure 61 were chosen using random sampling. The sample was used in the derivation of fusion model parameters. The remaining 33% of data points that were not part of the sample were used to test the fused DEMs. Spatial distribution of model and test points falling in different slope ranges over the six regions are shown in Figures 62 to 73.

The validation of the fused DEMs vertical accuracies was done using all the test points. The process included finding the height differences between the ground levelling data and the fused DEMs, then determining the statistical measures as discussed in section (3.2.2.2). Because some fusion methods may have a very high effect on improving the accuracy of the DEMs in certain slope ranges compared to others, the slope ranges were included in the validation. This was done to determine a combination of fusion methods that have a very high effect on improving the accuracy of the DEM's and using the

combination to generate a final fused DEM. The slope ranges included were (0° – 2.5°, 2.5° – 5.5°, 5.5° – 7.5°, 7.5° – 10°, 10° – 20°, >20°). The original DEMs (TanDEM-X, SRTM, ASTER, MERIT, AW3D30, and co-registered AW3D30) are also compared to the fused DEM. The comparison is done using height differences between 8,657 ground levelling test data points and the DEMs.

3.5.3 Results and discussion

3.5.3.1 Vertical accuracies of fusion methods in different regions

Tables 50 to 60 show the statistical results for the corrected DEMs and fused DEMs using different fusion methods for the six different regions.

Region 1

Table 50: Vertical accuracy comparison of different fusion methods using the ground levelling test data in region 1

	Corrected DEMs		DEM fusion results			
	AW3D30_Corr	TanDEM-X_Corr	Fusion (linear combination)	Fusion(Weighted averaging)	Fusion(Averaging DEMs)	Final DEM fusion
N	1219	1219	1219	1219	1219	1219
Min(m)	-29.07	-28.34	-28.48	-28.35	-28.70	-28.70
Max(m)	35.24	43.46	40.67	42.26	35.95	36.27
Mean (m)	0.383	0.475	0.460	0.530	0.429	0.389
STDV (±m)	5.722	4.998	4.973	5.189	5.079	4.897

Table 51: Vertical accuracy comparison of the different fusion methods in slope ranges using the ground levelling test data in region 1

	Corrected DEMs		DEM fusion results			
Slope ranges	AW3D30_Corr	TanDEM-X_Corr	Fusion (linear combination)	Fusion(Weighted averaging)	Fusion(Averaging DEMs)	Final DEM fusion
0 < Slope < 2.5						
N	571	571	571	571	571	571
Min(m)	-8.91	-8.43	-7.28	-7.96	-6.39	-7.28
Max(m)	35.24	36.66	36.27	36.38	35.95	36.27
Mean (m)	0.990	1.090	1.061	1.076	1.040	1.061
STDV (±m)	5.054	4.675	4.640	4.645	4.689	4.640
2.5 < Slope < 5.5						
N	350	350	350	350	350	350
Min(m)	-25.46	-25.56	-25.54	-25.46	-25.51	-25.56
Max(m)	29.95	29.66	29.73	29.95	29.80	29.66
Mean (m)	0.175	-0.200	-0.109	0.175	-0.012	-0.200
STDV (±m)	5.926	5.033	5.094	5.925	5.276	5.033
5.5 < Slope < 7.5						
N	88	88	88	88	88	88
Min(m)	-29.07	-28.34	-28.48	-28.35	-28.70	-28.70
Max(m)	28.18	42.40	39.69	42.26	35.29	35.29
Mean (m)	-0.227	-0.426	-0.388	-0.424	-0.327	-0.327
STDV (±m)	6.349	6.065	5.967	6.058	5.960	5.960
7.5 < Slope < 10						
N	73	73	73	73	73	73
Min(m)	-13.26	-12.38	-12.52	-13.22	-12.82	-13.22
Max(m)	22.86	43.46	40.67	22.86	33.16	22.86
Mean (m)	-0.703	0.212	0.079	-0.740	-0.246	-0.740
STDV (±m)	5.236	6.183	5.917	5.074	5.385	5.074
10 < Slope < 20						
N	110	110	110	110	110	110
Min(m)	-11.80	-7.38	-8.31	-7.38	-9.59	-7.38
Max(m)	26.38	26.80	22.90	26.80	17.57	26.80
Mean (m)	0.206	0.206	0.206	0.325	0.206	0.206
STDV (±m)	7.156	4.188	4.329	4.273	5.047	4.188
Slope > 20						
N	27	27	27	27	27	27
Min(m)	-13.84	-6.57	-7.76	-6.57	-9.73	-7.76
Max(m)	7.56	12.24	9.20	12.24	6.94	9.20
Mean (m)	-4.109	0.981	-0.071	0.981	-1.564	-0.071
STDV (±m)	5.971	5.024	4.756	5.024	4.817	4.756

In Table 51, the final fusion is a combination of the linear combination for slope less than 2.5° and greater than 20°, TanDEM-X for slope 2.5° to 5.5° and 10° to 20°, averaging for slope 5.5° to 7.5°, and weighted averaging for slope 7.5° to 10°. The methods are adopted because, after fusion of the DEMs, there is a remarkable decrease in standard deviations in those slope ranges, meaning an improvement in the vertical accuracy.

Region 2

Table 52: Vertical accuracy comparison of different fusion methods using the ground levelling test data in region 2

	Corrected DEMs		DEM fusion results			
	AW3D30_Corr	TanDEM-X_Corr	Fusion (linear combination)	Fusion(Weighted averaging)	Fusion(Averaging DEMs)	Final DEM fusion
N	1095	1095	1095	1095	1095	1095
Min(m)	-12.07	-8.50	-9.58	-8.53	-10.29	-8.50
Max(m)	28.99	30.05	29.87	29.02	29.52	29.87
Mean (m)	-0.375	-0.253	-0.273	-0.387	-0.314	-0.280
STDV (±m)	4.328	3.412	3.429	3.524	3.668	3.397

Table 53: Vertical accuracy comparison of the different fusion methods in different slope ranges using the ground levelling test data in region 2

	Corrected DEMs		DEM fusion results			
Slope ranges	AW3D30_Corr	TanDEM-X_Corr	Fusion (linear combination)	Fusion(Weighted averaging)	Fusion(Averaging DEMs)	Final DEM fusion
0 < Slope < 2.5						
N	413	413	413	413	413	413
Min(m)	-6.87	-4.89	-4.55	-6.80	-4.80	-4.55
Max(m)	28.99	30.05	29.87	29.02	29.52	29.87
Mean (m)	-0.819	-0.374	-0.446	-0.810	-0.596	-0.446
STDV (±m)	3.900	3.757	3.730	3.891	3.737	3.730
2.5 < Slope < 5.5						
N	283	283	283	283	283	283
Min(m)	-6.77	-4.36	-4.44	-4.41	-5.08	-4.44
Max(m)	19.98	28.65	27.60	26.74	24.31	27.60
Mean (m)	0.020	-0.007	-0.006	0.013	0.007	-0.006
STDV (±m)	4.215	3.624	3.607	3.629	3.727	3.607
5.5 < Slope < 7.5						
N	122	122	122	122	122	122
Min(m)	-7.95	-4.65	-4.71	-4.92	-5.79	-4.65
Max(m)	18.58	17.16	17.02	16.63	16.39	17.16
Mean (m)	0.367	-0.066	-0.030	0.094	0.150	-0.066
STDV (±m)	4.798	2.996	3.073	3.278	3.675	2.996
7.5 < Slope < 10						
N	95	95	95	95	95	95
Min(m)	-9.18	-3.77	-3.64	-3.77	-6.03	-3.77
Max(m)	9.30	5.41	5.63	7.31	6.90	5.41
Mean (m)	0.028	-0.120	-0.112	-0.037	-0.046	-0.120
STDV (±m)	3.951	2.146	2.194	2.344	2.843	2.146
10<Slope<20						
N	163	163	163	163	163	163
Min(m)	-11.95	-7.67	-8.45	-7.69	-9.72	-7.67
Max(m)	16.64	8.82	8.84	8.82	11.40	8.82
Mean (m)	-0.917	-0.549	-0.595	-0.550	-0.733	-0.549
STDV (±m)	4.421	2.958	3.012	2.959	3.463	2.958
Slope > 20						
N	19	19	19	19	19	19
Min(m)	-12.07	-8.50	-9.58	-8.53	-10.29	-8.50
Max(m)	27.25	6.05	7.63	6.03	13.37	6.05
Mean (m)	1.240	-0.615	-0.113	-0.603	0.312	-0.615
STDV (±m)	8.631	3.221	4.000	3.229	5.305	3.221

In Table 53, the final fusion is a combination of the linear combination for slope less than 5.5°, and TanDEM-X for slope greater than 5.5°. The methods are adopted because, after fusion of the DEMs, there is a remarkable decrease in standard deviations in those slope ranges, meaning an improvement in the vertical accuracy.

Region 3

Table 54: Vertical accuracy comparison of different fusion methods using the ground levelling test data in region 3

	Corrected DEMs		DEM fusion results			
	AW3D30_Corr	TanDEM-X_Corr	Fusion (linear combination)	Fusion(Weighted averaging)	Fusion(Averaging DEMs)	Final DEM fusion
N	1901	1901	1901	1901	1901	1901
Min(m)	-37.95	-21.94	-18.97	-22.18	-20.06	-22.18
Max(m)	50.46	62.92	56.55	62.90	55.74	48.56
Mean (m)	-0.460	-0.067	-0.187	-0.398	-0.263	-0.211
STDV (±m)	4.622	4.396	3.666	3.959	3.966	3.556

Table 55: Vertical accuracy comparison of the different fusion methods in different slope ranges using the ground levelling test data in region 3

	Corrected DEMs		DEM fusion results			
Slope ranges	AW3D30_Corr	TanDEM-X_Corr	Fusion (linear combination)	Fusion(Weighted averaging)	Fusion(Averaging DEMs)	Final DEM fusion
0 < Slope < 2.5						
N	638	638	638	638	638	638
Min(m)	-14.28	-9.43	-8.77	-13.20	-8.44	-8.77
Max(m)	27.18	27.92	27.85	27.25	27.55	27.85
Mean (m)	-0.638	0.146	0.073	-0.565	-0.246	0.073
STDV (±m)	3.456	2.923	2.920	3.361	3.045	2.920
2.5 < Slope < 5.5						
N	617	617	617	617	617	617
Min(m)	-37.95	-9.27	-10.02	-9.57	-20.06	-9.27
Max(m)	18.58	12.92	12.63	12.82	11.10	12.92
Mean (m)	-0.590	-0.236	-0.266	-0.250	-0.413	-0.236
STDV (±m)	3.710	2.004	2.032	2.017	2.568	2.004
5.5 < Slope < 7.5						
N	161	161	161	161	161	161
Min(m)	-16.19	-7.57	-7.11	-12.25	-9.44	-7.57
Max(m)	19.66	19.44	19.43	19.33	19.37	19.44
Mean (m)	0.007	-0.337	-0.315	-0.237	-0.165	-0.337
STDV (±m)	4.403	2.752	2.768	3.274	3.267	2.752
7.5 < Slope < 10						
N	178	178	178	178	178	178
Min(m)	-9.07	-9.93	-9.61	-9.01	-6.77	-6.77
Max(m)	13.89	42.12	40.20	13.83	26.36	26.36
Mean (m)	-0.515	-0.411	-0.418	-0.515	-0.463	-0.463
STDV (±m)	4.247	4.089	3.999	4.230	3.726	3.726
10<Slope<20						
N	236	236	236	236	236	236
Min(m)	-11.95	-10.25	-10.08	-10.70	-10.50	-10.08
Max(m)	50.46	24.60	22.51	22.38	24.41	22.51
Mean (m)	-0.071	-0.870	-0.720	-0.661	-0.471	-0.720
STDV (±m)	6.563	4.335	4.331	4.423	4.811	4.331
Slope > 20						
N	71	71	71	71	71	71
Min(m)	-22.18	-21.94	-18.97	-22.18	-19.32	-22.18
Max(m)	48.56	62.92	56.55	62.90	55.74	48.56
Mean (m)	0.061	3.632	0.809	0.628	1.847	0.061
STDV (±m)	10.530	16.351	11.169	12.113	11.816	10.530

In Table 55, the final fusion is a combination of the linear combination for slope less than 2.5° and 10° to 20°, TanDEM-X for slope 2.5° to 7.5°, averaging for slope 7.5° to 10°, and AW3D30 for slope greater than 20°. The methods are adopted because, after fusion of the DEMs, there is a remarkable decrease in standard deviations in those slope ranges, meaning an improvement in the vertical accuracy.

Region 4

Table 56: Vertical accuracy comparison of different fusion methods using the ground levelling test data in region 4

	Corrected DEMs		DEM fusion results			
	AW3D30_Corr	TanDEM-X_Corr	Fusion (linear combination)	Fusion(Weighted averaging)	Fusion(Averaging DEMs)	Final DEM fusion
N	1500	1500	1500	1500	1500	1500
Min(m)	-15.75	-19.74	-14.15	-15.44	-14.65	-15.75
Max(m)	28.22	31.97	29.60	31.96	28.91	29.61
Mean (m)	-0.151	-0.070	-0.042	-0.056	-0.111	-0.066
STDV (±m)	4.012	3.311	2.946	3.081	3.248	2.925

Table 57: Vertical accuracy comparison of the different fusion methods in different slope ranges using the ground levelling test data in region 4

	Corrected DEMs		DEM fusion results			
Slope ranges	AW3D30_Corr	TanDEM-X_Corr	Fusion (linear combination)	Fusion(Weighted averaging)	Fusion(Averaging DEMs)	Final DEM fusion
0 < Slope < 2.5						
N	500	500	500	500	500	500
Min(m)	-6.25	-7.63	-7.61	-6.83	-5.90	-7.61
Max(m)	13.15	11.85	11.83	11.18	10.48	11.83
Mean (m)	-0.530	-0.179	-0.180	-0.187	-0.355	-0.180
STDV (±m)	2.626	1.552	1.552	1.586	1.877	1.552
2.5 < Slope < 5.5						
N	448	448	448	448	448	448
Min(m)	-11.72	-7.13	-7.16	-8.65	-9.42	-7.13
Max(m)	28.22	29.61	29.60	29.05	28.91	29.61
Mean (m)	-0.025	-0.087	-0.087	-0.041	-0.056	-0.087
STDV (±m)	3.806	2.478	2.481	2.885	2.930	2.478
5.5 < Slope < 7.5						
N	145	145	145	145	145	145
Min(m)	-7.61	-4.61	-4.58	-4.58	-5.54	-4.61
Max(m)	22.72	13.13	13.29	13.14	17.92	13.13
Mean (m)	0.454	0.048	0.055	0.049	0.251	0.048
STDV (±m)	4.518	2.741	2.754	2.753	3.443	2.741
7.5 < Slope < 10						
N	145	145	145	145	145	145
Min(m)	-10.33	-14.23	-14.15	-14.18	-12.28	-14.15
Max(m)	12.98	9.15	9.01	9.03	8.57	9.01
Mean (m)	-0.040	-0.028	-0.028	-0.027	-0.034	-0.028
STDV (±m)	4.252	2.971	2.962	2.965	3.230	2.962
10<Slope<20						
N	196	196	196	196	196	196
Min(m)	-12.96	-7.17	-7.00	-7.17	-8.28	-7.00
Max(m)	25.03	31.97	25.92	31.96	21.56	25.92
Mean (m)	-0.234	0.025	-0.040	0.025	-0.104	-0.040
STDV (±m)	5.009	4.094	3.879	4.093	4.001	3.879
Slope > 20						
N	66	66	66	66	66	66
Min(m)	-15.75	-19.74	-12.57	-15.44	-14.65	-15.75
Max(m)	23.32	30.28	20.89	22.92	20.87	23.32
Mean (m)	0.538	0.241	1.044	0.299	0.389	0.538
STDV (±m)	7.322	10.167	7.429	7.362	7.565	7.322

In Table 57, the final fusion is a combination of the linear combination for slope less than 2.5° and 7.5° to 20°, TanDEM-X for slope 2.5° to 7.5°, and AW3D30 for slope greater than 20°. The methods are adopted because, after fusion of the DEMs, there is a remarkable decrease in standard deviations in those slope ranges, meaning an improvement in the vertical accuracy.

Region 5

Table 58: Vertical accuracy comparison of different fusion methods using the ground levelling test data in region 5

	Corrected DEMs		DEM fusion results			
	AW3D30_Corr	TanDEM-X_Corr	Fusion (linear combination)	Fusion(Weighted averaging)	Fusion(Averaging DEMs)	Final DEM fusion
N	965	965	965	965	965	965
Min(m)	-12.55	-7.65	-7.34	-6.61	-7.31	-7.34
Max(m)	23.61	22.65	22.89	23.31	23.13	22.89
Mean (m)	0.591	0.269	0.324	0.436	0.430	0.325
STDV (±m)	4.152	3.520	3.515	3.668	3.654	3.494

Table 59: Vertical accuracy comparison of the different fusion methods in different slope ranges using the ground levelling test data in region 5

	Corrected DEMs		DEM fusion results			
Slope ranges	AW3D30_Corr	TanDEM-X_Corr	Fusion (linear combination)	Fusion(Weighted averaging)	Fusion(Averaging DEMs)	Final DEM fusion
0 < Slope < 2.5						
N	536	536	536	536	536	536
Min(m)	-6.27	-7.65	-7.34	-6.61	-6.96	-7.34
Max(m)	23.61	22.65	22.89	23.31	23.13	22.89
Mean (m)	0.407	0.036	0.122	0.305	0.221	0.122
STDV (±m)	3.601	3.295	3.265	3.423	3.314	3.265
2.5 < Slope < 5.5						
N	269	269	268	268	268	268
Min(m)	-12.55	-4.73	-4.59	-4.67	-7.31	-4.73
Max(m)	20.31	22.02	21.48	21.44	20.12	22.02
Mean (m)	0.267	0.160	0.174	0.173	0.214	0.157
STDV (±m)	4.346	3.456	3.508	3.469	3.725	3.462
5.5 < Slope < 7.5						
N	68	68	68	68	68	68
Min(m)	-6.32	-2.83	-2.86	-5.06	-3.97	-2.83
Max(m)	18.02	19.24	19.19	18.20	18.63	19.24
Mean (m)	1.009	1.056	1.055	1.077	1.033	1.056
STDV (±m)	4.899	3.604	3.627	4.502	4.084	3.604
7.5 < Slope < 10						
N	36	36	36	36	36	36
Min(m)	-6.19	-3.96	-3.91	-4.18	-4.27	-3.96
Max(m)	14.62	6.55	6.85	10.64	10.58	6.55
Mean (m)	0.409	0.309	0.313	0.420	0.359	0.309
STDV (±m)	4.967	2.775	2.810	3.486	3.628	2.775
10<Slope<20						
N	48	48	48	48	48	48
Min(m)	-6.79	-4.64	-4.61	-4.50	-5.52	-4.50
Max(m)	17.43	13.14	12.96	12.60	13.46	12.60
Mean (m)	2.781	0.743	0.804	0.948	1.762	0.948
STDV (±m)	4.959	4.202	4.180	4.125	4.176	4.125
20 < Slope						
N	8	8	8	8	8	8
Min(m)	2.80	5.55	5.54	5.70	6.11	5.70
Max(m)	18.50	17.91	17.91	17.97	18.21	17.97
Mean (m)	8.025	9.803	9.786	9.614	8.914	9.614
STDV (±m)	4.613	3.636	3.632	3.596	3.774	3.596

In Table 59, the final fusion is a combination of the linear combination for slope less than 2.5°, TanDEM-X for slope 2.5° to 10°, and weighted averaging for slope greater than 10°. The methods are adopted because, after fusion of the DEMs, there is a remarkable decrease in standard deviations in those slope ranges, meaning an improvement in the vertical accuracy.

Region 6

Table 60: Vertical accuracy comparison of different fusion methods using the ground levelling test data in region 6

	Corrected DEMs		DEM fusion results			
	AW3D30_Corr	TanDEM-X_Corr	Fusion (linear combination)	Fusion(Weighted averaging)	Fusion(Averaging DEMs)	Final DEM fusion
N	1977	1977	1977	1977	1977	1977
Min(m)	-17.02	-20.70	-18.12	-18.54	-17.64	-18.12
Max(m)	46.34	48.18	47.84	48.16	47.26	47.84
Mean (m)	-0.078	0.765	0.664	0.786	0.344	0.768
STDV (±m)	6.082	6.043	5.860	5.918	5.887	5.841

Table 61: Vertical accuracy comparison of the different fusion methods in different slope ranges using the ground levelling test data in region 6

	Corrected DEMs		DEM fusion results			
Slope ranges	AW3D30_Corr	TanDEM-X_Corr	Fusion (linear combination)	Fusion(Weighted averaging)	Fusion(Averaging DEMs)	Final DEM fusion
0 < Slope < 2.5						
N	1262	1262	1262	1262	1262	1262
Min(m)	-17.02	-18.26	-18.12	-18.26	-17.64	-18.12
Max(m)	46.34	48.18	47.84	48.16	47.26	47.84
Mean (m)	-0.656	0.938	0.686	0.927	0.141	0.686
STDV (±m)	5.348	5.030	5.028	5.030	5.093	5.028
2.5 < Slope < 5.5						
N	481	481	481	481	481	481
Min(m)	-15.98	-11.91	-12.94	-13.59	-13.94	-15.98
Max(m)	43.17	44.20	43.95	43.88	43.68	43.17
Mean (m)	0.701	0.776	0.758	0.754	0.738	0.701
STDV (±m)	7.419	7.632	7.500	7.463	7.420	7.419
5.5 < Slope < 7.5						
N	82	82	82	82	82	82
Min(m)	-1.50	-5.75	-3.68	-5.18	-3.07	-1.50
Max(m)	28.80	39.18	34.70	38.34	32.49	28.80
Mean (m)	4.846	0.533	2.045	0.883	2.690	4.846
STDV (±m)	5.550	6.930	6.256	6.777	6.002	5.550
7.5 < Slope < 10						
N	66	66	66	66	66	66
Min(m)	-8.75	-5.89	-5.80	-5.51	-6.29	-8.75
Max(m)	30.05	35.07	29.56	31.14	29.64	30.05
Mean (m)	0.443	0.580	0.532	0.572	0.511	0.443
STDV (±m)	6.898	7.624	7.019	7.373	6.909	6.898
10<Slope<20						
N	71	71	71	71	71	71
Min(m)	-10.21	-6.81	-7.32	-10.07	-8.51	-7.32
Max(m)	6.18	9.72	8.57	6.09	7.56	8.57
Mean (m)	-2.004	-2.361	-2.310	-2.019	-2.182	-2.310
STDV (±m)	3.612	2.638	2.551	3.537	2.803	2.551
Slope > 20						
N	15	15	15	15	15	15
Min(m)	-7.04	-20.70	-8.55	-18.54	-13.16	-7.04
Max(m)	16.02	43.71	23.46	23.75	26.62	16.02
Mean (m)	3.497	2.807	2.955	3.577	3.152	3.497
STDV (±m)	7.199	14.576	8.719	10.247	9.908	7.199

In Table 61, the final fusion is a combination of the linear combination for slope less than 2.5° and 10° to 20°, and AW3D30 for slope 2.5° to 10° and greater than 20°. The methods are adopted because, after fusion of the DEMs, there is a remarkable decrease in standard deviations in those slope ranges, meaning an improvement in the vertical accuracy.

3.5.3.2 Vertical accuracy of the final fused DEM over South Africa

The final fused DEM for the whole of South Africa is shown in Figure 76. Tables 62 and 63 show the statistical results for the comparison of the corrected DEMs and final fused DEM over South Africa.

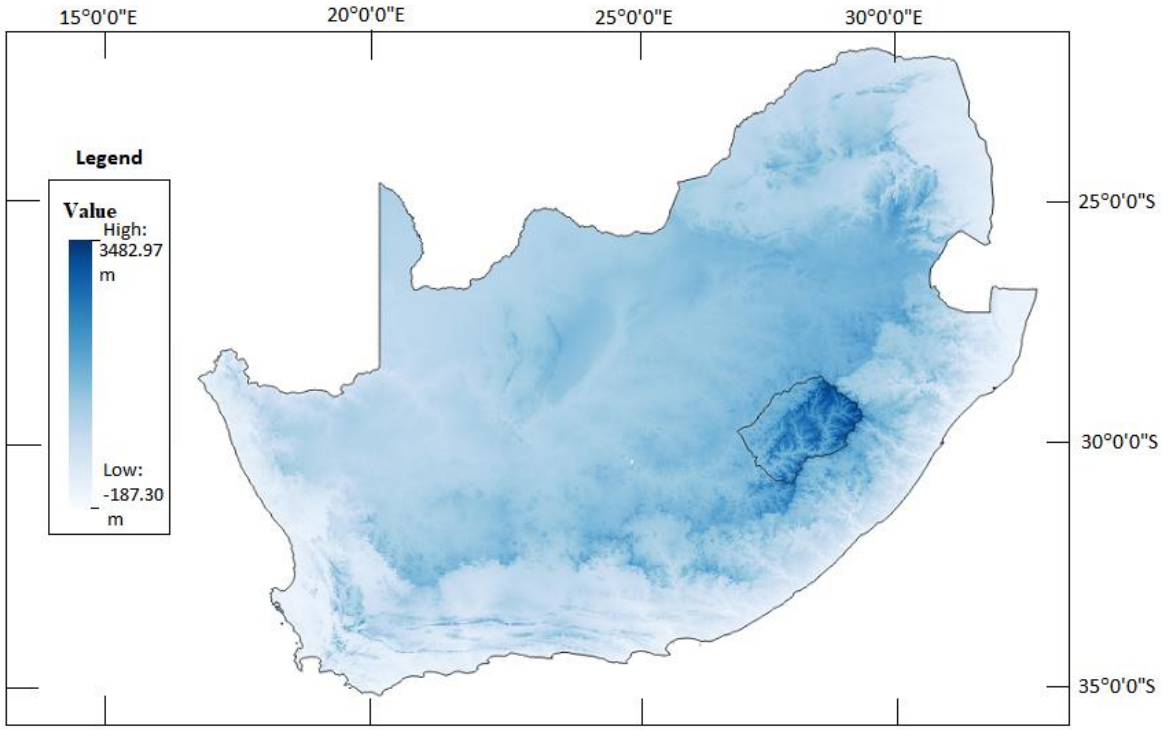

Figure 76: Final fused DEM for South Africa (units are in m)

Table 62: Vertical accuracy comparison of the corrected and final DEM fusion

	Corrected AW3D30	Corrected TanDEM-X	Final DEM fusion
N	8657	8657	8657
Min(m)	-37.95	-28.34	-28.70
Max(m)	50.46	62.92	48.56
Mean (m)	-0.073	0.213	0.173
STDV (±m)	4.995	4.582	4.290

Table 63: Vertical accuracy comparison of the corrected and final DEM fusion in different slope ranges

Slope ranges	Corrected AW3D30	Corrected TanDEM-X	Final DEM fusion
0 < Slope < 2.5			
N	3920	3920	3920
Min(m)	-17,02	-18,26	-18,12
Max(m)	46,34	48,18	47,84
Mean (m)	-0,269	0,427	0,334
STDV (±m)	4,420	4,037	4,016
2.5 < Slope < 5.5			
N	2448	2448	2448
Min(m)	-37,95	-25,56	-25,56
Max(m)	43,17	44,20	43,17
Mean (m)	0,041	0,065	0,050
STDV (±m)	5,126	4,491	4,417
5.5 < Slope < 7.5			
N	666	666	666
Min(m)	-29,07	-28,34	-28,70
Max(m)	28,80	42,40	35,29
Mean (m)	0,837	0,034	0,578
STDV (±m)	5,224	4,173	4,200
7.5 < Slope < 10			
N	593	593	593
Min(m)	-13,26	-14,23	-14,15
Max(m)	30,05	43,46	30,05
Mean (m)	-0,173	-0,040	-0,188
STDV (±m)	4,759	4,434	4,014
10<Slope<20			
N	824	824	824
Min(m)	-12,96	-10,25	-10,08
Max(m)	50,46	31,97	26,80
Mean (m)	-0,241	-0,484	-0,440
STDV (±m)	5,700	3,953	3,887
Slope > 20			
N	206,00	206,00	206,00
Min(m)	-22,18	-21,94	-22,18
Max(m)	48,563	62,921	48,563
Mean (m)	0,336	1,986	0,756
STDV (±m)	8,790	12,272	8,224

In Table 62, the final DEM fusion has a smaller standard deviation compared to the corrected DEMs. In Table 63, the final DEM fusion has smaller standard deviation in slopes ranging from 0° - 5.5° and greater than 7.5°. The results indicate that the final fused DEM has a better performance in these slope ranges. The vertical accuracies of the corrected DEMs and final fused DEM still decreases at steeper slopes, but fused DEM shows better performance compared to the corrected DEMs at these slopes.

3.5.3.3 Comparison of the original DEMs and fused DEM over South Africa

The statistical results for the vertical accuracies of the original DEMs and final fused DEM over the whole of South Africa using the combination of all the ground levelling (trigonometrical beacon) test data at 8, 657 points are shown in Table 64.

Table 64: Statistics of the height difference between the DEMs and the ground levelling data heights over South Africa

	ASTER	SRTM	MERIT	AW3D30 before coregistration	AW3D30 after coregistration	TanDEM-X	Final DEM Fusion
N	8657	8657	8657	8657	8657	8657	8657
Min(m)	-35.50	-37.80	-12.82	-34.90	-34.90	-23.08	-28.70
Max(m)	91.50	91.40	116.43	66.00	62.20	73.32	48.56
Mean (m)	9.995	3.851	8.497	2.768	3.867	4.250	0.174
Range (m)	127.00	129.20	129.25	100.90	97.10	96.40	77.26
STDV (±m)	9.732	7.293	9.275	4.784	5.745	5.073	4.290
RMSE (±m)	13.950	8.247	12.579	5.528	6.925	6.618	4.294

In the statistical results in Table 64, the final DEM fusion has a smaller range, mean, standard deviation, and RMSE over South Africa compared to all other DEMs applied in this study. These results indicate that the final DEM fusion achieves better absolute vertical accuracy compared to all other DEMs followed by the original AW3D30, TanDEM-X, co-registered AW3D30, SRTM, MERIT, and ASTER, in the order of decreasing vertical accuracy. The AW3D30 before co-registration, TanDEM-X, and MERIT standard deviations are within the vertical accuracy specifications of better than ±5, ±10 and ±12 m, respectively. The SRTM and ASTER vertical accuracy specifications of better than ±16 m are met. The AW3D30 after co-registration does not meet the original specification of better than ±5 m.

Chapter four: PROPOSED FRAMEWORK FOR THE DEVELOPMENT OF ACCURATE DIGITAL ELEVATION MODEL FROM GROUND AND SATELLITE DATA OVER SOUTH AFRICA

4.6 Introduction

The data sources, methods and techniques that have worked for the development of an accurate digital elevation model from ground and satellite data over South Africa are presented. The reference data, DEMs, correction models applied, fusion methods, application areas, and challenges with the use of the final fused DEM are discussed.

4.7 Prospects for development of accurate digital elevation model from ground and satellite data over South Africa

4.7.1 Data sources and error modelling strategies for DEM fusion

The ground levelling (trigonometrical beacon) and LiDAR work well as reference data for absolute and relative assessment, respectively. The AW3D30, TanDEM-X, SRTM, and MERIT DEMs can be used to develop an accurate DEM over South Africa. However, the most accurate DEMs that give better results are the AW3D30 and TanDEM-X. These DEMs are also the best candidate DEMs for fusion over South Africa because of the higher vertical accuracies in different geomorphological ranges compared to the other DEMs tested in this study. According to Santillan et al. (2016), the AW3D30 has always shown stable and high performance, and this has been supported by Uuemaa et al. (2020) and Mahesh et al. (2021). According to Han et al. (2021), the TanDEM-X has a better performance compared to the SRTM.

Segmenting the DEM into different regions and modelling DEM errors by the derivation of model parameters using a sample of points from the ground levelling data covering each region of interest provides better results, compared to the derivation of model parameters in a small region with LiDAR as reference and applying the models to the whole study area. In other words, correction parameters derived in one region, even if they are based on accurate reference DEM like LiDAR, cannot be used effectively in another region.

Using simple linear and multiple regression as a function of (slope, aspect, and surface roughness) to predict height errors, improves the errors in the DEMs (TanDEM-X and AW3D30). The adaptive terrain dependent method proposed by Zhou et al. (2020) also improves the errors in the DEMs. However, modelling DEMs errors using a combination of these methods, by selecting models that have a very high effect on improving the accuracy of the DEM's in certain slope ranges (0° – 2.5°, 2.5° – 5.5°, 5.5° – 7.5°, 7.5° – 10°, 10° – 20°, >20°) provides a remarkable improvement in DEM errors modelling.

4.7.2 Fusion methods and strategies that improved DEMs fusion

Segmenting the DEMs into different regions and fusing DEMs using models in which parameters are derived using a sample of points from the ground levelling data covering each region of interest provides better results, compared to the derivation of fusion parameters in regions with LiDAR as a reference and applying the fusion parameter to the whole study area.

Using linear combination, weighted averaging, averaging of the DEMs and fusion based on selected data by slope range (TanDEM-X, 0° – 20° & AW3D30, > 20°) results in a surface that improves the DEMs. However, using a combination of these fusion methods, by selecting methods that have a high effect on improving the accuracy of the DEM's in certain slope ranges (0° – 2.5°, 2.5° – 5.5°, 5.5° – 7.5°, 7.5° – 10°, 10° – 20°, >20°) provides more accurate final fused DEM that improves both the AW3D30 and TanDEM-X vertical accuracies.

4.7.3 Application and challenges of the final fused DEM

The final fused DEM generated has high resolution and national coverage and can be widely used in various research fields. Because the final fused DEMs includes elevations from DEMs which achieve better vertical accuracy, it can be applied in areas with different elevations and slopes. However, the proposed applications are in areas with slopes less than 20°, as better terrain representation is achievable. In the steepest areas, it can still achieve better vertical accuracy compared to other free satellite-based DEMs (SRTM, ASTER, MERIT, TanDEM-X, and AW3D30).

The developed DEM can be used for various applications, which include but are not limited to geological studies (detection of the geological structure, geological mapping, and analysis of tectonic evolution), geomorphology (volcano and aeolian), water resources, and hydrology (hydrologic modelling and reconstruction of palaeodrainage), evaluation of natural hazards (flooding and tsunami, earthquake), vegetation surveys and gravity modelling.

The challenge with the use of the DEM is that a full understanding of the consistency and homogeneity of the DEM is still necessary before it can be employed in various applications. The fused DEM still has challenges of decreasing vertical accuracy as slope increases. However, it still provides better results compared to other free satellite-based DEMs tested over South Africa.

Chapter five: CONCLUSION AND FUTURE WORK

5.1 Conclusion

This study aimed to contribute to developing a digital elevation model using satellite-based DEMs and ground levelling data over South Africa. This was achieved by preparing satellite-based DEMs, assessing the quality of the DEMs, selecting candidate DEMs for fusion, co-registration of DEMs, modeling candidate DEM errors, and fusing DEMs using such data and information. In this final chapter, the approach is reviewed by revisiting the stated research objectives, identifying weaknesses, and exploring avenues for future research.

The findings indicated that the absolute height differences had standard deviations of ±5.09 m for AW3D30 implied heights, ±7.03 m for SRTM, ±9.20 m for ASTER, ±4.99 m for TanDEM-X, and ±8.36 m for MERIT. In terms of the assessment results for the whole of South Africa, the AW3D30 and TanDEM-X showed better performance compared to all other DEMs. The ASTER showed the worst performance compared to all other DEMs.

Variation in elevation and slope affect accuracy of satellite-based DEMs. As elevation increases, the vertical accuracy of the DEMs decreases. As the slope increases, only the vertical accuracy of ASTER and MERIT decreases, and in other DEMs, there is no clear trend. Most high accuracies are achieved by these DEMs in areas with an elevation below 500 m and flat areas with slope angles between 0° to 2°. The lowest accuracies are observed in the steepest slopes and highest elevation areas.

Assessments in land use/cover categories show significant decrease in the accuracy of DEMs with increase in elevation in the low and high land use/cover areas. In medium land use/cover, only the ASTER vertical accuracy decreases as elevation increases. The rest of the DEMs show unclear trends and have low vertical accuracies in the elevation range (1000 - 1250 m). The reason for the unclear trend may be attributed to the smaller amount of ground levelling available, especially in higher elevation areas. In low land use/cover, all the DEMs vertical accuracies decrease as the slope becomes steeper. In medium land use/cover, only the SRTM, ASTER, and MERIT vertical accuracies are affected by slope change. In high land use/cover, the MERIT vertical accuracy decreases as the slope becomes steeper, and for the AW3D30 and TanDEM-X, higher vertical accuracies are found on steeper slopes. The absolute vertical accuracy of the AW3D30 and TanDEM-X varies less compared to all other DEMs over all land use/cover.

The findings indicated that the AW3D30 and TanDEM-X had the least height error standard deviations relative to LiDAR in all different geomorphological ranges compared to other DEMs and were better candidate DEMs for fusion. In the LiDAR area adopted in this study, an increase in the geomorphological factors (elevation, slope, and surface roughness) results in a decrease in the DEM's vertical accuracy. Most low vertical accuracies are achieved by these DEMs in areas with the highest (elevation, slope, and surface roughness). In all land uses/covers, most relatively low vertical accuracies are achieved by the DEMs in areas with the highest (elevation, slope, and surface roughness). In addition, there is no clear relationship between aspect change and height errors.

The co-registration of AW3D30 to grid lines of the DEMs (SRTM, ASTER, and TanDEM-X) decreases the vertical accuracy of the original DEM. Although a shift in the northwest direction was adopted for subsequent analysis, co-registration to the southeast offers better vertical accuracy compared to other directions when validated using 8,657 ground levelling data.

The approach for modeling DEM errors, which is made up of a combination of simple linear regressions, multiple linear regressions, and adaptive terrain-dependent methods over South Africa, provided a remarkable improvement in the vertical accuracy of the DEMs. After validating the DEMs using 8,657 ground levelling test data, there was a decrease in mean and standard deviation values. The standard deviation of the discrepancies decreased from ±5.745 to ±4.995 m for AW3D30 and ±5.073 to ±4.582 m for TanDEM-X, and the models had more effect over slope ranges, greater than 10°.

Deriving fusion parameters using ground levelling model points and selecting a combination of the best fusions from (linear combination, weighted averaging, (TanDEM-X (from 0° – 20°) & AW3D30 (> 20°)), and simple averaging) provided a remarkable improvement in the vertical accuracy of corrected DEM's. After validating the AW3D30, TanDEM-X, and final fused DEM using 8,657 ground levelling data points, the standard deviations of the discrepancies were ±4.995, ±4.582, and ±4.290 m, respectively. In slopes, less than 20°, the final fused DEM achieved the best accuracy.

The findings also indicated that the final DEM fusion achieves better absolute vertical accuracy compared to all the original satellite-based DEMs used in this study, followed by the original AW3D30, TanDEM-X, co-registered AW3D30, SRTM, MERIT, and ASTER, respectively. The fused DEM can be applied in all elevation and slope ranges. However, better terrain representation is achievable in areas with slopes less than 20°. The fused DEM is expected to be used in scientific research and geospatial applications, which include but are not limited to geological studies, geomorphology, water resources and hydrology, evaluation of natural hazards, vegetation surveys, and gravity modelling.

A full understanding of errors in the fused DEM is still necessary before it can be employed in various engineering and scientific applications. The DEM still has challenges of decreasing vertical accuracy as slope increases. However, it still provides better vertical accuracy compared to the freely available satellite-based DEMs (SRTM, ASTER, MERIT, TanDEM-X, and AW3D30) in all slope ranges in South Africa.

5.2 Future work

Experiments with raster data that have national coverage are very time-consuming, requiring days to run processes. Therefore, many different tests and experiments have been left for the future due to lack of time. Future work for this research concerns a deeper analysis of the final fused DEM and new proposals to try different methods. The following ideas could be tested for future work:

It is recommended that a DEM assessment may include not only the vertical accuracy but also the horizontal accuracy. The original heights of the TanDEM-X were ellipsoidal and were converted to spheroidal orthometric using the geoidal heights model interpolated by IDW. It could be interesting to use other interpolation techniques such as, kriging, artificial neuron networks, among others, and assess different TanDEM-X orthometric heights.

The co-registered AW3D30 to grid lines of the DEMs (SRTM, ASTER, and TanDEM-X) in the northwest direction was used for all subsequent analyses. However, the findings indicate that the southeast offered better vertical accuracy. Therefore, further research is recommended using the DEM co-registered to the southeast direction.

A similar process used to generate a SUDEM can be tested. However, in this case, this can be done using either AW3D30 or TanDEM-X. The process that was followed by Yamazaki (2018) in developing a Multi Error- Removed Improved Terrain (MERIT) DEM can be replicated in South Africa using the

TanDEM-X and AW3D30. The vertical accuracy of DEMs could be improved through the use of very high-resolution satellite data from InSAR techniques.

A more improved DEM can be generated by combining the final fused DEM with multiple sources of elevation data, namely large-scale contours, and spot heights. With available larger storage and robust processing software, the final fused DEM can be resampled to very high resolutions, and integration using ground levelling data can be tested to improve the accuracy of the DEM.

References

Abrams, M. (2016). ASTER GLOBAL DEM VERSION 3, AND NEW ASTER WATER BODY DATASET. ISPRS – International Archives of the Photogrammetry, Remote Sensing and Spatial Information Sciences, XLI-B4, pp.107-110. Available at: https://doi.org/10.5194/isprs-archives-XLI-B4-107-2016

Airbus. (2015). TerraSAR-X Image Product Guide: Basic and Enhanced Radar Satellite Imagery. Available at: https://www.intelligence-airbusds.com/files/pmedia/public/r459_9_20171004_tsxx-airbusds-ma-0009_tsx-productguide_i2.01.pdf

Ali, M., Shaker, I. and Saba, N. (2018). Enhancement of SRTM and ASTER Elevations Using GPS Control Points and Polynomial Regression Model. Al-Azhar University Civil Engineering Research Magazine, 40(2), pp.68-70.

Bagheri, H., Schmitt, M. and Zhu, X. (2018). Fusion of TanDEM-X and Cartosat-1 elevation data supported by neural network-predicted weight maps. ISPRS Journal of Photogrammetry and Remote Sensing, 144, pp.285-297. Available at: https://doi.org/10.1016/j.isprsjprs.2018.07.007

Baqersad, J., Poozesh, P., Niezrecki, C. and Avitabile, P. (2017). Photogrammetry and optical methods in structural dynamics – A review. Mechanical Systems and Signal Processing, 86, pp.17-34. Available at: https://doi.org/10.1016/j.ymssp.2016.02.011

Bates, J. and Granger, C. (1969). The Combination of Forecasts. Journal of the Operational Research Society, 20(4), pp.451-468. Available at: https://doi.org/10.2307/2581301

Csanyi, N. and Toth, C. (2007). Improvement of Lidar Data Accuracy Using Lidar-Specific Ground Targets. Photogrammetric Engineering & Remote Sensing, 73(4), pp.385-396. Available at: https://doi.org/10.14358/PERS.73.4.385

ElSayed, M. and Ali, A. (2016). Improving the Accuracy of the SRTM Global DEM Using GPS data fusion and regression Model. International Journal of Engineering Research, 5(3), pp.190-196. Available at: https://doi.org/10.17950/ijer/v5s3/305

Fuss, C., Berg, A. and Lindsay, J. (2016). DEM Fusion using a modified k-means clustering algorithm. International Journal of Digital Earth, 9(12), pp.1242-1255. Available at: https://doi.org/10.1080/17538947.2016.1208685

Gesch, D., Oimoen, M., Danielson, J. and Meyer, D. (2016). Validation of the ASTER Global Digital Elevation Model version 3 over the conterminous united states. ISPRS – International Archives of the Photogrammetry, Remote Sensing and Spatial Information Sciences, XLI-B4, pp.143-148. Available at: https://doi.org/10.5194/isprs-archives-XLI-B4-143-2016

Gómez, M., Lencinas, J., Siebert, A. and Díaz, G. (2012). Accuracy Assessment of ASTER and SRTM DEMs: A Case Study in Andean Patagonia. GIScience & Remote Sensing, 49(1), pp.71-91. Available at: https://doi.org/10.2747/1548-1603.49.1.71

Gorokhovich, Y. and Voustianiouk, A. (2006). Accuracy assessment of the processed SRTM-based elevation data by CGIAR using field data from USA and Thailand and its relation to the terrain characteristics. Remote Sensing of Environment, 104(4), pp.409-415. Available at: https://doi.org/10.1016/j.rse.2006.05.012

Han, H., Zeng, Q. and Jiao, J. (2021). Quality Assessment of TanDEM-X DEMs, SRTM and ASTER GDEM on Selected Chinese Sites. Remote Sensing, 13(7), 1304. Available at: https://doi.org/10.3390/rs13071304

Honikel, M. (1998). Fusion of optical and radar digital elevation models in the spatial frequency domain. Workshop on retrieval of Bio- And Geo-Physical Parameters from SAR Data for Land Applications, ESA-ESTEC, 21-23 Oct.

Huang, N., Shen, Z., Long, S., Wu, M., Shih, H., Zheng, Q., Yen, N., Tung, C. and Liu, H. (1998). The empirical mode decomposition and the Hilbert spectrum for nonlinear and non-stationary time series analysis. Proceedings of the Royal Society of London. Series A: Mathematical, Physical and Engineering Sciences, 454(1971), pp.903-995. Available at: https://doi.org/10.1098/rspa.1998.0193

Ismail, Z. and Jaafar, J. (2013). DEM Derived from Photogrammetric Generated DSM using Morphological Filter. 2013 IEEE 4th Control and System Graduate Research Colloquium. pp.103-106. Available at: https://doi.org/10.1109/ICSGRC.2013.6653284

Japan Aerospace Exploration Agency (2021). ALOS World 3D 30-meter DEM. V3.2, Jan 2021. Distributed by OpenTopography. Available at: https://doi.org/10.5069/G94M92HB

Jing, C., Shortridge, A., Lin, S. and Wu, J. (2013). Comparison and validation of SRTM and ASTER GDEM for a subtropical landscape in Southeastern China. International Journal of Digital Earth, 7(12), pp.969-992. Available at: https://doi.org/10.1080/17538947.2013.807307

Johnston, K., Ver Hoef, J., Krivoruchko, K. and Lucas, N. (2004). Using ArcGIS geostatistical analyst. ESRI Press, pp.131-166. Available at: https://www.researchgate.net/publication/200043204_Using_ArcGIS_geostatistical_analyst

Karkee, M., Steward, B. and Aziz, S. (2008). Improving quality of public domain digital elevation models through data fusion. Biosystems Engineering, 101(3), pp.293-305. Available at: https://doi.org/10.1016/j.biosystemseng.2008.09.010

Kass, M., Witkin, A. and Terzopoulos, D. (1988). Snakes: Active contour models. International Journal of Computer Vision, 1(4), pp.321-331. Available at: https://doi.org/10.1007/BF00133570

Kroenung, G., Strebeck, J., & Grohman, G. (2006). Filling SRTM Voids: The Delta Surface Fill Method. Photogrammetric Engineering and Remote Sensing, 72, pp.213-216.

Li, Y., Sun, Y., Huang, X., Qi, G., Zheng, M. and Zhu, Z. (2018). An Image Fusion Method Based on Sparse Representation and Sum Modified-Laplacian in NSCT Domain. Entropy, 20(7), 522. Available at: https://doi.org/10.3390/e20070522

Luebke, R. (2019). Assessing Vertical Accuracy of Digital Elevation Models. Available at: https://www.intermap.com/blog/2018/11/assessing-vertical-accuracy-of-digital-elevation-models-0

Mahesh, R., Jayadevan Sarunjith, K., Rajakumari, S., Muruganandam, R. and Ramesh, R. (2021). Quality assessment of open-sourced digital elevation models in southeast coast of India. The Egyptian Journal of Remote Sensing and Space Science, 24(2021), pp.745-754. Available at: https://doi.org/10.1016/j.ejrs.2021.03.006

Mapware (2020), Lidar vs Photogrammetry: Types of Remote Sensing. Available at: https://mapware.com/blog/lidar-vs-photogrammetry-types-of-remote-sensing/

Mikhail, E. M., Bethel, J. S., & McGlone, J. C. (2001). Introduction to Modern Photogrammetry. New Yord: John Wiley & Sons, Inc.

Mohamed, M. and Saleh, S. (2018). Fusion of SRTM and ASTER GDEM2 DEMs based on height error weighted average technique. Australian Journal of Basic and Applied Sciences, 12(6), pp.23-29. Available at: https://doi.org/10.22587/ajbas.2018.12.6.5

Nex, F. and Rinaudo, F. (2011). LiDAR or Photogrammetry? Integration is the answer. Italian Journal of Remote Sensing, 43(2), pp.107-121. Available at: https://doi.org/10.5721/ItJRS20114328

Oksanen, J. (2021). Digital Elevation Model | National Land Survey of Finland. Available at: https://www.maanmittauslaitos.fi/en/research/interesting-topics/digital-elevation-model

O'Loughlin, F., Paiva, R., Durand, M., Alsdorf, D. and Bates, P. (2016). A multi-sensor approach towards a global vegetation corrected SRTM DEM product. Remote Sensing of Environment, 182, pp.49-59. Available at: https://doi.org/10.1016/j.rse.2016.04.018

Papasaika, H., Poli, D. and Baltsavias, E. (2009). Fusion of Digital Elevation Models from Various Data Sources. 2009 International Conference on Advanced Geographic Information Systems & Web Services, pp.117-122. Available at: https://doi.org/10.1109/GEOWS.2009.22

Papasaika, H., Kokiopoulou, E., Baltsavias, E., Schindler, K. and Kressner, D. (2011). Fusion of Digital Elevation Models Using Sparse Representations. Photogrammetric Image Analysis, 6952, pp.171-184. Available at: https://doi.org/10.1007/978-3-642-24393-6_15

Pham, H., Marshall, L., Johnson, F. and Sharma, A. (2018). A method for combining SRTM DEM and ASTER GDEM2 to improve topography estimation in regions without reference data. Remote Sensing of Environment, 210, pp.229-241. Available at: https://doi.org/10.1016/j.rse.2018.03.026

Qiu, Z., Yue, L. and Liu, X. (2019). Void Filling of Digital Elevation Models with a Terrain Texture Learning Model Based on Generative Adversarial Networks. Remote Sensing, 11(23), 2829. Available at: https://doi.org/10.3390/rs11232829

Reinartz, P., Müller, R., Hoja, D., Lehner, M. and Schroeder, M. (2005). Comparison and fusion of DEM derived from SPOT-5 HRS and SRTM data and estimation of forest heights. Earsel Symposium, Porto, Portugal, 6 -11 June.

Rodríguez, E., Morris, C. and Belz, J. (2006). A Global Assessment of the SRTM Performance. Photogrammetric Engineering & Remote Sensing, 72(3), pp.249-260. Available at: https://doi.org/10.14358/PERS.72.3.249

Ronald, T. (1987). Terrain models — A tool for natural hazard Mapping. In: Avalanche Formation, Movement and Effects (Proceedings of the Davos Symposium, September 1986), 162.

Roth, A., knöpfle, W., Strunz, G., Lehner, M. and Reinartz, P. (2002). Towards a global elevation product: combination of multi-source Digital Elevation Models. Proc. of the Joint International Symposium on Geospatial Theory, Processing and Applications, Ottawa, 2002, pp.1-5.

Santillan, J. and Makinano-Santillan, M. (2016). VERTICAL ACCURACY ASSESSMENT OF 30-M RESOLUTION ALOS, ASTER, AND SRTM GLOBAL DEMS OVER NORTHEASTERN MINDANAO, PHILIPPINES. ISPRS - International Archives of the Photogrammetry, Remote Sensing and Spatial Information Sciences, XLI-B4, pp.149-156. Available at: https://doi.org/10.5194/isprsarchives-XLI-B4-149-2016

Schenk, T. (2005). Introduction to Photogrammetry. Department of Civil and Environmental Engineering and Geodetic Science Ohio State University, Columbus, OH.

Schindler, K., Papasaika-Hanusch, H., Schütz, S. and Baltsavias, E. (2011). Improving Wide-Area Dems Through Data Fusion - Chances and Limits. Institute of Geodesy and Photogrammetry, ETH Zürich, Switzerland, pp.3-14.

Schultz, H., Hanson, A., Riseman, E., Stolle, F., Zhu, Z. and Dong-Min, W. (2002). A Self-consistency Technique for Fusing 3D Information. Proceedings of the fifth IEEE international conference on information fusion, 2, pp.1106-1112. Available at: https://doi.org/10.1109/ICIF.2002.1020936

Setiyoko, A., Arymurthy, A. and Basaruddin, T. (2019). DEM fusion concept based on the LS-SVM cokriging method. International Journal of Image and Data Fusion, 10(4), pp.244-262. Available at: https://doi.org/10.1080/19479832.2019.1664647

Shortridge, A. and Messina, J. (2011). Spatial structure and landscape associations of SRTM error. Remote Sensing of Environment, 115(6), pp.1576-1587. Available at: https://doi.org/10.1016/j.rse.2011.02.017

Singh, S. (2019). Difference between DEM/DTM and DSM. GIS Resources. Available at: http://www.gisresources.com/confused-dem-dtm-dsm/

Su, Y. and Guo, Q. (2014). A practical method for SRTM DEM correction over vegetated mountain areas. ISPRS Journal of Photogrammetry and Remote Sensing, 87, pp.216-228. Available at: https://doi.org/10.1016/j.isprsjprs.2013.11.009

Su, Y., Guo, Q., Ma, Q. and Li, W. (2015). SRTM DEM Correction in Vegetated Mountain Areas through the Integration of Spaceborne LiDAR, Airborne LiDAR, and Optical Imagery. Remote Sensing, 7(9), pp.11202-11225. Available at: https://doi.org/10.3390/rs70911202

Szabó, S., Enyedi, P., Horváth, M., Kovács, Z., Burai, P., Csoknyai, T. and Szabó, G. (2016). Automated registration of potential locations for solar energy production with Light Detection and Ranging (LiDAR) and small format photogrammetry. Journal of Cleaner Production, 112, pp.3820-3829. Available at: https://doi.org/10.1016/j.jclepro.2015.07.117

Tachikawa, T., Hato, M., Kaku, M. and Iwasaki, A. (2011). Characteristics of ASTER GDEM version 2. *2011 IEEE International Geoscience and Remote Sensing Symposium*, pp.3657-3660. Available at: https://doi.org/10.1109/IGARSS.2011.6050017

Tarekegn, T. and Sayama, T. (2013). Correction of SRTM DEM artefacts by fourier transform for flood inundation modeling. Journal of Japan Society of Civil Engineers, Ser. B1 (Hydraulic Engineering), 69(4), pp.193-198. Available at: https://doi.org/10.2208/jscejhe.69.I_193

Tian, Y., Lei, S., Bian, Z., Lu, J., Zhang, S. and Fang, J. (2018). Improving the Accuracy of Open-Source Digital Elevation Models with Multi-Scale Fusion and a Slope Position-Based Linear Regression Method. Remote Sensing, 10(12), 1861. Available at: https://doi.org/10.3390/rs10121861

Tran, T., Raghavan, V., Masumoto, S., Vinayaraj, P. and Yonezawa, G. (2014). A geomorphology-based approach for digital elevation model fusion – case study in Danang City, Vietnam. Earth Surface Dynamics Discussions, 2(1), pp.255-296. Available at: https://doi.org/10.5194/esurfd-2-255-2014

Uuemaa, E., Ahi, S., Montibeller, B., Muru, M. and Kmoch, A. (2020). Vertical Accuracy of Freely Available Global Digital Elevation Models (ASTER, AW3D30, MERIT, TanDEM-X, SRTM, and NASADEM). Remote Sensing, 12(21), 3482. Available at: https://doi.org/10.3390/rs12213482

van Niekerk, A. (2015). Stellenbosch University Digital Elevation Model (SUDEM) Product Description v15.15.

van Niekerk, A. (2021). 5 m Stellenbosch University Digital Elevation Model (SUDEM). Geosmart.space. Available at: https://geosmart.space/products/sudem.html

Verhulp, J. (2015). Towards a national digital elevation model. Proceedings of the Geomatics Indaba Conference Proceedings, 11-13 August, Ekurhuleni, South Africa.

Vermeer, M. and Ayehu, G. (2018). Digital Aerial Mapping - a Hands-On Course. Finland.

Weydahl, D., Bretar, F. and Bjerke, P. (2005). Comparison of RADARSAT-1 and IKONOS satellite images for urban features detection. Information Fusion, 6(3), pp.243-249. Available at: https://doi.org/10.1016/j.inffus.2004.07.001

Yamazaki, D., Ikeshima, D., Tawatari, R., Yamaguchi, T., O'Loughlin, F., Neal, J., Sampson, C., Kanae, S. and Bates, P. (2017). A high-accuracy map of global terrain elevations. Geophysical Research Letters, 44(11), pp.5844-5853. Available at: https://doi.org/10.1002/2017GL072874

Yamazaki, D. (2018). MERIT DEM: Multi-Error-Removed Improved-Terrain DEM. Hydro.iis.u-tokyo.ac.jp. Available at: http://hydro.iis.u-tokyo.ac.jp/~yamadai/MERIT_DEM/

Yang, B. and Li, S. (2010). Multifocus Image Fusion and Restoration with Sparse Representation. IEEE Transactions on Instrumentation and Measurement, 59(4), pp.884-892. Available at: https://doi.org/10.1109/TIM.2009.2026612

Zhou, C., Zhang, G., Yang, Z., Ao, M., Liu, Z. and Zhu, J. (2020). An Adaptive Terrain-Dependent Method for SRTM DEM Correction Over Mountainous Areas. IEEE Access, 8, pp.130878–130887. Available at: https://doi.org/10.1109/ACCESS.2020.3009851